THESIS AND ABSTRACT

The role of autophagy in mature adipocytes during homeostasis and intestinal inflammation

by Felix Clemens Richter



St. Hilda's College, University of Oxford
Kennedy Institute of Rheumatology, NDORMS

Thesis submitted in fulfilment of the requirements for the degree of Doctor of Philosophy, University of Oxford

Hillary Term 2021

Abstract

The role of autophagy in mature adipocytes during homeostasis and intestinal inflammation

by Felix C. Richter

Thesis submitted in fulfilment of the requirements for the degree of Doctor of Philosophy, University of Oxford, Hillary Term 2021

Autophagy is an evolutionary conserved lysosomal degradation pathway, which can control cell-intrinsic functions such as differentiation and cellular metabolism. The cell-intrinsic role of autophagy is of particular importance to immune cells, but autophagy also has a cell-extrinsic role in the tumour environment. It remains unclear whether autophagy in the tissue environment can alter immune responses. The release of free fatty acids (FFA) from adipocytes in times of high energy demands (e.g. inflammation) classically depends on the function of cytosolic lipases, however, the contribution of autophagy to this process remains unknown.

Here we investigated the role of autophagy in mature adipocytes during colitis, and its impact on intestinal inflammation and the immune response. Induction of intestinal inflammation using dextran sulphate sodium (DSS) increased autophagic flux in adipose tissues. Furthermore, the adipocyte-specific deletion of *Atg7*, an essential autophagy gene, resulted in an exacerbation of intestinal inflammation upon DSS treatment. We found that loss of adipocyte autophagy impaired optimal lipolytic secretion and availability of FFA during intestinal inflammation. Adipose tissue macrophages react to local FFA availability by altering the expression of the FFA transporter CD36. In line with this, restricting FFA from LPS-stimulated macrophages blunted CD36 expression and reduced IL-10 secretion, while supplementation of the FFA linoleic acid rescued IL-10 expression. Accordingly, we found that during DSS colitis IL-10 secretion from adipose tissues and serum IL-10 levels were reduced in mice with adipocyte-specific autophagy loss.

This study highlights an underappreciated anti-inflammatory function of adipose tissues

during intestinal inflammation. Future studies will be required to investigate whether this anti-inflammatory pathway is conserved in human inflammatory bowel disease and whether it can be exploited therapeutically. Overall, results presented in this study revealed a novel cell-extrinsic function of autophagy in the metabolic regulation of immune responses, mediated by the provision of adipocyte-derived FFAs for IL-10 production.

Author's Publications

Simon Group

Alsaleh G*, Panse I*, Swadling L, Zhang H, **Richter FC**, Meyer A, Lord J, Barnes E, Klenerman P, Green C, Simon AK (2020) Autophagy in T cells from aged donors is maintained by spermidine and correlates with function and vaccine responses. *eLife*, **9**, e57950.

Richter FC, Obba S, Simon AK (2018) Local exchange of metabolites shapes immunity. *Immunology*, **155**, 309-319.

Riffelmacher T, Clarke A, **Richter FC**, Stranks A, Pandey S, Danielli S, Hublitz P, Yu Z, Johnson E, Schwerd T, McCullagh J, Uhlig H, Jacobsen SEW, Simon AK (2017) *Immunity*, **47**, 46-480.e5.

Riffelmacher T, **Richter FC**, Simon AK (2017) Autophagy dictates metabolism and differentiation of inflammatory immune cells. *Autophagy*, **14**, 1-8.

Simmons Group

Kinchen J*, Chen HH*, Parikh K*, Antanaviciute A, Jagielowicz, Fawkner-Corbett D, Ashley N, Cubitt L, Mellado-Gomez E, Attar M, Sharma E, Wills Q, Bowden R, **Richter FC**, Ahern D, Puri KD, Henault J, Gervais F, Koohy H, Simmons A (2018) Structural Remodeling of the Human Colonic Mesenchyme in Inflammatory Bowel Disease. *Cell*, **175**, 372 - 386.

Oxford-Cardiff COVID-19 Literature Consortium

Richter FC*, Alrubayyi A*, Teijeira Crespo A*, The Oxford-Cardiff COVID-19 Literature Consortium, Hulin-Curtis S*, (2021) Impact of obesity on host defences: Implications for SARS-CoV-2 infection. *Oxford Open Immunology*, **1**.

*Author's contributed equally

Scourfield DO, Reed SG, Quastel M, Alderson J, Bart VMT, Teijeira Crespo A, Jones R, Pring E, **Richter FC**, The Oxford-Cardiff COVID-19 Literature Consortium, Burnell SEA (2021) The Role and Uses of Antibodies in COVID-19 Infections: A Living Review. *Oxford Open Immunology*, **1**.

Hanna SJ, Codd AS, Gea-Mallorquì E, Scourfield DO, **Richter FC**, Ladell K, Borsa M, Compeer EB, Moon OR, Galloway SAE, Dimonte S, Capitani L, Shepherd FR, Wilson JD, Uhl LFK, The Oxford-Cardiff COVID-19 Literature Consortium, Gallimore AM, Milicic A (2020) T cell phenotypes in COVID-19. *Oxford Open Immunology*, **1**.

Rodrigues PRS, Alrubayyi A, Pring E, Bart VMT, Jones R, Clarissa C, Fangfang L, Tellier M, Maleki-Toyserkani S, **Richter FC**, Scourfield DO, Gea-Mallorquí E, Davies LC, The Oxford-Cardiff COVID-19 Literature Consortium (2020) Innate immunology in COVID-19—a living review. Part II: dysregulated inflammation drives immunopathology. *Oxford Open Immunology*, **1**.

Clarissa C, Tellier M, Fangfang L, Maleki-Toyserkani S, Jones R, Bart VMT, Pring E, Alrubayyi A, **Richter FC**, Scourfield DO, Rehwinkel J, Rodrigues PRS, Davies LC, Gea-Mallorquí E, The Oxford-Cardiff COVID-19 Literature Consortium (2020) Innate immunology in COVID-19—a living review. Part I: viral entry, sensing and evasion. *Oxford Open Immunology*, **1**.

Acknowledgements

Academia can be incredibly intimidating, maybe especially here in Oxford. While working next to some of the most talented and amazing researchers teaches you a lot, it does nurture your own imposter syndrome. In particular during my first rotation in my first year, I was close to drop out. However, thanks to an incredible support from my friends, my family, my lab mates, my partner and, foremost, my supervisor, I still had a great experience and want to thank you all here. I am lucky to have found incredibly supportive friends with whom I had a feeling of family away from my family. In particular, I want to thank the "OxFam" (Alina, Sara, Lion, Pablo, Mathilde, Matthias, Anne, David, Lilian) and the "Brunch Club" (Johannes, Juli, Athena, Jonny and Armin) for all their help throughout, for allowing to complain, to cheer and to share my feelings. I sincerely treasure these newly found long-term friendships. One says that singing 'Piano Man' together, binds one together. I am happy to have found these great friends:

"Sing us a song you're the piano man

Sing us a song tonight

Well we're all in the mood for a melody

And you got us feeling alright"

Excerpt of 'Piano Man' by Billy Joel, 1973

Next I want to thank my parents, Ute and Hartmut Richter, for their continuous support throughout my life. They are certainly the most important pillar in my life and make a lot of life's hardships easier to bear. I feel very privileged to have had the possibility to go the academic route that I was going due to their support. My brother, Simon Richter, is and always has been a major inspiration to me. I really enjoyed experiencing the DPhil journey with you. I am grateful for many supportive calls, our thesis writing retreat and that we continue going through life together.

I want to thank my partner Sarah Wideman, an outstanding scientist and a "soon-to-be" DPhil as well. She not only helped me during my long experimental days, but also lifted me up when I was down and helped me not to forget there is more to life than just science. Thank you for all your support throughout the years and more to come.

Along this DPhil, I was lucky to learn from many excellent researchers who are or were part of our lab. I selected coming to this lab in parts because of the great group atmosphere and I was never disappointed. I want to thank all previous and current members for inspirational discussions and encouraging word when experimental depression have set in: Alex Clarke, Thomas Riffelmacher, Sandrine Obba, Ghada Alsaleh, Mariana Borsa, Dingxi Zhou, Houfu Leng, Hanlin Zhang, Paula Hahn, Cristina Dumitru, Klara Piletic and Ana Victoria Lechuga-Vieco.

In particular, I want to thank Thomas Riffelmacher and Ghada Alsaleh, who have both influenced and inspired my research. You showed me that it is important to not make science the center of your life and to not loose sight of the life outside of the lab. You are both two of the most brilliant researchers I met during my time in Oxford, always approachable and someone I hope to stay in touch with in future.

I want to thank the many groups that I was in contact with in order to seek for advice and learn experimental techniques for a adipose project no one could equip me for. Special thank you to Cécile Bénézech and William Cawthorn (University of Edinburgh) and Irina Guschina (Cardiff University) for her help with the lipidomics.

This project would have been impossible without the help of an entire team of supervisors who helped me to navigate through my project and allowed me several new insights into my project. In particular, the help of Mathilde Pohin, Matthias Friedrich, Henk Schipper and Ghada Alsaleh have enabled me to progress with my project into the field of IBD research and adipose tissue biology.

This gratitude naturally extends to my co-supervisor Prof. Claire Edwards, an amazing supervisor with an open ear and encouraging words. Despite it not having become a bone marrow project, it was inspiring joining your lab meetings and having your support.

Lastly, I need to thank my main supervisor Prof. Katja Simon to bear with me during this incredibly challenging project. Although I have watched your supervision closely, I hope one day to be able to be as good of a researchers as you do and keep my life balance. Your supervision has made me into the independent researcher I am today. I am very grateful to have had such a role model as supervisor and hope that I can pass

on many of the virtues you taught me.

Contents

1 General Introduction **18**

1.1 Autophagy 18

1.1.1 Types of autophagy 18

1.1.2 Mechanism and receptors of autophagy 22

1.1.3 Regulation of autophagy 25

1.1.4 Autophagy in the immune system 27

1.2 Adipocytes and adipose tissues 30

1.2.1 Introduction to the role and function of adipocytes 30

1.2.2 Regulation and control of lipolysis 32

1.2.3 Immune cells in the adipose tissue 35

1.3 Metabolic crosstalk between immune cells and stroma 36

1.3.1 Amino acid crosstalk 37

1.3.2 Free fatty acid crosstalk 38

1.3.3 Organelle crosstalk 39

1.4 Inflammatory bowel disease 40

1.4.1 Immunopathology of IBD 41

1.4.2 Links of autophagy and IBD 44

1.5 Thesis hypothesis and objectives 46

2 Materials and Methods **48**

2.1 Mice 48

2.2 DSS-induced and *Helicobacter hepaticus*-induced colitis 48

2.3 Bone marrow transplantation 49

2.4 Hematopoietic progenitor colony-forming unit assay 49

2.5 Genotyping 49

2.6 Cell culture 51

2.7 Lentiviral transduction and shRNA cell lines 52

2.8 Adipose Tissue Explant Culture 52

2.9 Adipose Tissue and Colon Digestion 53
2.10 Flow cytometry 54
2.11 Polymerase chain reaction (PCR) 54
2.12 Quantitative PCR (qPCR) 56
2.13 Bulk RNA sequencing 57
2.14 Shotgun lipidomics 58
2.15 Free fatty acid analysis 59
2.16 Immunoblotting 59
2.17 Transmission electron microscopy 60
2.18 Epifluorescence and confocal microscopy 62
2.19 Osmium Tetroxide Staining 63
2.20 Cytokine analysis 63
2.21 Bone marrow-derived macrophage culture 64
2.22 Statistical Analysis 64

3 Experimental models to study autophagy in mature adipocytes 66

3.1 Introduction 66
3.1.1 Adipogenesis and the role of autophagy 66
3.1.2 Overview of existing experimental models to study adipocytes *in vitro* and *in vivo* 67
3.1.3 Aim of this chapter 68
3.2 Results 69
3.2.1 Establishment and validation of an inducible autophagy-KD adipocyte cell line 69
3.2.2 Establishment and validation of an inducible adipocyte-specific KO mouse model 75
3.3 Discussion 87
3.3.1 shRNA-mediated knockdown of *Atg5* and *Atg7* in ST2 cells is insufficient for further experimental assessment 87
3.3.2 Efficient deletion of *Atg7* in a tamoxifen-inducible, *Adipoq*-driven Cre mouse model 88

3.4 Conclusion 90

4 Homeostatic effects of autophagic loss in mature adipocytes 91

4.1 Introduction 91

4.1.1 Adipose tissue lipid metabolism 91

4.1.2 Immune cells in adipose tissues 92

4.1.3 Bone marrow adipose tissue and hematopoiesis 93

4.1.4 Context and aim of this chapter 94

4.2 Results 95

4.2.1 Long-term loss of adipocyte autophagy leads to decreased adipose tissue size 95

4.2.2 Adipocyte autophagy loss controls adipocyte size and lipolysis without changing systemic lipid levels 97

4.2.3 Adipocyte loss does not alter immune homeostasis in adipose tissues 103

4.2.4 Hematopoietic reconstitution may be affected by loss of autophagy in mature adipocytes 106

4.3 Discussion 111

4.3.1 Autophagy in adipocytes controls FFA secretion from adipocytes 111

4.3.2 Adipose tissue immune cells are unaffected by homeostatic loss of adipocyte autophagy 113

4.3.3 Loss of autophagy in bone marrow adipose tissue may control hematopoietic recovery 113

4.4 Conclusion 115

5 Loss of autophagy in mature adipocytes exacerbates intestinal inflammation 116

5.1 Introduction 116

5.1.1 IBD is linked to autophagy and adipose tissues 116

5.1.2 Murine models of intestinal inflammation 117

5.1.3 Context and aim of this chapter 118

5.2 Results 119

5.2.1 Low-dose DSS administration induces intestinal inflammation and leads to adipose tissue inflammation and increased adipose tissue autophagy . . . 119
5.2.2 DSS-induced colitis is exacerbated in adipocyte autophagy-deficient mice . . . 128
5.2.3 Helicobacter hepaticus-driven inflammation is not influenced by the loss of adipocyte autophagy . . . 136
5.3 Discussion . . . 139
5.3.1 Adipose tissues respond to murine models of colitis and induce autophagy . . . 139
5.3.2 Adipocyte autophagy controls the inflammation in DSS but not *H. hepaticus*-induced colitis, and not under homeostatic conditions 141
5.4 Conclusion . . . 144

6 Adipocyte autophagy contributes to the anti-inflammatory response to DSS-induced colitis 145

6.1 Introduction . . . 145
6.1.1 Mesenteric adipose tissue in IBD pathologies and murine models of colitis . . . 145
6.1.2 Adipose tissue macrophages in health and disease . . . 147
6.1.3 Context and aim of this chapter . . . 148
6.2 Results . . . 148
6.2.1 Adipose tissue increases IL-10 expression upon DSS colitis in an adipocyte autophagy dependent manner . . . 148
6.2.2 Autophagy-deficient adipocytes differentially secrete free fatty acids 155
6.2.3 IL-10 production in macrophages is dependent on FFA availability 164
6.3 Discussion . . . 170
6.3.1 An anti-inflammatory role of adipose tissues during inflammation 170
6.3.2 Acute loss of adipocyte autophagy contributes to FFA generation without fundamentally altering adipocyte identity . . . 173
6.3.3 Controlling IL-10 production in macrophages by FFA restriction 176

6.4 Conclusion 179

7 General Discussion and Conclusion 180

7.1 Adipose tissues as a central hub for immunity 180

7.2 Adipose tissues – the Jekyll and Hyde of IBD? 182

7.3 Cell-extrinsic effects of autophagy 184

7.4 Adipocyte autophagy involvement for other pathologies 187

7.5 Thesis Summary and Outlook 189

A Appendix 1 246

Abbreviations

4EBP1	Eukaryotic translation factor 4E-binding protein-1
ADIPOQ	Adiponectin
ADP	Adenosine diphosphate
AKT	AKT serine/threonine kinase
ALA	α-linolenic acid
AMBRA1	BECN1 regulator 1
AML	Acute myeloid leukemia
AMP	Adenosine monophosphate
AMPK	Adenosine Monophosphate-activated Protein Kinase
Ap2	Adipocyte protein 2
APC	Antigen-presenting cell
ARG1	Arginase 1
ATDC	Adipose tissue dendritic cell
ATG	Autophagy-related
ATGL	Adipose triglyceride lipase
ATM	Adipose tissue macrophage
ATP	Adenosine triphosphate
BAC	Bacterial artificial chromosome
BafA1	Bafilomycin A1
BAT	Brown adipose tissue
BECN1	Beclin-1
BMA	Bone marrow adipocyte
BMAT	Bone marrow adipose tissue
BMDM	Bone marrow-derived macrophage
BNIP3	BCL2 Interacting Protein 3
BNIP3L	BCL2 Interacting Protein 3 Like
C/EBP	CCAAT/Enhancer Binding Protein
CBS	Cystathionine beta synthase

CD	Crohn's disease
CFU	Colony forming units
cLP	Colonic lamina propria
CLS	Crown-like structure
CMA	Chaperone-mediated autophagy
cMAT	Constitutive marrow adipose tissue
CREB	cAMP response element-binding protein
DHA	Docosahexaenoic acid
DIO	Diet-induced obesity
DPX	Di-n-butylphthalate
DSS	Dextran Sulphate Sodium
EPA	Eicosapentaenoic acid
FABP4	Fatty acid binding protein 4
FAME	Fatty acid methyl ester
FAO	Fatty acid oxidation
FBS	Fetal bovine serum
FDR	False discovery rate
FFA	Free Fatty Acids
FIP200	FAK family interacting-protein of 200 kDa
FMO	Fluorescence minus one
FOXO	Forkhead box protein O
FOXP3	Forkhead box P3
FUNDC1	FUN14 Domain Containing 1
G0S2	G0/G1 switch protein 2
GALT	Gut-associated lymphoid tissues
GMP	Granulocyte/monocyte progenitors
GWAS	Genome-wide association study
gWAT	Gonadal white adipose tissue
Hh	Helicobacter hepaticus
HSC	Hematopoietic stem cell

HSL	Hormone sensitive lipase
HSPA8	Heat shock protein family A member 8
IBD	Inflammatory bowel disease
IBMX	3-isobutyl-1-methylxanthine
IDL	Intermediate-density lipoprotein
IFN	Interferon
IL-10R	Interleukin-10 receptor
ILC	Innate lymphoid cell
iNKT	invariant NK-T cell
IRF5	Interferon regulatory factor 5
IRGM	Immune-related GTPase M
iWAT	Inguinal white adipose tissue
KO	Knock-Out
LA	Linoleic acid
LAL	Lysosomal acid lipase
LAM	Lipid-associated macrophages
LAMP2A	Lysosome-associated membrane glycoprotein 2A
LAP	LC3-associated phagocytosis
LDL	Low-density lipoprotein
LIR	LC3-interactin region
LPS	Lipopolysaccharide
LRRK2	Leucine-rich repeatkinase 2
MAAC	Mature adipocyte aggregate culture
MEP	Megakaryocyte–erythroid progenitors
MGL	Monacylglycerol lipase
MHC	Major histocompatibility complex
MMe	Metabolically-activated macrophage
MOI	Multiplicity of infection
MSC	Mesenchymal stem cell
MTOR	Mechanistic target of rapamycin

MTORC	Mechanistic target of rapamycin complex
mWAT	Mesenteric white adipose tissue
NK	Natural killer cell
NOD2	Nucleotide-binding oligomerization domain 2
OPTN	Optineurin 1
oWAT	Omental white adipose tissue
OXPHOS	Oxidative phosphorylation
PA	Palmitic acid
PCA	Principal component analysis
PCR	Polymerase chain reaction
PE	Phosphatidylethanolamine
PFA	Paraformaldehyde
PI3K	Phosphoinositide 3-kinase
PI3P	Phosphatidylinositide-3-phosphate
PKA	Protein kinase A
PKC	Protein kinase C
PLIN	Perilipin
PPAR	Peroxisome proliferator-activated receptor
RAPTOR	Regulatory Associated Protein Of MTOR Complex 1
RHEB	Ras homolog enriched in brain
RICTOR	RPTOR Independent Companion Of MTOR Complex 2
rMAT	Regulated marrow adipose tisse
RNAi	Interference RNA
ROS	Reactive oxygen species
rpWAT	Retroperitoneal white adipose tissue
S6K	Ribosomal protein S6 kinase beta-1
SASP	Senescence-associated secretory phenotype
SCF	Stem cell factor
scRNAseq	Single cell RNA sequencing
SEM	Standard error of the mean

SIRT1	Sirtuin 1
SQSTM1	Sequestosome 1
STAT3	Signal transducer and activator of transcription 3
SVF	Stromal vascular fraction
TAG	Triacylglycerides
TFEB	Transcription factor EB
TGF	Transforming growth factor
Th	T helper
TLC	Thin layer chromatography
TLR	Toll-like receptor
Tmem	T memory
TNF	Tumour necrosis factor
TNFR1	Tumour necrosis factor receptor 1
TRE3G	Tet-On 3G transactivator protein
Treg	T regulatory
TSC1/2	Tuberous sclerosis protein 1/2 complex
UC	Ulcerative colitis
UCP-1	Uncoupling protein-1
ULK1	Unc51-like autophagy activating kinase 1
visWAT	Visceral white adipose tissue
VLDL	Very low-density lipoprotein
VSP34	Phosphatidylinositol 3-kinase VPS34
WIPI	WD-repeat protein interacting with phosphoinositides

1 General Introduction

1.1 Autophagy

The discovery of lysosomes in 1955 by Christian de Duve marked the first milestone of a new research field focussing on a biological process involved in the degradation of cellular contents via the lysosome [1]. Eight years later, this process was first termed 'autophagy' (from the Greek word meaning 'self-devouring' or 'self-eating'). Despite this discovery, it took another three decades until seminal work from the laboratory of Yoshinori Ohsumi discovered key genes involved in the regulation and function of autophagy pathways in yeast [2]. At the time, 15 AuTophaGy-related (ATGs) genes capable of controlling the delivery of autophagic cargo to the lysosome were identified in yeast. Today, the yeast ATG protein family consists of 41 members, many of which are structurally conserved across mammals and plants. This discovery sparked the formation of an entire research field dedicated to defining the molecular machinery involved in the autophagy pathway and its function in health and disease. For his ground-breaking discoveries and as a representative for the entire field of autophagy research, Yoshinori Ohsumi was awarded the Nobel Prize in Physiology or Medicine in 2016. Nowadays, autophagy is defined as a conserved lysosomal degradation pathway which serves to maintain vital cellular functions during times of stress or fasting. While autophagy has been considered for a long time to be a nonselective process, studies over the past years have revealed that autophagy can selectively degrade unwanted or potentially harmful cellular components, including damaged mitochondria or protein aggregates. In this capacity, autophagy is crucial for controlling cellular health and survival. In addition, autophagy takes part in cell differentiation and development in a variety of mammalian cell types, which is central to human health [3, 4].

1.1.1 Types of autophagy

Autophagy can be separated into three distinct subtypes based on how the autophagosomal cargo enters in the degradative pathway. The three major subtypes include microautophagy, macroautophagy and chaperone-mediated autophagy (CMA) (summarized in

Fig.1). To facilitate discussion and nomenclature in the autophagy research field, two bona fide hallmarks that characterize classical or canonical autophagy have been established, that (I) the cargo needs to be of cytoplasmic origin and (II) lead to its degradation by the lysosome [5].

Microautophagy describes the process of selective or non-selective uptake of cytosolic content directly into lysosomes or late endosomes by membrane invagination. This process was first described in yeast for the degradation of peroxisomes [6]. Over the years, other organelles were similarly shown to be degraded through microautophagy including parts of the nucleus [7], damaged mitochondria [8] and lipid droplets [9, 10]. Intriguingly, some microautophagy processes require proteins involved in macroautophagy (e.g. ATG7, ATG8, ATG9) for cargo targeting and internalization [11]. The main function of microautophagy lies in the control of biosynthetic pathways, metabolic adaptation, regulation of organelle size and quality control of damaged proteins [12].

Macroautophagy is arguably the best-studied autophagy pathway and is characterized by the distinct formation of vesicular structures. These vesicles are named autophagosomes and consist of a double membrane vesicle containing cytosolic content which are subsequently targeted towards lysosomal fusion and degradation. Similar to microautophagy, the uptake of cytosolic cargo during macroautophagy can be either non-selective or selective. It degrades proteins as well as cellular organelles, which can be used to further discriminate different forms of autophagy depending on the autophagosomal cargo. For instance, the degradation of mitochondria has therefore been referred to as mitophagy [8], of lipid droplets as lipophagy [13] and of the endoplasmic reticulum as ERphagy [14]. Mechanistically, macroautophagy can generally be subdivided into three phases: (I) Initiation of autophagosome formation, (II) elongation and engulfment of cytoplasmic components by the growing autophagosome and (III) closure of the autophagosome and its fusion with the lysosome (Fig.2). At this latter step, the fused autophagosome is referred to as autolysosome and is effectively degrading the autophagosomal content through the action of lysosomal hydrolases. The generated macromolecules (e.g. amino acids, lipids) can subsequently be used for other energetic

or biosynthetic pathways. Since autophagy requires lysosomes for the degradation of cellular content, researchers use lysosomal inhibitors (e.g. Bafilomycin A1(BafA1)) to accumulate autolysosomes [15]. These structures are often identified by the autophagy marker protein Microtubule-associated proteins 1A/1B light chain 3B (hereafter referred to as LC3), which is typically degreaded in the autolysosome together with the cargo. Inhibition of lysosomes prevents this degradation and thus accumulates $LC3^+$ autolysosomes, allowing for a quantitative measure of autophagic flux [16]. While there is much insight regarding the core autophagy machinery and its regulation, several research questions remain open [17]. This includes the source of membranes during autophagosomal initiation [18, 19], the role of specific lipid sources in this process [20] and the necessity of distinct autophagosomal proteins such as ATG8 in the autophagic process [21].

CMA refers to the direct delivery of selective cargo to the lysosome by chaperone-mediated translocation of proteins across the lysosomal membrane [22]. Proteins targeted for CMA-mediated degradation contain a KFERQ-like motif which is recognized in the cytosol by the heat shock protein family A member 8 (HSPA8), the main CMA chaperone [23]. Roughly 30% of the cytosolic proteome contains KFERQ-like motifs and are therefore potentially targets for CMA. Beside the role of HSPA8 in CMA, this process requires the function of the lysosomal protein LAMP2A which binds to the cytosolic autophagic cargo and multimerized to form a translocation process and thus enabling cargo import into the lysosome [24]. The latter requirement of LAMP2A involvement is characteristic for CMA and distinguishes CMA from selective microautophagy which also uses HSPA8 for the uptake of KFERQ-containing proteins due to its ability to bind to phosphatidylserines on the outside of endosomes [25]. Unsurprisingly, CMA has been found to be a crucial pathway for many biological processes including protein turnover [26], antigen presentation [27], T cell function [28] and regulation of systemic metabolism [29].

However, in recent years this classic separation has become outdated due to discoveries of **non-canonical autophagy pathways**. During LC3-associated phagocytosis (LAP) LC3 is conjugated to a single membrane phagosome and subsequently targeted for lyso-

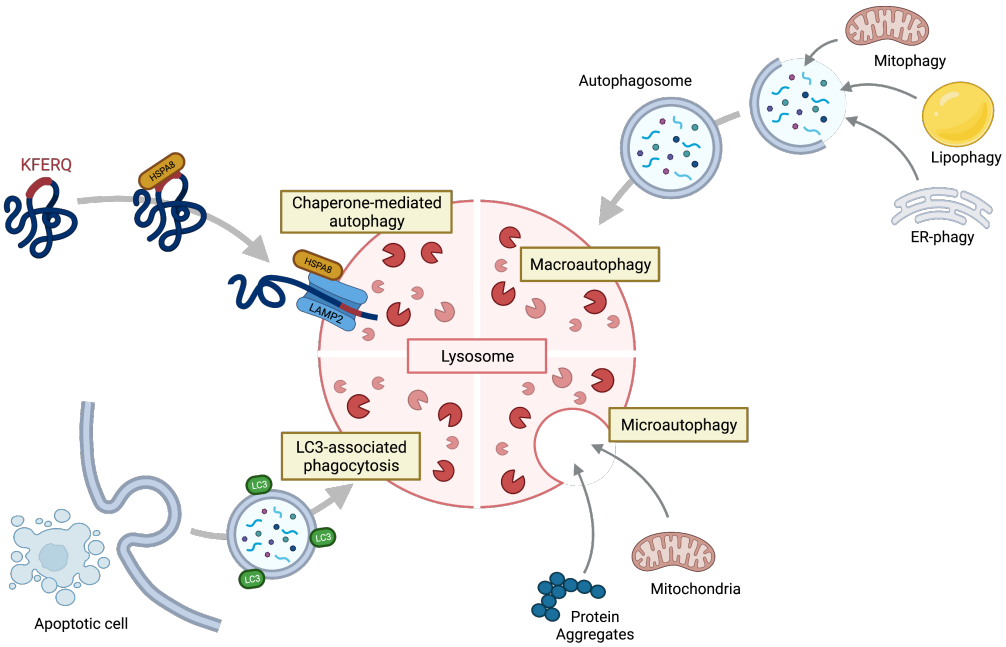

Figure 1: Types of autophagy. Autophagy is classically divided into three subtypes including micro-, macro- and chaperone-mediated autophagy (CMA). Microautophagy is based on the invagination of the lysosomal membrane and uptake of cargo both selectively and non-selectively directly into the lysosome. Macroautophagy is based on the formation of double membrane vesicles sequestering cytosolic cargo which is targeted for lysosomal degradation. Proteins containing a KFERQ-like motif are recognized by specific cytosolic chaperones (e.g. HSPA8) and brought to the lysosomal protein LAMP2A which translocates the protein across the lysosomal membrane. Lastly, LC3-associated phagocytosis, a non-classical autophagy pathway, is used for the degradation of extracellular cargo such as apoptotic cell debris. Phagosomes thereby get tagged by the autophagy marker LC3 and ultimately targeted to the lysosome for degradation.

somal degradation [30, 31]. This process involves some, but not all, components of the autophagic machinery [30]. Other ATG proteins have been implicated in controlling secretion of cellular content, a process called secretory autophagy. This pathway does not ultimately lead to lysosomal degradation of its cargo, but instead the secretion of extracellular proteins and the release of secretory granules [32, 33]. This includes the recently described release of exosomes into circulation [34, 35]. In addition, LC3-bearing exospheres have been found to contribute to the release of mitochondria from cardiac tissue [36]. However, the functions and contributions of several proteins of the autophagic machinery to non-canonical autophagy are still not completely understood. The emergence of functions of ATG proteins outside of classical autophagy pathways, however,

highlights the diversity of this process regulating several cellular processes. The next section will summarize the main molecular processes involved in macroautophagy at each phase of its life cycle.

1.1.2 Mechanism and receptors of autophagy

The term autophagic machinery describes a set of proteins critical for the formation, elongation and maturation of the autophagosome (Fig.2). Generally, proteins involved in these processes form four distinct complexes, each with a distinct role in the autophagy pathway. During the phagosome formation, an initiation complex is formed in response to the dephosphorylation of the unc51-like autophagy activating kinase 1 (ULK1 or ATG1 in yeast) [37, 38]. This signal is sufficient to trigger the recruitment of several proteins (including FAK family interacting-protein of 200 kDa (FIP200), ATG13 and ATG101) that in turn are capable of phosphorylating beclin-1 (BECN1 or ATG6 in yeast) and ATG9, promoting membrane elongation and phagosome formation [39, 40]. BECN1 is a core component of the class III phosphoinositide 3-kinase (PI3K) complex and interacts with ATG14L1, VSP34, autophagy and BECN1 regulator 1 (AMBRA1) and p115 [41, 42]. This second complex is crucial to increase the concentration of phosphatidylinositide-3-phosphate (PI3P) at the site of the nascent autophagosome, which is then capable of attracting proteins with a PI3P binding motif, such as members of the WD-repeat protein interacting with phosphoinositides (WIPI) protein family. WIPI2 has been demonstrated to interact with ATG16L1, a protein that takes part in one of two ubiquitin-like conjugation systems [43]. More precisely, ATG16L1 in complex with ATG5, ATG7, ATG10 and ATG12 form the so called ATG12 conjugation system. In contrast, ATG3, ATG4, ATG7 and ATG8 are components of the ATG8 conjugation system. The ATG12 complex is crucial for the covalent binding of ATG12 to ATG5, thereby forming an essential E3-ligase which takes part in the ATG8 conjugation system [44]. The function of this system is to transfer phosphatidylethanolamine (PE) moieties onto ATG8 homologues, such as LC3, and thus anchors it in the inner and outer membrane of the growing autophagosome [45]. This lipidation of LC3 from its cytosolic form (referred to as LC3-I) to its lipidated form (referred to as LC3-II) is

central to the autophagic process, and inhibition of this conversion effectively stops autophagic flux. Over the course of several maturation steps, the autophagosome closes and is then transported to the lysosome in a RAB7-dependent manner [46]. Once the autophagosome has fused with the lysosome, the autophagic cargo is degraded by lysosomal acid hydrolases into its rudimental components, which in turn can be recycled by the cells during starvation or cellular stress. Of note, in recent years, a small number of reports have demonstrated that autophagy can occur independent of some of the classical autophagy core components (e.g. ATG5), suggesting alternative autophagy pathways, which still remain to be fully characterized [47].

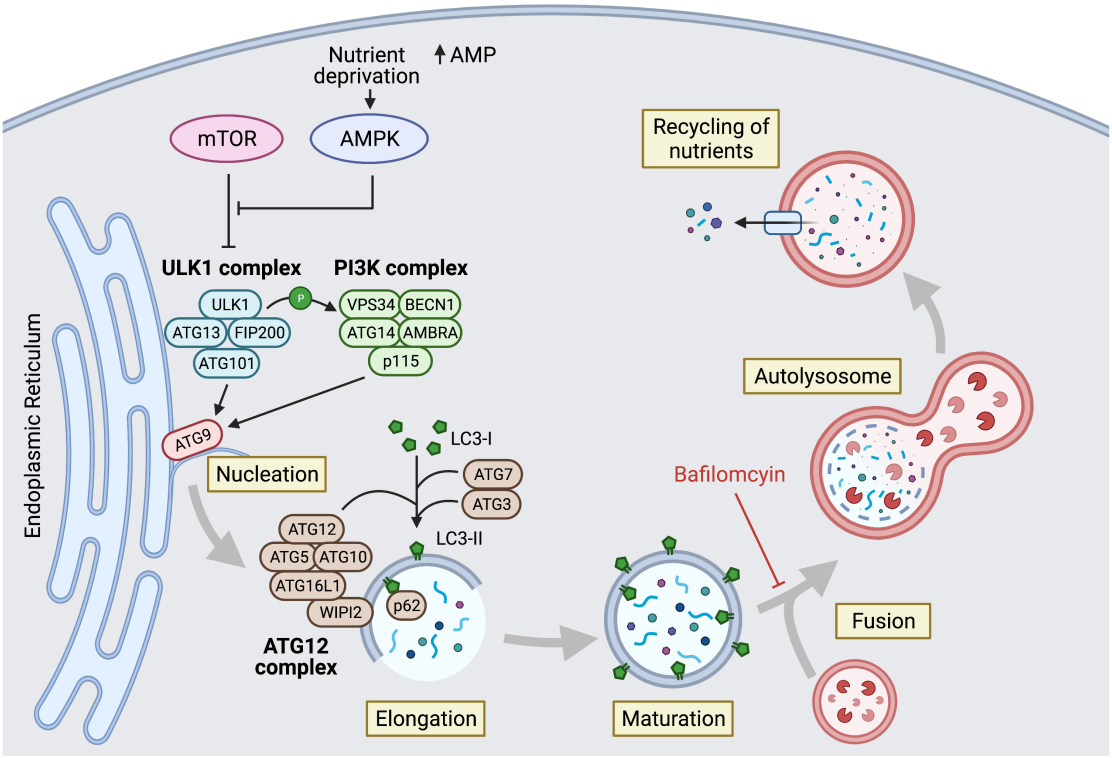

Figure 2: Core autophagy pathway. Nutrient deprivation and subsequent low AMP levels inhibit mTOR leading to the activation of ULK1 complex. This leads to the phosphorylation of BECN1 and the formation of PI3K complex. These complexes associate with the ER transmembrane protein ATG9 and start the formation of the autophagosome. WIPI2 associates to the growing autophagosome and recruits ATG16L1 which is covalently bound to ATG5 via the activity of ATG7 and ATG10, which forms the E3-ligase ATG12 complex. Next, cytosolic LC3-I is lipidated by addition of PE to LC3-II through the E1-ligase ATG7, the E2-ligase ATG3 and the ATG12 complex. Using the membrane bound LC3-II, certain autophagy receptors (e.g. p62) can bind to LC3 and target specific organelles and proteins for degradation (e.g. through ubiquitinylating). The lysosomal degradation of the matured autophagsome can be inhibited using the V-ATPase inhibitor Bafilomycin A1. After fusion with the lysosome, autophagic cargo is degraded by lysosomal hydrolases and nutrients can be recovered.

Originally, it was assumed that autophagy is a non-selective process, but recent discoveries of receptors for autophagic cargo have shifted the view on the specificity and selectivity of autophagy. Although basal autophagy may be continuously active and maintains basic cell homeostasis, the notion of selective degradation of cellular components in times of high cellular stress has become increasing popular. To this end, the identification of a series of proteins capable of interacting with ATG8 homologues (including LC3) has sparked the interest of the research community, and may even suggest that many more cellular components than those known today are putative targets for autophagosomal degradation. The mammalian genome encodes for seven ATG8 protein family members: MAP1LC3A, MAP1LC3B/B2, MAP1LC3C, GABARAP, GABARAPL1, and GABARAPL2 (GATE-16). This evolutionary diversification of ATG8 may indicate in mammalian systems the existence of distinct autophagosomes which regulate their cellular cargo through expression and incorporation of specific ATG8 homologues. The targeting of specific cellular components into autophagosomes requires adaptor proteins or autophagy receptors which contain an LC3-interacting region (LIR) motif [48]. This short four amino acid sequence, consisting of a leucine, isoleucine or valine at the first position and a hydrophobic residue in the last position, anchors the LIR-containing protein and its binding partners into the phagophore membrane. The best characterized autophagy receptor is p62 also known as sequestosome-1 (SQSTM1), which binds to ubiquitinylated protein aggregates in the cytoplasm via its ubiquitin-binding domain, and targets it for lysosomal degradation through LIR-dependent binding of LC3 [49, 50]. In addition to p62, several more autophagy receptors have been identified and can degrade a variety of cargo. For instance, optineurin (OPTN) has been shown to promote targeting of intracellular bacteria [51], protein aggregates [52] and mitochondria [53]. While a multitude of autophagy receptors have been described for macroautophagy pathways (reviewed extensively by [54]), the receptor targeting lipid droplets for degradation via lipophagy remains unknown. The interaction of autophagy receptors and LC3 is often regulated by phosphorylation at the N-terminus of the LIR domain as described for the mitophagy receptors BNIP3L [55], BNIP3 [56] and FUNDC1 [57]. While our understanding of autophagy receptors has significantly increased over the past decade,

it remains to be seen how many receptors for known autophagosomal substrates can be identified with future technological advances (e.g. by peroxidase APEX2-tagged variants of ATG8 proteins and known autophagy receptors [58, 59, 60]).

1.1.3 Regulation of autophagy

The autophagy pathway is regulated on both the transcriptional and post-transcriptional level. On a transcriptional level, the FoxO family of forkhead transcription factor family (FOXO) [61] and transcription factor EB (TFEB) [62, 63], among others, are well known to control autophagy gene expression. Despite their essential role in autophagy gene expression, changes in autophagy status does not always correlate with transcriptional changes [16]. In fact, the dominant factors controlling autophagic flux are the mechanistic target of rapamycin (MTOR) and AMP-activated protein kinase (AMPK) signalling pathways, which are controlled post-transcriptionally. Both proteins are sensitive to the energy and nutrient status in cells, but they can also integrate signals from cytokines and growth factors (e.g. insulin signalling). Regulation of mTOR signalling has been extensively reviewed elsewhere [64] and summarized in Fig.3 .

In brief, the **mTOR pathway** can generally be distinguished into two distinct branches, with each pathway's core complex at the centre: mTOR complex (MTORC) 1 and 2. Intracellular amino acid levels (in particular of arginine and leucine) as well as growth factor receptor signalling control mTORC1 activation and its location to the lysosome, where it associates with Rag proteins on the lysosomal membrane [65]. While amino acids activate mTORC1 via binding to SESTRIN and CASTOR, insulin signalling requires AKT-dependent phosphorylation of heterodimeric tuberous sclerosis 1/2 complex (TSC1/2). TSC1/2 can in turn activate the Ras homologue enriched in brain (RHEB) GTPase, which is also located at the lysosomal membrane and is an important activator of mTORC1 activity. This activation promotes phosphorylation of downstream targets including translational regulators S6 kinase (S6K) and eukaryotic translation factor 4E-binding protein-1 (4EBP1), resulting in an increased rate of translation and protein biosynthesis. In contrast, inhibition of mTORC1 activity by rapamycin treatment induces autophagy, thus mTORC1 activity represses autophagy. mTORC1 inhibits the au-

tophagy initiation complex by phosphorylating ULK1 [66, 67]. More recently, mTORC1 has also been shown to interact with TFEB on the lysosomal surface and, consequently, prevent its translocation into the nucleus to drive the gene expression of ATG genes [68]. While mTORC1 has been well-described over the years, mTORC2 remains somewhat more elusive. mTORC2 is known to phosphorylate AKT serine/threonine kinase (AKT), thus connecting mTORC1 and mTORC2, however, this process is not necessary for mTORC1 signalling. The activation of mTORC2 seems to regulate the organization of the actin cytoskeleton [69], ion transport [70] and pro-survival functions via activation of AKT-FOXO pathways [71], which is particularly important for controlling lipid catabolism in brown adipocytes. Deletion of the mTORC2 core component RICTOR increases thermogenesis and prevents diet-induced obesity (DIO), thus implicating mTORC2 signalling in lipid metabolism [72]. While direct links connect mTORC1 to autophagy repression, the relationship of mTORC2 and autophagy may be more complex. The mTORC2-AKT-dependent phospho-inhibition of FOXO3 protects mice from fasting-induced muscle atrophy by inhibiting autophagy [73]. However, at the same time mTORC2-dependent activation of protein kinase C (PKC) has been shown to increase actin cytoskeletal activity at the plasma membrane and thus promote the formation of autophagosome precursors [74]. Overall, mTOR signalling has a central role in the regulation of metabolic pathways and autophagy, often leading to opposing behaviours between the two pathways [75].

AMPK is a kinase consisting of three subunits (α, β and γ) and it takes part in the regulation of cellular energy homeostasis, thereby controlling glucose and lipid uptake, as well as, mitochondrial respiration and fatty acid oxidation (FAO). At times of low cellular energy levels, AMPK is activated through binding of intracellular AMP and adenosine diphosphate (ADP) to cystathionine beta synthase (CBS) domains in the γ subunit [76]. While the activation of AMPK promotes catabolic pathways and downregulates anabolic pathways, its effects on mTORC1 are of particular importance with regards to autophagy activation. AMPK phosphorylates RAPTOR, a core component of the mTORC1 complex, thus inhibiting it from complexing with its other components [77]. In addition, AMPK activates ULK1 through phosphorylation at two sites (S317

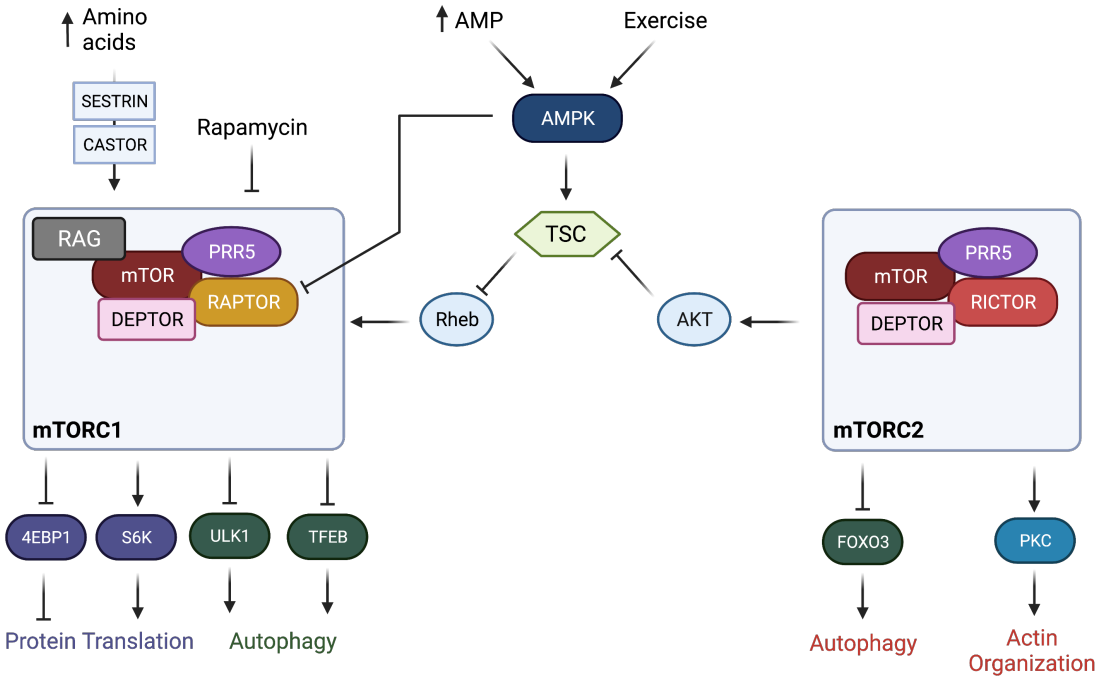

Figure 3: AMPK and mTOR regulatory pathways. AMPK and mTOR signalling pathways can regulate cellular autophagy levels. mTOCR1 is activated by high intracellular levels of amino acids (e.g. leucine), which then associates to Rag proteins located at the lysosomal membrane. This promotes biosynthetic processes such as protein translation through phosphorylation of S6K and 4EBP1, whilst inhibiting catabolic processes including autophagy. In contrast, activation of AMPK by high intracellular AMP levels or exercise leads to the activation of TSC, which in turn inhibits the mTOR activator Rheb resulting in the inhibition of mTORC1 signalling and, thus, activation of autophagy. In parallel,the activation of mTORC2 promotes mTORC1 signalling via AKT-dependent TSC inhibition. mTORC2 can inhibit autophagy by phospho-inhibition of the transcription factor FOXO3.

and S777), thus promoting autophagy [66]. Conversely to the deletion of RICTOR, adipocyte-specific deletion of AMPK subunits results in an impaired cold response and increased susceptibility to DIO, thus highlighting the opposing effects of mTOR and AMPK signalling [78]. The balance of AMPK and mTOR signalling is central for the regulation of autophagy in various cell types, including immune cells and non-immune cells such as adipocytes [75, 79, 80, 81](75, 79-81).

1.1.4 Autophagy in the immune system

The cell-intrinsic effects of autophagy in immune cells for their maintenance, differentiation and function have been well-characterized over the past 20 years [82]. Here is a summary of the work done in the Simon lab, however, many other studies contributed to this field. While there is indisputable evidence for the central role of this pathway

in regulating a balanced immune response, its precise contribution to different cellular pathways remains less well understood. Three dominant themes have emerged over the years in which autophagy can contribute to (I) differentiation, (II) maintenance of long-lived immune cells and (III) prevention of cellular aging. Metabolic control by autophagy can be closely linked to all of these themes.

Due to its ability to degrade entire organelles, autophagy is crucial for **cell differentiation** by regulating cellular organelle homeostasis and metabolism. During erythropoiesis, the maturation of reticulocytes into erythrocytes requires mitophagy. Lack of autophagy will prevent erythrocyte differentiation and cause anaemia [83, 84]. Moreover, immune cell subsets which rely on oxidative phosphorylation (OXPHOS) as their main energy-providing pathway, require autophagy to control mitochondrial health. During OXPHOS, reactive oxygen species (ROS) are produced which can damage the mitochondria. T cells which are cell-intrinsically deprived of autophagy, subsequently loose the capacity to remove damaged mitochondria, rendering the cells increasingly glycolytic, prompting an inflammatory or even apoptotic phenotype [85, 86]. Similarly, the inhibition of autophagy in human liver-derived $CD8^+$ lymphocytes decreases mitochondrial health and preserves tissue resident features [87]. Beside the metabolic control of OXPHOS in the mitochondria, autophagy also regulates cellular lipid metabolism in several immune cell types [88, 89, 90]. In an atherosclerotic setting, lipid loaded macrophages, called foam cells, require autophagy for the breakdown of cholesterol species and subsequent reverse cholesterol export, and may enhance atherosclerotic lipid accumulation [90]. In contrast, the degradation of lipid droplets during the differentiation of neutrophil precursors is essential for the generation of adenosine triphosphate (ATP). In a CCAAT/Enhancer Binding Protein (C/EBP)α-driven genetic mouse model, the cell-intrinsic loss of autophagy in neutrophil precursors blocks their differentiation and consequently impairs their potential to clear bacterial infections [88]. Interestingly, the C/EBPα-driven system has significant off-target effects in both hepatocytes and adipocytes. The use of bone marrow transplantation models demonstrates the cell-intrinsic nature of this mechanism. However, strikingly the effect on neutrophil differentiation blockage is more pronounced in $C/EBP\alpha$ x $Atg7^{f/f}$ mice, compared to the

transplanted mice (unpublished data from our lab) [91]. This may indicate a role of cell-extrinsic effects of autophagy loss in hepatocytes and adipocytes on neutrophil differentiation, possibly through alterations in exogenous lipid provision by adipocytes. Lastly, loss of autophagy in $CD4^+$ cells shifts the balance of T helper (Th) 2 and T regulatory (Treg) cell towards Tregs in the intestine, leading to spontaneous intestinal inflammation [92]. Furthermore, deletion of Atg16l1 specifically in Tregs, switches their cellular metabolism from FAO to glycolysis in the intestine, but not in the spleen [92]. However, the precise reason for this metabolic shift remains unknown. In line with these findings, colonic Tregs are expanded and IL-10 production is increased in response to spermidine, a microbial-derived polyamine and known autophagy inducer [93].

Some immune cells, such as memory cells, persist in the bone marrow and other tissues and remain quiescent until re-infection. During this time, **autophagy is essential for these long-lived cells to maintain cell homeostasis and self-renewal**. Loss of autophagy in T memory (Tmem) or B memory cells results in their loss and decreased protection from re-infection [63, 85]. In addition, fetal liver-derived, innate-like B1 cells also rely on autophagy for their self-renewal, by maintaining FAO and mitochondrial health [89]. This concept also holds true for hematopoietic stem cells (HSC), which divide only once every 40 weeks, and need to self-renew constantly [94]. Loss of autophagy in HSCs leads to a massive expansion of hematopoietic progenitor populations, severe myeloproliferation and lethal HSC exhaustion [95].

The **regulation of cellular aging** is the third theme by which autophagy regulates immune cells. Autophagy levels decrease in several immune and stromal cells with age. Falling levels of autophagy with age have been observed in both murine and human B cells and have been linked to reduced circulating levels of spermidine [63, 96]. The decrease in autophagic flux is mechanistically linked to an increase in several hallmarks of aging [97], including a senescence-associated secretory phenotype (SASP). Spermidine supplementation has been shown to improve function of B cells by promoting eIF5A-dependent, post-transcriptional hypusination of TFEB [96]. Interestingly, the loss of autophagy in macrophages reduces pathogenic killing capacities, while leading to a low-

grade pro-inflammatory shift reminiscent of aged macrophages and SASP [98].

While much is known about the cell-intrinsic effects of autophagy in immune cells, it remains unclear whether the loss of autophagy in other cell types can impact on immune cell function. Immune cells are either resident in complex environments or circulate and move between different organs. In either case, immune cells are likely to encounter different metabolic and nutritional milieus when travelling through the organism. Today, an increasing number of studies started to investigate how the specific tissue environment shapes cellular metabolism and alters immune cell functions [99, 100]. Adipose tissues present a particularly complex tissue environment, due to their lipid-rich and metabolic nature.

1.2 Adipocytes and adipose tissues

1.2.1 Introduction to the role and function of adipocytes

Traditionally, adipocytes are seen as highly specialized cells, responsible for the storage of energy in the form of lipids. While adipocytes long remained understudied, due to the presumption of their sole role in lipid storage, research over the past few decades has highlighted a significant diversity of adipose tissues with distinct origins, locations and functions [101, 102]. Adipocytes are roughly divided based on their histological characteristic into three subtypes: (I) white adipocytes, which account for more than 95% of adipose mass, have a marked unilocular lipid droplets taking up most of the cytoplasm, (II) brown adipocytes, which represent 1-2% of adipose mass and contain multilocular lipid droplets, and (III) beige adipocytes, which are typically found in white adipose tissues upon cold exposure and have similar characteristics as brown adipocytes. White adipocytes serve as nutrient storage and control systemic energy balance and metabolism [102]. In contrast, brown and beige adipocytes are rich in mitochondria which catabolize lipids through uncoupled mitochondrial respiration, thus releasing energy in the form of heat. In this process the action of uncoupling protein-1 (UCP-1), which is markedly increased in brown and beige adipocytes, is essential, possibly by acting as a long-chain fatty acid/H+ symporter [103]. Humans usually loose brown adipose tissue mass during

childhood and adolescence, however, chronic exposure to cold conditions or sustained catecholaminergic exposure can maintain brown fat tissues [104, 105]. Interestingly, autophagy is important in the beige into white adipose tissue transformation, since loss of *Atg5* or *Atg12* prevents mitochondrial clearance and preserves the beige adipocyte phenotype after cold exposure [106]. In line with this, the deletion of *Tfeb* from brown adipocytes preserves mitochondrial mass in brown adipocytes [107]. Due to their high metabolic activity and potential to 'burn' fatty acids, brown and beige adipose tissues have become a main therapeutic avenue to combat increasing population adiposity and obesity [108]. In this context, adipocyte autophagy may present an exciting drug target to maintain brown/beige adipose tissues [109].

White adipose tissue can be further subdivided based on their location into subcutaneous and visceral adipose tissue depots. The latter has been associated with metabolic disease, while subcutaneous fat may even lower the risk for particular diseases [110]. Yet, this classification may be an oversimplification, especially since visceral adipose tissues can be further divided based on their location and association with particular organs into gonadal, omental, mesenteric and retroperitoneal white adipose tissue depots, among others. Although the conservation (in terms of size and position) of these adipose tissues across mammalian species is not very well conserved, much can be learned about adipose tissue physiology by studying rodent models. Nowadays, it is believed that visceral adipose tissue depots may have distinct origins which determine cytokine secretion and lipid turnover [111]. Interestingly, adipocyte precursors, so called preadipocytes, have depot-specific gene signatures which they maintain ex vivo, suggesting a cell-intrinsic program which predefines adipocytes in each depot [112]. The development of white adipose tissues requires the activation of a series of transcription factors, such as the peroxisome proliferator-activated receptor (PPAR)γ, and C/EBPα [113, 114]. Both transcription factors are essential for normal adipocyte differentiation (also referred to as adipogenesis) [115]. Interestingly, autophagy takes part in the adipogenic process, since deletion of *Atg5* or *Atg7* in preadipocytes leads to lipodystrophy in rodents [116, 117]. Although the precise mechanism for this remains unknown, it has been reported that autophagy may increase PPARγ stability and promote adipogenesis

[116, 118]. While the necessity for autophagy during adipogenesis is clear, the mode by which autophagy affects the function of mature adipocytes remains largely unexplored.

The role of adipose tissues as endocrine organ started to emerge in the mid 1990's, when both leptin and tumour necrosis factor (TNF)α were found to be secreted from adipose tissues, to regulate systemic metabolism and obesity [119, 120]. Since these initial discoveries, the list of factors secreted from adipose tissues has gradually increased to encompass a multitude of cytokines, hormones, glucocorticoids, steroids, and coagulation and completement factors. A notable addition to this list was the complement-related protein adiponectin (ADIPOQ), which is exclusively produced by mature adipocytes and has been shown to correlate with reduced risk of obesity, diabetes and cardiovascular disease [121]. While the endocrine function of adipocytes allows cross-communication with several other tissues, at its heart its evolutionary purpose is likely to be seeded in lipid handling and prevention of lipotoxicity.

1.2.2 Regulation and control of lipolysis

The major function of white adipocytes remains the control of lipid storage and release during times of nutrient access and starvation, respectively. When systemic energy demands exceed energy generation from dietary source, adipocytes hydrolyse stored triacylglycerides (TAG) to generate and secrete free fatty acids (FFA), a process called lipolysis. Lipolysis is typically induced by stimulation of β-adrenergic receptor signalling. However, other inducers, including inflammatory cytokines such as TNFα, promote FFA release from adipocytes [122, 123]. The hydrolyzation of stored TAGs requires a series of events that regulate proteins on the lipid droplet surface, as well as, three major cytosolic enzymes and their cofactors. In particular, the enzymes adipose triglyceride lipase (ATGL), hormone sensitive lipase (HSL) and monacylglycerol lipase (MGL) mediate TAG hydrolyzation to diacylglycerol, to monoacylglycerol, and to glycerol, respectively. At each step, each lipase liberates one FFA moiety, however ATGL seems to be the rate limiting step crucial for lipolysis. In addition to the cytosolic degradation of TAGs, which usually occurs at pH $\sim$7 (often referred to as 'neutral' lipolysis), TAGs are degraded in the lysosome by the action of the lysosomal acid lipase (LAL) in a process referred to as

'acid' lipolysis. Genetic loss of *Lal* results in a marked lipid dysbalance, hepatomegaly and shorter life span in mice highlighting its central role in lipid metabolism [124].

Lipolysis is regulated on several levels, both transcriptionally as well as post-transcriptionally. On a transcriptional level, *Atgl* gene expression is controlled by FOXO1, PPARγ and the PPARγ co-activator 1α (PGC1α). In a similar fashion, *Hsl* transcription is regulated by PPARγ/PGC1α. Strikingly, the autophagy master transcription factor TFEB can control expression of *Ppar* and *Pgc1α* in muscle and liver, and thus indirectly impact lipolysis [125]. The same study found that TFEB also drives *Lal* gene expression, in line with its role in lipophagy [125]. In addition, FOXO1 activation by Sirtuin 1 (SIRT1)-dependent deacetylation promotes *Lal* expression [126].

Post-transcriptional regulation of neutral lipolysis often occurs on the surface of lipid droplets. The lipid droplet consists of a cholesterol and TAG-rich lipid core, surrounded by a shell of more than 100 lipid droplet associated proteins [127]. In particular, two proteins can interact with the enzymatic domain of ATGL, and thus control its activity. Interaction of the lipid droplet binding protein CGI58 activates ATGL, while binding of G0/G1 switch protein 2 (G0S2) inactivates ATGL [128, 129]. In addition, the lipid droplet coating protein perilipin (PLIN)-1 sequesters CGI-58 under basal conditions preventing its interaction with ATGL [130]. Upon lipolysis induction, protein kinase A (PKA) phosphorylates several lipolysis proteins including PLIN1, CGI-58 and HSL. The phosphorylation of PLIN1 releases CGI-58 and consequently initiates the lipolytic process. At the same time, PKA-mediated phosphorylation of HSL promotes its recruitment to the lipid droplet where it binds to PLIN1 [131]. HSL contains five distinct serine residues which are differentially phosphorylated and can either activate or inhibit HSL activity [132].

While these phosphorylation events are well described for stimulation via β-adrenergic signalling, the activation of molecular pathways after TNFα stimulation are less well defined. Although it is clear that activation via the tumour necrosis factor receptor 1 (TNFR1) is required and sufficient to promote TNFα-induced lipolysis [133, 134], the precise signalling pathways downstream (JNK, ERK1/2, AMPK, PKA and IKK) remain

less understood. Since the effects of TNFα on lipolysis are not immediate, it appears that TNFα-induced lipolysis is regulated on a transcriptional level [123, 135, 136]. However, the precise regulation of TNFα-induced lipolysis on a post-transcriptional level remains incompletely understood.

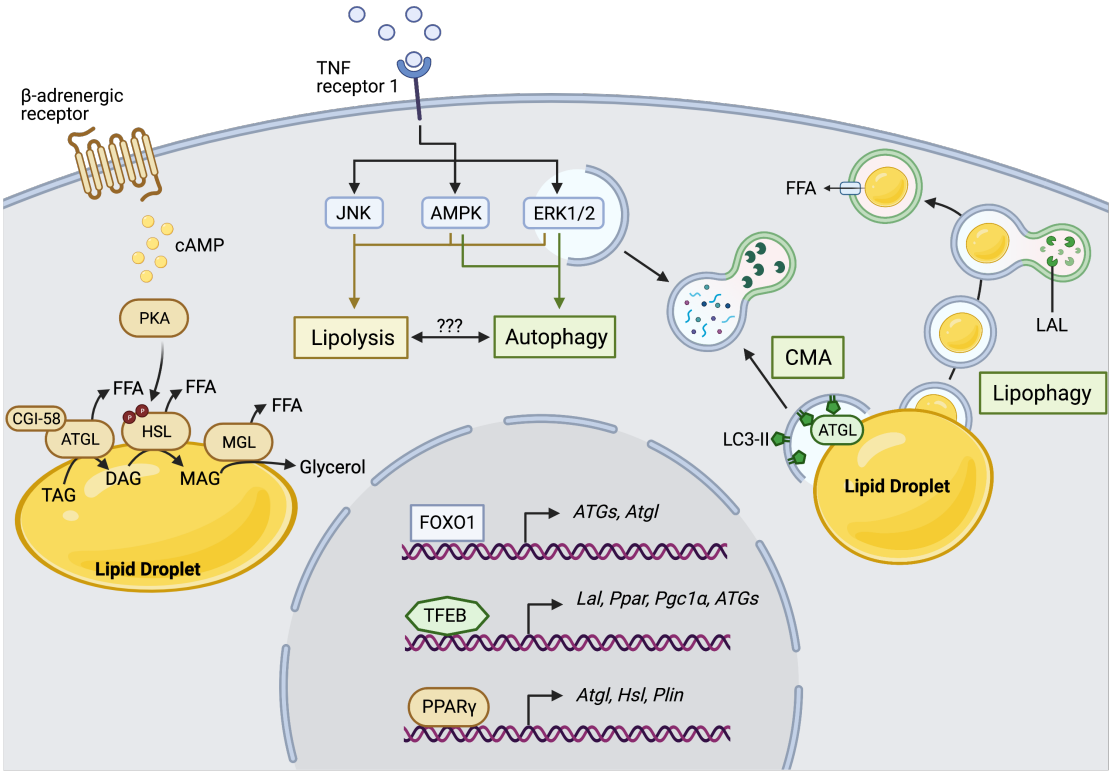

Figure 4: Relationship between autophagy and lipolysis. Lipolysis is classically driven through the degradation of TAGs to glycerol and FFAs via the activity of cytosolic lipases ATGL, HSL and MGL. Lipolysis enzyme ATGL is regulated through co-activator CGI-58, whereas HSL is specifically phosphorylated by HSL to induce lipolysis. Lipolysis is also induced during TNF signalling via stimulation of cytosolic kinases. In addition, AMPK can regulate autophagy by inactivation of mTOR signalling pathways. ERK1/2 can be selectively degraded via autophagy thus downregulating lipolytic pathways. The direct degradation of lipid droplets via the autophagic machinery is referred to as lipophagy. In addition, autophagy can regulate proteins involved in lipolysis pathways such as ATGL. Lastly, autophagic and lipolytic pathways share common transcriptional regulation via TFEB, FOXO1 and PPAR activity.

As expected, nutrient providing pathways, such as lipolysis and autophagy share common transcriptional pathways (e.g. FOXO and TFEB), thus linking them on a molecular level. In addition, autophagy and lipolysis share common metabolic regulators such as mTOR, AMPK and ERK [137]. Intriguingly, both ERK and ATGL can directly interact with LC3-II [138, 139]. ATGL contains a LIR domain which is essential for ATGL recruitment to the lipid droplet and may target ATGL for autophagic degradation [139].

In addition, CGI-58 controls BECN1 cleavage by caspase 3 which further connects autophagy and lipolysis on a post-transcriptional level [140]. Taken together, research in recent years has demonstrated a tight-knit relationship between autophagy and lipolysis in adipocytes and other cell types (Fig.4), however how these processes communicate and influence (patho)physiological behaviour in mammals, under homeostasis or disease, remains unanswered. In particular, the effects of alterations of lipolytic or autophagic processes on other cell types in adipose tissues has not yet been investigated.

1.2.3 Immune cells in the adipose tissue

Curiously, only 20-40% of the cells in adipose tissues are adipocytes, despite them accounting for more than 90% by volume. During obesity, more than half of this non-adipocyte fraction consists of immune cells, making the adipose tissue an immunological tissue [121]. In this context, immune cells present the main cellular source of TNFα secreted from adipose tissues, although adipocytes themselves can produce TNFα as well [119, 141]. In lean conditions, adipose tissues are enriched in macrophages which express high levels of the tissue resident marker CD206 and maintain tissue homeostasis via expression of anti-inflammatory IL-10. Macrophage-specific loss of the PPARγ impairs anti-inflammatory macrophage polarization in vivo and promotes development of DIO, insulin resistance and glucose intolerance [142]. Obesity leads to a significant influx of inflammatory macrophages expressing the surface marker CD11c and producing TNFα and IL-6. This takeover of inflammatory macrophages can eventually lead to insulin resistance [143].

Tregs are enriched in adipose tissues and they can control tissue homeostasis, in part via macrophages. Treg accumulation in visceral adipose tissues is increased in male compared to female mice, which is regulated via androgen-regulated IL-33 expression from GP38$^+$ adipose stromal cells [144]. Expression of IL-33 is an important stromal cue for the maintenance of adipose tissue Tregs which recognized via their receptor ST2 [145]. In addition, adipose tissue Treg express high levels of PPARγ, particularly in tissues from male animals, and PPARγ is required for Treg accumulation in the tissue [144, 146]. However, during obesity these cells are gradually lost [147]. Other T cell

subsets such as Th2 cells are typically found in adipose tissues under homeostasis and they are associated with reduced metabolic dysfunction and inflammation [148]. During obesity, the number of Th2 cells is reduced, whereas $CD8^+$ T cells increase. This increase in $CD8^+$ T cells precedes the macrophage infiltration and is required for macrophage recruitment [149]. In lean animals, adipose tissues are enriched in Tmem, and promote their function [150]. However, obesity induction subverts the endogenous function of adipocytes and negatively impacts recall responses [151]. Increasing evidence suggests other T cell subsets such as $\gamma\delta$ T cells, which are also enriched in adipose tissues, regulate adipose tissue physiology. In the case of adipose tissue $\gamma\delta$ T cells, they are crucial for regulating expansion of Tregs and controling thermogenesis via production of IL-17A, which stimulates IL-33 expression in stromal subsets [152]. These complex cross-talks between immune cells, stromal cells and adipocytes are common in adipose tissues, and control the systemic metabolic regulation.

While other cells of the innate and adaptive immune system can be found in the adipose tissues, including B cells, natural killer (NK) cells, innate lymphoid cells (ILCs), eosinophils, neutrophils and invariant NK-T cells, their presence and function is highly dependent on the metabolic challenges in situ. Overall, obesity promotes a shift towards type I (pro-inflammatory) immune cells, whereas homeostasis and thermogenesis drive the expansion of immune cell populations involved in type II immunity [153, 154]. The advent of single cell technologies enables studying adipose tissue immune cell populations in greater detail and slowly uncovers both tissue- and disease-specific immune cell adaptations [155]. In general, the research efforts in the past years have increasingly provided a better insight into the immunology of adipose tissues and underline the importance of immune cells in tissue homeostasis and inflammation. However, despite the great depth of immune cell phenotyping, the field is still just beginning to understand the mechanistic cues that drive immune-metabolic crosstalk under different situations.

1.3 Metabolic crosstalk between immune cells and stroma

Immune cells exert their function in distinct tissue environments which differ significantly in the availability of oxygen, micronutrients (such as vitamins and iron), amino

acids and fatty acids. Stromal cells, here defined as non-immune cells, in the tissue environment compete for the same nutrients, thereby taking part in the regulation and control of local metabolite availability. In some cases, stromal cells can also alter immune cell behaviour through the provision of sources of energy such as amino acids and fatty acids. This complex local metabolic interaction between immune cells and stromal cells was recently referred to as 'local metabolism' [156]. Much of this crosstalk was originally discovered in cancer cell interactions with their microenvironment, however this concept appears to be equally applicable to immune regulation. This includes several autophagy-dependent processes.

1.3.1 Amino acid crosstalk

Amino acids are essential for cell metabolism and function. In particular, the tumour environment can restrict the availability of specific amino acids, and thereby suppress anti-tumoral immune responses. For instance, myeloid suppressor cells in the tumour microenvironment metabolize large amounts of arginine and subsequently render T cells anergic in the tumour microenvironment [157, 158]. In addition, autophagy in hepatocytes controls the secretion of the arginine-degrading enzyme arginase 1 (ARG1). Once autophagy is lost, either in all cells or specifically in hepatocytes, ARG1 levels in the circulation increase and deplete systemic arginine. This decrease in systemic arginine levels subsequently reduces the growth of several murine cancers, however, it is independent of the T cell mediated anti-tumour response [159]. The effect of autophagy on cancer progression, however, may depend on the tumour mutational burden. A second study, using cancer models with high mutational burden implicate hepatocyte autophagy in the generation of a tumour immune tolerant environment by enhancing Treg function and suppressing interferon (IFN)γ production [160]. Although the crosstalk between hepatocytes and tissue resident immune cells has not ultimately been resolved, a metabolic component appears likely. The concept of autophagy-dependent amino acid provision has also been studied in the context of pancreatic cancer. In this case, pancreatic cancer cells induce autophagy in stellate cells to promote the secretion and provision of alanine to the tumour [161]. This metabolic support seems to be evolutionarily conserved, since

even in Drosophila non-autonomous autophagy, induced by the cancer cells, was shown to promote cancer growth via amino acid provision [162]. Overall, these landmark studies have established the idea that autophagy can provide amino acids to local cancer cells and may even be able to control local immune responses, however, more work is needed to show this in a tumour-free context.

1.3.2 Free fatty acid crosstalk

While activated and pro-inflammatory immune cells typically use glycolysis to meet their metabolic demands, quiescent and anti-inflammatory immune cell types, such as anti-inflammatory macrophages, Tmem and Tregs, rely more strongly on FAO [163]. It is therefore unsurprising that the lipid-rich environment of adipose tissues predominantly attracts FAO-driven immune cell subsets [156]. Interestingly, the uptake of FFA from the environment is crucial to the function of several immune cells. Indeed, adipose tissue ILC2 require exogenous FFA uptake for energy generation and effective protection against helminth infection [164]. Interestingly, the study also showed that uptake of FFA was increased in the mesentery compared to other barrier sites like the gut, suggesting a tissue-dependent adaptation to local FFA availability. In line with this, adipose tissue Tmem significantly increase FFA uptake and activation potential during reinfection challenges [150]. This is in line with the requirement for exogenous FFA uptake in $CD8^+$ tissue-resident Tmem for their long-term survival [165]. Although adipocytes are a likely source of FFA, it remains unclear whether adipocytes can indeed alter immune cell behaviour through FFA provision. In contrast, the functional impact of adipocyte-derived FFA on cancer growth has been well established. For instance, lipolysis-induced FFA secretion from human omental adipocytes can drive β-oxidation in ovarian metastatic cancer cells, thus underlining the close metabolic interaction between cancer cells and their tumour environment [166]. Similar lipid transfer has been observed in the case of acute myeloid leukemia (AML) in the bone marrow [167]. Interestingly, the uptake of adipocyte-derived FFA requires expression of the fatty acid translocase CD36 on the cancer cell surface and promotes cancer aggression [168, 169]. In addition to its role in fuelling cellular metabolism, uptake of exogenous FFA can also promote cell prolif-

eration, as observed for fibroblasts [170]. Taken together, it has become apparent that resident immune cell populations require FFA catabolism to meet their metabolic needs (Fig.5), however, if and how adipocytes supply this energy source to immune cells during times of local or systemic inflammation remains unexplored.

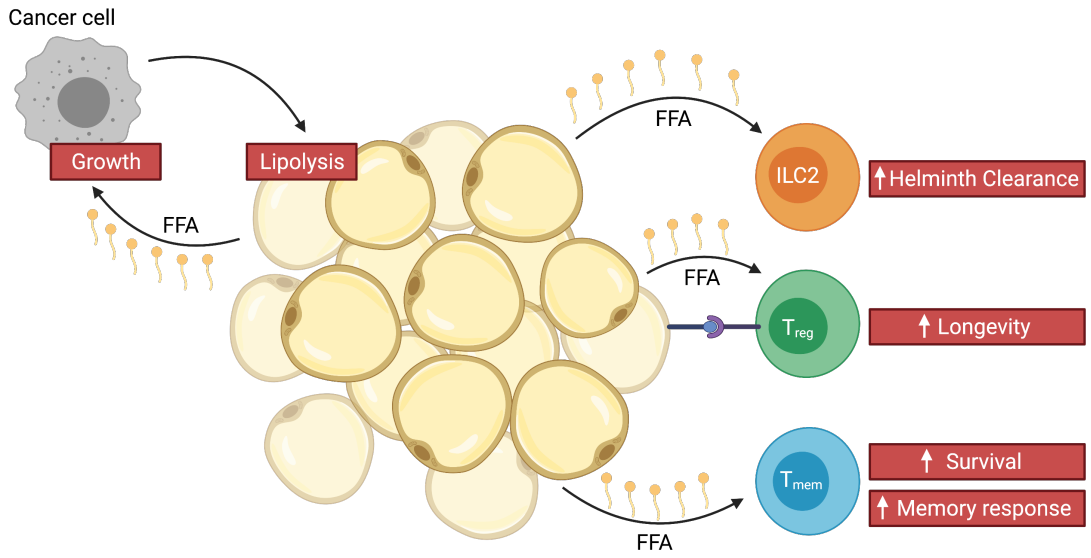

Figure 5: Local FFA exchange in the adipose tissue. Several cancer types (e.g. breast cancer, ovarian cancer, AML) promote lipolysis in adipocytes and use secreted FFA for their own growth. Similarly, lymphocytes take up FFA from their environment in order to fuel their metabolism for long-term survival or immunological function. Figure was adapted from Richter *et al.* [156]

1.3.3 Organelle crosstalk

Changes in cellular metabolism often depend on the utilization of the mitochondria. While metabolic changes are often regulated on a cell-intrinsic level, recent reports of mitochondrial transfer between cell types upon injury, allowed a new perspective on metabolic crosstalk [171, 172]. Even under homeostatic conditions, cardiomyocytes release dysfunctional mitochondria via exophers, in a process involving LC3 and some components of the autophagic machinery [36]. The released mitochondria are ultimately taken up and degraded by myocardial macrophages in order to maintain cardiac health and function. In the adipose tissue, mitochondria released from adipocytes are sequestered by macrophages [173]. While this transfer ensures metabolic tissue homeostasis, disruption of this process during obesity exacerbates adipocyte expansion and

lowers energy expenditure. It remains unclear however, whether adipocytes, analogous to cardiomyocytes, use exosphers for this transfer. However, adipocytes are capable of releasing lipid droplets containing exosomes, which are phagocytosed by adipose tissue macrophages (ATMs) and consequently promote expression of tissue resident markers [174]. It remains unclear whether autophagy, or its related molecules, are required for this metabolic organelle crosstalk.

Studies from the past decade have highlighted the close metabolic interaction between distinct cell subsets and their tissue environment. While much has been learned from cancer cells, it remains unclear how much of this crosstalk occurs in a non-cancer setting. Since immune cells react to infections and inflammation by shifting their metabolism to allow for cell proliferation and activation, immune cell metabolism is often compared to the metabolism observed in cancer cells [175]. However, to-date little is known about the molecular mechanisms of the metabolic cell-cell communication occurring between immune cells and their tissue environment. The adipose tissue presents a reservoir of many immune cells and is an important metabolic player. This raises the question of whether adipocytes can control local or even systemic immune responses through the regulation of nutrient release. In particular, their role in chronic inflammation, known to impact energy metabolism and expenditure, is less well studied [176].

1.4 Inflammatory bowel disease

Systemic chronic inflammation has become the primary cause of death, with more than 50% of all fatalities associated with inflammation-related diseases such as stroke, diabetes, autoimmune, neurodegenerative diseases, cancer, among others [177]. While not all chronic diseases lead to death, they can significantly impair patient quality of life. Increasing evidence suggests that the prevalence of systemic chronic inflammation depends on certain risk factors such as age, infections, diet, physical activity and stress [178]. Inflammatory bowel disease (IBD) is a general term for chronic inflammatory pathologies affecting the gastrointestinal tract. The prevalence of IBD for a large UK cohort was recently estimated at about 0.7% (7 in 1000 individuals) with the incidence rising 94% among the adolescent population over the past 20 years [179]. Interestingly,

the incidence of IBD is paralleling the increase in obesity and overweight in the general population [180], but possible links between obesity and IBD remain largely unexplored with respect to its effects on disease initiation, disease course and therapy. The most prevalent forms of IBD are ulcerative colitis (UC) and Crohn's disease (CD) with 54% and 38% of all IBD cases, respectively [179]. UC is characterised by a continuous and uniform inflammation of the superficial colonic mucosa, whereas CD manifests in discontinuous lesions of the small and large intestine with transmural inflammation [181]. Interestingly, a common symptom associated with CD is the expansion and wrapping of the mesenteric adipose tissue around the inflamed intestine, a phenomenon referred to as 'creeping fat tissue' (further introduced in Chapter 5). The aetiology of IBD remains incompletely understood, however, a combination of factors, including genetic predisposition, environmental factors and the microbiota, are associated with IBD pathogenesis. Independent of the combination of triggers required, IBD pathology ultimately results in a breakdown of immune tolerance towards commensal intestinal microorganisms in the affected areas of the gut. This may include a destruction of the intestinal epithelial barrier, which has been demonstrated in murine models of colitis [182] and the activation of innate and adaptive immune cells. An exacerbated inflammatory response is the main feature of IBDs, it is therefore not surprising that anti-inflammatory and immune suppressive drugs are the primary treatment options for IBD patients.

1.4.1 Immunopathology of IBD

The immunopathology of IBD is a complex network of innate and adaptive immune pathways communicating predominantly via cytokines [183]. Intestinal homeostasis is largely regulated via the function of dendritic cells and macrophages, which promote tolerance largely coordinated by a continuous expression of IL-10 [184]. However, other cell types such as Tregs and epithelial cells contribute to the maintenance of intestinal health. Upon breakdown of the intestinal barrier, these cells are the first to respond to the intrusion of the commensal microbiota. Bacteria are sensed via pattern recognition receptors and phagocytosed by antigen-presenting cells (APCs), such as dendritic cells and macrophages, in the mucosa. Upon bacterial sensing APCs activate and increase

pro-inflammatory and stimulatory cytokine production including TNFα, IL-1β, IL-12, IL-23, among others. Intestinal dendritic cells can then migrate to lymphoid organs including gut-associated lymphoid tissues (GALT) to activate naïve T cells. The persistent activation of the adaptive immunity represents a key step in the transition to chronic inflammation in IBD. Antigens presented to $CD4^+$ T cells promote their differentiation into effector subpopulations. Macrophage activation promotes IFNγ production, which subsequently shifts $CD4^+$ T cells towards a pro-inflammatory Th1 phenotype. In contrast, IL-4 production by APCs induces Th2 populations. Traditionally, CD has been associated with the expression of the Th1 cytokine IFNγ, whereas UC with higher levels of the Th2 cytokines IL-5 and IL-13 [185, 186, 187]. Later on, Th17 cells have been described as part of the immune response observed in both CD and UC patients. However, this classical perspective on IBD pathologies has been challenged in recent years. Increasing evidence suggest that the intestinal location of the inflammation may be a major determinant controlling Th response. Using a location-based stratification, IBD-associated Th17 responses are more pronounced in the ileum, while Th1 responses are both found in ileum and colon [188, 189, 190]. Importantly, anti-TNFα-resistant CD patients have an increased frequency of apoptosis-resistant intestinal $TNFR2^+$ $IL23R^+$ T cells in their colon, indicating a putative role of IL-23 in this patient subset [191]. Clinical trials using IL-12p40 targeting antibodies were effective in reducing disease burden in anti-TNFα resistant CD patients, suggesting that TNFα and IL-12p40 may belong to two distinct pathogenic pathways [192, 193]. Besides IL-12, the IL-12p40 subunit also forms IL-23, a cytokine secreted from intestinal APCs, which is capable of inducing Th17 responses [194, 195]. Stimulation of UC and CD-derived intestinal lymphocytes with IL-23 induces IL-17 and IFNγ, respectively [196]. Th17 populations are influenced by the microbiome and control intestinal bacterial or fungal infections by coordinating neutrophilic responses [197, 198]. Of note, the fungus *Debaryomyces hansenii* has recently been shown to interfere with intestinal wound healing in both mice and human underlining the importance of the mycobiota in CD [199]. Possibly due to this reason, blocking of IL-17A, the characteristic cytokine of Th17 cells, did not improve IBD pathologies in human trials [200]. In contrast, clinical trials targeting IL-23 subunits

(p40 or p19) are effective against CD and UC underlining the involvement of Th17 in the pathology [201].

In order to control immune cell activation, the secretion of the anti-inflammatory cytokines IL-10 and transforming growth factor (TGF)-β by intestinal Tregs is crucial. In addition to thymic-derived Tregs, the availability of TGF-β and antigen-recognition can induce local Treg development from naïve $CD4^+$ T cell populations in the intestine. Genetic loss of *Foxp3*, the dominant factor for Treg differentiation and function, in mice and humans, results in severe immune dysfunction and autoimmunity, which is often accompanied by intestinal inflammation [202]. However, even in individuals with normal FOXP3 expression, the differentiation of Tregs is outbalanced during IBD by the expansion of Th17 cells [203]. This balance of Tregs and Th17 differentiation depends on the activation of STAT3-mediated signalling pathways, which are induced by IL-6 and IL-23 [204]. As a result of a Treg/Th17 imbalance, the control of intestinal homeostasis can be impaired and lead to excessive inflammation. The contribution of TGF-β1 and IL-10 in this process has been extensively studied in mice and humans. The genetic loss of IL-10 expression in mice exacerbates intestinal inflammation and, similarly, mutations in genes involved in IL-10 signalling (ie. IL10RA, IL10RB, IL10) can result in severe early onset IBD in humans [205]. In particular, single nucleotide polymorphisms in the IL10 coding region have been linked to both CD and UC, underlining its central role in intestinal tissue homeostasis and in the control of excessive immune activation [206]. Since mutations in the IL-10 pathway are sufficient to induce intestinal inflammation and its immunopathology is distinct compared to 'classical' IBD, it is often classified as a monogenic 'IBD-like' pathology [207]. Curiously, the regulation of IL-10 production seems to depend on a variety of factors, including the microbiome. The presence of *Clostridium* species has been shown to induce FOXP3-expressing Tregs and production of IL-10 in the colon [208].

Although the importance of IL-10 to intestinal health is indisputable, the regulation of its expression locally and systemically remains incompletely understood. In addition, the administration of IL-10 has shown promising results in preclinical models of IBD,

pointing towards a role of systemic IL-10 in the pathology. In contrast, human clinical trials using recombinant IL-10 therapy were unsuccessful, however, differences in patient groups, disease progression and drug delivery may complicate data interpretation [209, 210]. In addition to its use as a therapy, it remains unclear whether 'non-gut' tissue sources of IL-10 can have a meaningful impact on intestinal health.

1.4.2 Links of autophagy and IBD

Several major genome-wide association studies (GWAS) have identified a multitude of single nucleotide polymorphisms in genes involved in autophagic pathways (e.g. *ATG16L1*, immune-related GTPase M (*IRGM*), leucine-rich repeatkinase 2 (*LRRK2*), nucleotide-binding oligomerization domain 2 (*NOD2*)) in CD patients [211, 212, 213, 214, 215, 216]. Since these early findings, murine studies using global and cell-type specific knock-out (KO) models have elucidated the function of autophagy in cell types involved in IBD. A particularly well-studied IBD susceptibility allele is a mutation in *ATG16L1*, leading to an amino acid change from tryptophan to alanine (T300A). Epithelial cells and dendritic cells harbouring this mutation are less antimicrobial, due to their inability to degrade bacteria in an autophagy-dependent manner [217]. This process is also referred to as xenophagy, and it has been proposed that a dysfunction in xenophagic pathways may increase IBD susceptibility. In line with this, the cytosolic bacterial sensor NOD2 interacts with ATG16L1 and other components of the autophagic machinery to clear intracellular pathogens and for DCs to antigen-present on major histocompatibility complex (MHC) class II to stimulate $CD4^+$ T cells. Identified human mutations in both *NOD2* and in *ATG16L1* impair these processes, and thus increase inflammation [218, 219]. Today, both an inactive and a hyperactive form of NOD2 has been associated with the risk for developing IBD, underlining the importance of well-balanced NOD2 signalling pathways in the maintenance and control of intestinal immunity. In general, NOD2 is a pleiotropic innate immune sensor and can, apart from autophagy induction, elicit a variety of effects, which include the regulation of ER stress, self-tolerance (via IL-10 release) and T cell regulation [216]. Interestingly, deletion of *Atg5*, *Atg7*, or the use of the hypomorphic T300A *Atg16l1* allele in intestinal epithelial cells leads to aber-

rant Paneth cells and lower antimicrobial peptide secretion [220, 221]. Curiously, the hypomorphic T300A variant is accompanied by a strong upregulation of genes involved in lipid metabolism, such as PPAR signalling and adipokine signalling [220]. Although this observation is still unexplained, it is plausible that Paneth cells may shift their metabolic sources towards lipids to compensate for the loss of autophagy. Importantly, the loss of autophagy can also impair immune cell function and lead to the development of spontaneous intestinal inflammation. For instance, genetic loss of *Atg16l1* in murine T cells skews the immune response towards a type 2 response to dietary and microbial antigens, thus promoting intestinal inflammation [92]. Mutations in *Irgm* can also lead to Paneth cell abnormalities and an increased susceptibility to intestinal inflammation [222]. Like ATG16L1 and NOD2, IRGM mediates this effect by directly impairing xenophagy [213, 223]. IRGM in mice can also regulate inflammasome assembly and degradation in an autophagy-dependent manner and thus control the level of pyroptosis and inflammation in the colon [224]. Other gene variants discovered through GWAS have also been functionally investigated, most of the gene variants caused a significant impairment in xenophagy (extensively reviewed in [225]).

Taken together, a combination of genetic and functional studies in both humans and mice underline that dysfunctional autophagy in various cell types, including epithelial and immune cells, contribute to the development of IBD. Autophagy contributes to a multitude of cellular pathways and its relevance for IBD pathology may therefore be cell type dependent. However, it remains crucial to use animal models to dissect the mechanisms of how autophagy contributes to the development and progression of IBD. While much research has focussed on the role of autophagy in cell types located in the intestine during inflammation, autophagy loss in other organs and their distal effects on the inflamed gut remain largely unknown. It remains to be explored whether loss of autophagy in other cell types, such as adipocytes in the mesentery, may contribute to IBD.

1.5 Thesis hypothesis and objectives

During infections and inflammatory processes, immune cells can quickly adapt their energy metabolism and biosynthetic pathways to promote immune cell growth, proliferation and effector functions. While the impact of immunometabolism on immune cell function is nowadays well established, little is known about the influence of the local tissue environment in directing immune cell metabolism and possibly their function. The adipose tissue represents a highly metabolic tissue environment, which releases energy-rich FFA during times of systemic energy deprivation. These situations can occur in chronic inflammatory conditions, such as IBD. Curiously, the phenomenon of the 'creeping fat tissue' observed in CD patients further indicates a direct involvement of adipose tissues in IBD pathology. Due to its close genetic link to autophagy pathways and the obvious involvement of adipose tissues in the pathology, we set out to study the role of autophagy in mature adipocytes during intestinal inflammation. We hypothesized that adipocyte autophagy contributes to the regulation of the immune response in intestinal inflammation (Fig.6). To test this, we aimed to address the following objectives in chapters 3-6, respectively:

3. Establish models to study autophagy in mature adipocytes.

4. Assess the role of adipocyte autophagy under homeostatic conditions.

5. Determine the impact of adipocyte autophagy on intestinal inflammation during colitis.

6. Analyse the mechanistic effect of adipocyte autophagy on metabolism and on local immune cell populations.

The results presented in this thesis suggest that adipocyte autophagy is required for the anti-inflammatory response upon intestinal injury. Mechanistically, adipocyte autophagy is required in colitic animals to promote the release of FFA from mature adipocytes. The lack of local FFA is responsible for the downregulation of IL-10 expression in ATMs, thus lowering systemic IL-10 levels and exacerbating intestinal in-

flammation. Overall, this thesis demonstrates a novel cell-extrinsic role of autophagy in tissue stromal cells, in regulating immune cell responses during inflammation.

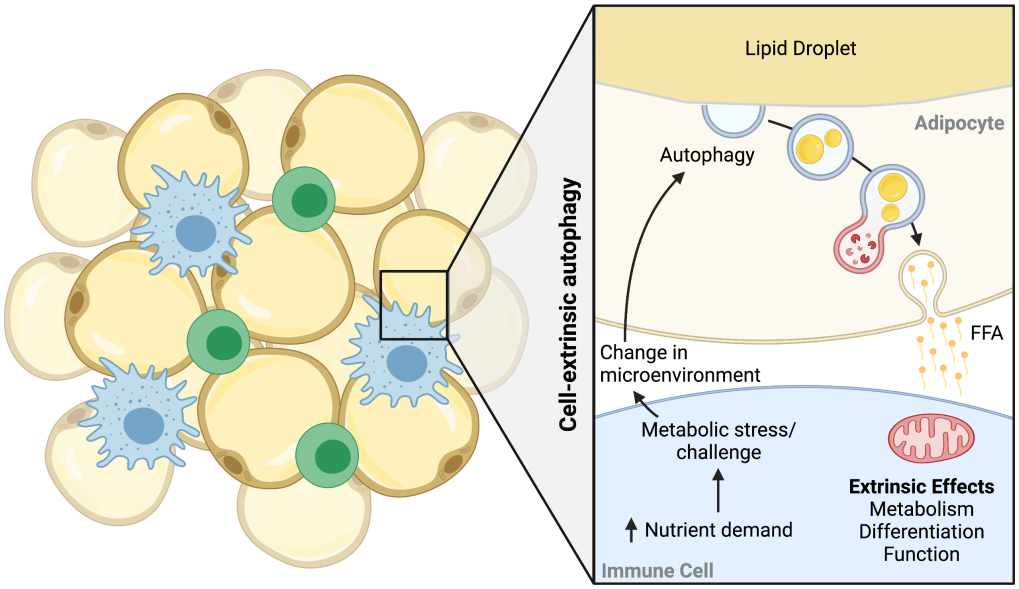

Figure 6: Graphical presentation of the central hypothesis of the thesis. Immune cell activation upon inflammatory stimulation promotes a metabolic shift/stress in adipose tissue-resident immune cells. Adipocytes react to the inflammatory environment through activation of autophagy, and release metabolites or other signals, such as cytokines, in an autophagy dependent manner. These adipocyte-derived metabolites or signals are required for appropriate immune cell activation, shift of metabolism, and function. This process was termed "cell-extrinsic autophagy".

2 Materials and Methods

2.1 Mice

Adipoq-Cre^{ERT2} mice [226] were purchased from Charles River, UK (JAX stock number: 025124) and crossed with either floxed *Atg7* (*Atg7*$^{f/f}$) mice [227], floxed *Atg16l1* (*Atg16l1*$^{f/f}$) mice [228] or *Ai14* tdTomato reporter mice [229] on a C57BL/6J background. Control mice were littermates, predominantly *Cre*$^{-}$ mice, and co-housed with the experimental animals. Wild-type C57BL/6J females, purchased from Charles River, UK (JAX stock number: 000664), were housed for 1-2 weeks prior to experimental start. C57BL/6 SJL CD45.1 for bone marrow transplantation were bred in-house. During all experiments, we used sex-matched and age-matched littermate controls. For colitis experiments, we balanced each cage with the same number of autophagy-deficient and control mice (where possible) to avoid cage effects. Genetic recombination was induced at 8-10 weeks of age by gavage with 4mg tamoxifen per mouse per day for five consecutive days. Tamoxifen was washed out over a two-week period before further experimental assessment. Mice were fed and housed under specific pathogen-free conditions in the Biological Service Unit, Kennedy Institute of Rheumatology, Oxford. All animal experiments were performed in accordance to approved experimental procedures by the Home Office and the Local Ethics Review Committee (University of Oxford) under UK project licence (PPL 30/3388 and P01275425).

2.2 DSS-induced and *Helicobacter hepaticus*-induced colitis

For DSS colitis experiments, mice were treated for five days with 1.5%-2% (w/v) DSS (MP Biomedicals, 160110) in drinking water, as indicated. Mice were sacrificed at day 7 and day 14 after initial DSS administration for peak inflammation and recovery experiments, respectively. For *Helicobacter hepaticus*-induced colitis [230], *H. hepaticus* (ATCC51449) was administrated by oral gavage for two consecutive days and anti-IL-10 receptor antibody (2BScientific) was injected intraperitoneally (1mg/20g mouse weight) on day 1 and day 7 of the model. For both colitis models, control (non-inflamed) animals were kept in separate cages on the same rack.

2.3 Bone marrow transplantation

Experimental setup was based on discussions with and protocols from Prof. Olaia Naverias [231]. Recipient mice (*Adipoq-Cre*$^{+}$ x *Atg7*$^{f/f}$ or *Adipoq-Cre*$^{-}$ x *Atg7*$^{f/f}$ on CD45.2^{+} background) were treated with tamoxifen. After 12 weeks, mice were irradiated with 4.25Gy per cycle for two irradiation cycles, 4 hours apart. Bone marrow cells from C57BL/6 SJL CD45.1^{+} mice were prepared from femur and tibia. Cells were counted using hemocytometer and diluted to a concentration of 1.25 x10^{6} cells/mL in PBS. Cell suspension was filtered (40µm strainer) shortly prior to intravenous injection of 100µL (equivalent to 1.25 x10^{5} cells/mouse). Mice were kept for two weeks post-transplantation on antibiotics (Enrofloxacin) in drinking water to avoid infections. During the course of the experiment, mice were bled at indicated time points.

2.4 Hematopoietic progenitor colony-forming unit assay

Colony forming unit (CFU) assay on hematopoietic progenitor cells were performed using methylcellulose-based medium with recombinant cytokines (M3434, Stemcell). MethoCult was prepared following manufacturer protocol. Bone marrow cells were isolated from one femur, one tibia and pelvic bones. Bones were crushed and filtered through 40µm strainer. CD45^{+} Terr119^{-} BM cells were counted using beads by flow cytometry. Total of 2.5 x10^{4} CD45^{+} Terr119^{-} cells were plated in six-well plates in technical duplicates. CFUs were counted eight days post-plating by blinded assessor (kind help by Dr. James Swann).

2.5 Genotyping

Ear clips were lysed in 100µL NaOH (50mM) lysis solution for 1 hour at 100°C and once vortexed after 30min of lysis. Lysis was quenched by adding 13µL of 1M Tris-HCl solution (pH∼8). Undigested tissue was pelleted at 16,000g for 5min. Polymerase chain reaction (PCR) was performed for each individual transgene in 20µL reactions using MyTaq™ Red Mix (BIO-25044, Bioline). All primers were used at a concentration of 100µM.

Volume (µL)	*Adipoq-Cre*	*Atg7$^{f/f}$*	*Atg16l1$^{f/f}$*	*Ai14*
Per primer (100µM)	0.25	0.25	0.1	0.2
2x MyTaq RedMix	10	10	10	10
RNase/DNase-free water	7	7.25	7.8	7.2
DNA sample	2	2	2	2

Primer sequences

Adipoq-Cre PCR

Adipoq-22925 5'- GAG TCT GCC TTT CCC ATG AC -3'

Adipoq-22926 5'- TCC CTC ACA TCC TCA GGT TC -3'

Adipoq-21173 5'- CCG CAT CTT CTT GTG CAG T -3'

Adipoq-21175 5'- ATC ACG TCC TCC ATC ATC C -3'

Atg7f/f PCR

Atg7-752 5'- CCA TGC TGA TGG CTA ATG TCT C -3'

Atg7-753 5'- CTG CAG GAA TTC GAT ATC ATA ACT TCG -3'

Atg7-14R 5'- GTC CAG AGT CCG GTC TCT GGT TG -3'

Atg16l1f/f PCR

Atg16l1-F 5'- CTT TCT CAA CAG AAC CAG CAG TAC -3'

Atg16l1-R 5'- GTA GAA AGA CTG GTG ATG GTA AAC C -3'

Ai14 PCR

IMR9020 5'- AAG GGA GCT GCA GTG GAG TA -3'

IMR9021 5'- CCG AAA ATC TGT GGG AAG TC -3'

IMR9103 5'- GGC ATT AAA GCA GCG TAT CC -3'

IMR9105 5'- CTG TTC CTG TAC GGC ATG G -3'

Cycling conditions

Step	*Adipoq-Cre*	*Atg7$^{f/f}$*	*Atg16l1$^{f/f}$*	*Ai14*
1	94°C, 2min	95°C, 1min	94°C, 2min	94°C, 1min
2	94°C, 20sec	95°C, 15sec	94°C, 15sec	94°C, 15sec
3	65°C, 15sec	64°C, 30sec	60°C, 15sec	60°C, 15sec
4	68°C, 10sec (to step 2, 10 cycles)	70°C, 10sec (to step 2, 32 cycles)	72°C, 10sec (to step 2, 30 cycles)	72°C, 10 sec (to step 2, 30 cycles)
5	94°C, 15sec	70°C, 2min	72°C, 2min	72°C, 2min
6	60°C, 15sec	4°C, Hold	4°C, Hold	4°C, Hold
7	72°C, 10sec (to step 5, 28 cycles)			
8	72°C, 2min			
9	4°C, Hold			

PCR products were separated on a 2% agarose gel, prepared from TAE buffer (40mM Tris-Acetate, 1mM EDTA) with SYBR® Safe DNA Stain (Invitrogen, S33102, Dilution 1:10,000), and were run at 120V for 25min until separated. Bands were visualized via G-Box (Syngene).

2.6 Cell culture

ST2 cells [232] and 3T3-L1 cells [233] were a kind gift from Prof. Claire Edwards and Dr. Henk Schipper, respectively. Both cell lines were maintained in stock medium (DMEM/High Modified (D6429, Sigma) supplemented with 10% FBS (Sigma, F9665) and 100U/ml Pen-Strep (Sigma, P0781) and passaged before reaching confluency. ST2 cell adipogenic differentiation was performed as previously described [234]. In brief, ST2 cells were seeded at 8x10^5 cells/well into a six-well plate. Upon reaching 80% confluency, cells were induced in stock medium with 100nM insulin (I9278, Sigma), 200µM freshly prepared Indomethacine (I7378, Sigma), 500µM 3-isobutyl-1-methylxanthine (IBMX) (I7018, Sigma) and 1µM Dexamethasone (D4902, Sigma). After three days of adipogenic induction, cells were switched to maintenance medium consisting of stock medium with 100nM insulin for another four days. shRNA mediated knockdown was induced over four days using indicated concentrations of freshly prepared doxycycline (D9891, Sigma). Doxycycline-containing medium was replaced every two days.

2.7 Lentiviral transduction and shRNA cell lines

Generation of inducible, shRNA-mediated *Atg5* and *Atg7* knockdown ST2 and 3T3-L1 cell lines were generated based on the LT3REVIR backbone [235], kindly provided by Prof. Johannes Zuber, and published shRNA sequences [236]. Control cell lines were constructed using a non-targeting shRNA sequence towards *Renilla*.

shRNA stem sequences

shRen	5'- CAG GAA TTA TAA TGC TTA TCT A -3'
shAtg7-131	5'- ACC AGA AGA AGT TGA ACG AGT A -3'
shAtg7-700	5'- AAA GGT CAA AGG ACA AAG ATA A -3'
shAtg5-1063	5'- CAC CCA GAT AAC TTT CTT CAT A -3'
shAtg5-1389	5'- AAC AGT TTG TAT TTC TGA TTA A -3'

shRNA fragments were cloned into LT3REVIR backbone using EcoRI and XhoI restriction enzyme sites. Clones were confirmed by Sanger sequencing. Selected and purified plasmids were packaged by co-transfection using the packing plasmid pMD2.G (Didier Trono, Addgene 12259) to generate lentiviral particles by WIMM Genome Engineering Facility. ST2 and 3T3-L1 cells were transduced with lentivirus with stock medium containing 6.5µg/mL polybrene (TR-1003-G, Millipore) and multiplicity of infection (MOI) of 0.25. After two days, cells were washed and after another 48h sorted by constitutive mVenus expression. Bulk sorted cell lines were split into two to three wells and expanded.

2.8 Adipose Tissue Explant Culture

Adipose tissues were collected from mice in fat medium (DMEM supplemented with 1% fatty acid free BSA (126609, Sigma) and 5% HEPES (15630-056, Gibco)). Explants were washed in PBS before performing explant culturing. For measurement of cytokine secretion, adipose tissue explants were cultured for either 6 or 24h in RPMI (R8758, Sigma) with 100U/ml Pen-Strep in the presence or absence of FBS as indicated. Supernatant was collected, spun down (400g, 5min) to remove cell debris and

then frozen until further analysis. For measurement of autophagic flux, adipose tissue explants were cultured for 4h in 100nM Bafilomycin A1. For lipolysis assays, adipose tissues were minced into 10-20mg pieces. Three pieces (∼50mg) were cultured in 200µL DMEM supplemented with 2% fatty-acid free BSA with/without isoproterenol (I6504, Sigma) or TNFα (315-01A, Peprotech). For isoproterenol-induced lipolysis (adapted from [237]), supernatant samples were collected after 1 and 2h of explant cultures. For TNFα-stimulated lipolysis (adapted from [238]), adipose tissues were cultured for 24h in medium containing TNFα (100ng/mL), then cells were washed, and adipose tissues were cultured for an additional 3h in fresh DMEM with 2% fatty-acid free BSA. Supernatant was collected and spun down (400g, 5min) to remove cell debris. Total FFA levels were quantified using Free Fatty Acid Assay Quantification Kit (ab65341, Abcam) following manufacturer protocol. For both assays, results were normalized to tissue input weight.

2.9 Adipose Tissue and Colon Digestion

Adipose tissues were collected in fat medium. Each tissue was weighed before placing into 2mL digestion medium consisting of fat medium with 0.2mg/mL Liberase TL (5401020001, Roche) and 20µg/mL DNase (11284932001, Roche). Tissues were minced in digestion medium and then incubated for 25-30min at 37°C under agitation (190rpm). Using first wide bore and then standard size pipette tips, tissue pieces were broken up by pipetting up and down. Cell suspensions were strained and digestions were quenched by adding fat digest medium containing 2mM EDTA (15575-020, Invitrogen). Cell suspension was pelleted by centrifugation (700g, 10min). Floating adipocyte fraction and pelleted vascular stromal fraction were collected for further analysis.

For colon digests, colons were collected, length measured and faeces removed and cleaned of any attached tissues. Sections for histology were fixed overnight in 10% neutral buffered formalin (HT5011, Sigma) before further processing. Equally sized proximal, mid and distal colon pieces were collected in RNAprotect Tissue Reagent (76104, Qiagen) for gene expression analysis. Colons were digested as previously described [230]. In brief, colons were cut open longitudinally, washed twice in RPMI containing 5% FBS and 5mM EDTA at 37°C under agitation to remove epithelium. Next, tissue was di-

gested for 45min in RPMI supplemented with 5% FBS, 1mg/mL collagenase type VIII (Sigma) and 40µg/mL DNaseI (Roche). Cells were strained through 40µm filter and pelleted (400g, 5min) at 4°C. Cells were resuspended in PBS containing 0.1% BSA (w/v) and 2mM EDTA and counted using CASY® cell counter (OMNI Life Science), if not otherwise indicated, prior to until further analysis (e.g. flow cytometry).

2.10 Flow cytometry

Staining for flow cytometry was performed as previously described [88]. In brief, single cell suspension were stained in round bottom 96-well plates in a total staining volume of 50µL. First, live dead staining and surface staining was performed using LIVE/DEAD Fixable Stains (ThermoFischer) and fluorochrome-conjugated primary antibodies (Biolegend, BD Bioscience, eBioscience), respectively. If not otherwise indicated, all cells were fixed either in 4% paraformaldehyde (PFA) for 10min at room temperature or using eBioscience™ Foxp3/ Transcription Factor Staining Set (00-5523-00, Invitrogen) for 30min at 4°C. Intracellular transcription factor staining was performed after fixation and permeabilization using fluorescently labelled primary antibodies. Intracellular cytokine staining was performed after 15min fixation using BD Cytofix/Cytoperm™ Fixation/Permeablization Kit (554714, BD Biosciences). For intracellular lipid quantification, PFA-fixed cells were stained for 30min with BODIPY™ 493/503 and then washed before acquisition on LSRII or Fortessa X-20 flow cytometers (BD Biosciences). Bead compensation controls were prepared. If cells were counted by beads on flow cytometer, 20,000 PE/FITC-fluorescent BD Calibrite™ Beads (349502, BD Bioscience) were added per sample before sample acquisition.

2.11 Polymerase chain reaction (PCR)

For quantification of genomic *Atg7* excision, genomic DNA from gonadal adipose tissue was extracted using DNeasy Blood & Tissue Kit (69504, Qiagen). PCR was prepared using LA Taq PCR kit (RR013A, Takara) in 20µL total reaction volume.

Reagent	Volume (µL/rxn)
Per primer (100µM)	0.2
10x LA Taq Buffer	2
LA Taq Polymerase	0.2
$MgCl_2$	2
dNTP	3.2
RNase/DNase-free water	11.2
DNA sample	1

Primer sequences

Hind-Fwd 5'- TGG CTG CTA CTT CTG CAA TGA TGT -3'

96-121c 5'- TTA GCA CAG GGA ACA GCG CTC ATG G -3'

Cycling conditions

1. 94°C, 5min
2. 98°C, 20sec
3. 68°C, 3min (Go to 2, 30 cycles)
4. 72°C, 10min
5. 4°C, hold

Quantification of cDNA by PCR was performed as previously shown [239]. In brief, total RNA from gonadal adipose tissues were extracted using TRI reagent (T9424, Sigma) and RNeasy Mini Kit (74104, Qiagen). For cDNA synthesis, 1µg of total RNA was reverse transcribed using High-Capacity RNA-to-cDNA™ kit (4388950, ThermoFischer). Primers were used at 20µM stock concentration.

Reagent	Volume (µL/rxn)
Per primer (20µM)	0.2
2x MyTaq RedMix	10
RNase/DNase-free water	8.6
DNA sample	1

Primer sequences

mAtg7-Fwd	5'- TGT GGA GCT GAT GGT CTC TG -3'
mAtg7-Rev	5'- TGA TGG AGC AGG GTA AGA CC -3'
mActin-Fwd	5'- GAG GCA CTC TTC CAG CCT TC -3'
mActin-Rev	5'- TAG AAG CAT TTG CGG TGG AC -3'

Cycling conditions

1. 98°C, 2min
2. 98°C, 20sec
3. 55°C, 15sec
4. 72°C, 1min (Go to 2, 30 cycles)
5. 72°C, 5min
6. 4°C, hold

PCR products were separated on a 1% agarose gel, prepared from TAE buffer (40mM Tris-Acetate, 1mM EDTA) with SYBR® Safe DNA Stain (Invitrogen, S33102, Dilution 1:10,000), and were run at 120V until separated. Bands were visualized via G-Box (Syngene).

2.12 Quantitative PCR (qPCR)

RNA extraction from whole adipose tissues and enriched adipocyte fractions was performed using TRI reagent (T9424, Sigma) extraction method. Colon tissues were lysed in RLT buffer containing 1,4-Dithiothreitol following RNeasy Mini Kit protocol. Colon tissues (equally sized pieces – proximal, mid, distal colon) and adipose tissues were lysed in 2mL tubes containing ceramic beads (KT03961-1-003.2, Bertin Instruments) using a Precellys 24 homogenizer (Bertin Instruments). After homogenisation, solution was further processed using RNeasy Mini Kit (74104, Qiagen) following manufacturer protocol for respective extraction method. For cDNA synthesis, total RNA was adjusted for whole adipose or colon tissue RNA, but not for adipocyte RNA, and reverse transcribed

using High-Capacity RNA-to-cDNA™ kit (4388950, ThermoFischer). Gene expression analysis was performed using validated TaqMan™ probes (Applied Biosystems) and run on a ViiA7 real-time PCR system (ThermoFischer) using TaqMan™ Fast Universal PCR Master Mix (4352042, Applied Biosystems). All assays were determined using comparative Ct method and either represented as relative expression ($2^{-\Delta Ct}$) or fold change ($2^{-\Delta\Delta Ct}$). Data was normalized to *Actin*, *Hprt*, *18S* rRNA or *Tbp*, after determination of most stable housekeeping gene expression. Samples were normalized as follows; colon samples were normalized to *Actin* and *Hprt*, adipose tissues were normalized to *18S* rRNA and *Tbp*, floating adipocytes were normalized to *18S* rRNA.

Cycling conditions

1. 50°C, 2min
2. 95°C, 20sec
3. 95°C, 1sec
4. 60°C, 20sec (Go to 3, 40 cycles)

TaqMan™ probes

Atg7 (Mm00512209_m1), Atg5 (Mm00504340_m1), Adipoq (Mm00456425_m1), Becn1 (Mm01265461_m1), Sqstm1 (Mm00448091_m1), Map1lc3b (Mm00782868_m1), Gabarap (Mm00490680_m1), Gabarapl1 (Mm00457880_m1), Gabarapl2 (Mm01243684_gH), Il33 (Mm00505403_m1), Tnfa (Mm00443258_m1), Ifng (mm01168134_m1), Cxcl9 (Mm00434946_m1), Il1a (Mm00439620_m1), Ptx3 (Mm00477268_m1), Il1b (Mm00434228_m1), S100a9 (Mm00656925_m1), Il10 (Mm00439614_m1), Il22 (Mm01226722_g1), Tgfb1 (Mm001178820_m1), Il23a(Mm00518984_m1), Actin (Mm02619580_g1), Hprt (Mm01545399_m1), Rn18s (Mm04277571_s1), Tbp (Mm01277042_m1).

2.13 Bulk RNA sequencing

RNA samples were prepared as described above and further processed by the Oxford Genomics Centre (University of Oxford). In brief, PolyA library was prepared from cDNA with end-reparation, A-tailing and adapter ligation. Samples were size selected,

multiplexed and GC'ed before paired end sequencing using NovaSeq6000 over one unit of a flow cells. Raw read quality control was performed using pipeline_readqc.py (`https://github.com/cgat-developers/cgat-flow`). Sequencing reads were matched to reference genome GRCm38/Mm10 with known slice site information of Ensemble 99 version annotation using the pseudoalignment method kallisto [240]. All samples passed quality control using FastQC v0.11.9. More than 90% of reads aligned to reference genome. Differential gene expression was analysed using DEseq2 v1.30.1 [241]. Pathway enrichment analysis for differentially expressed genes associated with intestinal inflammation was performed using *enrichGO* function for "Biological Pathway" annotations from the clusterProfiler R (v3.18.1) package [242]. Selected gene sets were visualized in heatmaps and z-scores (scaling per gene) were calculated based on $\log_2$-transformed normalized counts using the R package pheatmap.

2.14 Shotgun lipidomics

Serum samples (1µL/sample) were analysed using Shotgun Lipidomics platform by Lipotype GmbH (Dresden, Germany), as described previously [243]. In brief, lipids were extracted using methyl tert-butyl ether and methanol and then spiked using lipid class-specific internal standards. Extracts were dried and resuspended in MS acquisition buffer and analysed by mass spectrometry on a hybrid quadrupole/Orbitrap mass spectrometer. Lipids were identified using LipotypeXplorer software [244]. Prior to normalization, lipids were filtered according to mass accuracy, occupation threshold, noise and background. Lipid class-specific internal standards were used for lipid quantification. Data were returned when falling within limits of quantification and coefficient variation for different lipid classes. Sample preparation, mass spectrometry, initial quality control and processing were performed by LipoType GmbH (Germany). Raw data (in pmol and %pmol) were filtered to include only lipid species with no missing values (due to subthreshold or failed QC). Data were further processed in R.

2.15 Free fatty acid analysis

Total serum FFA levels were quantified using enzyme-based Free Fatty Acid Assay Quantification Kit (ab65341, Abcam) following manufacturer protocol. For analysis of specific FFA species, serum samples were analysed in collaboration with Dr. Irina Guschina (Cardiff University). In brief, lipids were extracted by Folch's method [245] and lipid extracts were stored at -20°C under nitrogen atmosphere prior to further analysis. Non-polar lipids, including FFAs, were separated using one-dimensional thin layer chromatography (TLC) on 10x10 cm silica gel G plates (Merck) in the solvent system hexane/diethyl ether/acetic acid (80:20:1, by vol.). FFAs separated by TLC were used for fatty acid methyl esters (FAMEs) preparation. FAMEs were prepared using a solution of 2.5% H_2SO_4 in dry methanol/toluene (2:1 (v/v)). Samples were heated to 70°C for 2h, with occasional vortexing. FAMEs were extracted by two additions of 3mL of hexane. The hexane fractions were transferred into clean glass tubes, evaporated under a stream of nitrogen and reconstituted in 50µL of hexane. All reagents for fatty acid extraction and derivatisation were of HPLC quality. FAMEs were analysed using a Clarus 500 GC with a flame ionisation detector (Perkin-Elmer). A Perkin-Elmer Elite 225 column (30m x 0.32mm x 0.25µm) was used with a nitrogen carrier gas constant pressure of 20psi. The oven temperature program began at 170°C for 3min, was ramped to 220°C at 4°C/min and was then held for 30min. FAMEs were identified by comparison of the peak retention times with those of a GC-411 standard mixture (Nu-Chek Prep. Inc). Perkin-Elmer TotalChrom software was used for data acquisition and calculation.

2.16 Immunoblotting

Adipose tissues were collected and snap frozen in liquid nitrogen or on dry ice. Adipose tissues were transferred in 2mL tubes filled with ceramic beads (KT03961-1-003.2, Bertin Instruments). Per 100mg of adipose, 200µL Laemmli buffer (4% SDS, 20% Glycerol, 125mM Tris-HCl) containing protease inhibitors (04693159001, Roche) and phosphoStop (04906837001, Roche) were added. Tissues were homogenised using Berkin Precellys 24 homogenizer (1-2 cycles, 6500rpm, 40sec). Tissues were incubated on ice for one hour, before tissue remnants were pelleted (16000g, 5min, 4°C). Subnatant was transferred

into fresh tubes. Samples were centrifuged (16000g, 5min, 4°C) and subnatant collected using insulin syringe and transferred into fresh tube avoiding aspiration of floating lipid layer. This process was repeated two more times. Cell lysates were sonicated for 40sec at 20% amplitude (one cycle). Finally, samples were centrifuged (16000g, 5min, 4°C) and subnatant collected in fresh tubes and stored until analysis at -20°C or -80°C. Cell lines were lysed in NP-40 buffer containing protease stop and phosphoStop for 45min on ice. Samples were centrifuged (16000g, 15min, 4°C) and supernatant collected. Protein concentration was determined using BCA Protein Assay Kit (23227, Thermo Scientific). Total of 15-30µg protein were loaded on 4-12% Bis-Tris SDS PAGE and separated at 120V. Proteins were transferred onto PVDF membranes using BioRad Turbo Blot (1704156, BioRad) for 7min at 25V (1.3A). Membranes were blocked in with 5% skimmed milk (Sigma). The following primary antibodies were used: LC3 (L8918, Sigma) (1:1500), ATG7 (ab133528, Abcam) (1:1500), ATG5 (D5F5U, Cell Signalling) (1:1000), ADIPOQ (ab3455, Abcam) (1:1000) β-ACTIN (8H10D10, Cell Signalling) (1:10000). Primary antibodies were visualized using IRDye secondary antibodies (LI-COR, Lincoln) (1:15000).

2.17 Transmission electron microscopy

Experimental instructions were provided by and transmission electron microscopy was performed by the Dunn School of Pathology EM facility (Dr. Errin Johnson). In brief, adipose tissues were harvested, cut into 1-2mm cubes and placed in freshly prepared fixative (2.5% glutaraldehyde, 4% paraformaldehyde, 0.1M sodium cacodylate buffer). After 2h fixation at room temperature, samples were stored at 4°C until further processing. Samples were then washed twice for 45min in 0.1M sodium cacodylate buffer (pH∼7.2) at room temperature with rotation and processed for EM using a Leica AMW automated microwave processing unit using the following program:

Automated processing program

1. 0.1M sodium cacodylate buffer pH∼7.2 (1min, 37°C, 20W, Slope) – two cycles
2. 0.1M sodium cacodylate buffer pH∼7.2 + 50mM glycine (1min, 37°C, 20W, Slope)

3. 0.1M sodium cacodylate buffer pH∼7.2 (1min, 37°C, 20W, Slope)
4. 0.1M sodium cacodylate buffer pH∼7.2 (1min, 37°C, 15W, Continuous)
5. 1% osmium tetroxide + 1.5% potassium ferricyanide in 0.1M sodium cacodylate buffer pH∼7.2 (12min, 37°C, 20W, Pulse)
6. MQ water (1min, 37°C, 15W, Continuous) – 7 cycles
7. 2% uranyl acetate in water (5min, 37°C, 20W, Continuous)
8. 2% uranyl acetate in water (2min, 20°C, 0W, Continuous)
9. 2% uranyl acetate in water (2min, 37°C, 15W, Continuous)
10. MQ water (1min, 37°C, 15W, Continuous) – 2 cycles
11. 30% Ethanol (1.5min, 37°C, 15W, Continuous)
12. 50% Ethanol (1.5min, 37°C, 25W, Continuous)
13. 70% Ethanol (2.5min, 37°C, 25W, Continuous)
14. 90% Ethanol (1.5min, 37°C, 25W, Continuous)
15. 95% Ethanol (1min, 37°C, 25W, Continuous)
16. 100% Ethanol (2min, 37°C, 25W, Continuous)
17. 25% TAAB Hard Plus epoxy resin in Ethanol (3min, 37°C, 10W, Continuous)
18. 50% TAAB Hard Plus epoxy resin in Ethanol (3min, 37°C, 10W, Continuous)
19. 50% TAAB Hard Plus epoxy resin in Ethanol (3min, 45°C, 12W, Continuous)
20. 75% TAAB Hard Plus epoxy resin in Ethanol (3min, 45°C, 12W, Continuous)
21. 100% TAAB Hard Plus epoxy resin (10min, 45°C, 12W, Continuous) – 2 cycles
22. 100% TAAB Hard Plus epoxy resin (15min, 45°C, 12W, Continuous) – 2 cycles
23. 100% TAAB Hard Plus epoxy resin (30min, 45°C, 12W, Continuous)

After cycling, samples were transferred into fresh TAAB Hard Plus epoxy resin, centrifuged (2min, 2000g) and then incubated at room temperature overnight with rotation. The next day, resin was replaced with fresh resin, centrifuged (2min, 2000g) and incubated for 3h at room temperature. This step was repeated and then transferred into Beem capsules filled with fresh resin and polymerised for 48h at 60°C. Polymerised blocks were sectioned using a Diatome diamond knife on a Leica UC7 Ultramicrotome. Ultrathin (90nm) sections were transferred onto 200 mesh copper grids and post-stained with lead citrate for 5min, washed and air dried. Grids were imaged with a Thermo Fisher Tecnai 12 TEM (operated at 120kV) using a Gatan OneView camera.

2.18 Epifluorescence and confocal microscopy

To test recombination specificity, *Adipoq-Cre^{ERT2}* mice were crossed to *Ai14* tdTomato reporter mice. After induction of deletion by tamoxifen, adipose tissues, lungs, liver and spleen were collected in PBS and kept on ice. Whole tissues were imaged macroscopically using epifluorescence stereomicroscope Olympus MVX10.

For confocal imaging, adipose tissues were fixed in 10% neutral buffered formalin and then embedded in paraffin or OCT (LAMB/OCT, ThermoScientific). Colons were open longitudinally, contents removed, colon washed and spread on a filter paper. Next, colon was tightly wrapped around wood stick and finally tissue was fixed in OCT. Frozen tissue blocks were sectioned using crytostat CM1900UV (Leica Camera AG) and counterstained in mounting medium with DAPI (H-1200, Vectashield). Images were acquired on Olympus FV1200 IX83 Confocal System (Olympus).

For colon and adipose tissue histology, adipose tissues and colons were fixed in 10% neutral buffered formalin for 4h and 24h, respectively. Tissues were washed in 70% ethanol until embedding in paraffin. 5µm paraffin sections were cut and stained with hematoxylin and eosin (H&E). In brief, sections were processes as follows for staining using DRS 2000 Stainer (Sakura): Xylene (5min), Xylene (5min), 100% Ethanol (1min), 100% Ethanol (1min), Water (1min), Haematoxylin Harris (6.5min), Water (2min), Acid Alcohol (40sec), Water (2min), Blueing aging (1min), Water (1min), 1% aqueous Eosin Y (1.75min), Water (3min), 100% Ethanol (1min), 100% Ethanol (1min), 100%

Ethanol (1min), Xylene (1min), Xylene (1min). Slides were mounted with with Di-n-butylphthalate (DPX) mounting media. Images were scanned on Hamamastu Nanoscanner S210 (Hamamastu) or imaged using Olympus BX51 (Olympus).

2.19 Osmium Tetroxide Staining

Osmium tetroxide staining was performed as previously described [234]. In brief, tibia were cleaned of soft tissue and fixed overnight in 10% neutral buffered formalin at room temperature. Formalin was washed off under running tap water and then decalcified for two weeks in 10% EDTA decalcification solution, with change of decalcification solution every three days. Bones were washed for 30min under running water and stained in 1% osmium tetroxide solution (AGR1022, Agar Scientific) for 48. Excesses osmium was removed by subsequent washing for more than 5-times in Sörensen's buffer (81mM KH_2PO_4, 19mM $Na_2HPO_4 \cdot 7H_2O$, pH∼7.4) over the course of several days. Stained bones were embedded in 1% agarose in cryovials. Bones were scanned on Quantum FX µCT machine (Perkin Elmer) at 90V, 200µA, FOV 20mm, scanning technique: 4.5min, capture size: small. Data was processed using Analyzer12.0 software. Thresholds were determined according to best discrimination of cortical bone and BMAT (BMAT: 5500-max; Bone: 3800-5499).

2.20 Cytokine analysis

Serum samples were harvested by cardiac puncture after mice had been killed and collected in BD Microtainer® blood collection tubes (365978, BD Bioscience). Blood samples were centrifuged for 1.5 minutes at 15,000g. Supernatant was collected and frozen in 50µL aliquots at -80°C until further analysis. Supernatants from mesenteric adipose tissue explants and serum samples were subjected to the LEGENDPlex™ Mouse Inflammation Panel (740446, Biolegend) for multiplexed cytokine analysis following manufacturer's instructions. Protocol was adapted to use half volumes. For subsequent measurements of adipose tissue explant cytokine secretion, IL-10 and TNFα was measured using TNFα Mouse Uncoated ELISA Kit (88-7324-86, Invitrogen) and IL-10 Mouse Uncoated ELISA Kit (88-7105-86, Invitrogen) following manufacturer's protocols.

2.21 Bone marrow-derived macrophage culture

Bones were harvested from mice and soft tissue was removed. Bone marrow from femur and tibia were flushed out into a sterile Petri dish with R_{10} (RPMI containing 10% FBS and 100U/ml Pen-Strep) using a 25G syringe. Bone marrow cells were strained through 40µm filter and centrifuged (5min, 400g, 4°C). Cells were resuspended in 1mL eBioscience™ 1x RBC lysis buffer (00-4333-57, Invitrogen) and incubated for 3min at room temperature. Cells were topped up with R_{10} and centrifuged (5min, 400g, 4°C). Cells were resuspended in 30mL R_{10} supplemented with a final concentration of 100ng/mL M-CSF (315-02, Peprotech) and split onto two non-adherent square plates (109-17, Thermo Scientific). Cells were fed after 72 hours with 5mL fresh R_{10} containing 400ng/mL M-CSF. Cells were fully differentiated at day 7. For macrophage polarization, cells were seeded at a concentration of 0.5-1x10^5 cells/well in a U-bottom 96 well plate in R_{10} containing 100ng/mL M-CSF. The next day, cells were adherent and washed. Macrophage polarization was induced in the indicated medium using the following cytokine: 100ng/mL M-CSF, 100ng/mL IFNγ (315-05, Peprotech), 100ng/mL LPS (L8274, Sigma), 20ng/mL IL-4 (214-14, Peprotech), 20ng/mL IL-13 (210-13, Peprotech). Generally, supernatants were harvested and cells were analysed 16h post-polarization start, if not otherwise indicated.

2.22 Statistical Analysis

Data were tested for normal distribution before using parametric or non-parametric tests. P-values were determined by unpaired Student's t-test or non-parametric Mann-Whitney test (for two group experimental setup). Comparison across more than two groups were performed by One-Way or Two-Way ANOVA with Tukey's multiple testing correction. Differences were considered statistically significant when $p<0.05$ (*$p<0.05$, **$p<0.01$, ***$p<0.001$, ****$p<0.0001$). Samples were typically pooled from several experiments, if not else indicated. Data points were pooled between experiments when control group was comparable between experiments. Data was typically not blocked for experiment, if not otherwise indicated, and therefore also includes inter-experimental variation. Data was presented as violin plots or as mean +/- standard error of the mean

(SEM). For statistical analysis of serum lipidomics, data was compared using linear regression model and subsequent multiple t-testing. Histopathology of colon sections was scored blinded by third-party experimenter (kind help by Dr. Mathilde Pohin). All experiments were performed in at least two independent experiments and data points were pooled, unless else indicated. Graphs were generated and statistics were calculated using GraphPad Prism 9 software, except for lipidomics and bulk RNA sequencing dataset, which were calculated using R software.

3 Experimental models to study autophagy in mature adipocytes

3.1 Introduction

This chapter will focus on the creation and validation of new experimental tools that will serve us subsequently as *in vitro* and *in vivo* models to study autophagy in mature adipocytes. While much is known about the importance of autophagy during adipogenesis, the role of autophagy in mature adipocytes remains unclear. In the following introduction, we highlight the current understanding of adipogenesis and strategies to target gene expression specifically in mature adipocytes.

3.1.1 Adipogenesis and the role of autophagy

Adipogenesis can be divided into two phases: the commitment phase of mesenchymal stem cells (MSC) to the adipogenic lineage forming fibroblast-like progenitor cells, called pre-adipocytes and the differentiation phase of these pre-adipocytes into round lipid-laden and terminally differentiated adipocytes [115]. Whilst the commitment of MSCs to the adipogenic lineage is thought to be influenced by extracellular matrix via WNT signalling, the terminal differentiation of pre-adipocytes depends on key transcription factors involved in the regulation of cellular lipid metabolism such as the activation of PPARγ and members of the C/EBP transcription factor family. To date, we differentiate several stages of terminal adipogenesis based on a variety of cell surface markers. In a seminal study by Berry and Rodeheffer, the loss of the surface marker CD24 distinguishes pre-committed adipocyte precursors and committed pre-adipocytes [246]. The authors could further demonstrate that pre-adipocytes express key transcriptions factors such as PPARγ and C/EBPs necessary for priming for adipogenic differentiation.

Autophagy plays a central role for the differentiation of many hematopoietic and mesenchymal cell types [82, 247]. In 2009, two landmark studies by Singh *et al.* and Zhang *et al.* were published demonstrating that autophagy is crucial for the development of

normal adipose tissue [116, 117]. Both studies used a transgenic mouse model to specifically delete essential autophagy genes in the adipogenic lineage. To target adipocytes, both studies used an adipocyte protein 2 (*Ap2*)-driven Cre recombinase system, a downstream target of PPARγ [248]. AP2 is today more commonly referred to as fatty acid binding protein 4 (FABP4), a protein expressed predominantly, but not exclusively, in adipocytes. Both studies revealed that *in vitro* deletion of *Atg7* or *Atg5* leads to reduced accumulation of intracellular TAG and expression of adipogenic marker genes including FABP4. *In vivo*, the loss of autophagy resulted in a dramatic decrease of white adipose tissue mass and a shift toward a more 'brown adipose tissue-like' cellular makeup characterized by accumulation of mitochondria and increased β-oxidation. In summary, these studies provided strong evidence for a central role of autophagy in the differentiation of white adipose tissue and its potential role in determining adipocyte phenotypes. Indeed, later studies confirmed that autophagy controls mitochondrial clearance in adipocytes and thus governs its metabolic state [106].

3.1.2 Overview of existing experimental models to study adipocytes *in vitro* and *in vivo*

Due to the crucial role of autophagy in adipogenesis, selection of the right molecular tools to study autophagy in mature adipocytes is crucial. Several comparative studies have investigated the best *in vivo* systems to target different cell types belonging to the adipogenic lineage [249, 250]. Due to a better understanding of the markers associated with adipocyte differentiation, we now know that the *Ap2-Cre* system, which was used initially, may have several potentially detrimental off-target effects. For instance, several *Ap2-Cre* mouse lines have shown *Ap2* to be highly expressed in endothelial cells [249]. On the other hand, new transgenic mouse lines based on mature adipogenic markers have been developed such as *Adipoq* for both constitutive as well as inducible experimental approaches [251, 226]. These mouse lines ensure that the gene deletion will occur after adipocyte differentiation. This is particularly important for this project in which we want to investigate for autophagy's role in mature adipocytes.

In vitro adipocytes are typically studied using established immortalized preadipocyte

cell lines such as the murine derived 3T3-L1 and ST2 cell lines. Alternatively, pre-adipocytes can be either isolated from primary adipose tissue or derived from murine embryonic fibroblasts. All of the methods mentioned above require further stimulation with agonists promoting adipogenic differentiation such as IBMX and dexamethasone which activate PPARγ and induce C/EBPδ and C/EBPβ [252, 253]. The addition of insulin into the differentiation media induces both lipogenesis and the growth of lipid droplets, as well as activation of cyclic AMP response element binding (CREB) proteins which are critical for adipogenesis [254, 255]. Previously, groups used siRNA or CRISPR technologies to delete genes from pre-adipogenic cell lines prior to their differentiation, however this may possibly impact on their adipogenic capacity. Using transfection approaches to delete or decrease gene expression are challenging in non-dividing cell types and have not been widely reported for differentiated adipocytes.

Lack of good *in vitro* adipocyte culture models have often posed issues in translating *in vitro* findings. Adipose tissue explant culture, though commonly used, show increased expression of hypoxia and inflammation markers, especially if in culture for more than 24 hours [256]. Until recently, there was no method that would allow long-term culture of fully differentiated mature adipocytes. However, the introduction of the membrane mature adipocyte aggregate cultures (MAAC) by Harms *et al.* allows the culture of human or murine adipocytes without changing their *in vivo* gene expression, whilst maintaining high viability [257]. MAAC provide possibilities to study interactions between adipocytes and immune cells closely mimicking *in vivo* conditions, although the impact of different medium conditions on this *ex vivo* crosstalk remains to be explored. Nevertheless, this method may prove particularly useful when culturing primary adipocytes from inducible transgenic mouse models.

3.1.3 Aim of this chapter

While the role of autophagy in pre-adipocytes is well-described [116, 117], the role of autophagy in mature adipocytes remains largely elusive. This was in part due to the lack of appropriate cellular and molecular tools to delete essential autophagy genes exclusively in mature adipocytes after they have fully differentiated. The aim of this

chapter was (1) to create the necessary biological tools to study autophagy in mature adipocytes, (2) to confirm that the transgenic constructs are expressed in the expected manner and (3) to validate that it will sufficiently inhibit autophagic flux.

3.2 Results

3.2.1 Establishment and validation of an inducible autophagy-KD adipocyte cell line

To prevent unwanted off-target effects of autophagy loss during adipogenesis, we started to investigate possibilities to inducibly knock-down essential proteins involved in the autophagic machinery. Interference RNA (RNAi) technologies are based on the evolutionary conserved mechanism of posttranscriptional regulation of messenger RNAs. We took advantage of plasmids and protocols from Prof. Johannes Zuber using their improved 'miR-E' system [235]. In order to create a cell line model that would not interfere with normal adipogenesis, we chose a lentiviral backbone with a tetracycline/doxycycline-inducible cassette, which was named LT3REVIR based on the original publication (Fig.7A). Addition of this cassette would ensure that we could induce the repression of autophagy-related genes by the addition of doxycycline to the medium once the cells have fully differentiated. Based on results from Ebner *et al.* [236], which was using a very similar expression vector, we obtained a list of candidate sequences available targeting known essential autophagy proteins. Based on the results of the screening (data not shown), we settled on two stem sequences for each of the two target transcripts *Atg7* and *Atg5* (Fig.7B). Whilst the shRNA targeting *Atg5* are both located at the 3' end of the transcript on the same exon, the *Atg7* shRNAs are located on different exons (Fig.7C). In particular, *shAtg7-700* targets *Atg7* by spanning over two exons. Using the restriction enzyme sites XhoI and EcoRI, we cloned the constructs and validated the resulting clones by enzymatic digestion and plasmid sequencing (data not shown). After the plasmid sequence was confirmed, we packaged the plasmid in lentiviruses and transduced in ST2 or 3T3-L1 cells as shown in Fig.7D. Using a multiplicity of infection (MOI) smaller than 1 reduced the likelihood of multiple integrations of viral DNA into the genome of the same cell. Cells were sorted according the stable expression of the

fluorescent protein mVenus. Bulk sorted cells were collected and expanded before use for subsequent analysis. Using bulk sorted cells, in comparison to clonally expanded cell lines, ensure that off-target effects based on the integration site are minimised, however at the same time increases heterogeneity of the sorted cell lines. In the end, we established five new cell lines per parental line either targeting a non-endogenous control transcript (*shRenila* (*shRen*)), the essential autophagy-related gene *Atg7* (*sh131*, *sh700*) or *Atg5* (*sh1036*, *sh1389*).

We next sought to test the cell lines by titrating the doxycycline concentration necessary to induce deletion of autophagy in the cells. First, we used the constitutive expression of mVenus in non-differentiated 3T3-L1 and ST2 cells as proxy for equal integration of the lentiviral construct into our cell lines. Indeed, we observed that mVenus expression among all mVenus$^+$ cells were comparable for both 3T3-L1 and ST2 cells (Fig.8A). Next, we could approximate the expression of the shRNA by measuring the expression of dsRED in undifferentiated ST2 cell upon doxycycline treatment using flow cytometry. Prior to doxycycline administration, no expression of dsRED was observed, suggesting that the integrated construct is tightly regulated and does not cause unwanted shRNA expression (Fig.8B). In contrast, administration of just 0.5µg/mL doxycycline elicited a strong increase in dsRED expression indicating the expression of the adjoining shRNA. More interestingly, the cells seem to express comparable amounts of dsRED independent of the dose of doxycycline (Fig.8C). However, we observe that the cell line constructs *sh131* and *sh700* are expressing higher amounts of dsRED in comparison to the other cell lines after 3 days of doxycycline treatment. These differences remain after 5 days of culture with doxycycline (Fig.8C,F). The relatively lower dsRED expression in *shRen* and *sh1389* could be explained through construct integration into heterochromatic structures leading to lower accessibility of the construct locus and reduced shRNA expression. In addition to measuring the levels of dsRED per cell, we observe that increasing concentrations of doxycycline are leading to increasing fraction of cells being positive for dsRED (Fig.8D) after 3 days. This reaches a plateau at a concentration of approximately 2µg/mL. However, a further increase in the percentage of dsRED expressing

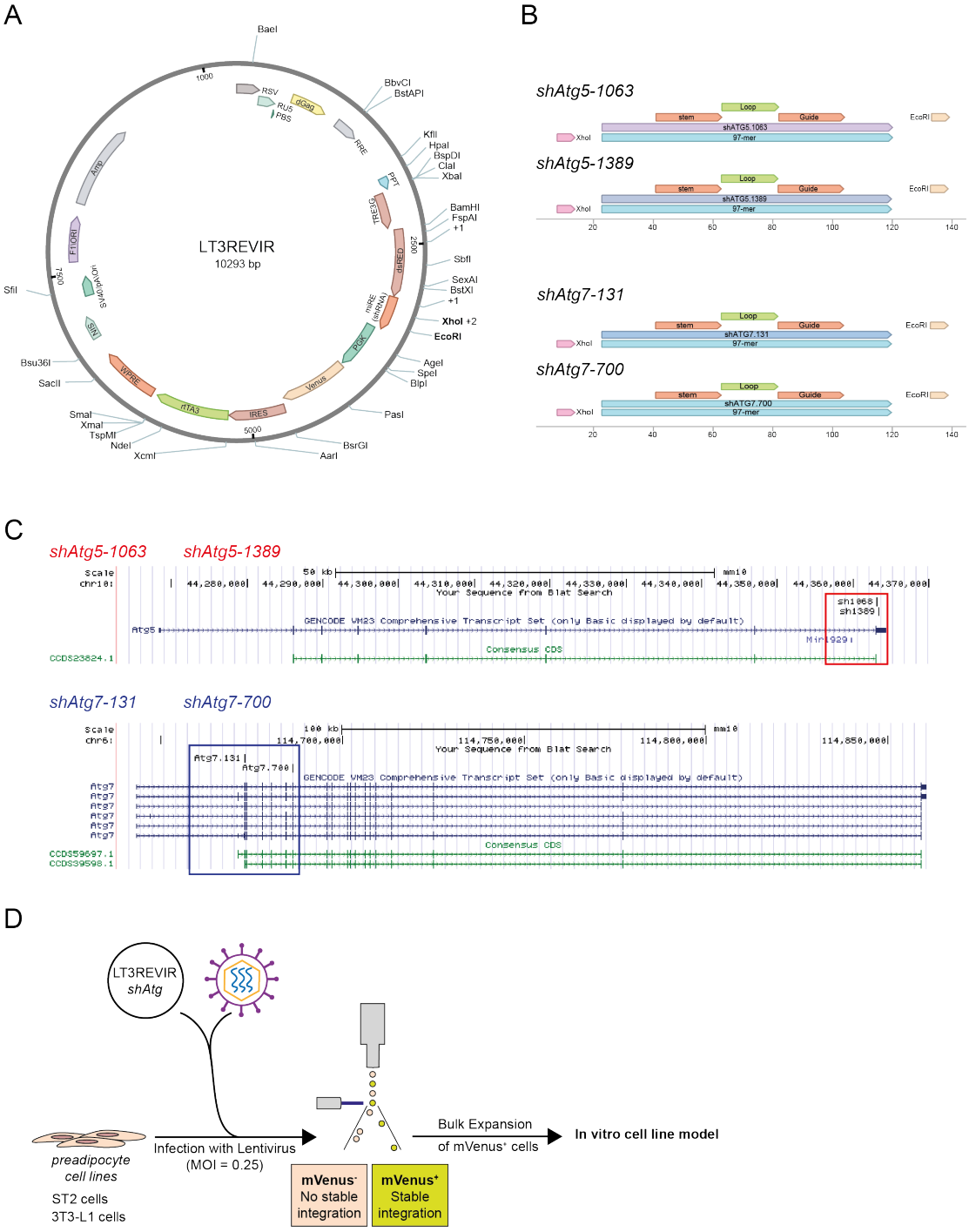

Figure 7: Overview of cell line construction. (A) Vector map of the doxycycline-inducible, lentiviral shRNA construct (kind gift from Prof. Johannes Zuber [235]). (B) Schematic representation of the four shRNAs targeting either *Atg5* or *Atg7* and additional restriction enzymes sites for integration into vector. (C) BLAT alignment of shRNA stem sequence to mouse genome shows specificity and location of stem sequence to transcripts. (D) Pre-adipocyte cell lines ST2 and 3T3-L1 were transduced with an MOI = 0.25 before FACS-sorted selection of mVenus$^+$ cells indicating lentiviral integration.

cells could be observed over a time course of 5 days (Fig.8D,E). Based on results of this experiment, we learned that we can effectively induce our transcript at a concentration of 2µg/mL doxycycline over a time course of approximately 4 days.

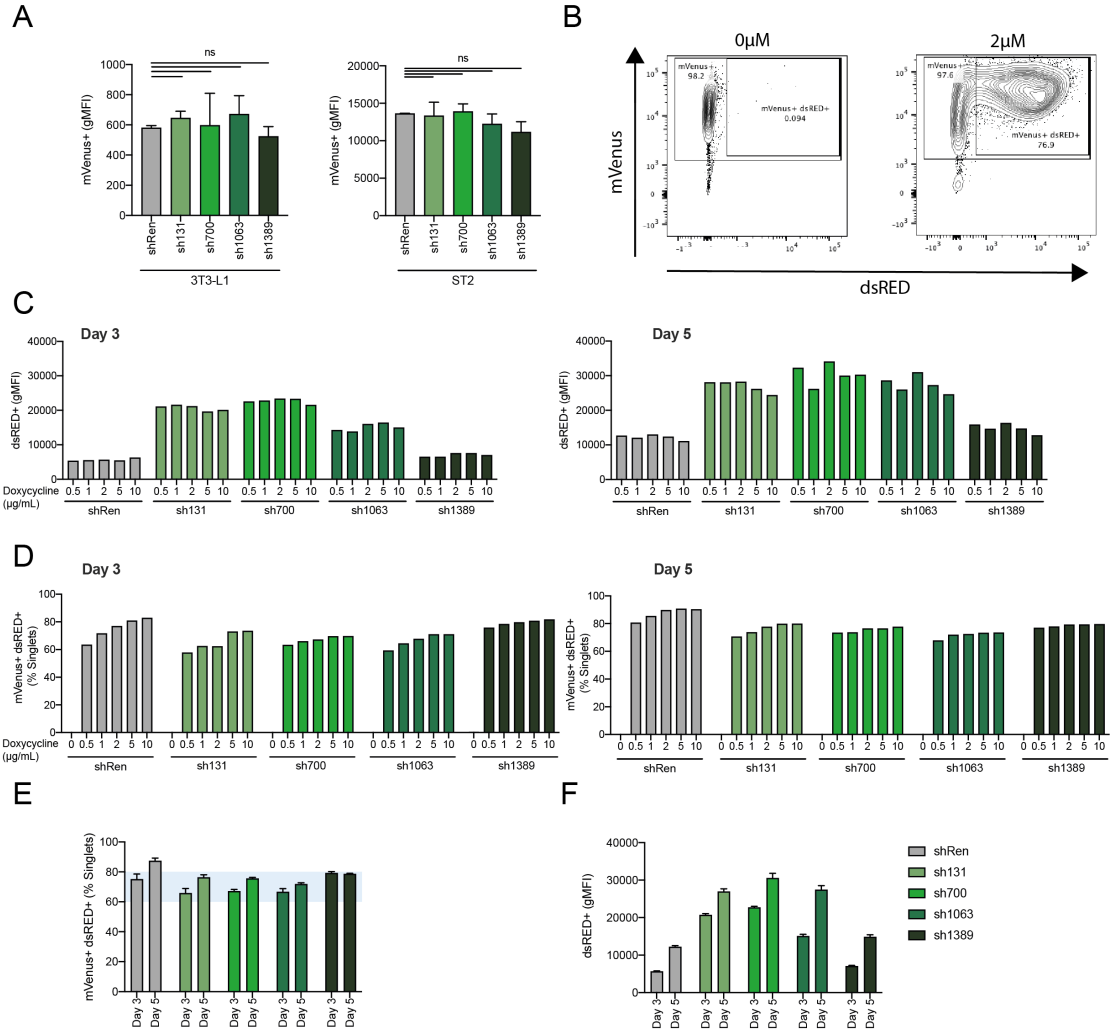

Figure 8: Lentiviral shRNA construct is tightly regulated and leads to strong and persistent induction of the construct after 5 days of doxycycline treatment. (A) Expression of mVenus measured in all mVenus expressing cells across the constructs. (n=2-3). Statistical analysis by One-Way ANOVA. (B) Representative FACS plots (taken from *shRen* – Day 5) showing that dsRED, a proxy for shRNA expression, is not expressed prior to doxycycline treatment and efficient shRNA expression upon doxycycline treatment. (C) Quantification of dsRED signal in all mVenus$^+$ dsRED$^+$ expressing cells shows that cells are expressing the inducible part of the shRNA to a different extent. That can only partially be recovered over time. (n=1) (D) Dose-response of dsRED-expressing mVenus$^+$ cells to increasing concentrations of doxycycline. From this data it seems that 2µg/mL is sufficient to reach plateau response in the cells. (n=1) (E) Summary of all cell lines (independent of their doxycycline concentration) shows that cell lines express/accumulate more dsRED fluorescent protein after 5 days of doxycycline treatment compared to 3 days. (n=5) (F) Summary of dsRED expression taken together all concentrations. *sh131*, *sh700* and *sh1389* are not showing much stronger dsRED expression anymore after day 3. (n=5))

We finally sought to validate our cell lines by evaluating their capacity to suppress the expression of *Atg5* and *Atg7* transcripts and proteins. For this, we optimized our protocol as shown in Fig.9A. As the shRNA is targeting specifically *Atg5* or *Atg7* transcripts to prompt them for degradation, we measured *Atg5* and *Atg7* transcript levels after 4 days of doxycycline treatment. We observed an efficient decrease of *Atg5* transcript levels (right panel, Fig.9B). In contrast, the KD efficiency of *sh131* and *sh700* was more variable with *sh131* showing increased capacity to reduce *Atg7* transcript levels (Fig.9B). We next assess the impact this KD has on ATG5 and ATG7 protein levels. We found that the reduction in ATG5 and ATG7 protein levels were most pronounced by *sh131* and *sh1389* targeting *Atg7* and *Atg5*, respectively (Fig.9C). We next assessed the potential of the cell lines to inhibit the autophagic flux by measuring the accumulation of LC3-II upon lysosomal inhibition using Bafilomycin A1 (BafA1). Unfortunately, we were unable to detect any significant differences in autophagic flux despite the overall reduction of ATG5 and ATG7 by their respective shRNAs. Preliminary data from experiments under starvation conditions did also not yield any significant changes in autophagic flux (data not shown). Of note, we also observed that adipogenesis varied between the clones as measured by the presence of ADIPOQ in Western Blot analysis (Data not shown). This may be explained by the differences in the genetic drift of the FACS-sorted population during cell expansion. We therefore recommend for future experiments to compare to the non-doxycycline treatment group for each cell lines since the differentiation stage (the ratio of differentiated vs. non-differentiated adipocytes) may have an impact on the overall autophagic flux observed in the culture dish.

Overall, our data show that we have created cell lines that can be efficiently knocked down for autophagy regulated genes on both transcript and protein level. However, the shRNA-mediated KD is still not profound enough to abrogate the autophagic flux in this experimental setting. Hence, we refrained from including the cell line in further mechanistic and cellular investigations in this study. Despite this rather discouraging result, we hope that other cell lines, derived from the well-known murine pre-adipocyte cell line 3T3-L1, may show better KD efficiency and inhibition of overall autophagic flux. Characterization of these 3T3-L1-derived cell lines is ongoing work carried out by

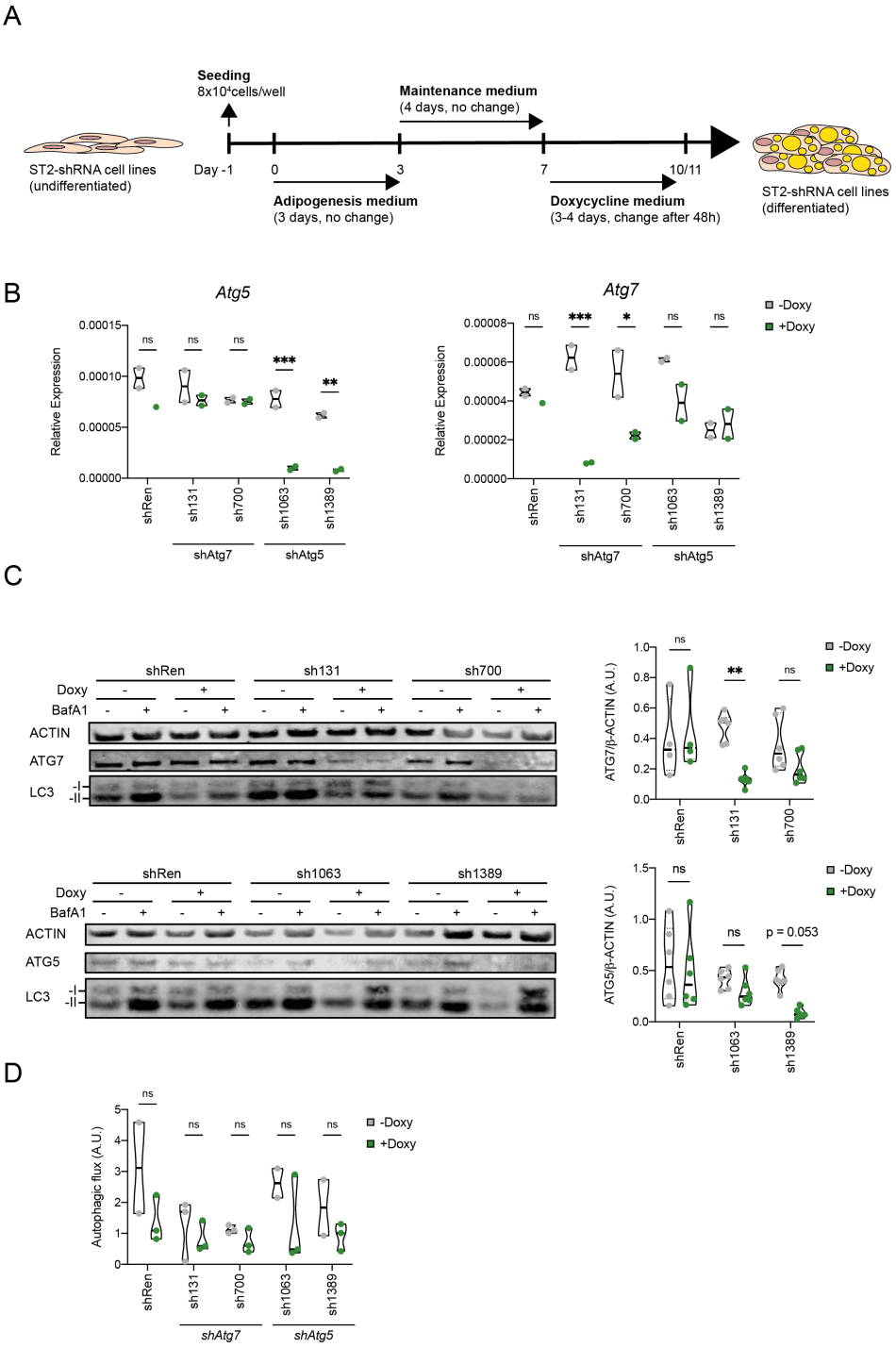

Figure 9: Assessment of KD efficiency in ST2 cell constructs. (A) Schematic overview of the differentiation protocol of ST2 cells with subsequent induction of shRNA expression by doxycycline treatment (2µg/mL). Doxycycline treatment was refreshed after 48 hours at a final concentration of 2µg/mL. (B) Expression of *Atg5* or *Atg7* transcript at 4 days post-doxycycline administration. (C) Western Blot and quantification analysis of ATG5 and ATG7 protein levels at 4 days post-doxycycline administration. (D) Quantification of autophagic flux as shown representatively in panel C. Statistical analysis by Two-Way ANOVA. Experiments in this figure were performed by and data is courtesy of Paula Hahn.

another DPhil student in our lab.

3.2.2 Establishment and validation of an inducible adipocyte-specific KO mouse model

We next sought to establish an animal model to study autophagy in mature adipocytes. From the literature we predicted that the best candidate for our purposes may be the *Adipoq*-driven Cre (*Adipoq-Cre*) recombinase system, as it is reported to target specifically mature adipocytes. Thus, we would circumvent unwanted effects during adipocyte differentiation. To validate, that the *Adipoq-Cre* system is the most appropriate for our purposes, we sought to understand the expression of the adipocyte maturity marker ADIPOQ relative to the dynamics of autophagic flux during adipocyte differentiation. During adipogenesis, ST2 cells are slowly losing their fibroblastic shape and become more rounded. The strongest cell morphological changes occur from day 4 to day 6 during this time, differentiating ST2 cells start accumulating intracellular lipids in form of multiple lipid droplets (Fig.10A). This morphology is common for differentiating ST2 cells. We confirmed that the intracellular vesicles are indeed lipid droplets by Oil Red O staining (Fig.10A). Every two days, we measured the autophagic flux and found that the accumulation of LC3-II is the strongest around day 4 and therefore just preceding the accumulation of lipid droplets in the cytoplasm. In addition, the appearance of lipid droplets in differentiating ST2 cells coincides the increase of ADIPOQ expression in the cells at day 4 and 6 (Fig.10B,C). The data indicates that the autophagic flux mostly precedes the increase in the adipogenic maturity marker ADIPOQ. As the decrease of autophagic flux and the increase ADIPOQ expression seem to be connected, we could not exclude the possibility that *Adipoq-Cre* driven deletion of autophagy impairs the differentiation potential of pre-adipocytes *in vivo*. Furthermore, it remains unclear if adipogenic differentiation *in vivo* follows a similar dynamic as in this *in vitro* model.

Adipoq-Cre systems are described to be very specific to adipose tissues [249]. To confirm this data, we evaluated the expression of both *Adipoq* transcript and ADIPOQ protein levels in various mouse tissues. We found that *Adipoq* was indeed specifically expressed in subcutaneous and visceral adipose tissues, but not in the spleen or the

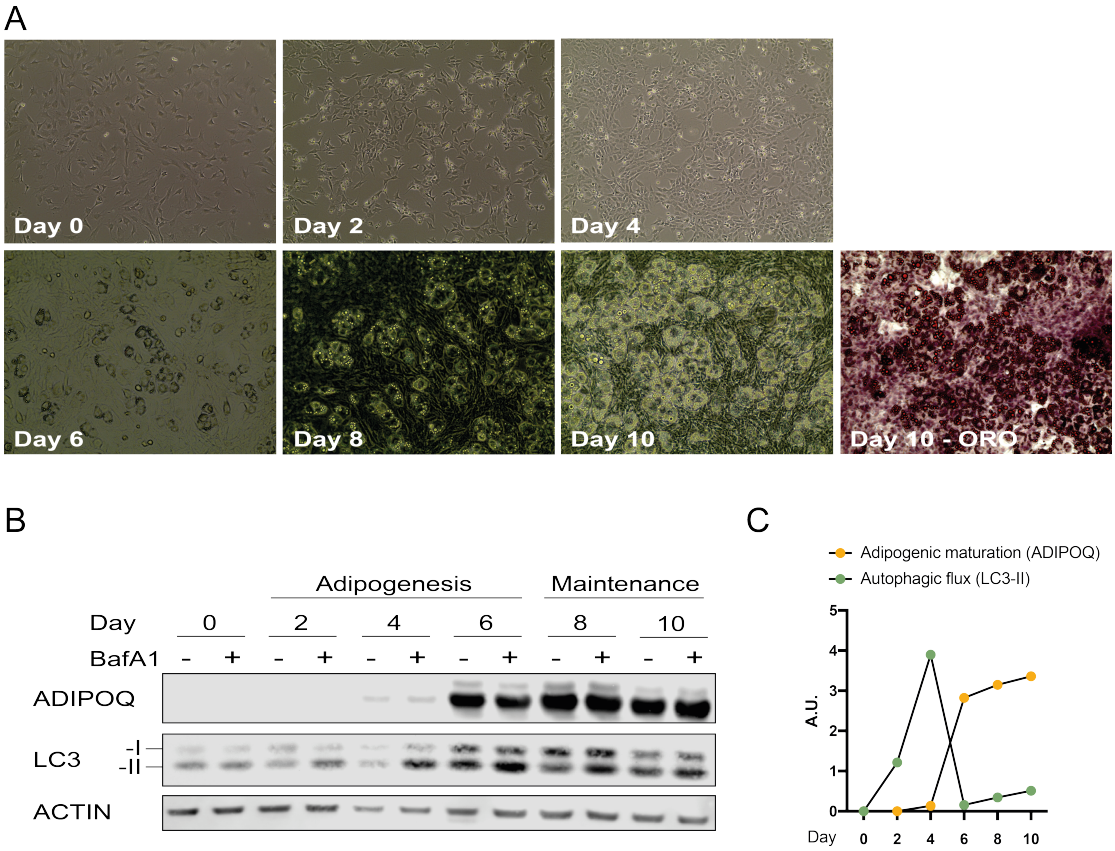

Figure 10: Increase of autophagic flux mostly proceeds expression of ADIPOQ during adipogenesis in ST2 cells. (A) Cells were assessed by brightfield microscopy every two days, showing characteristic morphological changes such as expansion of the cytoplasm and accumulation of intracellular lipid droplets over the course of differentiation. Presence of intracellular lipid droplets was confirmed by Oil Red O staining at the end of the differentiation protocol. (B) Western Blot of autophagic flux bases on accumulation of LC3-II band during lysosomal inhibition through the administration of BafA1 (100nM). Measurement of the expression of ADIPOQ during adipogenesis. (C) Semi-quantitative analysis of ADIPOQ protein expression and autophagic flux (as LC3-II signal of ((+Baf cond.)-(-Baf cond.))/(-Baf cond.)) shown in panel B. (n=1)

liver (Fig.11A). This was validated on protein levels showing ADIPOQ expression only in peripheral adipose tissues (Fig.11B). To ensure that *Adipoq* is not expressed in any off-target cells or adipogenic precursors, we used tissue transcriptomic datasets from Tabula Muris [258] (Fig.11C). Tabula Muris is a compendium of several single cell RNA (scRNAseq) datasets of a large variety of mouse organs. This resource allows for detailed transcriptional investigation in the expression of a gene of interest in various cell types present in different tissues. Here, we employed the adipose tissue scRNAseq dataset to explore the expression of *Adipoq* in adipose tissue stromal cells. Importantly, no expression of *Adipoq* was detected in various adipose tissue resident immune cells (incl. B cells,

T cells, myeloid cells and NK cells). Some limited expression could be observed in very few cells in the endothelial compartment. Interestingly, the lack of *Adipoq* expression in MSCs suggested that adipogenic precursors may not express this gene. We further looked at the expression of *Adipoq* in bone marrow adipocytes and found that these cells would be similarly targeted by the *Adipoq*-driven recombinase system (Fig.11D) confirming reports of bone marrow adipocytes as a major source for ADIPOQ [259]. Overall, this data suggest that an *Adipoq-Cre* system is a good candidate to use for adipocyte-specific deletion of autophagy.

To ensure that adipose tissues can develop normally, we decided to use a tamoxifen-inducible *Adipoq*-driven (*Adipoq-Cre*^{ERT2}) system created by Sassmann *et al.* rather than a constitutive system allowing more spatio-temporal control of the genetic deletion [226].We decided on a mouse model that expresses the Cre recombinase from a bacterial artificial chromosome (BAC) to ensures that endogenous gene expression remains undisturbed (Fig.12A). In classical mouse models, the recombinase is integrated into the endogenous gene locus and thus impairing gene expression from at least one of two alleles. Disruption of the endogenous gene locus, depending on the gene, can have significant impact on the phenotype observed and can be circumvented by using a BAC.

To make sure we would be able to track our transgene through various mouse generations, we first setup a new genotyping protocol based on two primer pairs suggested by Charles River. The first primer pair (22926+22925) anneals to the transgene. More specifically, the reverse primer 22925 specifically recognizes an intron region in the *Adipoq* genomic region, whereas the forward primer is located in the *Cre* recombinase coding sequence (Fig.12A,B). As a positive control for the genotyping, the primer pair 21175 and 21173 anneals to the coding sequence of the metabolic gene *Gapdh* (Fig.12A,B). After improving cycling conditions, we established a genotyping protocol that simultaneously amplifies both loci leading to two distinct fragments corresponding to either the transgene (272bp) or the positive control *Gapdh* (175bp) (Fig.12C). This protocol was subsequently used to verify genotypes of experimental animals and breeding.

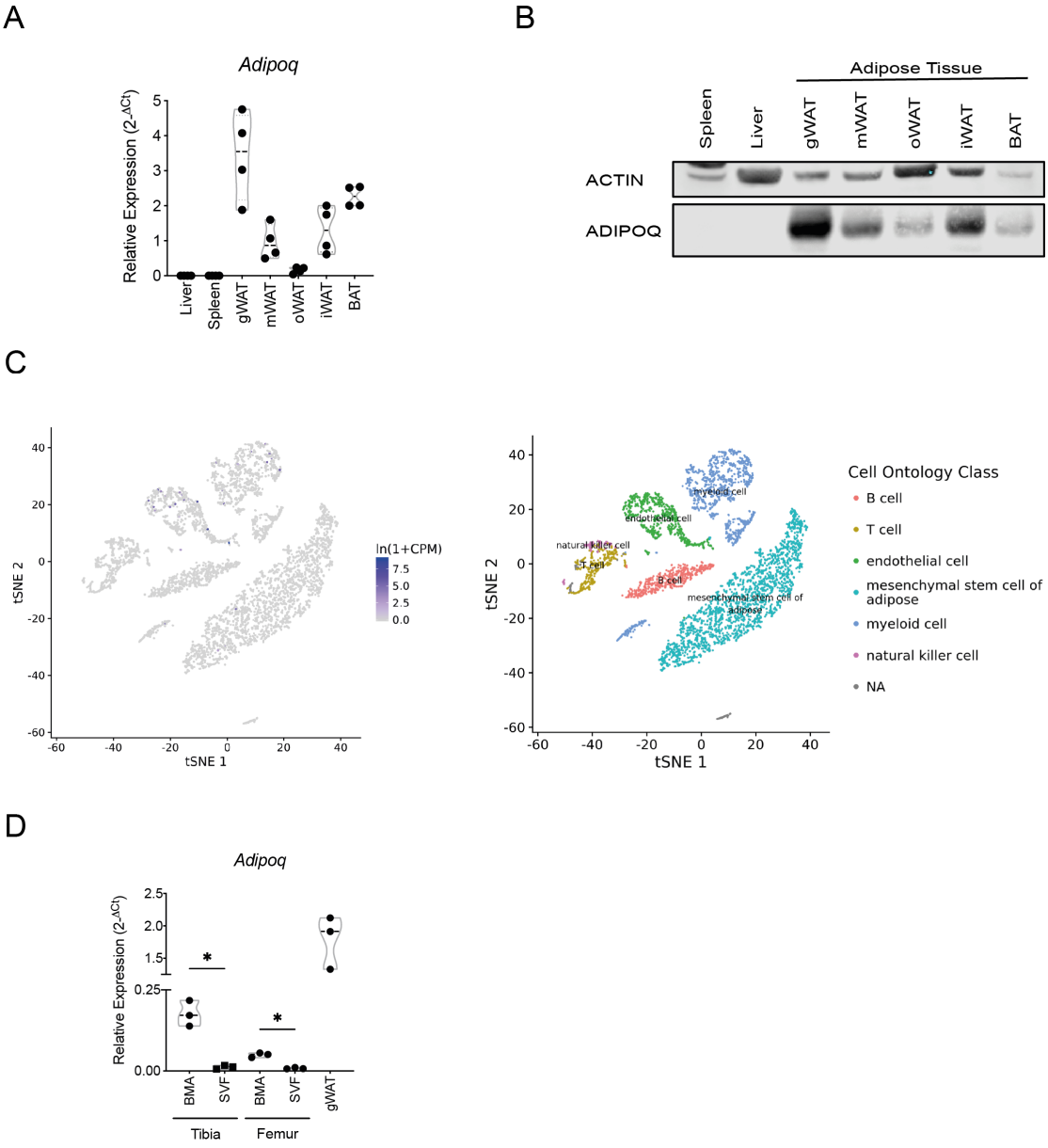

Figure 11: Adiponectin shows adipose tissue-specific gene expression and seems to be predominantly present in mature adipocyte. (A) Gene expression of *Adipoq* was evaluated using whole tissue RNA from spleen, liver, gonadal white adipose tissue (gWAT), mesenteric white adipose tissue (mWAT), omental white adipose tissue (oWAT), inguinal white adipose tissue (iWAT) and brown adipose tissue (BAT). (n=4) (B) Western blot analysis of ADIPOQ protein expression in the same tissues. (C) Single cell transcriptomic data from Tabula Muris (`https://tabula-muris.ds.czbiohub.org`) was used to identify *Adipoq* expression in various adipose tissue stromal cell populations including immune cells. Abundance of *Adipoq* transcript levels (left panel) were presented in identified adipose tissue cell subsets (right panel). (D) Expression of *Adipoq* transcript in bone marrow adipocytes (BMA) and stromal vascular fraction (SVF) after isolation according to Fan *et al.* [260]. (n=3) Statistical analysis by Two-Way ANOVA (excluding gWAT as positive control).

To study the leakiness and specificity of the recombinase system *in vivo*, we next crossed the *Adipoq-Cre*^{ERT2} mouse with a reporter mouse to obtain a mouse model that expresses

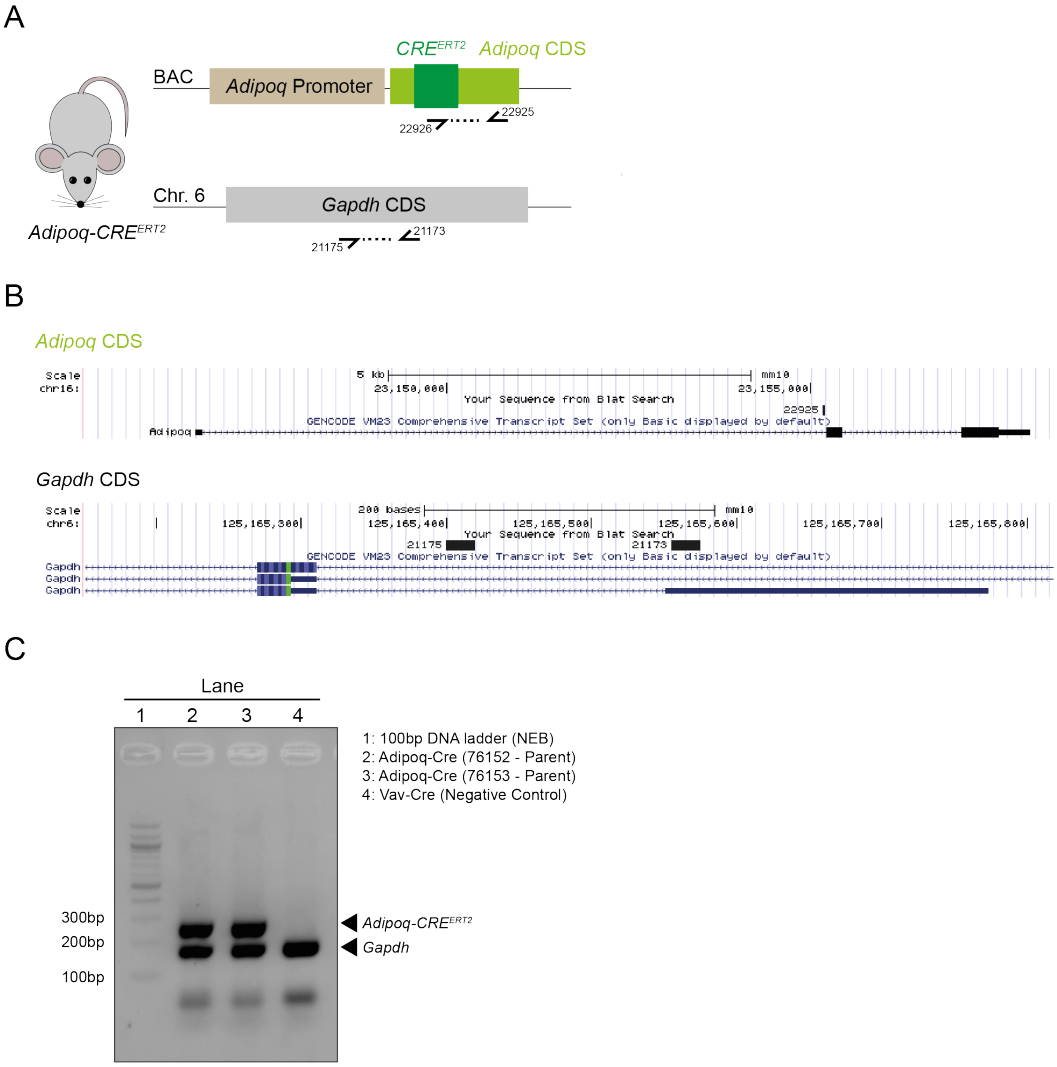

Figure 12: Genotyping of *Adipoq*-driven Cre recombinase mice. (A) Schematic overview of transgene design. The transgene Cre^{ERT2} recombinase is located under the control of the *Adipoq* promoter on a bacterial artificial chromosome (BAC), hence all endogenous gene loci are not affected by the transgene. (B) Schematic overview of primer binding sites. Two primers (22926+22925) target the *Adipoq-Cre*^{ERT2} transgene, whereas the other primer pair (21173+21175) is a positive control amplifying the endogenous GAPDH locus. (C) Example of genotyping results obtained for *Adipoq-Cre*^{ERT2}. Expected sizes for the fragments for the transgene are 272bp and for the internal positive control GAPDH 175bp. Fragments were resolved on a 2% agarose gel. Representative blot for many independent experiments (N>10).

the fluorescent protein tdTomato in cells upon recombination (Fig.13A). We observed that mice that were genotyped as Cre^{+} show a low expression of the fluorescent reporter when compared to Cre^{-} mice, even prior to tamoxifen administration (Fig.13B, upper two rows). This low fluorescent signal is heterogenous and detailed analysis shows that it seems some individual adipocytes show stronger tdTomato expression than others (Fig.13C). Upon administration of tamoxifen, we, however, observe a clear increase in

fluorescence in the adipose tissue (Fig.13B, third row), whereas off-target organs such as liver, spleen and lungs did not show any fluorescence indicating that the recombination was restricted to the adipose tissue. As our aim is to study the impact of autophagy-deficient adipocytes on immune cells, we wanted to make sure that the recombinase is not recombining in blood immune cells. We therefore bled mice two weeks post-tamoxifen treatment and measured the expression of tdTomato in blood immune ($CD45^+$) cells. We found no off-target expression in *Adipoq-Cre*^{ERT2} mice (Fig.13D), whilst mice from the ubiquitously expressed *Rosa-Cre*^{ERT2} were recombined in all tissues (data not shown).

Lastly, we wanted explored whether this mouse model shows off-target expression in different stromal cell types found in adipose tissues. To check for the stickiness of td-Tomato released during the tissue digestion process, we included Ter119, an erythrocyte marker, as a proxy for stickiness in the flow cytometry panel. Interestingly, cells with high tdTomato signal coincided with cells for Ter119 (Fig.14A) as shown in the color plot (second row). In contrast, immune cells isolated form mesenteric lymph nodes were negative for tdTomato expression and Ter119 (data not shown). This suggested that during adipose tissue digestion tdTomato may be released from dying adipocytes and stick to immune cells. After gating on $Ter119^-$ ('non-sticky') cells, we found that the strongest off-target tdTomato expression was present in endothelial cells ($CD31^+$) and barely any expression in immune cells (Fig.14B). The increased tdTomato signal in endothelial cells may be partially explained through increased autofluorescence in comparison to other cell types. Another explanation may be that these cells seem to be more 'sticky' in comparison to the other tested cell types. However, as also previously observed in the scRNAseq data from Tabula Muris (Fig.11C) some endothelial cells may actually be expressing *Adipoq*. On the other hand, we observed only very limited expression of tdTomato in pre-adipocytes or adipocyte precursor cells indicating that recombination in the tissue may indeed be limited to mature adipocytes rather than progenitor populations (Fig.14C), confirming that this model is optimal for our subsequent studies.

We further confirmed that the expression of tdTomato occurs in mature adipocytes by

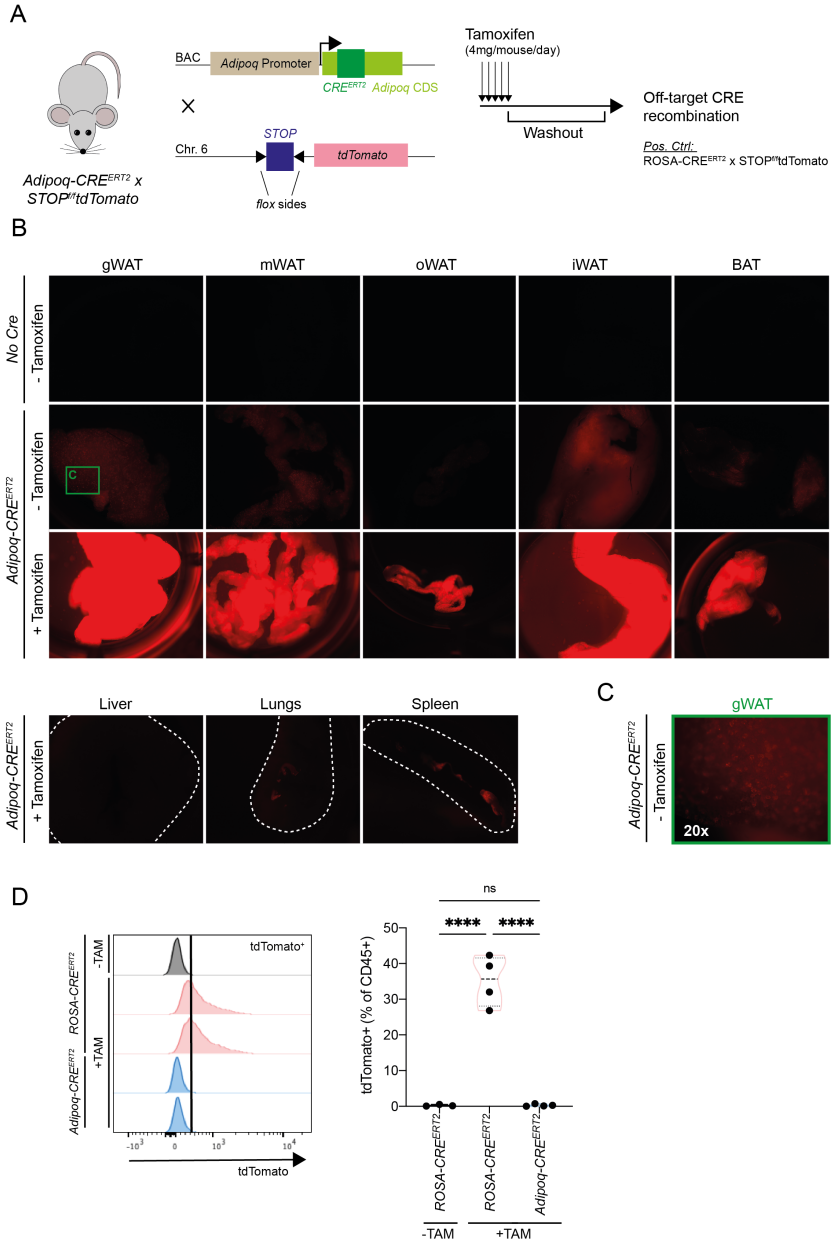

Figure 13: *Adipoq-Cre^{ERT2}* is adipose-tissue specific but shows minor leakage prior to tamoxifen administration. (A) Schematic overview of reporter mouse model. Administration of tamoxifen will lead to translocation of the Cre recombinase into the nucleus and excise the stop codon in front of the tdTomato reporter leading to its expression. (B) Stereo-fluorescence microscopy shows increased tdTomato expression prior to tamoxifen administration in mice genotyped as Cre^{+} when compared to Cre^{-} controls. However, tamoxifen administration strongly increases the expression of tdTomato. At the same time, no off-target expression of the recombinase could be observed in liver, lungs and spleen. gWAT: gonadal white adipose tissue, mWAT: mesenteric white adipose tissue, oWAT: omental white adipose tissue, iWAT: inguinal white adipose tissue, BAT: brown adipose tissue. (C) Magnified look at single recombined tdTomato^{+} adipocytes in gonadal white adipose tissue. (D) Expression of tdTomato in CD45^{+} circulating blood immune cells. (n=3-4). Statistical analysis by One-Way ANOVA. Representative for two independent experiments (microscopy) and one experiment (FACS).

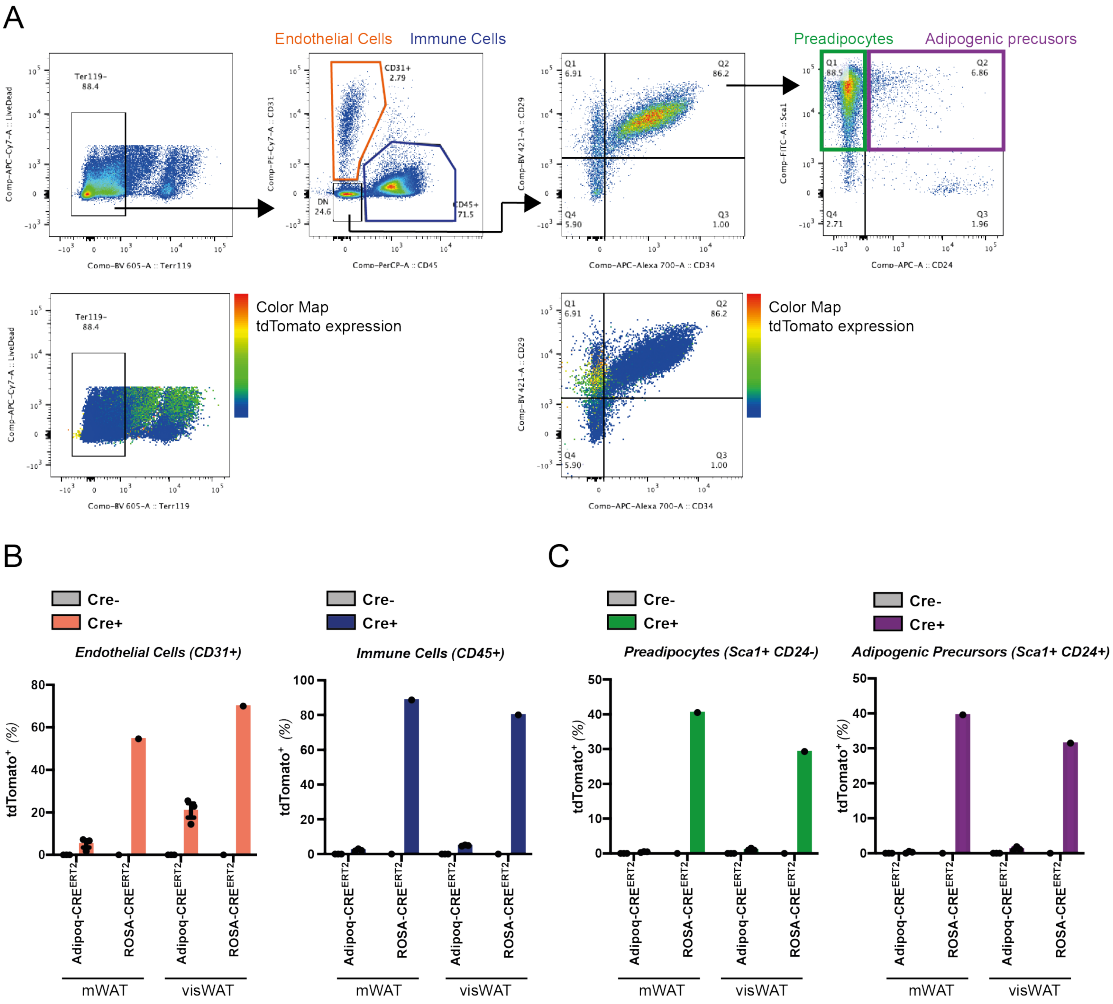

Figure 14: *Adipoq-Cre*^{ERT2} has some off-target expression in adipose endothelial cells. (A) Gating strategy of different stromal and immune cell populations isolated from adipose tissue based on Chau *et al.* [261]. (B) Some endothelial cells (CD31$^+$) are expressing tdTomato signal using the *Adipoq-Cre*^{ERT2} mice, whereas only minor tdTomato expression was observed in immune cells. (C) Expression of tdTomato in adipocyte progenitors was mostly absent from *Adipoq-Cre*^{ERT2} reporter mice. (n=1 (*ROSA-Cre*^{ERT2}), n=3 (*Adipoq-Cre*^{ERT2})). Data representative for two independent experiments.

co-staining with the lipid droplet protein PLIN1 (Fig 15A). We then wanted to exclude the possibility of unwanted expression of the recombinase in intestinal tissues that would cause concerns for using intestinal models of inflammation. For this we purpose we took frozen sections from either mWAT or colonic lamina propria (cLP) and only observed recombination in the mWAT but no recombination in the intestine of *Cre*$^+$ animals (Fig.15B).

In summary, the data supports the notion that the recombinase is expressed specifically in mature adipocytes. We could not observe any off-target expression in blood immune

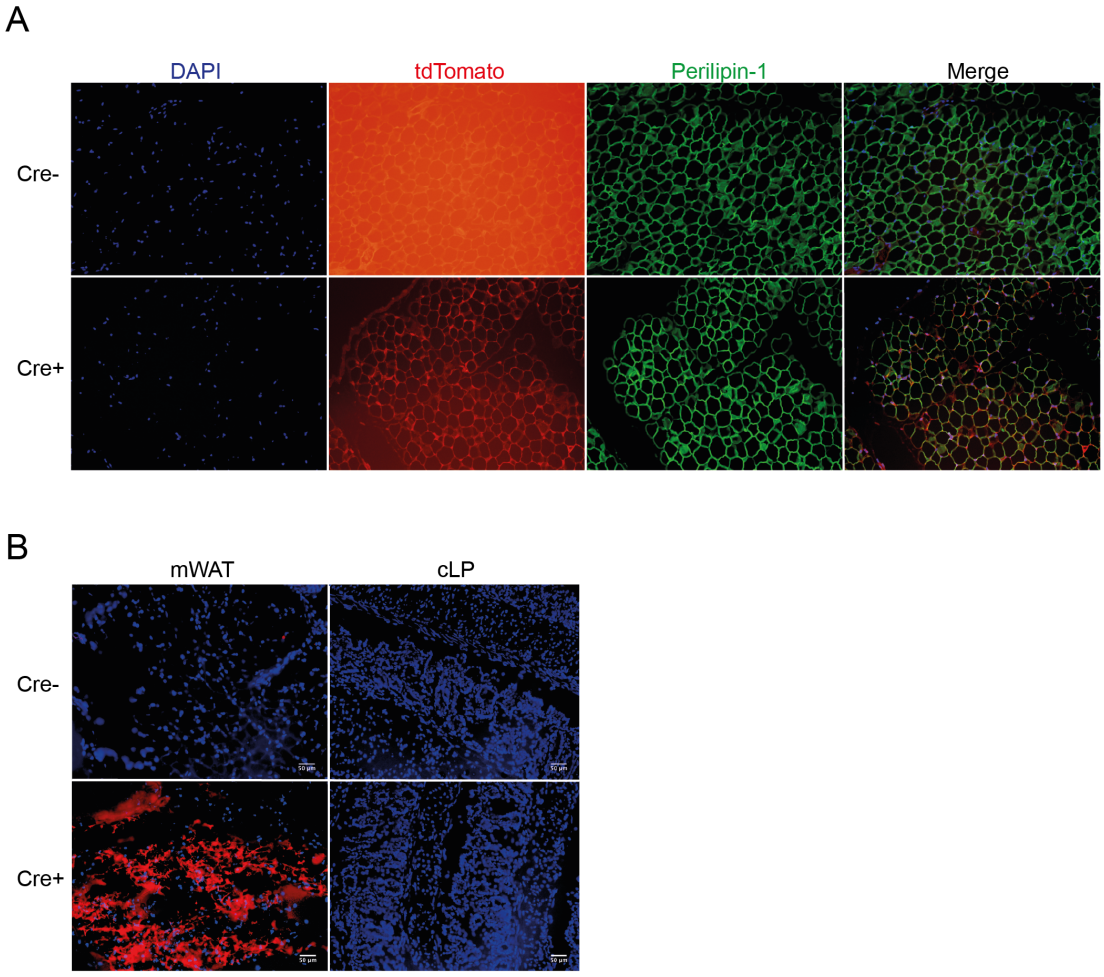

Figure 15: *Adipoq-Cre*^{ERT2} shows expression in predominantly mature adipocytes and is not expressed in the intestine. (A) Immunofluorescence microscopy of paraffin-fixed gWAT with co-staining for nuclear DNA using DAPI and lipid droplet structures using PLIN1. (n=3) Data from one independent experiment. (B) Expression of tdTomato in cross-sections of mWAT and cLP. (n=3). Data from one independent experiment.

cells or adipose tissue stroma, except potentially endothelial cells. This signal, however, may be an artefact introduced by the digestion process and further analysis will be required to exclude recombination in endothelial cells using the *Adipoq-Cre*^{ERT2} system. No off-target expression was detected in the intestine. Our data raised the concerns of a potential leakiness of the recombinase prior to tamoxifen administration which could lead to premature gene excision (Fig.13C). Based on this observation, we need to check for any unwanted recombination events in adipocytes prior to tamoxifen administration.

Next, we sought to examine the efficiency of deleting the essential autophagy gene *Atg7* in mature adipocytes using the *Adipoq-Cre*^{ERT2} driver. For this, we crossed mice with

the *Adipoq-Cre*^{ERT2} recombinase drive with mice containing floxed *Atg7*. The floxed sites are located around exon 14, which encodes the active site of the enzyme [227]. Administration of tamoxifen will therefore excise exon 14 from the genome and lead to the loss of ATG7 protein expression (Fig.16A). To evaluate the efficiency of genomic deletion, we extracted the whole DNA from gonadal adipose tissue of mice that were treated with tamoxifen. Next, we ran a PCR with primers annealing to the floxed site of *Atg7*-exon14. By identification of the fragment length, we could determine whether the allele was still floxed, excised or completely wild-type. We found that only upon administration of tamoxifen, the gene was efficiently excised from the genomic locus providing a partial deletion in mice that were previously genotyped as heterozygous and a complete deletion in mice that were identified as floxed homozygous mice (Fig.16B). Next, we sought to identify whether tamoxifen leads to a decrease in *Atg7* transcript levels. We first used semiquantitative measurements using reverse PCR and solved the amplified transcript fragment on a 1% agarose gel. We found that an approximately 50% reduction in *Atg7* transcript levels in comparison to tamoxifen-treated wild-type controls in whole tissue RNA lysates (Fig.16C).

As these lysates also contain RNA from other 'non-adipocyte' cell types found in adipose tissues, we aimed to improve our analysis by digesting the adipose tissue first and collect the floating adipocytes after low-speed centrifugation. The collected floating fraction is enriched in adipocytes and no apparent contamination could be detected under light and fluorescence microscopy according to their morphology (data not shown). Using this fraction, we extracted the RNA and measured *Atg7* transcript levels using qRT-PCR. We observed a >80% reduction in *Atg7* transcript levels upon tamoxifen treatment (Fig. 16D). In contrast, prior to tamoxifen treatment no reduction in expression levels were noted. Lastly, we quantified ATG7 protein levels in whole tissue lysates and found that ATG7 was indeed efficiently reduced (Fig. 16E). Semiquantitative analysis revealed about 50% reduction on protein level corroborating the reduction of *Atg7* transcript levels in whole tissue lysates in figure panel C. In summary, our data demonstrates efficient excision of the floxed *Atg7* locus and reduction of *Atg7* transcript and protein levels. We observed no major changes of *Atg7* transcript levels prior to tamoxifen

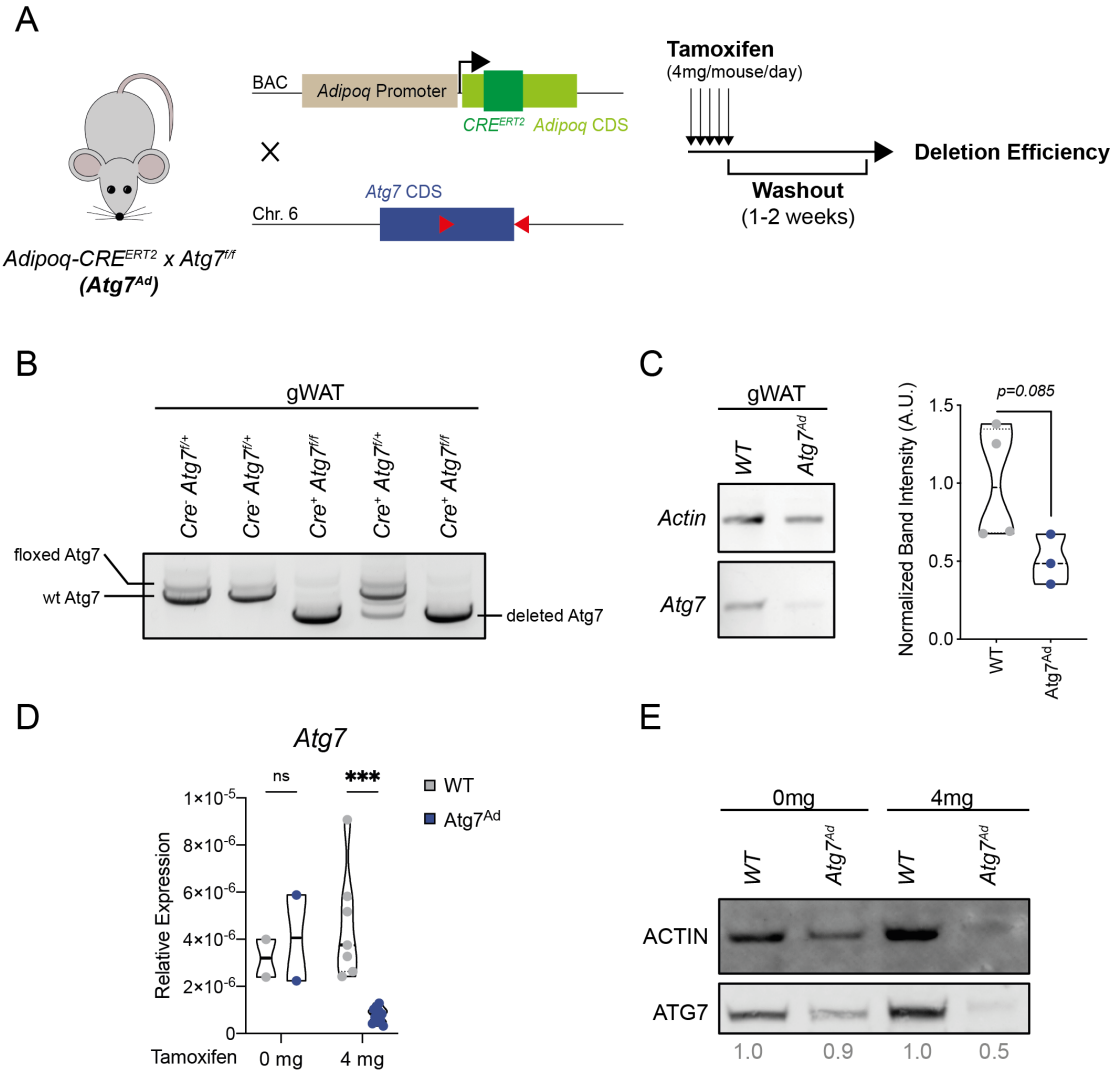

Figure 16: Efficient deletion of *Atg7* on transcriptional and protein level. (A) Schematic of the genetics behind our experimental model referred to as $Atg7^{Ad}$. Flox sites are marked by red triangles in the *Atg7* coding sequence. (A-E) Mice were analyzed two weeks after last tamoxifen administration by gavage. (B) Genomic excision of *Atg7* in DNA extracts from whole gWAT. Representative of two independent experiments. (C) Semiquantitative analysis of *Atg7* transcript in gWAT extracts. (each dot is one biological replicate/mouse). Statistical analysis by Student's t-test (D) Expression of *Atg7* transcripts in mature, enriched gonadal adipocytes measured by qRT-PCR. Representative of four independent experiments. (n=2 (0mg group), n=7-11 (4mg group)). Statistical analysis by Two-Way ANOVA. (E) Representative Western Blot for ATG7 and β-ACTIN protein expression in iWAT. Representative of two independent experiments.

administration, confirming that the *Adipoq-Cre*^{ERT2} system is not leaky.

However, as mentioned before, ATG7 is an E1-like ligase and as an enzyme capable to catalyse LC3 lipidation even at low levels to maintain autophagic flux. Therefore, we wanted to assess the impact of *Atg7* deletion on the autophagic flux *in vivo*. We collected adipose tissues from either tamoxifen-treated or non-treated mice and extracted proteins.

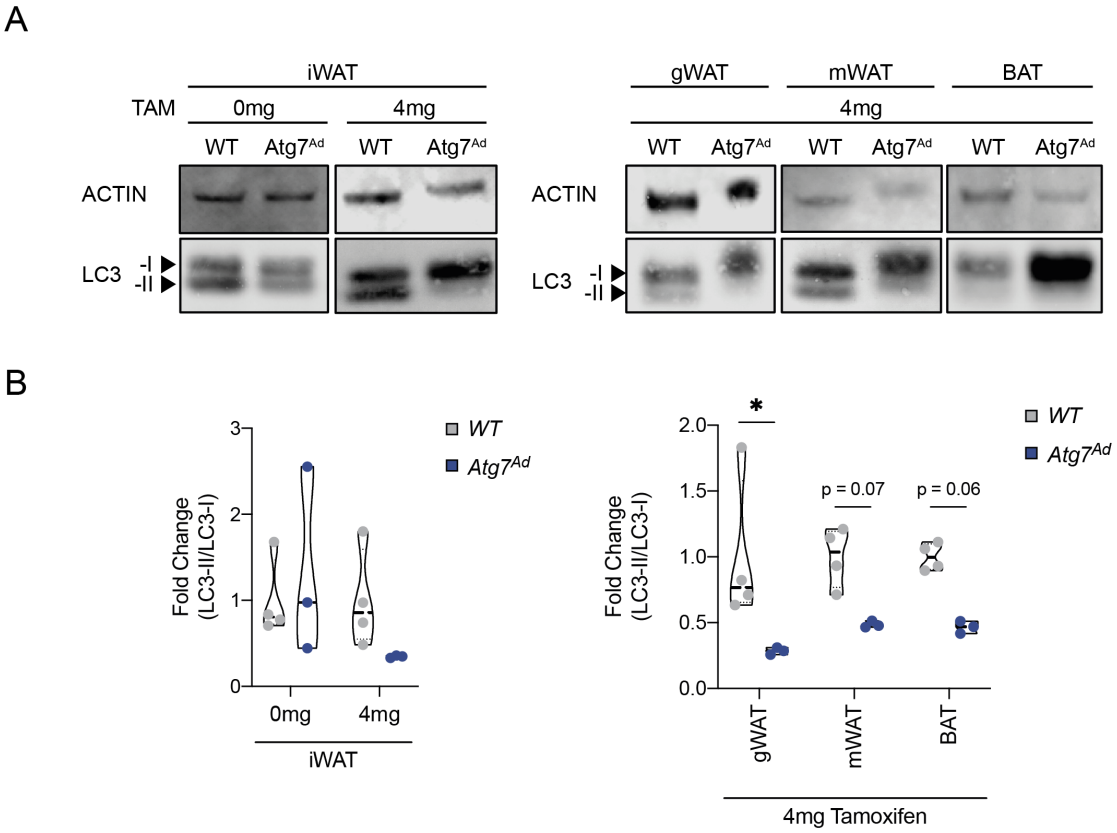

Figure 17: *Atg7^{Ad}* mouse model efficiently inhibits LC3 lipidation and reduces autophagy. (A) Western Blot analysis of LC3 expression level in various adipose tissues. (B) Semiquantitative analysis of protein levels several adipose tissues (n=3-4). Statistical analysis by Two-Way ANOVA. Representative for three independent experiments.

Next, we measured the presence of LC3 in these adipose tissues. Based on the function of ATG7 in the autophagic lipidation machinery, we were expecting a shift in the balance of LC3-II/LC3-I with an accumulation of cytosolic LC3-I and potentially a reduction of lipidated LC3-II, leading to a decreased LC3-II/LC3-I ratio. First, we observed a reduction of LC3-II/LC3-I ratio upon administration in tamoxifen in iWAT compared to wild-type controls whereas there was no difference prior to tamoxifen administration. Comparable to iWAT, we observed a significant reduction of LC3-II/LC3-I ratio in BAT and other visceral white adipose tissues (visWAT) including mWAT and gWAT (Fig.17A,B).

In conclusion, these results validated an efficient loss of adipocyte autophagy in this mouse model and was therefore used in all subsequent experiments in this thesis.

3.3 Discussion

3.3.1 shRNA-mediated knockdown of *Atg5* and *Atg7* in ST2 cells is insufficient for further experimental assessment

In this chapter, we aimed to suppress autophagy-regulated gene expression using a doxycycline-inducible shRNA system in the murine pre-adipocyte cell lines ST2 and 3T3-L1. After transduction, we found that integration efficacy of the lentiviral construct did not differ between cell lines and clones, but that there was a difference in the levels of dsRED expression between the cell lines. The most likely explanation for this may be that there are differences in the construct induction in the different cell lines. Differences between cell lines could potentially be associated with the integration site in the genome such as integration into a heterochromatic region. Using bulk sorted cells, in contrast to single cell derived clones, should circumvent the possible impact of the integration site into the genome. Another possible explanation may be that, although the constructs all have been cloned from the same backbone, mutations may have occurred in the Tet-On 3G transactivator protein (TRE3G) element. Variation in shRNA expression between constructs complicates data interpretation from these cell lines since an increased shRNA expression in one cell line compared to another may cause other unwanted off-target effects (e.g. saturation of endogenous miRNA pathways [262]). This can be controlled for by comparing always within the same cell lines in the absence or presence of doxycycline. Besides, performing experiments in this manner would remove any possible phenotypes caused by site-specific differences in lentiviral integration into the genome.

Although previous studies have successfully employed methods of transient or stable knockdown autophagy-related genes in a variety of cell lines [236, 263, 264], we were unable to find sufficient reduction in LC3 conversion in our stably transfected cell lines. The estimated half-life of ATG5 is about 30 hours [265], therefore it seems unlikely that the protein level will not be depleted after 4 days of shRNA expression. Despite observing significant reduction of both *Atg7* and *Atg5* transcript and protein levels by their respective shRNAs, the enzyme levels may remain sufficiently expressed to uphold

the lipidation of LC3 and hence maintains functional autophagy, an observation that our lab had previously made with other cells and RNAi systems. Another explanation may be that not all cells express or induce the construct after adipogenesis. This can be followed up on by investigating the expression of dsRED after adipogenesis by confocal microscopy. Overall, our data underlines the need for further optimization of the protocol. For instance, we want to investigate if the cell lines show autophagy inhibition after prolonged doxycycline treatment (e.g. after six days [235]) or after actively inducing autophagic flux by starvation (as previously reported [236]).

Lastly, during the validation of the cell lines we observed that adipogenesis was reduced in some cell lines compared to others. It has been described that increased number of pre-adipocyte passages can lead to loss of adipogenic capacity, especially in the absence of the PPARγ agonists such as rosiglitazone [266]. We therefore tried to limit passage number when expanding mixed clones. This could however still lead to some clonal shifts and explain differences observed in the cell lines capacity to undergo adipogenesis and consequently their decreased expression of ADIPOQ. Addition of rosiglitazone to the differentiation medium may help promote adipogenesis in these cell lines.

3.3.2 Efficient deletion of *Atg7* in a tamoxifen-inducible, *Adipoq*-driven Cre mouse model

The first adipocyte-specific gene deletion in an animal models has been described in the early 2000s using the *Ap2-Cre* transgenic mouse line as driver of the Cre recombinase [267]. Due to marked off-target expression in other cell types, it soon was replaced with the *Adipoq-Cre* mouse lines, which show an improved specificity in mature adipocytes [249], which was corroborated in our experiments. ADIPOQ is an adipokines and is often associated with anti-inflammatory and tissue protective functions. ADIPOQ is, similar to FABP4, a target gene for PPARγ and its expression can therefore be induced upon treatment with thiazolidinediones, a type 2 diabetes drug class of PPAR agonists [268]. We decided to use a tamoxifen-inducible *Adipoq-Cre*^{ERT2} mouse line as driver for our genetic deletion in order to avoid any chance of basic developmental differences occurring in the murine adipose tissues during adolescence. However, our data shows

that the upregulation of ADIPOQ occurs shortly after the peak of autophagy during adipogenesis. In the next chapter we will confirm that adipose tissues develop normally *in vivo* when *Atg7* is deleted. After the start of my project other groups published a similar approach to study autophagy specifically in mature adipocytes [269, 270], and some have shown efficient deletion of genes involved in autophagy pathways using constitutive Cre lines [271, 272].

Tamoxifen-inducible Cre transgenics are created by the fusion of the Cre recombinase to a mutated form of the estrogen receptor. Once tamoxifen is administrated, it gets converted *in vivo* to is active form 4-hydroxy-tamoxifen, which is then capable to specifically bind to this mutated form of the estrogen receptor [273]. Sassmann *et al.* published an improved version of the mutated estrogen receptor (Cre^{ERT2}) which increases its sensitivity to 4-hydroxy-tamoxifen by 10-fold [274]. The binding of 4-hydroxy-tamoxifen results in the activation of this nuclear receptor and the import of the fusion protein into the nucleus, where the Cre recombinase excises the gene of interest. Since estrogen is known to control and regulate systemic metabolism, recent studies have investigated the effect of tamoxifen on the systemic metabolism. Treatment with tamoxifen can alter lipid metabolism and lead to tissue browning as well as control thermogenesis [275, 276]. Moving forward, to ensure that effects are due to genetic deletion rather than tamoxifen treatment, both wild-type and KO mice need to be treated with tamoxifen.

As shown in this chapter, our inducible-transgenic mouse model leads to an efficient excision and genetic abrogation of *Atg7* gene expression. Although encouraging, other Cre-associated adverse effects may occur and need to be investigated further [277]. Since the Cre is expressed from a BAC, the risk of disruption of endogenous gene expression is avoided. However, Cre toxicities have been described leading eventually to cell death caused by off-target genome cuts at endogenous pseudo-*loxP* sequences [277]. Lastly, the usage of reporter mice, whilst helping to identify tissue specificity on a histological and microscopy level, one needs to refrain from using it as approximation for target gene deletion. The deletion efficiency of a specific genetic target remains subject to both the expression and type of Cre recombinase as well as the accessibility of the target *loxP* sequence in the genome. This being said, deletion of *Atg7* was sufficient to decrease

both transcript and protein levels and to impair conversion of LC3-I to LC3-II, thus indicating a successful inhibition of autophagic flux in adipocytes using this system and experimental setup.

3.4 Conclusion

Whilst establishing an *in vitro* system to study the role of autophagy in mature adipocytes has not been entirely successful, we are focussing the following chapter on the *in vivo* role of autophagy in mature adipocytes and how it affects metabolic and immunological characteristics of adipose depots under homeostatic conditions. Several cell types, including immune cells, are living in lipid-rich environments such as adipose tissue depots and have adopted metabolic features characterized by increased lipid uptake and catabolism [156]. Whether the loss of autophagy in mature adipocytes is however sufficient to cause cellular adaptations of these cells remains to be established.

4 Homeostatic effects of autophagic loss in mature adipocytes

4.1 Introduction

4.1.1 Adipose tissue lipid metabolism

Adipocytes are well known to store and release lipids and FFA in times of nutrient excess and deprivation, respectively. Intracellular lipids can be degraded via one of two major lipid degradation pathways: lipolysis or lipophagy. Lipolysis describes the degradation of stored TAG through enzymatic hydrolysation to FFA and glycerol during times of metabolic stress/demand (i.e. increased energy expenditure such as exercise, inflammation). Loss of adipocyte lipolysis is associated with reduced levels of circulating FFA under basal and fasting conditions [278]. Lipophagy refers the degradation of lipid droplets via an autophagosomal-lysosomal pathway. Immune cells such as neutrophils use lipophagy to generate intracellular FFA to fuel FAO, ATP generation and ultimately their differentiation [88]. Hepatocytes use lipophagy during periods of stress to mobilize lipids from lipid droplets [13]. As summarized in the general introduction, the precise interplay of lipolysis and lipophagy remains incompletely understood. Interestingly, lipolysis in hepatocytes appears to provide small amendable lipid droplets for lipophagic degradation suggesting a sequential order of these processes [279]. Whether autophagy can control FFA output by either lipophagy or autophagy-dependent regulation of lipolysis factors in adipocytes remains largely elusive.

In addition to the control of serum FFA levels via lipolysis, adipocytes take part in a systemic lipid handling system based on lipoprotein particles delivering cholesterol and TAG between the gut, liver, adipose tissues, muscle and other peripheral organs. TAG-rich very low-density lipoproteins (VLDL) are released by the liver and adipose tissues secrete lipoprotein lipases to liberate TAGs from the lipoprotein particles and store them in lipid droplets. Due to this process, the particles become cholesterol-rich intermediate (IDL) or low-density lipoproteins (LDL) depending on the degree of hydrolyzation. LDLs are then transported back to the liver or can be further used as

cholesterol source in peripheral tissues. This process of lipid storage in adipocytes is essential in avoiding ectopic lipotoxicities and metabolic dysfunction.

A common feature of metabolic diseases is a state of abnormal levels of lipids present in the blood, which is often referred to as dyslipidemia. For instance, increased levels of TAG occur frequently during obesity and can lead to ectopic deposition of fat in peripheral tissues such as muscle [280]. Furthermore, disturbance of lipid metabolism occurs often during infections and inflammatory conditions [281, 282]. Whether changes in lipid metabolism are systemic, potentially involving several metabolic organs, or whether metabolic changes can be more locally restricted is often not very well discriminated in these studies.

4.1.2 Immune cells in adipose tissues

Immune cells monitor and react to changes in their local and systemic metabolic environment. Induction of lipolysis, adipose tissue hypertrophy and thermogenesis all are capable to elicit immune activation and infiltration into associated metabolic tissues [283]. Obesity-induced adipose tissue expansion and hypertrophy increases the presence of ATMs. In lean individuals, ATMs resemble phenotypically alternatively activated 'M2-type' macrophages with high expression of CD206, ARG1 and CD301. Increasing adiposity leads to an increased fraction of ATMs expressing CD11c consistent with a pro-inflammatory 'M1-type' polarization. While both $CD11c^{+}$ and $CD11c^{-}$ ATM population expand during obesity, there is an overall shift from 'M2-type' to 'M1-type' ATMs. However, recent reports reveal a broader ATM diversity suggesting that this dichotomous classification is likely an oversimplification [284, 285]. The function and plasticity of ATMs during different metabolic conditions remain incompletely understood.

Obesity leads to the increase of adipocyte size, referred to as hypertrophy. Excessive adipocyte size expansion can lead to adipocyte death, and dying cells are surrounded by ATMs [286]. These histological structures are often referred to as so-called crown-like structures (CLS). Inhibition of lipolysis by genetic ablation of *Hsl* leads to a marked increase in adipocyte size and CLS [286]. Beside macrophages, other myeloid cell types are readily present in adipose tissues including eosinophils, ILC2, adipose tissue den-

dritic cells (ATDC) and neutrophils. The latter have been described to expand during obesity and can promote inflammation and insulin resistance [287]. Whilst B and T cell populations increase during obesity, regulatory subpopulations such as FOXP3$^+$ Tregs are lost in the process [147]. Interestingly, their loss seems to precede adipose tissue inflammation and macrophage infiltration [147]. Invariant NKT (iNKT) cells are also enriched in lean adipose tissues and are capable of regulating Treg and ATM phenotypes [288, 289]. iNKT cells are unique in their ability to present lipid antigens via CD1d on their surface [290].

In summary, adipose tissue immune cell populations shift from a tissue homeostatic 'type 2' towards a pro-inflammatory 'type 1' phenotype when the metabolic and/or inflammatory state of the adipose tissue changes. Especially since deletion of other genes involved in adipose tissue function (e.g. *Atgl*-KO and *Hsl*-KO) have shown altered immune cell populations [283, 286], it is central to assess the adipose tissue immune cells in our model.

4.1.3 Bone marrow adipose tissue and hematopoiesis

Bone marrow adipose tissue (BMAT) has long been considered as a mere space filler of the bone marrow, although it accounts for up to 70% of the total bone volume in adult humans [259]. Only in past decade, the hemato-regulatory and metabolic role of BMAT has come to light. BMAT is distinct from white and brown adipose tissues by its location, functions and metabolic features [291, 292, 293]. Compared to brown and white adipose tissue, BMAT arises from its own specialized progenitor population in the bone marrow, known as adipogenic progenitor cells [294, 295]. Interestingly, it has been shown that like other adipose tissues, BMAT expresses high levels of the adipocyte marker ADIPOQ and can be targeted using *Adipoq-Cre* driven mouse models [259, 296]. Typically, BMAT is subdivided into two distinct compartments, constitutive and regulated marrow adipose tissue (cMAT and rMAT, respectively) [297]. While cMAT is predominantly found in regions of 'yellow marrow', an area of high marrow adiposity perinatally (distal tibia, vertebrae and tail), rMAT regions are governed by external factors such as age or calorie restriction and appear in areas of hematopoietically active

'red marrow' (proximal tibia, femur). The relationship of BMAT and hematopoiesis is incompletely understood. Using a lipodystrophic animal model (so called *A-Zip* mice with a dominant-negative form of C/EBP under the *Ap2* promoter), BMAT ablation in caudal vertebrae (consisting mostly of cMAT) leads to increased hematopoietic recovery suggesting a net negative effect of adipocytes on hematopoiesis in these bones [231]. In line with this, intra-tibial injection of bone marrow adipocyte precursors did impair hematopoietic recovery, while co-lateral tibias, which have not been injected, reconstitute efficiently [294]. However, contrasting reports have recently appeared revealing some supportive functions of BMAT in hematopoiesis. Ablation of adipocytes in long bones like the femur (with high composition of rMAT upon irradiation) impairs hematopoietic recovery [296]. This effect is likely mediated by the release of a key cytokine for hematopoiesis and HSC self-renewal called stem cell factor (SCF) [296, 298]. In addition, the release of FFA from BMAT supports megakaryocyte maturation [299]. The effect of BMAT on HSCs remains still unclear and may depend on the experimental setup and model used. Age-associated increase of BMAT is associated with increased myelopoiesis [300]. Further evidence points towards a functional role of BMAT in myelopoiesis since leukemic suppression of BMAT impairs myelo-erythroid maturation, which can be rescued by promoting BMAT differentiation using PPARγ agonists [301]. It was further reported that AML cancer cells can take up BMAT-derived FFA to fuel its growth and survival [167]. Detailed analysis of homeostatic hematopoiesis is central to understand possible effects on peripheral immune cells during loss of autophagy in mature adipocytes.

4.1.4 Context and aim of this chapter

The interactions of adipocytes with immune and hematopoietic cells are becoming an increasing focus of interest. Loss of key adipocyte processes (such as lipolysis) increases inflammation [302]. We therefore set out to investigate whether loss of autophagy in mature adipocytes would alter adipose tissue biology and influence immune cells living therein under unchallenged conditions. We hypothesized that loss of adipocyte autophagy may impact on immune and/or hematopoietic cell phenotypes in adipose tissue

environments under homeostatic conditions. This chapter aims (1) to give a macroscopic overview of the impact of adipocyte autophagy on adipose tissue morphology and on functional lipid metabolism and (2) to examine the impact of adipocyte autophagy loss on immune and hematopoetic cells within adipose tissues and the bone marrow.

4.2 Results

4.2.1 Long-term loss of adipocyte autophagy leads to decreased adipose tissue size

Autophagy is known to be central for normal adipose tissue development during adolescence [116, 117], however the short- and long-term impact of autophagic loss specifically in mature adipocytes remains largely unknown. To assess mice after tamoxifen-induced autophagy deletion, we monitored their body and adipose tissue weight after 2 weeks of deletion (short-term) and after 8 weeks of deletion (long-term) (Fig.18A). Directly after giving tamoxifen, body weight development stalls briefly in both genotypes before recovering in both female and male $Atg7^{Ad}$ mice and littermate controls (Fig.18B). Similarly, body weight in either of the sexes at the end of our short-term or long-term observation period were comparable (Fig.18C). We next sought to measure adipose tissue mass at the different time points. Whilst we did not observe any differences in adipose tissue after short-term deletion of autophagy in visceral adipose tissues, we found that long-term deletion leads to a reduction in the overall visceral adipose tissue mass (Fig.18D – left panel) and in individual visceral adipose tissues including the mesentery and omentum (Fig. 18D – middle and right panels). After splitting the long-term deletion cohort by sex, we found a similar trend to reduced adipose tissue mass in autophagy-deficient adipose tissues in both sexes (Fig.18E).

We next sought to assess the BMAT development post-deletion. Since BMAT increases with age, we used three cohorts, taken down at different time points post-deletion, to quantify differences in BMAT development over a three-month period. Using osmium tetroxide staining, tibias from $Atg7^{Ad}$ mice showed decreased levels of bone marrow adiposity compared to their littermate controls over time (Fig.19A+B). Strikingly, BMAT

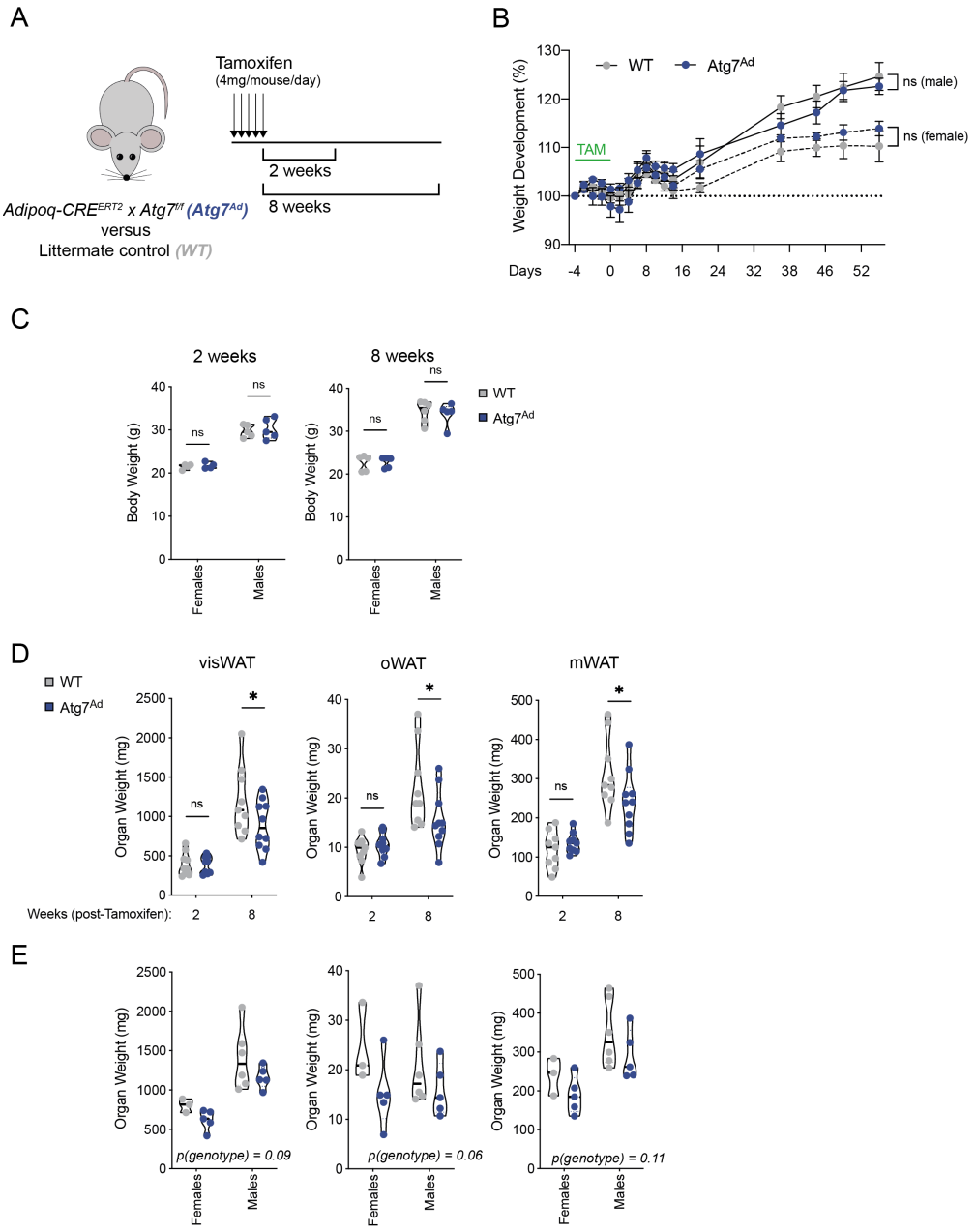

Figure 18: Body weight and adipose tissue mass decreases 8 weeks after autophagy deletion. (A) Schematic of experimental setup of short-term (2 weeks) and long-term (8 weeks) deletion of autophagy in adipocytes. (B) Body weight development separated by sex in $Atg7^{Ad}$ and littermate (WT) controls. (C) Body weight at the end of observation period in both sexes. (D) Adipose tissue mass of omental white adipose tissue (oWAT), mesenteric white adipose tissue (mWAT) and the collection of visceral adipose tissues including gonadal white adipose tissue (gWAT), mWAT, oWAT and retroperitoneal white adipose tissue (rpWAT). (E) Splitting adipose tissue weight after 8 weeks post-tamoxifen administration by sex. (B-E) Statistical analysis by Two-Way ANOVA. Each data point represents one biological replicate.

reduction was due to the loss of rMAT, whilst the cMAT remained unchanged (Fig.19B). This suggests that the loss of autophagy in the bone marrow affected predominantly

newly generated adipocytes in rMAT. This was further verified using H&E staining of tibias where adipocyte abundance in the proximal tibial epiphysis, a region known to increase rMAT with age, appears to be reduced (Fig.19C). Of note, no particular sex differences were observed in BMAT loss, although BMAT quantity was generally increased in female mice compared to male mice, as has been previously reported [303].

Taken together, the increase of adipose tissue mass with age is impaired in both peripheral adipose tissue depots and in BMAT in the adipocyte autophagy-KO model. A significant reduction in adipose tissue weight was only observed at 8 weeks post-deletion. This loss in adipose tissue mass may possibly be explained through an unwanted deletion in 'late' adipogenic progenitor populations, which in turn impaired adipose tissue growth over time. Alternatively, adipocytes may become smaller or more apoptotic.

4.2.2 Adipocyte autophagy loss controls adipocyte size and lipolysis without changing systemic lipid levels

Adipose morphology is described by the size and number of adipocytes in the tissue. Hypertrophic adipose tissues are characterized by an increased adipocyte size and decreased adipocyte number, whereas increased adipocyte number and reduced cell size is indicative for a hyperplastic tissue. The reduction in adipose tissue mass, previously observed in our autophagy-deficient adipose tissues after 8 weeks, could therefore be explained by a reduction of adipocyte size; by reduced adipocyte proliferation; by a higher metabolic demand shifting adipocytes towards a 'beige' phenotype; or by increased cell death. To address whether any of these changes occur in adipose tissues after the loss of autophagy in adipocytes, we performed Hematoxylin and Eosin (H&E) staining on our visceral adipose tissues. To assess the size and number of adipocytes within adipose tissue, we established an image-based pipeline (Fig.20A). We confirmed that this pipeline was fit for purpose delivering consistent results over several histological sections of the same sample (Fig.20A). Comparing adipocyte size between control or $Atg7^{Ad}$ mice, we found that adipocyte size was increased after deletion of autophagy suggesting that autophagy alters lipid handling in the tissue (Fig.20B+C). Furthermore, adipocyte numbers were decreased in the $Atg7^{Ad}$ mice indicating that autophagy-deficient adipose

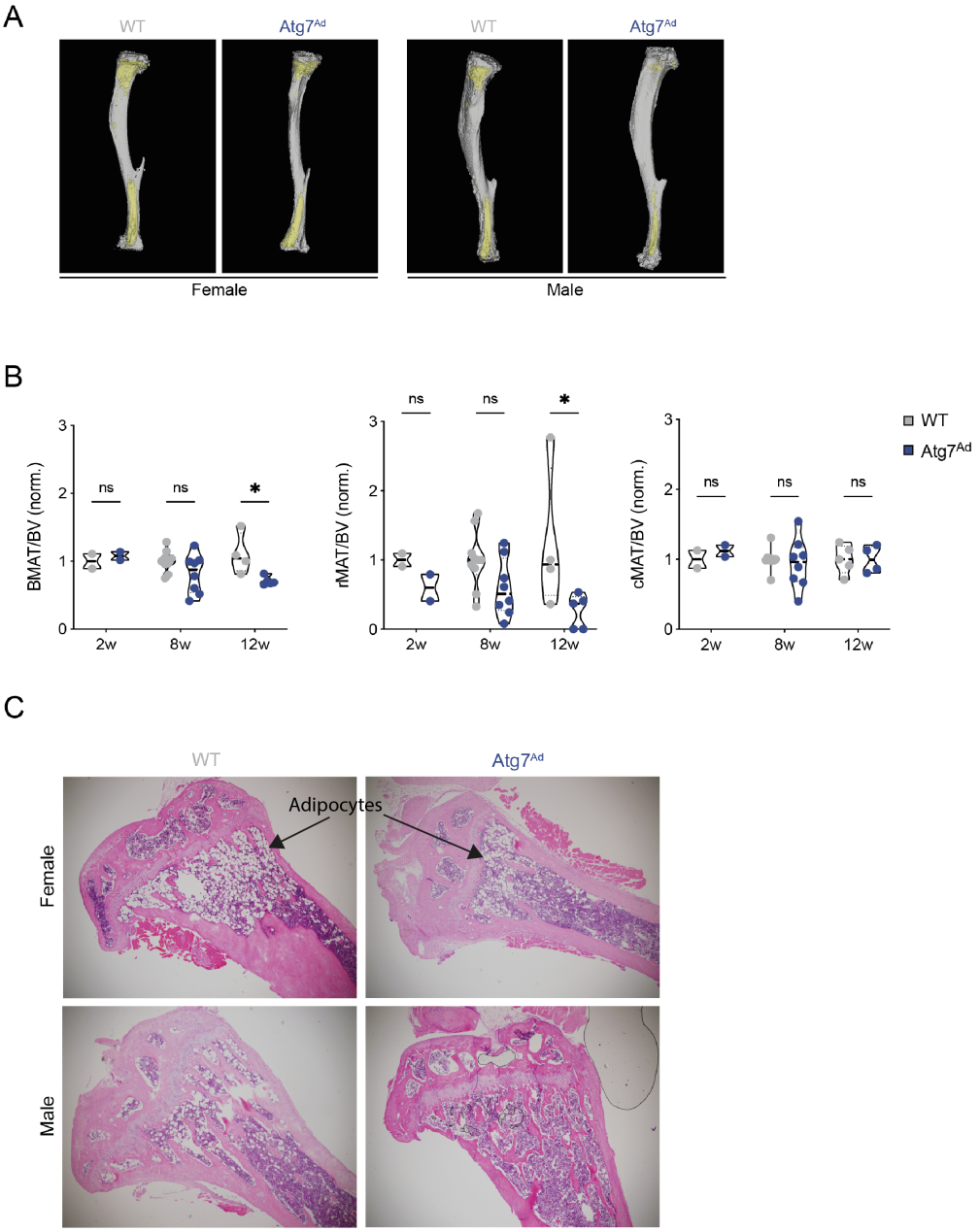

Figure 19: Bone marrow adipose tissue development is impaired in adipocyte autophagy-deficient mice. (A) Representative µCT images of tibias (in grey) stained with osmium tetroxide (in yellow) from adipocyte-autophagy deficient mice and littermate controls by sex. (B) Quantification of BMAT, rMAT and cMAT relative to the total bone volume (BV) and normalised to cage internal wild-type controls to exclude cage bias. (n=2-9) (C) H&E staining of tibias from $Atg7^{Ad}$ mice and controls. Adipocytes appear as white large cells in the epiphysis close to the knee joint. Statistical analysis by Two-Way ANOVA. Each data point represents one biological replicate.

tissue undergoes hypertrophy (Fig.20B+D).

Hypertrophic adipose tissues are associated with insulin resistance and lipid dysbalance leading to the development of metabolic diseases such as diabetes and obesity [304].

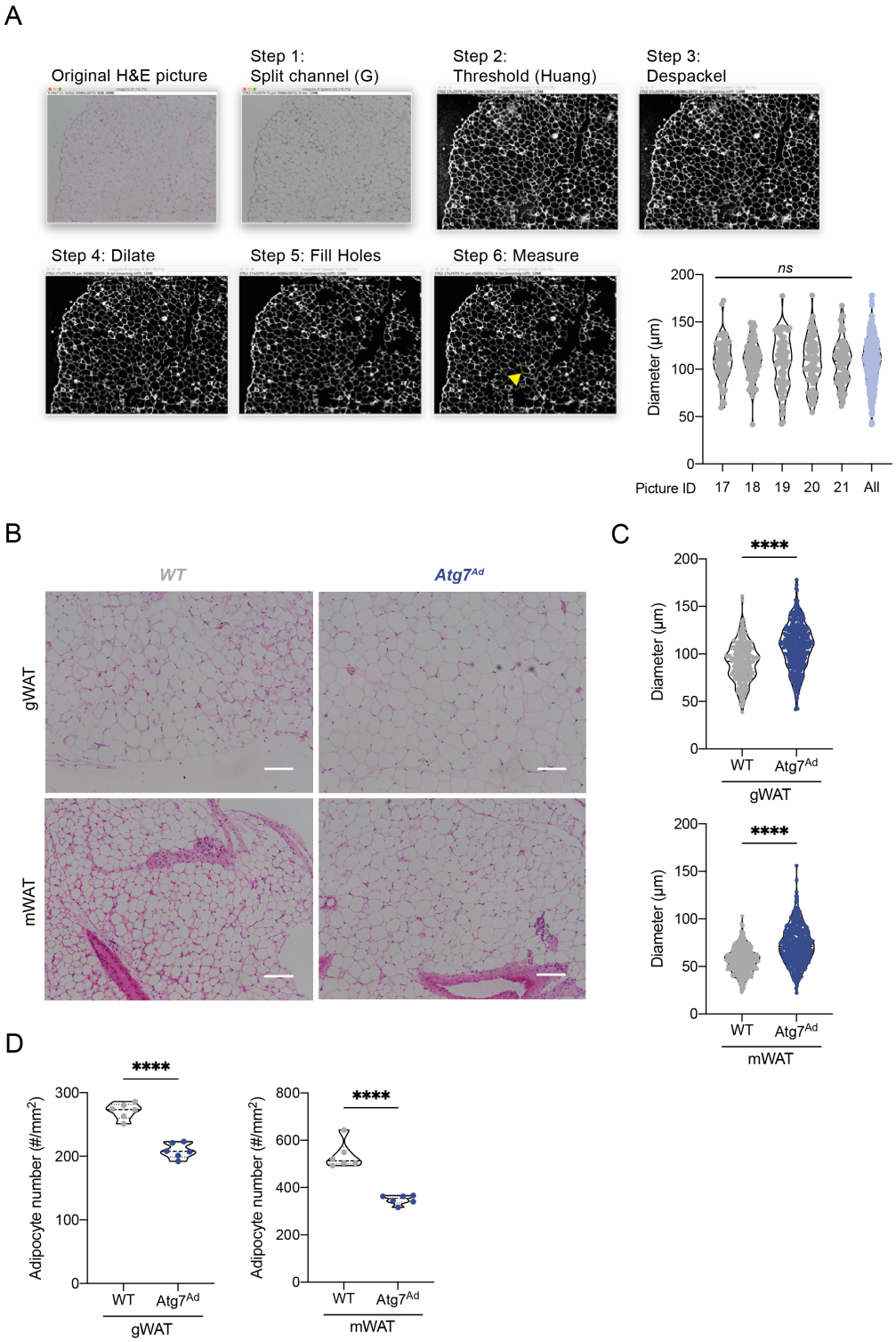

Figure 20: Adipocyte autophagy loss increases adipocyte size after 8 weeks. (A) Pipeline steps to process adipose tissue H&E staining for measurement of adipocyte size. High inter-section reproducibility of the same sample. (B) Representative H&E histology of gWAT and mWAT at 8 weeks post-tamoxifen administration. Scale bar: 200µm. (C) Adipocyte size measured from several sections of the same sample. (D) Adipocyte number in gWAT and mWAT after 8 weeks post-deletion. One biological replicate per group was used for this time point, variation representative for technical variation. Statistical analysis by One-Way ANOVA (A) or Student's t-test (C-D).

In addition, hypertrophic adipocytes have increased levels of basal lipolysis compared to smaller adipocytes [305]. The role of autophagy in regulating lipolysis in mature adipocytes remains largely unknown. Using gWAT explants from adipocyte autophagy-deficient and control mice, the lipolytic potential was measured under either basal (non-stimulated) or isoproterenol-induced conditions (Fig.21A). Basal lipolysis levels were not significantly reduced, indicating that autophagy does not affect the homeostatic lipolytic capacity of adipocytes (Fig. 21B). In contrast, using the β-adrenergic receptor agonist isoproterenol, adipocytes quickly increased their lipolytic output. Isoproterenol-induced lipolysis was impaired in adipose tissues made autophagy-deficient either through the loss of *Atg7* (right panel) or *Atg16l1* (left panel), as measured by the secretion of FFA into the supernatant (Fig.21C).

Systemic lipid homeostasis is regulated by a fine balance between lipid synthesis, storing and degradation. Adipocytes prevent systemic lipotoxicity by storing lipids and FFA. Hypertrophic adipocytes are less capable to store and retain FFA [306]. Although basal lipolysis was only marginally affected by the loss of autophagy, it was central to get a better understanding of the system lipid homeostasis in adipocyte autophagy-KO mice. Circulating levels of glycerol and FFA were measured 8 weeks post-tamoxifen treatment. Loss of *Atg7* did not affect circulating FFA or glycerol levels (Fig.22A). Even after splitting the cohort by sex, no major differences in circulating FFA levels were observed within each sex group (Fig.22B). When corrected for sex, a trend to decreased circulating FFA levels in $Atg7^{Ad}$ mice appears (Fig.22B). This is in line with the marginal decrease in basal lipolysis observed previously.

Systemic lipid metabolism is a complex interplay of lipid uptake by the intestine, lipid handing and metabolization in adipose tissues, liver and muscle. Beside FFA, other lipid species have been shown to be implicated in the regulation of systemic metabolism. To ensure that the loss of adipocyte autophagy does not alter other systemic lipid parameters, more than 400 serum lipids spanning 12 lipid classes were analysed by shotgun lipidomics [243]. Lipid species with missing values were excluded from the analysis resulting in a dataset of 148 detected lipids detected in all samples. Global

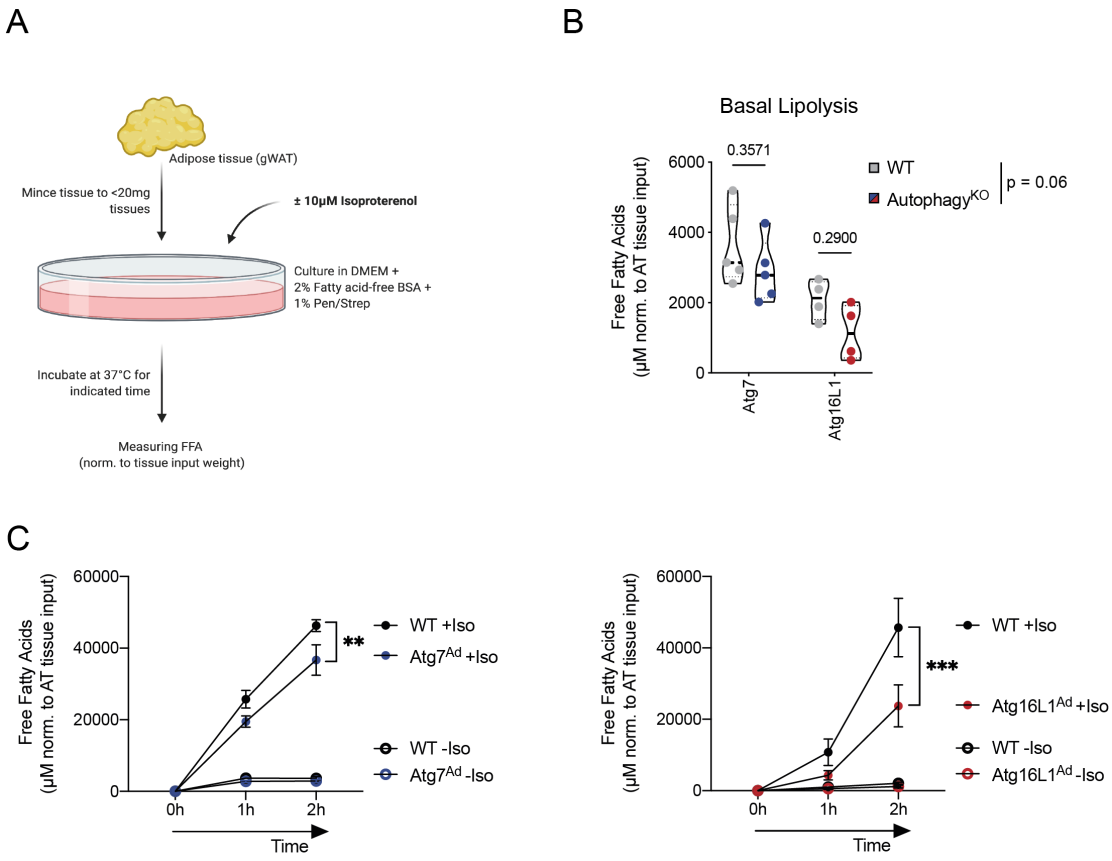

Figure 21: Autophagy partially controls isoproterenol-induced lipolysis. (A) Experimental schematic of lipolytic measurements of adipose tissue explants. (B) Measurement of basal (non-induced) lipolysis in explants from two different adipocyte autophagy-KO mouse models targeting either *Atg7* (blue points) or *Atg16l1* (red dots) with their corresponding littermate controls (grey dots). (n=4-5). (C) Representative experiments to measure basal and isoproterenol-induced lipolysis in adipose tissue explants with or without adipocyte-specific autophagy deletion. (n=4-5). Statistical analysis by Two-Way ANOVA. Each data point represents one biological replicate.

comparison of serum lipid profiles adipocyte autophagy KO and littermate control mice by principal component analysis (PCA) did not show any distinct clusters suggesting that the overall lipid profile is not altered based on the genotype or sex (Fig.23A). We next analysed whether specific lipid species were differentially regulated. After linear regression and correction for multiple testing, no lipids were found to be differentially expressed due to the loss of autophagy in mature adipocytes (Fig.23B). Based on this data, we were unable to determine any significant impact of adipocyte autophagy on systemic lipid metabolism during homeostasis.

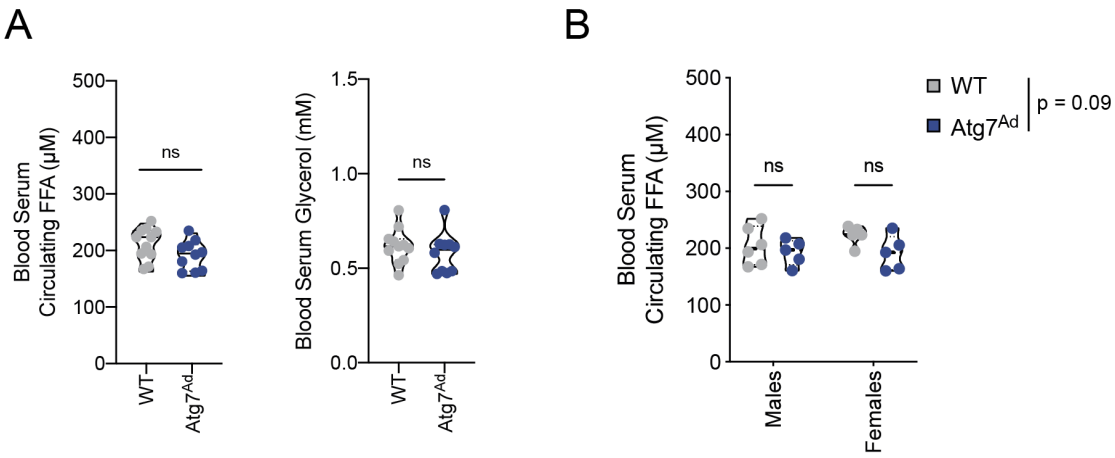

Figure 22: Serum free fatty acid and glycerol levels are not altered by autophagy loss in adipocytes. (A) FFA and glycerol measured in serum of mice 8 weeks post- tamoxifen administration. (n=10-11). (B) FFA measurements split by sex (n=5-6/group). Statistical analysis by Student's t-test (A) and Two-Way ANOVA (B). Each data point represents one biological replicate.

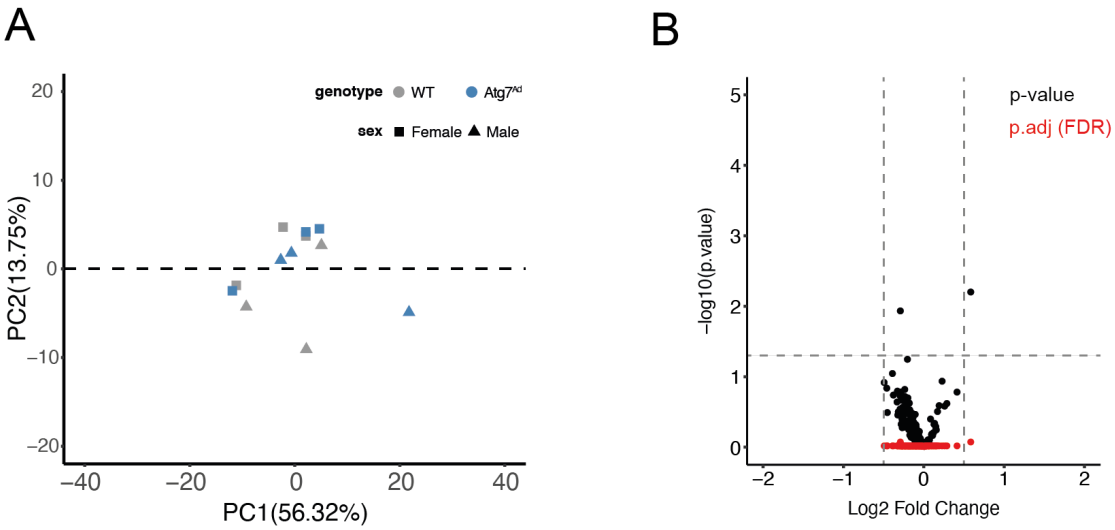

Figure 23: Serum lipidome remained unchanged two weeks after autophagy deletion from adipocytes during homeostasis. (A) Principal component analysis on serum lipidomics from a homeostatic cohort (3 males + 3 females per genotype) two weeks after deletion of autophagy in adipocytes. Each data point represents one biological replicate. (B) Differentially regulated serum lipids based on genotype after linear regression and multiple correction using Benjamini, Hochberg and Yekutieli correction (FDR). Data presented as non-corrected p-value (black dots) and adjusted p-value after FDR correction (red dots).

4.2.3 Adipocyte loss does not alter immune homeostasis in adipose tissues

Immune cells are responsive to changes in the adipose tissue environment, so we quantified the changes in immune cell composition two weeks post-autophagy deletion in visceral adipose tissue depots. Since we were aiming to investigate proximal and distal adipose tissues in the context of intestinal inflammation later on, the gut-associated mesenteric adipose tissue was analysed separately from a collection of visWAT depots (gWAT, rpWAT and oWAT). As previously reported [307], ATMs displayed a high level of autofluorescence, and express surface markers such as F4/80, CD206 and CD11c (Fig.24A). We also observed that adipose tissue eosinophils have a F4/80^{int} phenotype as previously reported [307]. After having established a functional flow cytometry panel to assess myeloid cell populations in adipose tissue, we analysed adipose tissue immune cells collected from $Atg7^{Ad}$ mice and littermate control mice. While we found that a higher fraction of CD45$^+$ cells was present in mesenteric adipose tissue (possibly representing higher density of immune cells in comparison to other visceral adipose tissues [308], Fig.24B), we did not find any changes in the number of immune cells in the adipose tissues (Fig.24C). Furthermore, we did not observe any differences in the frequency of specific myeloid cell populations in the tissue, except a slight increase in M2-type ATMs frequency in the mWAT. Similarly, we were unable to find any significant differences in immune cell composition after long-term deletion (data not shown). Overall, these findings suggest that adipocyte autophagy is dispensable for the immune phenotype in visceral adipose tissues under homeostasis over the observed time.

Although ATMs present the most common cell population in lean adipose tissues, lymphoid cells are also resident in adipose tissue. To investigate changes in the adipose tissue lymphocytes, we first established a gating scheme to identify several lymphoid cell populations (Fig.25A). The frequency of T cell subsets and B cells in both visWAT and mWAT did not changed in response to loss of adipocyte autophagy after two weeks of deletion (Fig.25B). The proportion of different CD4$^+$ T cells subsets remained unaffected by the loss of autophagy after stratification of CD4$^+$ T cells by their lineage-specific transcription factors GATA3$^+$ (Th2), RORγt$^+$ (Th17) and FOXP3$^+$ (Tregs)

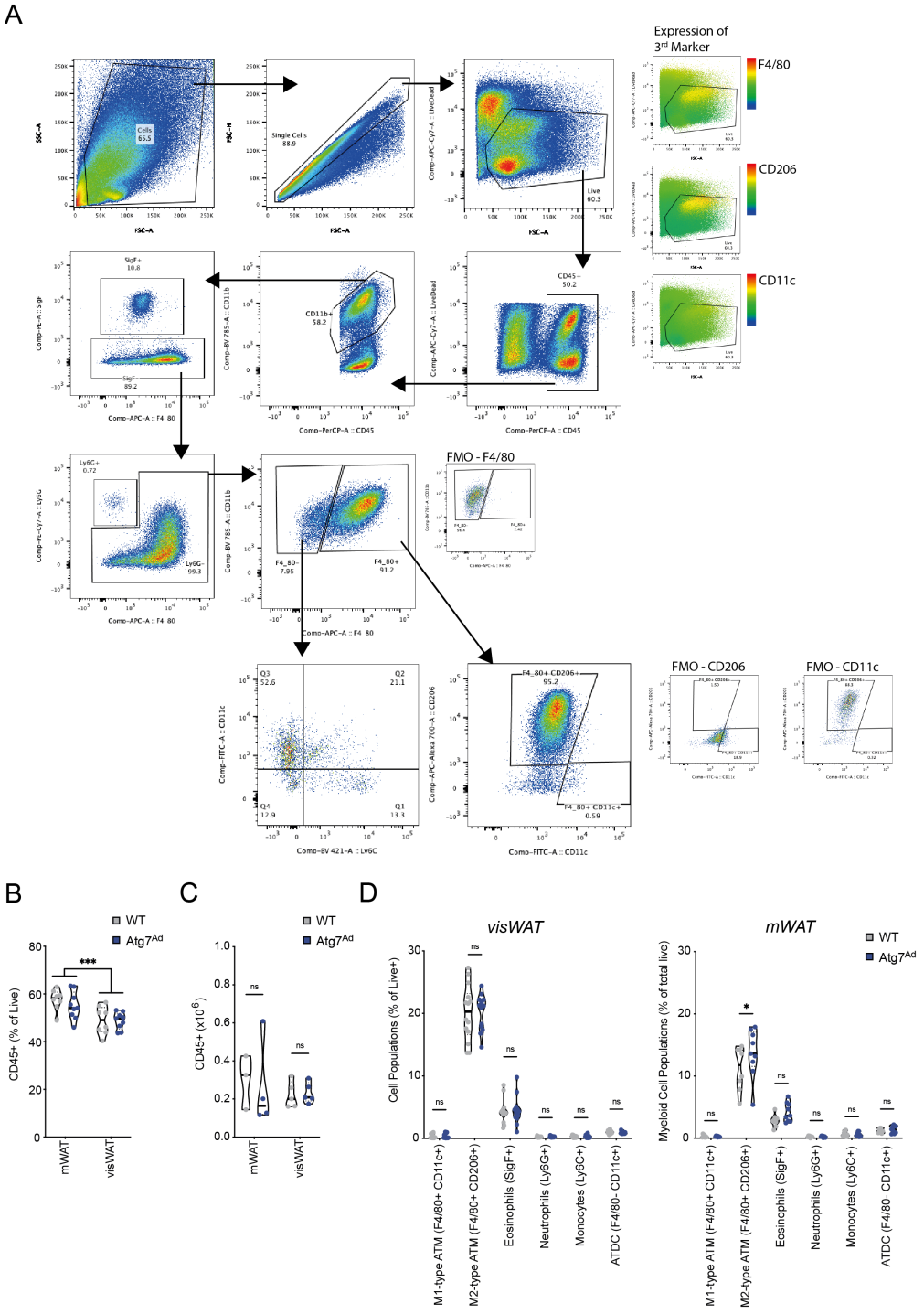

Figure 24: Adipocyte autophagy deletion does not alter myeloid presence in visceral adipose tissue depots. (A) Gating strategy for adipose tissue myeloid cell population. Single live cells were gated, including autofluorescencehigh cell populations, before myeloid cells were gated by $CD45^+$ $CD11b^+$. Eosinophils express a $F4/80^{int}$ phenotype and were therefore first gated by expression of $SigF^+$. Neutrophils ($F4/80^-$ $Ly6G^+$) were removed before separating into $F4/80^{low}$ and $F4/80^{int\text{-}high}$, based on 'fluorescence minus one' (FMO) control. $F4/80^{int\text{-}high}$ were further separated into 'M1-type' ($CD11c^+$) or 'M2-type' ($CD206^+$) macrophages. $F4/80^{low}$ were separated finally separated into $Ly6C^+$ monocytes and $CD11c^+$ ATDC. This panel was used in subsequent experiments. (B) Frequency of immune cells within total stromal vascular fraction (SVF). (C) Absolute immune cell presence in mWAT and visWAT. (D) Frequency of myeloid cell populations among SVF in mWAT (n=9) and visWAT (n=14). Statistical analysis by Two-Way ANOVA. Each dot represents one biological replicate.

(Fig.25C). Following the results of the myeloid compartment, we did not observe any changes in lymphoid immune cell populations associated with the loss of adipocyte autophagy, neither at 2 nor 8 weeks post-deletion (data not shown).

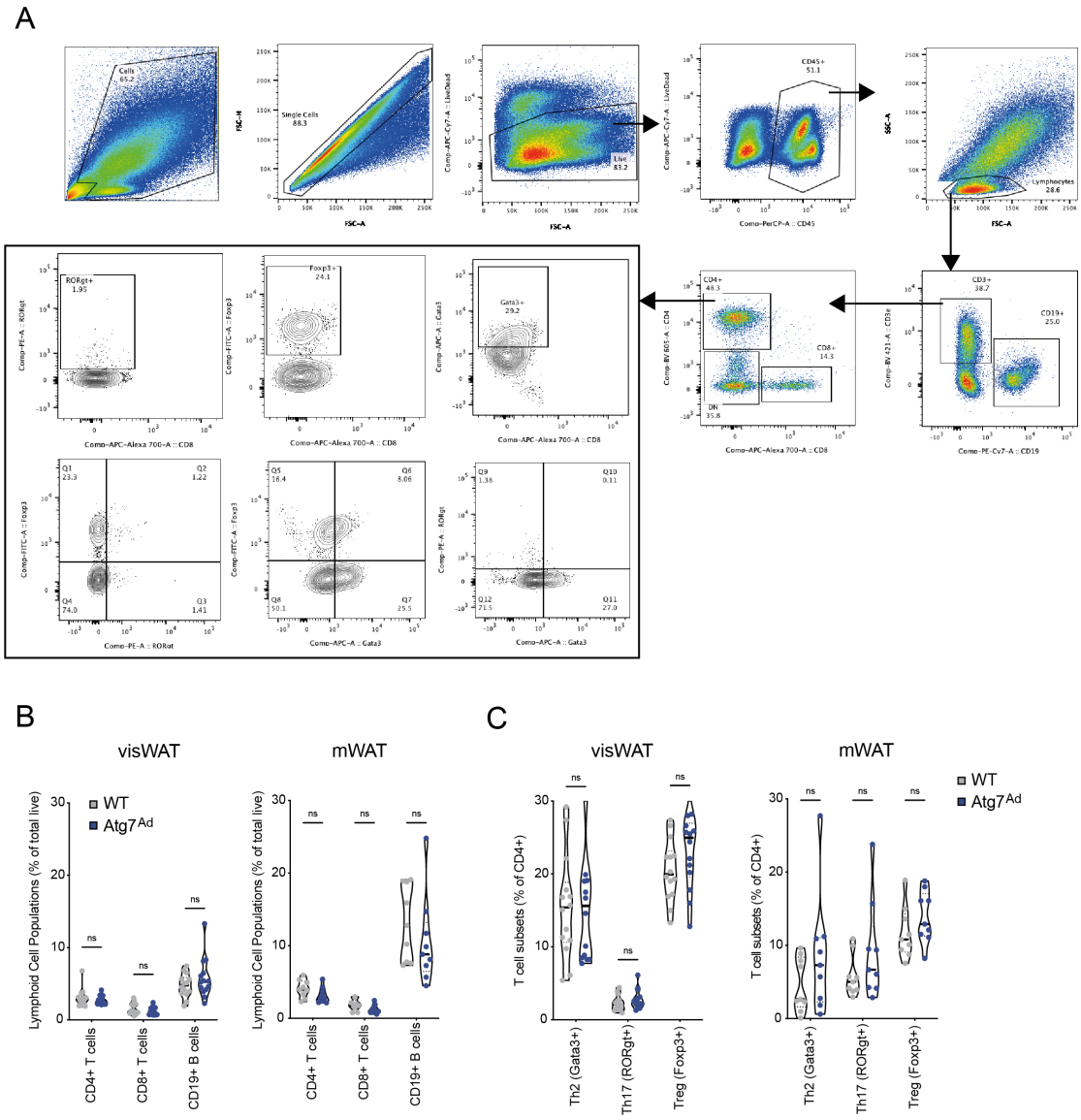

Figure 25: Lymphoid cell populations were unaffected by the loss of autophagy. (A) Gating strategy for adipose tissue lymphocytes: Single live cells were gated for CD45$^+$ immune cells prior to lymphocyte gating. Next, cells were stratified by expression of CD3$^+$ (T/NKT cells) and CD19$^+$ (B cells). CD3$^+$ T cells were further gated by CD4$^+$ and CD8$^+$ expression. Lastly, CD4$^+$ T cells were analysed by expression of key transcription factors, GATA3$^+$ (Th2), RORγt$^+$ (Th17) and FOXP3$^+$ (Treg). (B) Frequency of lymphocyte subpopulations in visWAT (n=14) and mWAT (n=9) after two weeks of autophagy deletion in mature adipocytes. (C) Proportion of CD4$^+$ T cell subsets in visWAT (n=14) and mWAT (n=9) two weeks post-tamoxifen treatment. Statistical analysis by Two-Way ANOVA. Each dot represents one biological replicate.

In summary, deletion of autophagy did not alter adipose tissue immune cell populations

under homeostatic conditions despite showing increased adipocyte hypertrophy. This suggests that hypertrophy at this time point does not lead to tissue inflammation as defined by immune cell composition and total numbers. Further studies should be undertaken to examine the functional and activation status of adipose tissue immune cells under homeostatic deletion. An important measure for adipose tissue health is the balance of adipose tissue macrophage polarization which appears to be unaltered in our model under homeostasis.

4.2.4 Hematopoietic reconstitution may be affected by loss of autophagy in mature adipocytes

Since the loss of adipocyte autophagy impairs BMAT expansion over time, it might have potential effects on hematopoiesis. To investigate the impact of autophagy-deficiency in adipocytes on hematopoiesis, we assessed hematopoietic progenitor populations by flow cytometry 8 weeks after tamoxifen administration (Fig.26A). No differences in the frequency of hematopoietic progenitor populations were observed (Fig.26B) suggesting that the autophagy loss in BMAT does not impede on normal hematopoiesis at this time point.

The bone marrow microenvironment has a particularly important role during hematopoietic challenges such as irradiation and hematopoietic transplantation. Irradiation ablates endogenous HSCs, which will require the transplantation of new bone marrow cells to reconstitute the hematopoietic compartment and ensure the survival of the animal. Interestingly, irradiation also results in a spontaneous expansion of rMAT [309]. Although initial studies suggest a net negative effect of BMAT on hematopoiesis, others could show that the secretion of SCF from bone marrow adipocytes is important in hematopoietic recovery [296, 298]. Since the role of autophagy in bone marrow adipocytes may become more apparent during stress situations, we sought to understand whether hematopoietic reconstitution might be impaired or accelerated in our model. To investigate this, adipocyte autophagy was depleted prior to irradiation and bone marrow transplantation. Since rMAT expansion is impaired after autophagy-deletion from adipocytes during aging, we presumed that rMAT expansion after irradiation may be equally impaired.

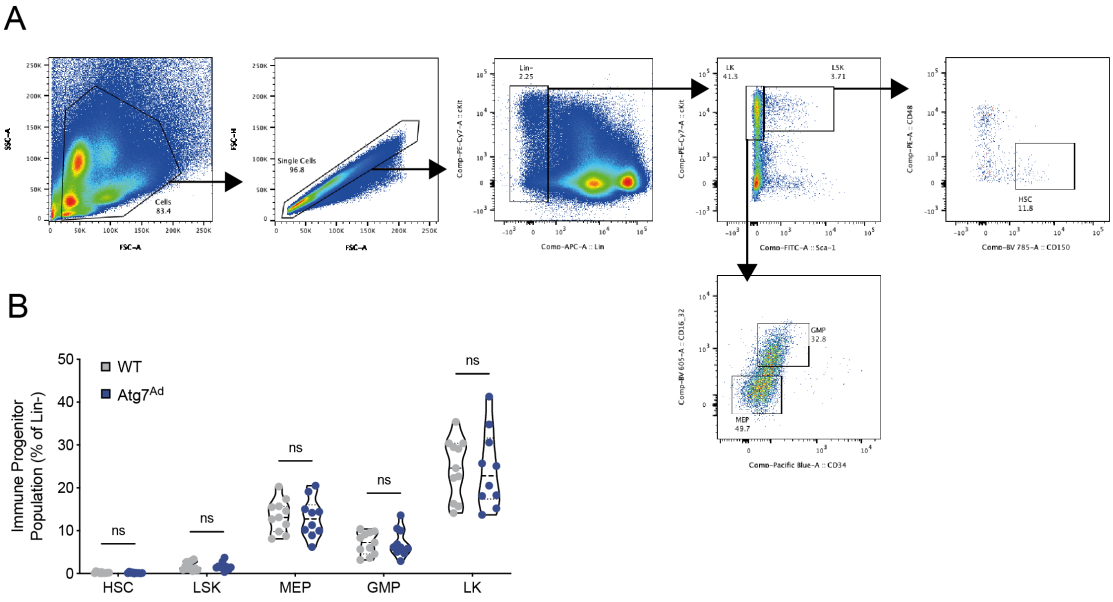

Figure 26: Hematopoiesis is unchanged even 8 weeks after loss of adipocyte autophagy. (A) Gating strategy of hematopoietic progenitor populations. Total BM cells were gated on single, live cells, lineage negative to identify hematopoietic progenitor population. Consequently LK (Lin^-, $cKit^+$, $Sca\text{-}1^-$) and LSK (Lin^-, $cKit^+$, $Sca\text{-}1^+$) populations were identified. LK population was further subdivided into megakaryocyte–erythroid progenitors (MEP; $CD16/32^-$, $CD34^-$) and granulocyte/monocyte progenitors (GMP; $CD16/32^+$, $CD34^+$). HSC ($CD150^+$, $CD48^-$) population was further assessed among LSK population. (B) Frequency of hematopoietic progenitor populations 8 weeks post-tamoxifen administration. (n=10-11). Statistical analysis by Two-Way ANOVA. Each dot represents one biological replicate.

Reconstitution was evaluated by bleeding after 14 days and 19 days post-transplantation (Fig.27A). Irradiation led to loss of bone marrow cellularity in both autophagy-deficient and control animals (Fig.27B). Extramedullary hematopoiesis remained comparable as assessed by splenic weight (Fig.27C). White blood and red blood cell counts were comparable between genotypes, while mice with autophagy-deficient adipocytes showed a trend for faster platelet recovery (Fig.27D).

Aging is not only associated with an expansion of BMAT, but also with an increased myeloid bias [310]. Conclusive causal links between these two phenomena have not yet been successfully established. We therefore sought to analyse whether loss of adipocyte autophagy may alter myeloid-lymphoid balance. We used the congenic marker CD45.1 to track the hematopoietic reconstitution of donor-derived cells in our model. Mice were bled 14 days after reconstitution and blood immune cells populations were analysed by flow cytometry. Strikingly, blood cell numbers contained a substantial frac-

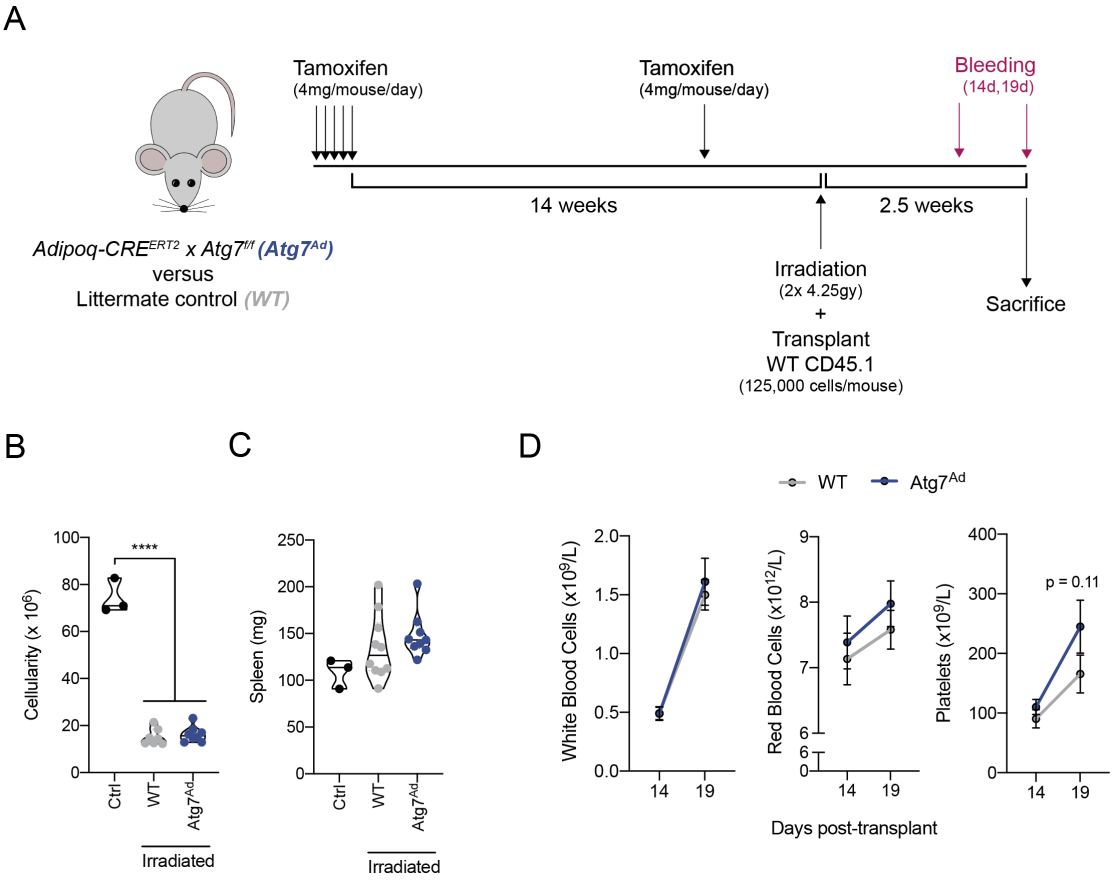

Figure 27: Hematopoietic recovery after irradiation shows trend to increased platelet recovery. (A) Experimental overview of transplantation experiment. (B) Cellularity of bone marrow after irradiation. (C) Spleen weight. (D) Peripheral blood cell populations after 14- and 19-days post-transplantation. Statistical analysis by One-Way ANOVA (B-C) and Two-Way ANOVA (D). Each dot represents one biological replicate.

tion of CD45.1$^-$ recipient-derived immune cells suggesting that the irradiation was sub-optimal and did not remove all recipient hematopoietic stem/progenitor cells (Fig.28A). Chimerism between the recipient groups was, however, comparable. Since both donor-derived (CD45.1$^+$) and recipient-derived (CD45.1$^-$) progenitor cells can be considered wild-type due to the tissue specific deletion of autophagy occurring only in adipocytes, we analysed all blood immune cells independent of their CD45 status. Taking together all immune cells, we observed an increased frequency of circulating lymphoid cells in $Atg7^{Ad}$ mice compared to wild-type littermates (Fig.28B). In contrast, myeloid frequency was reduced when adipocyte autophagy was lost in the microenvironment (Fig.28B). This points towards a shift in the myeloid:lymphoid ratio potentially as a consequence of decreased rMAT expansion in the KO animals after irradiation. If the effect was due

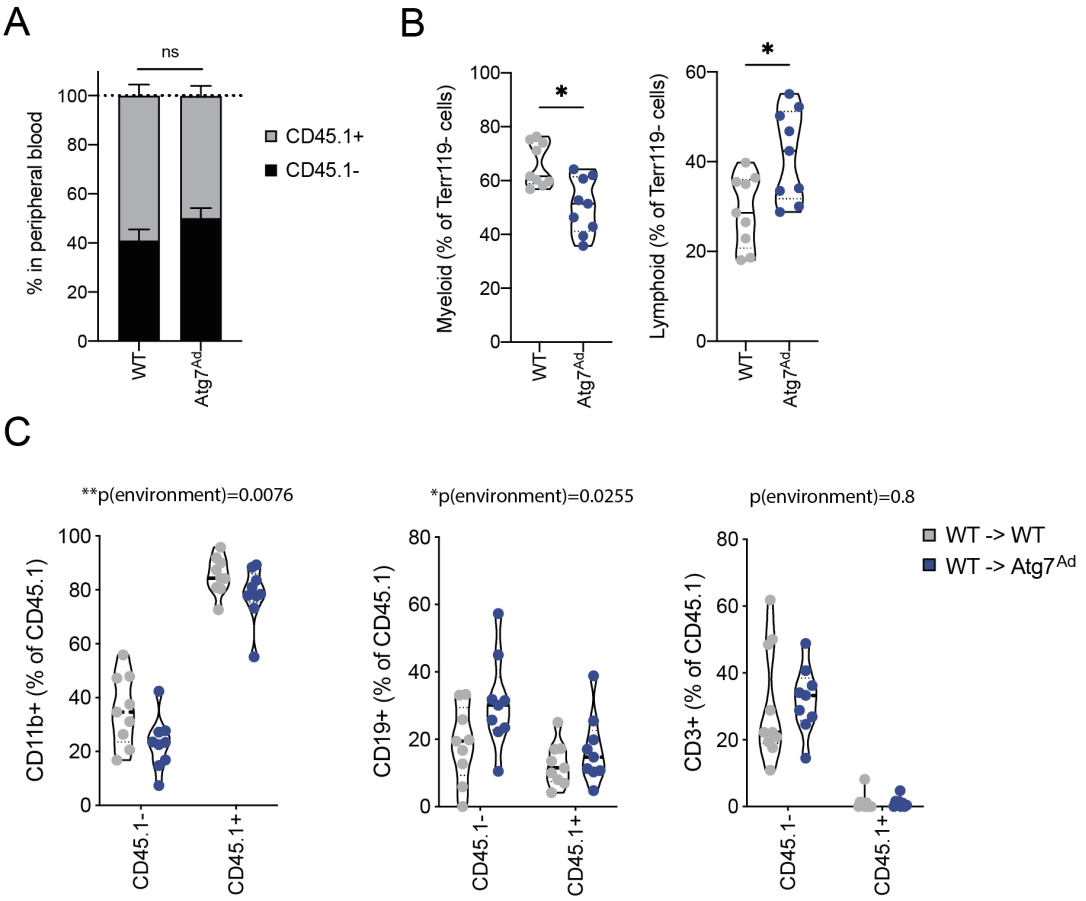

Figure 28: Loss of adipocyte autophagy shifts myeloid-lymphoid balance after irradiation. (A) Fraction of CD45.1$^+$ vs. CD45.1$^-$ blood immune cells from mice with or without deletion of adipocyte autophagy deletion. (n=9-10) (B) Shift of myeloid-lymphoid balance in peripheral blood after 14 days post-deletion. (C) Myeloid cell (CD11b$^+$), B cell (CD19$^+$) and T cell (CD3$^+$) reconstitution in peripheral blood after 14 days post-deletion. (n=9-10). Statistical analysis by Two-Way ANOVA (A,C) and Mann-Whitney test (B). Each dot represents one biological replicate.

to a change in the microenvironment of the hematopoietic cells, then the effects on lineage bias should be comparable between CD45.1$^+$ donor-derived cells and CD45.1$^-$ recipient-derived cells. Thus, we stratified our analysis for each congenic marker and found that, although there were substantial differences in the overall frequency of different immune cell populations, the myeloid populations in both cohorts (CD45$^+$ and CD45$^-$) trended towards a decreased frequency while B cell frequencies were increased and T cells unchanged (Fig.28C).

Changes in peripheral blood immune cell composition may reflect alterations of hematopoietic progenitor populations in the bone marrow. Therefore, we sacrificed the mice 20

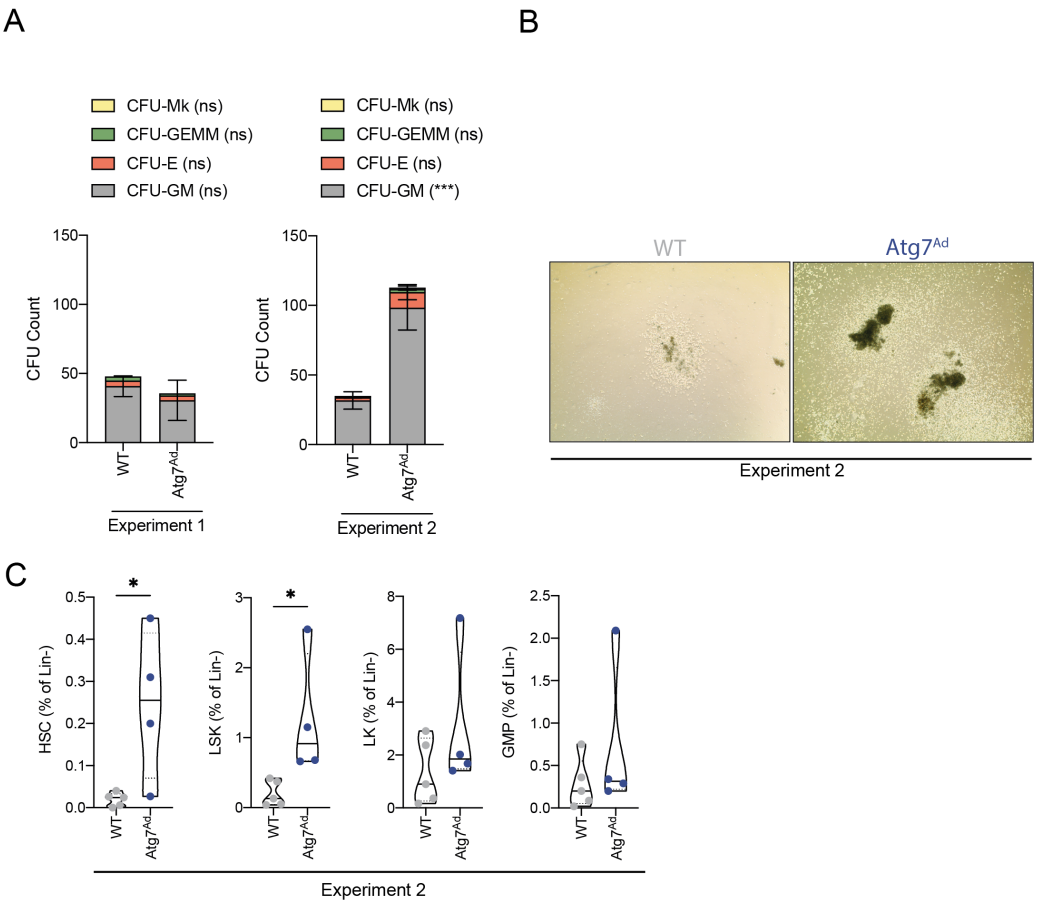

Figure 29: Loss of adipocyte autophagy promotes hematopoietic progenitor expansion after irradiation. (A) CFU counts of methylcellulose colony forming assay from two independent experiments (n=4-5/group/experiment) after eight days of culture in M3434 medium. (B) Representative images of CFUs observed in the second independent experiment (n=4-5). (C) Frequencies of hematopoietic progenitor populations found in the bone marrow 20 days post-transplantation in the second experiment. (n=4-5). Statistical analysis by Two-Way ANOVA (A) and Mann-Whitney test (C).

days after transplantation and assessed the abundance and potency of its progenitor populations isolated from either $Atg7^{Ad}$ mice or littermate controls. To this end, we used a methylcellulose CFU assay by plating 250,000 bone marrow cells from each mouse. Colonies were identified and blindly counted eight days after initial plating. While the first experiment did not show any differences between the different environments, the second experiment showed a marked increase in total colonies counted, especially in CFU derived from GMPs (Fig.29A). However, CFU size was comparable between the conditions, indicating that progenitors from $Atg7^{Ad}$ microenvironment are more abundant but are not more potent than those from control mice (Fig.29B, quantification not shown). Lastly, frequencies of progenitor cell populations were also increased in bones isolated

from adipocyte autophagy-deficient background in the second experiment (Fig.29C). These experiments should ideally be repeated. However, in the next chapter we shifted our attention to the role of adipocyte autophagy during inflammation.

Taken together, hematopoiesis was unaltered under homeostatic conditions after eight weeks post-autophagy deletion from adipocytes. After bone marrow insult by irradiation, hematopoietic recovery revealed a slightly improved platelet reconstitution, a shift of the myeloid-lymphoid balance and a putative increase in hematopoietic progenitor populations. However, these preliminary conclusions require further optimization and confirmation through additional experiments.

4.3 Discussion

4.3.1 Autophagy in adipocytes controls FFA secretion from adipocytes

The importance of lipolysis in lipid catabolism is well documented, however, whether autophagy contributes to degradation of stored lipids in mature adipocytes remained largely unknown [137]. Interestingly, our data shows that deletion of autophagy in mature adipocytes leads to a hypertrophic phenotype resembling adipose tissues from *Hsl*-KO mice [311]. In contrast, however, adipose tissue-specific deletion of *Atgl* did not alter adipocyte size possibly indicating the existence of counter-mechanisms to reduce lipid uptake and cytotoxicity [302]. Recently, two studies have described the role of autophagy in mature adipocytes using inducible mouse models [269, 270]. In line with our findings, Cai *et al.* found that adipocyte number was reduced [269]. In addition, both studies found that adipocyte lipid droplet size was heterogenous in white adipose tissue depots while accumulation of lipid droplets in brown adipose tissue were frequently observed in adipocyte autophagy-deficient mice.

Autophagy is crucial for the clearance of mitochondria from beige adipocytes, allowing the hypothesis that autophagy in white adipocytes may control mitochondrial clearance [106]. Indeed, long-term deletion of *Atg3* from adipocytes leads to the accumulation of mitochondrial proteins such as aconitase and heat shock protein-60, however no accumulation of the beige/brown adipocyte marker UCP-1 was observed [269]. However, the inducible deletion of *Becn1* did reveal a significant decrease of UCP-1 expression

after cold exposure suggesting that adipocyte autophagy may indeed contribute to the transition from white-to-beige adipose tissue in this condition [270, 107].

Interestingly, there is now a growing body of evidence (which includes our own findings) that demonstrate that lipolysis is reduced upon β-adrenergic receptor stimulation (e.g. using isoproterenol) in autophagy-deficient adipocytes [269, 270, 272]. While most studies did not find any substantial effect of autophagy loss on basal lipolysis, Zhang *et al.* could demonstrate that adipocyte-specific deletion of *Raptor*, a positive regulator mTORC1 signalling promotes basal lipolysis in an autophagy-dependent manner [272]. In the same study, electron microscopy images reveal lysosomal structures containing lipid droplets allowing for possible involvement of lipophagy in the FFA output from adipocytes. However, the precise mechanism involved in decreased lipolytic output remains unclear. Chaperone-mediated degradation of lipid droplet associated proteins, called perilipins, via the autophagosomal-lysosomal machinery has been found to regulate lipolysis by increasing the access of cytosolic lipases to TAGs stored in the lipid droplet in hepatocytes and adipocytes [312, 238].

Decrease of lipolytic potential in adipocytes had neglectable effect on circulating FFA levels and no substantial effect on the general serum lipidome. Interestingly, Cai *et al.* found that after long-term deletion of adipocyte autophagy for 12 weeks increases lipid peroxides which are part of HDL particles [269]. In our screen, we did not find any significant differences in the serum lipidome between adipocyte autophagy-deficient and littermate controls. However, it remains to be investigated whether the loss of adipocyte autophagy will eventually lead to the ectopic deposition of lipids in other metabolic organs such as the liver or muscle. In summary, the data presented with regards to the short-term metabolic effects of autophagy loss revealed no significant involvement of adipocyte autophagy under homeostatic conditions. However, the loss of autophagy does impair lipolysis, which may become more relevant during times of high nutrient demand.

4.3.2 Adipose tissue immune cells are unaffected by homeostatic loss of adipocyte autophagy

Adipose tissue immune cells can regulate adipocyte homeostasis and *vice versa*. We had observed that white adipose tissues from adipocyte autophagy KO mice were hypertrophic, however this did not lead to increased presence of macrophages in the adipose tissue. This is in contrast to previous reports in which the inducible deletion of autophagy in short-term (2 weeks post-tamoxifen) and long-term (12 weeks post-tamoxifen) led to a significant increase of F4/80$^+$ ATMs and CLS in the adipose tissues suggesting increased tissue inflammation, possibly through induction of adipocyte cell death [269, 270]. The disparity may arise from technical differences in detecting the ATMs. While the published studies have predominantly used immunostaining to identify ATMs in the tissue, we used flow cytometry. Another reason for differences in the immunological state may be due to differences in tamoxifen administration (intraperitoneal vs. gavage, drug dosing) and the genes targeted. Overall, we did not observe strong immunological changes in the adipose tissue by flow cytometry and did not observe obvious differences in CLS formation when histology was assessed. However, to detect possible immunological changes in the adipose tissue, we could perform immunohistology or whole tissue transcriptomics (as done by Cai *et al.* and Son *et al.*) [269, 270].

Thus far, our data did not reveal any major immunological differences caused by the deletion of autophagy under homeostatic conditions suggesting that adipocyte autophagy may be dispensable for adipose tissue immune homeostasis. We therefore decided that we can group homeostatic wild-type and adipocyte autophagy-deficient mice together as 'control' group to compare with inflamed mice in future experiments.

4.3.3 Loss of autophagy in bone marrow adipose tissue may control hematopoietic recovery

In this chapter, we demonstrated that rMAT expansion was decreased with age. This can be explained by the necessity of adipocytes to have intact autophagic flux to differentiate and form their characteristic morphology. Since adipocytes in the bone marrow

are distinct from peripheral adipocytes, little is known about the requirements of bone marrow adipocytes during differentiation. Recently, a study identified that the bone marrow harbours a subpopulation of non-lipid laden, ADIPOQ$^+$ stromal subpopulation which eventually will form mature adipocytes using both scRNAseq and lineage tracing approaches [295]. In line with our data from Chapter 3, where we had observed a slight overlap of autophagy and ADIPOQ expression in bone marrow stroma-derived ST2 cells, it is plausible that this overlap may prevent the full maturation of bone marrow adipocyte late progenitors into lipid-laden, mature adipocytes. Importantly, the study by Zhong *et al.* also reported that visceral fat tissue does not contain ADIPOQ$^+$ adipogenic progenitor populations [295]. The reduced expansion of BMAT with age did not impair hematopoiesis under homeostatic conditions. We can only speculate on the effects that longer deletion of autophagy in adipocytes would have on the aging hematopoietic compartment. Aging is a clear and strong driver of BMAT expansion, similarly several studies revealed a possible connection between the amount of BMAT on myelo- and granulopoiesis [298, 301]. Interestingly, we had observed a similar phenomenon in early studies during this PhD in which granulopoiesis was promoted in tibias compared to femurs in wild-type animals possibly correlating with the amount of bone marrow adipose tissue (data not shown).

After hematopoietic transplantation, we observed a shift towards increased lymphopoiesis in mice without adipocyte autophagy in their environment. Unfortunately, we were unable to quantify BMAT content of femurs and tibias from transplanted animals in order to confirm the expected reduced expansion of BMAT (especially rMAT) upon irradiation in adipocyte autophagy-deficient animals. The bones have been collected and will be added to the analysis. However, from the aged adipocyte autophagy-deficient mice, it seems likely that BMAT expansion during irradiation in these mice will be impaired. A major caveat of this experiment was the insufficient depletion of endogenous hematopoietic cells after transplantation. About half of the cells were still recipient-derived suggesting that the irradiation was sub-lethal and the irradiation conditions need to be optimized. However, since donor- and recipient bone marrow are both wild-type cells and the chimerism is comparable between the recipient mice, we can

attempt to draw some careful conclusions on the impact of the two microenvironments on hematopoiesis. In adipocyte autophagy-deficient recipient mice, we observed an overall shift in myeloid-lymphoid balance towards increased lymphopoiesis. This is in line with literature describing a negative impact BMAT has on B cell lymphopoiesis, possibly through the secretion of adiponectin which in turn can enhance myelopoiesis [313, 314]. Loss of BMAT can therefore promote lymphopoiesis. Lastly, we also found in these preliminary experiments that the loss of adipocyte autophagy may actually promote hematopoietic recovery by increasing progenitor cell in the bone marrow resembling data from lipodystrophic *A-Zip* mice [231]. Newer studies show that adipocytes in the bone marrow can have numerous effects on hematopoiesis after insult such as myocardial infarction (Nahrendorf lab, unpublished data) or hematopoietic transplantation via the release of nutrients (e.g. FFA) and soluble cytokines, respectively [296].
Overall, our data revealed that deletion of autophagy in adipocytes did not alter homeostatic hematopoiesis. Furthermore, it provided a glimpse into the possible role of adipocyte autophagy during hematopoietic recovery. These experiments require, however, further optimization and repetition to confirm the preliminary findings presented here.

4.4 Conclusion

In this chapter we have explored the impact of inducible autophagy deletion in adipocytes on different adipose tissues and the immune cells harboured within them. We found that upon induction of lipolysis, autophagy-deficient adipocytes secrete less FFA into their environment, however, homeostatic conditions did not alter immune state and composition of the animals. Thus, in the next chapter, we will use experimental models to evaluate the function of adipocyte autophagy in the context of intestinal inflammation.

5 Loss of autophagy in mature adipocytes exacerbates intestinal inflammation

5.1 Introduction

5.1.1 IBD is linked to autophagy and adipose tissues

IBD pathologies are thought to be of multifactorial origin, evoked by a combination of environmental and host factors. Data from over 75,000 IBD patients identified nearly 200 susceptibility loci [215, 315]. Data from these genome-wide association studies highlighted enriched signatures of classical inflammatory (e.g. NFκB signalling, TNF signalling, IL-10 and IL-23 pathways) and autophagy pathways (e.g. *ATG16L1*, *IRGM*, *NOD2*) [211, 316]. Autophagy has been studied in many intestinal cell types, most notably revealing a pivotal role in controlling intestinal epithelial cell function [317]. By contrast, the adipocyte-specific role of autophagy during intestinal inflammation has not been studied. In spite of a rising obesity epidemic, the clinical links between obesity and IBD are still controversial, with studies claiming an increased disease burden and surgery, whereas other reports did not corroborate these findings. The increased prevalence of IBD in industrialized countries may, however, suggest a link to lifestyle, including obesity. However, disease severity was increased in CD patients highlighted by an increased occurrence of anoperineal abscesses, decreased chance of remission and more active disease [318, 319]. Nevertheless, future studies will be required to better understand obesity-associated inflammation in IBD pathogenesis and drug therapies. More directly associated to CD is the phenomenon of the 'creeping fat' tissue. This adipose tissue phenomenon was first noted by Burrill Crohn in 1932 and describes an expansion of mesenteric adipose tissue that covers more than half of the intestinal circumference at the inflammation site [320]. A recent MRI-based study found that at least 20% of CD patients present with creeping fat tissue at the inflammation site [321]. In patients undergoing intestinal resections, over 60% of patients have creeping fat tissues, possibly suggesting that creeping fat tissue can be used as a marker for disease severity [322]. However, its role, whether protective or pathological, remains enigmatic.

Nevertheless, it points towards a potential link between mesenteric and possibly other 'non-adjacent' adipose tissues (hereafter referred to as 'distal' adipose tissues) with CD and/or other forms of IBD. Interestingly, the lack of adipose tissue-derived leptin in a lipodystrophic CD patient was shown to exacerbate intestinal inflammation in a TNFα-dependent manner [323].

5.1.2 Murine models of intestinal inflammation

Over the past decades, several murine colitis models have been established which can be divided into different classes [324]. The most common models of colitis are induced by administration of chemical agents such as dextran sulfate sodium (DSS). DSS leads to epithelial damage which exposes the lamina propria to the luminal content resulting in myeloid-driven intestinal inflammation. The initiation of this model is independent of T cells as inflammation develops equally in lymphocyte-deplete *Rag*$^{-/-}$ and *SCID* mice compared to immunocompetent mice [325, 326]. This has led to the discovery that monocytes, macrophages and neutrophils in concert contribute to the inflammation upon tissue injury [327]. In contrast, eosinophils appear to be anti-inflammatory in the context of DSS-induced colitis, possibly through production of soluble lipid mediators [328].

Another class of murine colitis models relies on the genetic or adaptive disruption of the intestinal immune tolerance. IL-10 is a crucial cytokine for controlling immune activation and, in the intestine, is a key contributor to establishing and maintaining immune tolerance to the commensal microbiome [329]. Genetic deletion of IL-10 results in the expansion of Th1 and Th17 cells leading to chronic inflammation, however the onset depends on the microbial composition [330]. Interestingly, Treg-derived IL-10 is an important regulator of intestinal tissue homeostasis, since deletion of IL-10 specifically in FOXP3^{+} Tregs leads to development of spontaneous colitis [331, 332]. The sensing of IL-10 by innate immune cells is essential for the regulation of intestinal homeostasis [205]. Consequently, intestinal inflammation can be induced in immunocompetent animals by the administration of the pathobiont *Helicobacter hepaticus* (*Hh*) when an anti-IL10 receptor (IL-10R) blocking antibody is administered. Without the disruption of IL-

10-dependent pathways, immunocompetent mice are able to control *Hh* infection [333, 334]. Similar to *IL10*$^{-/-}$ mice, this model is driven by IFNγ and IL-23, corresponding to Th1 and Th17 responses, respectively [334]. Macrophage-specific deletion of IL-10Rα increases IL-23 production, Th17 activation and the development of spontaneous colitis [335]. Subsequently, *Hh*-induced T cell activation predominantly was shown to drive Th17 cells with a strong Th1 gene expression *in vivo*, although Th1 cells could also induce colitis in an adoptive T cell transfer model [336].

Other models of colitis have been developed, and include models driven by the adoptive transfer of T cells into lymphocyte-deficient *Rag*$^{-/-}$ mice, or intestinal infections with enteric pathogens (e.g. *Salmonella thypimurium*, *Clostridium rodentium*) [337, 338]. Although all of the herein mentioned animal models of IBD reflect some aspects of IBD pathology, arguably none of them entirely reflects human IBD. For instance, most murine colitis models mimic UC rather than CD pathology, except for three described CD-like ileitis mouse models: one mouse model of chronic TNFα overexpression (*TNFdARE*), one model of intestinal epithelial cell-specific deletion of *Atg16l1* and the *SAMP1/YitFc* mouse strain [339, 340, 341]. In addition, the adoptive T cell transfer model cause pathological lesions, including epithelial hyperplasia and immune cell infiltration whilst maintaining tissue integrity, that resemble CD-like disease [342]. Although no known colitis models adequately reproduce the phenomena of 'creeping fat' observed in CD patients, some attempts have been made using chemically induced models [343]. However, some insights into the role of adipose tissues in murine colitis models and in humans have been gained over the past years and will be introduced in the next chapter. Yet, much remains unclear on the regulatory role adipose tissues play during intestinal inflammation.

5.1.3 Context and aim of this chapter

Given the strong genetic link between autophagy regulated genes, creeping fat, and IBD, we sought to investigate the role of adipocyte autophagy in different models of intestinal inflammation. Existing models of small intestinal inflammation are either not amenable to mechanistic studies (*SAMP1/Yitc*), or driven by a single inflammatory

mediator (*TNFdARE*) that might not be of high relevance to adipose tissue-mediated regulation of inflammation. We therefore chose a more unbiased approach, studying an acute (DSS) and a chronic model of intestinal inflammation (IL10R+*Hh*), each of which can be used in the setting of genetic manipulation (*Cre-loxP*). To this end, we (1) set up and characterise the effects of DSS-induced colitis on the adipose tissue and the immune cells therein and (2) evaluate the effects of autophagy loss in adipocytes for the response to acute and chronic intestinal inflammation.

5.2 Results

5.2.1 Low-dose DSS administration induces intestinal inflammation and leads to adipose tissue inflammation and increased adipose tissue autophagy

Acute intestinal inflammation was induced by administration of DSS in drinking water. While the precise mode of action of DSS remains unknown, it causes inflammation through epithelial destruction and breaking the natural barrier between the gut microbiome and immune cells. This model, which resembles human UC most closely [344, 345], leads to an acute body weight loss in mice. Since this could be a consequence of reduced fat mass, we were keen to lower the dose of DSS in drinking water to enable sufficient intestinal inflammation without excessive body weight and adipose tissue loss. Mice were treated with 1.5-2% DSS in drinking water over five days, the lowest concentrations that were previously established to induce reproducible colitis. The inflammatory phenotype was assessed at day 7 after initial DSS treatment, representing peak inflammation. Administration of DSS in drinking water for five days resulted in a significant decrease in body weight at day 7 (∼5% of initial body weight) (Fig.30A) suggesting ongoing inflammation. In line with this, DSS treatment led to a significant destruction of the colonic epithelial architecture, including a loss of goblet cells and crypt structures (Fig.30B). This increase in inflammation could be further confirmed through blinded scoring of colonic histopathology (Fig.30B) and decreased colon length, a characteristic hallmark of this disease model (Fig.30C). Furthermore, we found that mesenteric lymph nodes were significantly increased as measured by weight, while spleen

weight remained unchanged (Fig.30D). To assess the altered immune state in response to DSS-induced colitis, single-cell suspensions from the colonic lamina propria were stained for different immune cell subsets by flow cytometry. This analysis demonstrated a significant increase in total CD45$^+$ immune cells (Fig.30E), which was predominantly due to increases in CD11b$^+$ myeloid and B220$^+$ B cells (Fig.30F).

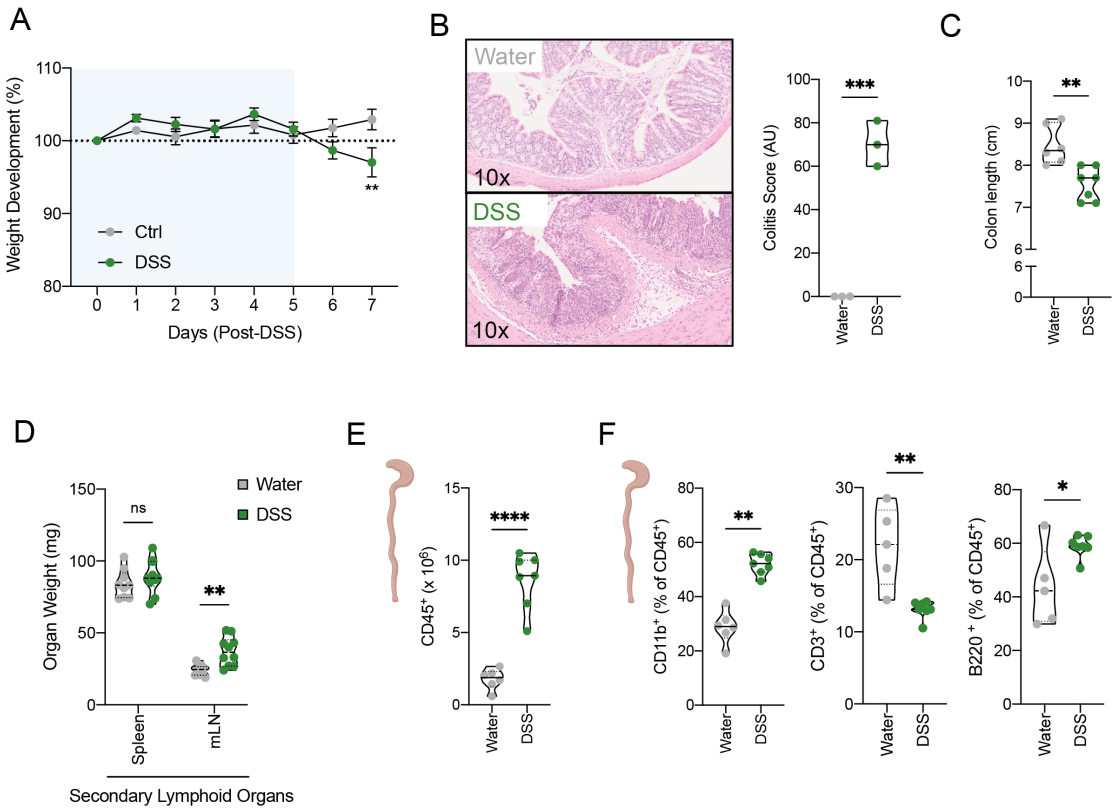

Figure 30: DSS treatment regime results in significant intestinal inflammation. (A) Body weight development of wild-type mice on water with or without 1.5% DSS for five days, as indicated by blue shading. Body weight loss coincides with returning animals to water after five-day DSS regime. (B) Representative images of histopathology and scoring of intestinal inflammation. (C) Measurement of colon length 7 days after initial DSS treatment. (D) Weight of secondary lymphoid organs upon DSS-induced colitis. mLN: mesenteric lymph nodes. (E) Absolute number of CD45$^+$ immune cells in colonic lamina propria at day 7 post-DSS treatment start. (F) Proportion of CD11b$^+$ myeloid cells, CD3$^+$ T and B220$^+$ B cells among all immune cells. Statistical analysis by Student's t-test (B-C, E-F) and Two-Way ANOVA (D). Each data point represents one biological replicate, pooled from at least two independent experiments.

Having confirmed that DSS robustly induces colitis, potential changes in the adipose tissues were investigated next. There was a collective decrease in omental, mesenteric and visceral adipose tissue mass (Fig.31A). We concluded that this treatment regime induced a myeloid-dominant intestinal inflammation and slightly reduced adipose tissue

mass. This was in line with observations that DSS colitic mice showed a significant reduction in circulating levels of FFA in the blood (Fig.31B).

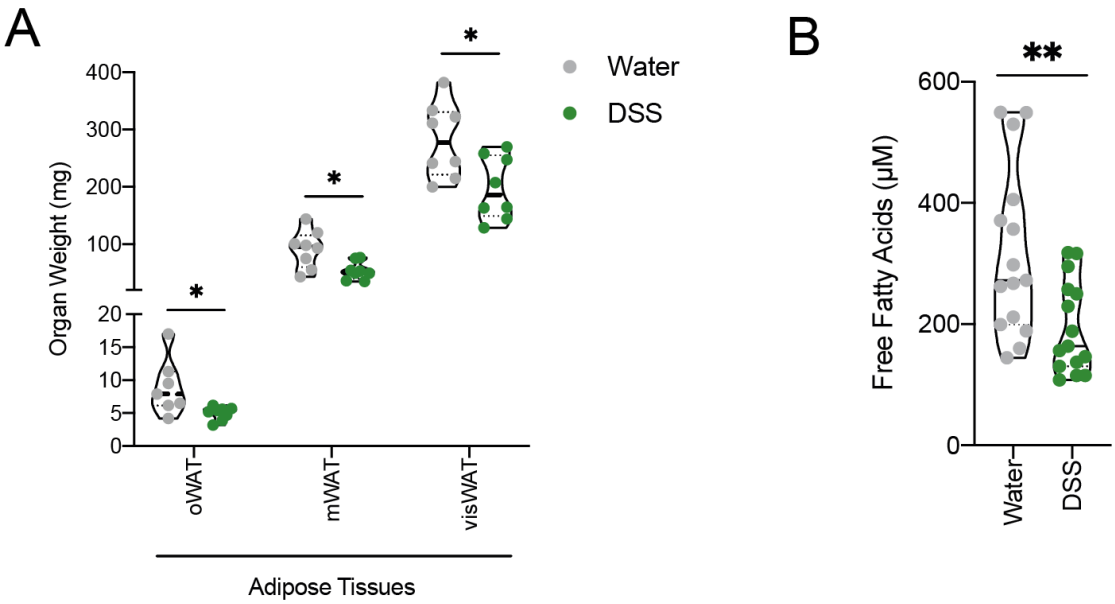

Figure 31: DSS treatment results in limited reduced body and adipose tissue weight. (A) Tissue weights measured in omental (oWAT), mesenteric (mWAT) and visceral white adipose tissue (visWAT) at day 7 after start of DSS regime. (B) Circulating levels of FFA in blood serum at day 7 post-DSS start. Statistical analysis by Two-Way ANOVA (A) and Student's t-test (B). Each data point represents one biological replicate, pooled from at least two independent experiments.

The uptake of long-chain FFA is regulated through expression of the fatty acid transporter CD36, among others [346]. DSS-induced colitis leads to acute inflammation, adipose tissue loss and reduced FFA levels, which prompted the question whether certain intestinal immune cell subsets may sense the difference in circulating FFA evoked by intestinal inflammation. To address this, we first investigated the expression of CD36 on intestinal immune cell subsets (Fig.32). Only $CD206^+$ tissue-resident, intestinal macrophages increase CD36 expression upon DSS-induced colitis, among all quantified myeloid populations (Fig.32A,B). This was in line with a trend in increased intracellular lipids in $CD206^+$ intestinal macrophages as quantified by the neutral lipid dye BODIPY (Fig.32C). Of note, this is however accompanied by a shift in the macrophage balance away from $CD206^+$ tissue-resident towards pro-inflammatory $CD206^-$ macrophage types during DSS colitis (Fig.32D) suggesting a shift towards cells with low CD36 expression during peak inflammation. In contrast to myeloid cells, $CD3^+$ T cells show a signifi-

cant decrease of CD36 expression on their surface (Fig.32E,F). In particular, antigen experienced $CD44^+CD4^+$ and $CD44^+CD8^+$ T cell subsets decreased CD36 expression (Fig.32G). Overall, DSS-induced inflammation reduced the expression of CD36 on intestinal T cells, but increased CD36 on $CD206^+$ tissue resident macrophages. Despite this increase, the expression of CD36 in all myeloid cells remained fairly unaltered suggesting that other colonic immune cells may not require CD36-mediated FFA uptake during peak inflammation.

Adipose tissues provide FFA during times of high energy demand, it is therefore possible that intestinal inflammation may impact on proximal adipose tissues such as the mesenteric white adipose tissue (mWAT) and distal visceral adipose tissue (visWAT) depots. To investigate this, we analysed the impact of DSS-driven intestinal inflammation on immune cell populations in adipose tissues. For this purpose, we isolated immune cells from the proximal mWAT and distal visWAT. We found that there was an increase in total cell numbers isolated from mWAT during DSS-induced colitis after normalization to tissue input, which was not observed in visWAT (Fig.33A). However, we did not observe an increased proportion of $CD45^+$ immune cells among all live cells (Fig.33B, left panel), but a significant increase in $CD45^+$ immune cell numbers (Fig.33B, right panel), indicating an overall increase in adipose tissue cell density. Interestingly, we found a significant increase in $F4/80^+$ ATM numbers in mWAT (Fig.33C). In contrast, $CD19^+$ B cells did increase significantly in mWAT of inflamed mice (Fig.33D). We did, however, find a slightly increased presence of $FOXP3^+$ adipose tissue Tregs (Fig.33E). Overall, this data suggests that DSS-induced colitis leads to an increased cell density in the mWAT potentially due to the loss of adipose tissue during DSS-induced inflammation.

These findings parallel reports from human IBD patients which show an increase in macrophage and T cell number in the mesentery of CD patients [347]. ATMs are the predominant cell type in adipose tissues in mice with and without intestinal inflammation. These cells are well known to be sensitive to local changes in lipid availability by increasing CD36 expression as seen during obesity or by stimulation with the fatty acid palmitate [284]. To understand whether lipid availability was changed in

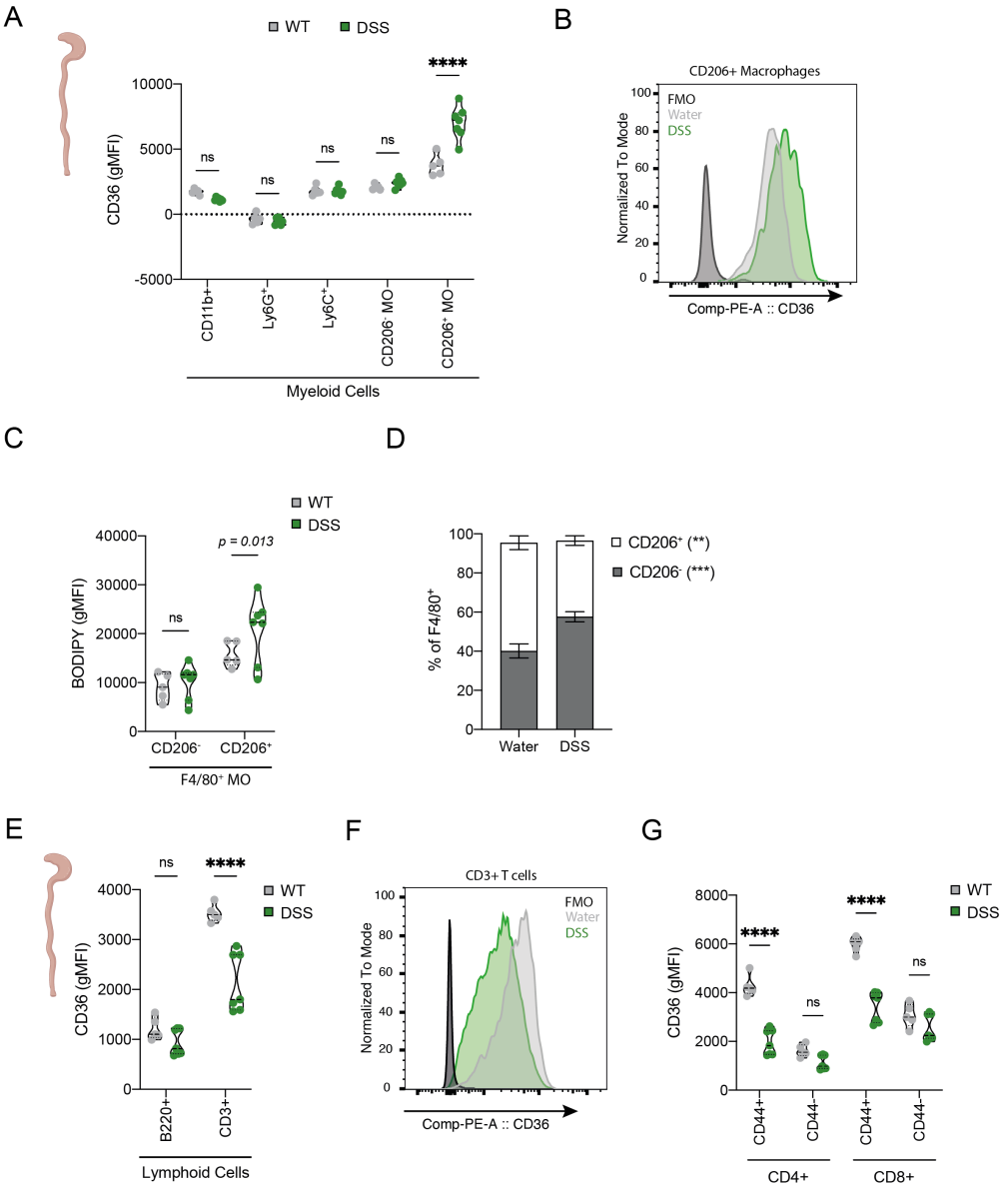

Figure 32: Expression of fatty acid translocase CD36 is increased on intestinal CD206$^+$ macrophages but decreased on antigen-experienced T cells. (A) Geometric mean fluorescence intensity of CD36 on myeloid (CD11b$^+$) cell types including neutrophils (Ly6G$^+$), monocytes (Ly6C$^+$) and macrophage (F4/80$^+$) subsets. (B) Representative histogram of CD36 expression on CD206$^+$ macrophages from water- or DSS-treated animals. (C) Intracellular lipid droplets stained by BODIPY in CD206$^-$ and CD206$^+$ macrophage populations. (D) Proportion of CD206$^-$ vs. CD206$^+$ macrophage subsets shift upon DSS-induced inflammation in the colon. (E) Surface expression of CD36 on CD3$^+$ T and B220$^+$ B cells as presented by the geometric MFI. (F) Representative histogram of CD36 expression on CD3$^+$ T cells upon DSS-induced colitis. (G) Surface expression of CD36 on CD4$^+$ and CD8$^+$ T cell subsets divided into antigen-experienced CD44$^+$ and naïve CD44$^-$ T cells. Statistical analysis by Two-Way ANOVA. Each data point represents one biological replicate, pooled from at least two independent experiments (A-D) and representative data shown for two independent experiments (E-G).

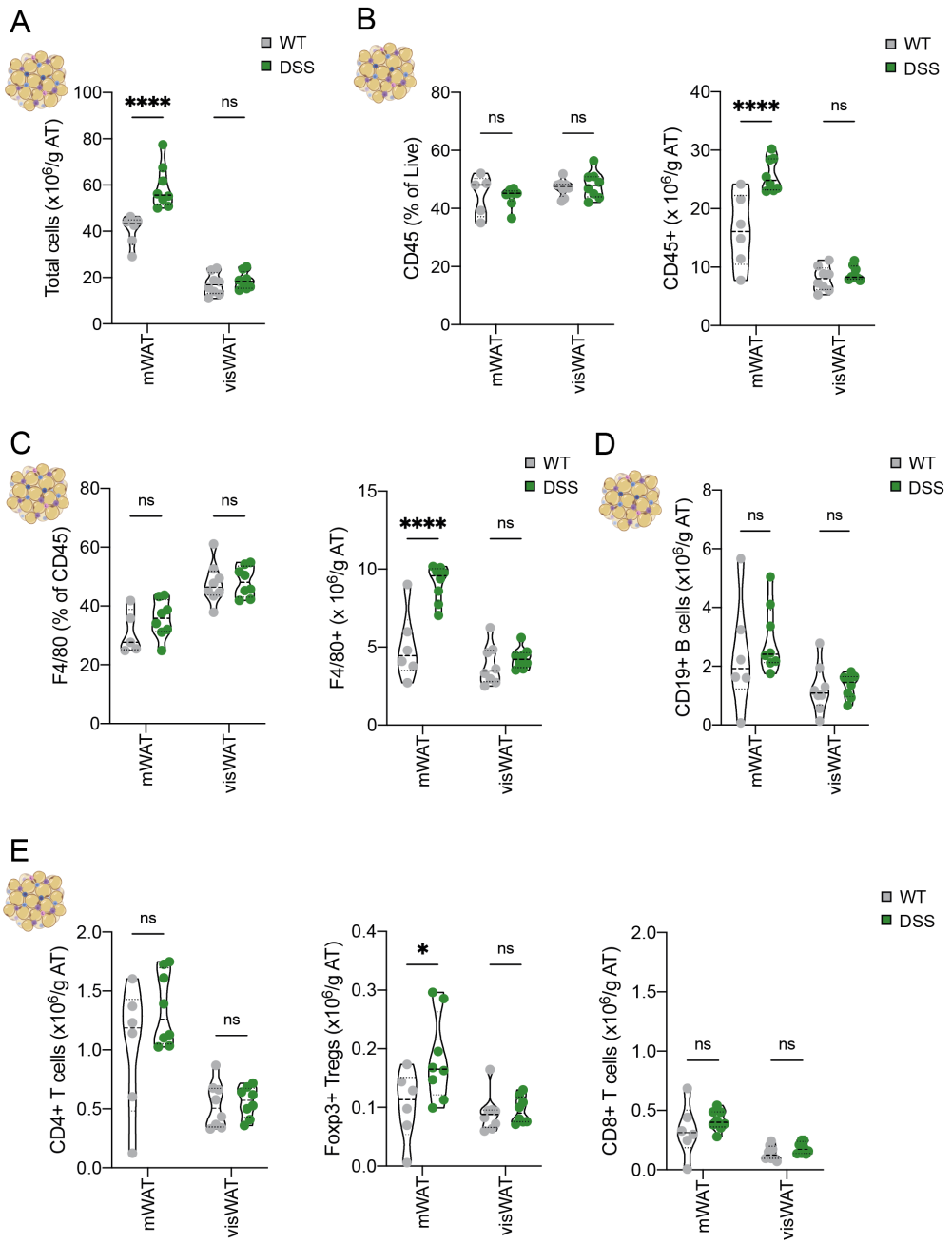

Figure 33: Increased presence of ATMs and adipose tissue Tregs in mesenteric adipose tissue upon DSS-induced intestinal inflammation. (A) Absolute number of live cells in mWAT and visWAT normalized to adipose tissue weight. (B) Frequency of $CD45^+$ of total live cells and absolute number of $CD45^+$ immune cells in mWAT and visWAT of mice treated with water or DSS. (C) Frequency and absolute number of $F4/80^+$ macrophages in adipose tissues upon DSS-induced colitis. (D) Absolute number of $CD19^+$ B cells in mWAT and visWAT. (E) Absolute number of $CD4^+$ and $CD8^+$ T cells and $FOXP3^+$ Tregs in adipose tissues upon DSS-induced colitis. Data pooled from two independent experiments. Statistical analysis by Two-Way ANOVA. Each data point represents one biological replicate, pooled from at least two independent experiments.

the adipose tissue during DSS-induced colitis, we quantified CD36 on ATMs. Interestingly, we found that CD36 expression was significantly increased on ATMs during DSS-induced colitis in both mWAT and visWAT (Fig.34A). This may indicate that both adipose tissue depots undergo lipolysis *in vivo* during acute intestinal inflammation. We did not find any changes in the overall lipid droplet mass as quantified by BODIPY staining in ATMs (data not shown), however ATMs displayed a significant increase in the pro-inflammatory transcription factor Interferon regulatory factor 5 (IRF5) (Fig.34B,C). In contrast, DSS-induced colitis did not alter the expression of the tissue resident marker CD206 on ATMs (Fig.34B,C). This may indicate that ATM become more pro-inflammatory during intestinal inflammation. Together with the up-regulation of CD36, this may be a reaction to increased FFA presence, potentially through increased adipocyte lipolysis [283].

Autophagy is frequently increased in a variety of cell types in response to stress and inflammation [348]. Since energy demands increase during DSS colitis and autophagy in adipocytes can contribute to the release of FFA from adipose tissues [269, 270, 272], we sought to investigate whether autophagy levels were altered upon DSS-induced inflammation in the adipose tissue. To address this, mWAT explants from water- or DSS-treated animals were harvested at day 7 and cultured for 4 hours in the absence or presence of the lysosomal inhibitor BafA1. Upon DSS-induced colitis, autophagic flux significantly increased in mWAT as observed by the accumulation of LC3-II upon lysosomal inhibition (Fig.35A). Although we observed an increase in the tissue autophagy levels upon DSS-induced colitis, it remains unclear whether this increase is due to changes in the autophagic flux in the mature adipocytes or another stromal cell component of the adipose tissue. We therefore employed transmission electron microscopy to confirm autophagosomal structure initiation in the cytoplasm of mature adipocytes upon DSS-induced colitis. Double membrane structures, a hallmark of autophagosomes, were identified in mature adipocyte upon DSS-induced colitis (green arrowhead, Fig.35B). In order to confirm that autophagy is specifically altered in mature adipocytes, we fractionated visceral adipose tissue depots (which did not contain mWAT) into their adipocyte and stromal vascular cell fraction. The choice to use visceral adipose tissues

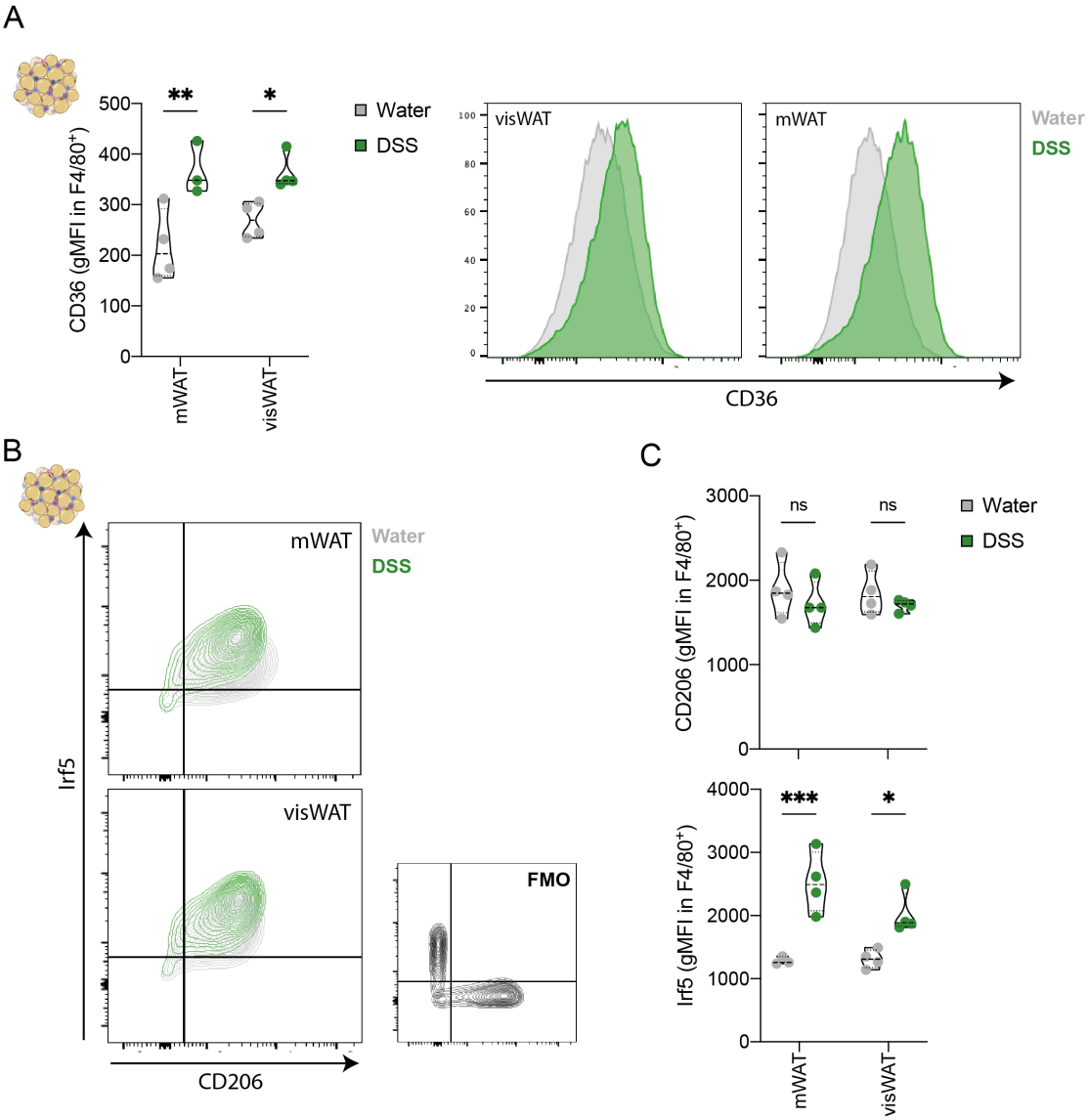

Figure 34: ATMs significantly upregulate CD36 and IRF5 expression during DSS-induced intestinal inflammation in both mWAT and visWAT. (A) Surface expression of CD36 on F4/80$^+$ ATMs in mWAT and visWAT upon DSS-induced inflammation. (B) Representative histograms of IRF5 and CD206 expression on F4/80$^+$ ATMs from water-treated (grey) or DSS-treated mice (green). Gates were set according to fluorescence minus one (FMO) controls (black). (C) Quantification of gMFI of IRF5 and CD206 on ATMs. Representative data shown from two independent experiments. Statistical analysis by Two-Way ANOVA. Each data point represents one biological replicate, data representative for two independent experiments (D).

was based on the limited recovery of floating mesenteric adipocytes after tissue digestion. Gene expression of the *Atg8* homologues, *Map1lc3b* and *Gabarapl1*, were increased upon DSS treatment specifically in the adipocyte, but not in the stromal vascular fraction (Fig.35C). Taken together, our data suggests that autophagy is altered in mesenteric and likely visceral adipocytes upon DSS-induced colitis. However, it remains unclear

whether this increase in adipocyte autophagy is initiated through local changes (e.g. bacterial translocation) or through alterations in systemic mediators such as cytokines. Anyhow, these findings raised the possibility of an important role of adipocyte autophagy in DSS-induced inflammation. Thus, we next sought to use our adipocyte specific KO model to characterise the impact of adipocyte autophagy loss on the intestinal immune response to DSS-induced colitis.

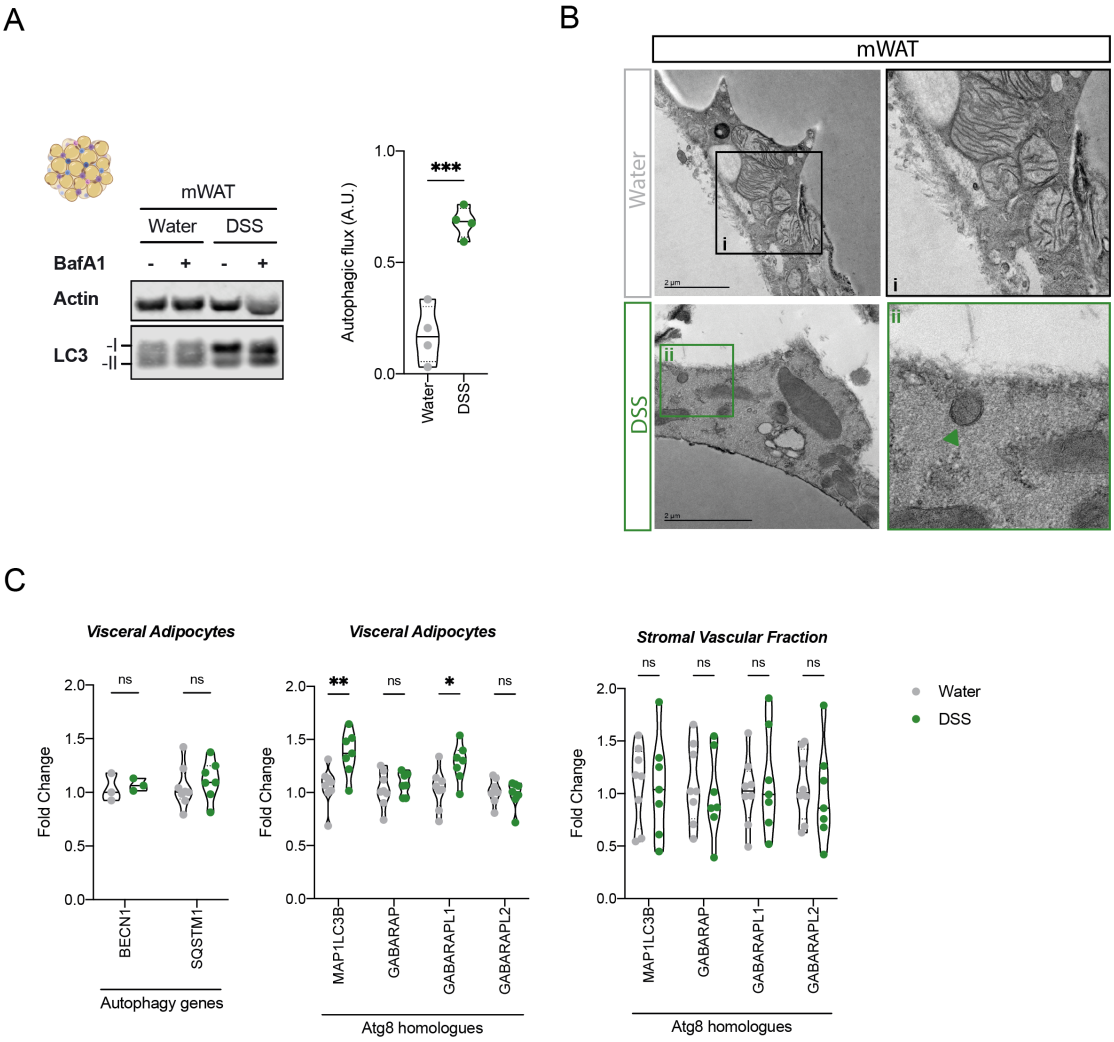

Figure 35: Autophagy is increased during DSS-induced colitis in mesenteric, and potentially visceral adipose tissues. (A) mWAT explants were cultured in the absence or presence of 100nM BafA1 and LC3-II accumulation was analysed by western blotting. (B) Representative transmission electron microscopy images of mesenteric adipose tissue, identifying double membrane structures resembling autophagosomes (green arrowhead). (C) Gene expression of autophagy-related genes in purified visceral adipocytes and visceral stromal vascular fraction. Pooled data from two independent experiments presented as fold change ($2^{-\Delta\Delta Ct}$). Statistical analysis by Student's t-test (A) and Two-Way ANOVA (C). Each data point represents one biological replicate, pooled from at least two independent experiments.

5.2.2 DSS-induced colitis is exacerbated in adipocyte autophagy-deficient mice

We first wanted to investigate whether deletion of adipocyte autophagy can spontaneously lead to intestinal inflammation. Thus, we assessed intestinal inflammation by histopathology of immune cell infiltrates, two weeks after autophagy deletion in adipocytes. Short-term deletion of adipocyte autophagy did not alter the histological architecture of the colon or lead to increased immune cell presence or tertiary lymphoid structure formation (Fig.36A). This was further confirmed by blinded histopathological scoring (Fig.36A). In addition, colon length was comparable between the genotypes (data not shown). The loss of adipocyte autophagy also did not elevate the proportion of total number of $CD45^+$ immune cells in the colonic lamina propria (Fig.36B). Using an established gating strategy for colonic myeloid cells from Jones *et al.* [349] (Fig.36C), we were unable to find any significant increases in myeloid cell populations (Fig.36D).

In addition, we looked specifically at lymphoid cells in the colon (Fig.37A). Analogous to the myeloid compartment, we were unable to detect any differences in the overall T and B cell compartment between mice deficient for autophagy in their adipocytes and littermate controls (Fig.37B). Finally, we also investigated whether the loss of adipocyte autophagy would shift the balance of different $CD4^+$ T cell subsets, potentially due to cell-intrinsic differences in their cell metabolism. T cells subsets were stratified by the expression of lineage specific key transcription factors. However, we were unable to find any differences in $CD4^+$ T cell subsets between the genotypes (Fig.37C).

Overall, our data suggests that short-term deletion of adipocyte autophagy does not alter intestinal homeostasis. This is in line with the observation that homeostatic mice show only little to no autophagic flux as seen in figure 35A. Long-term deletion of 8 weeks equally did not change intestinal inflammation (data not shown). Therefore, we conclude that adipocyte autophagy appears to be dispensable for intestinal health under homeostatic conditions.

Since autophagy in adipose tissues was strongly induced upon intestinal injury, we next

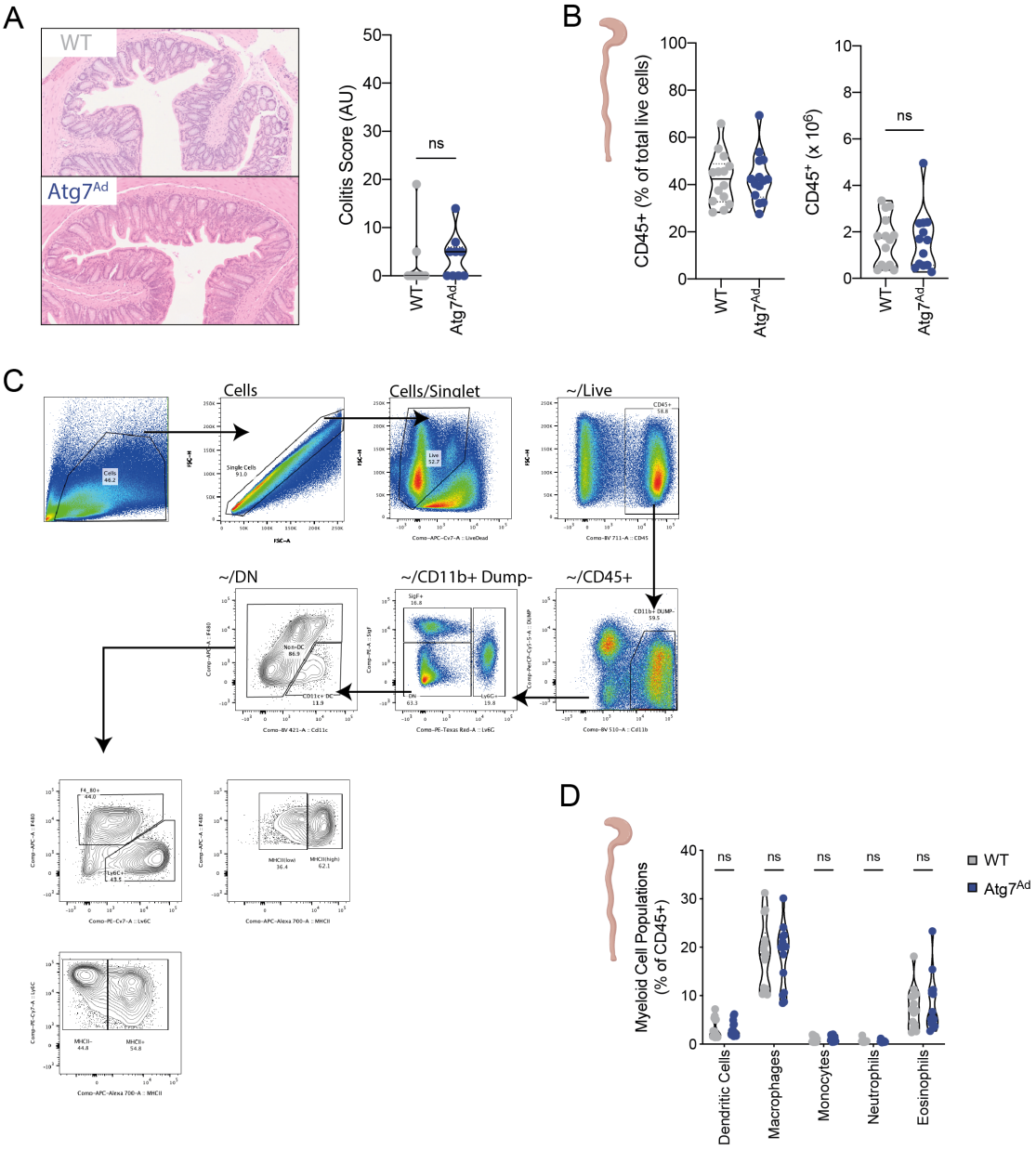

Figure 36: Intestinal health is maintained in adipocyte-autophagy KO mice two weeks post-deletion. (A) Representative images of distal colon (left) and histopathological scores of sections (right) from WT (Cre^{-} $Atg7^{f/f}$) and adipocyte autophagy KO mice ((Cre^{+} $Atg7^{f/f}$) two-week post-deletion. (B) Frequency (right) and absolute number of $CD45^{+}$ immune cells present in colons as measured by flow cytometry. (C) Intestinal myeloid gating strategy adapted from Jones *et al.* (40). (D) Frequency of colonic myeloid cell populations from adipocyte autophagy deficient ($Atg7^{Ad}$) mice and littermate controls (WT). Statistical analysis by Student's t-test (A-B) and Two-Way ANOVA (C). Each data point represents one biological replicate, pooled from two independent experiments.

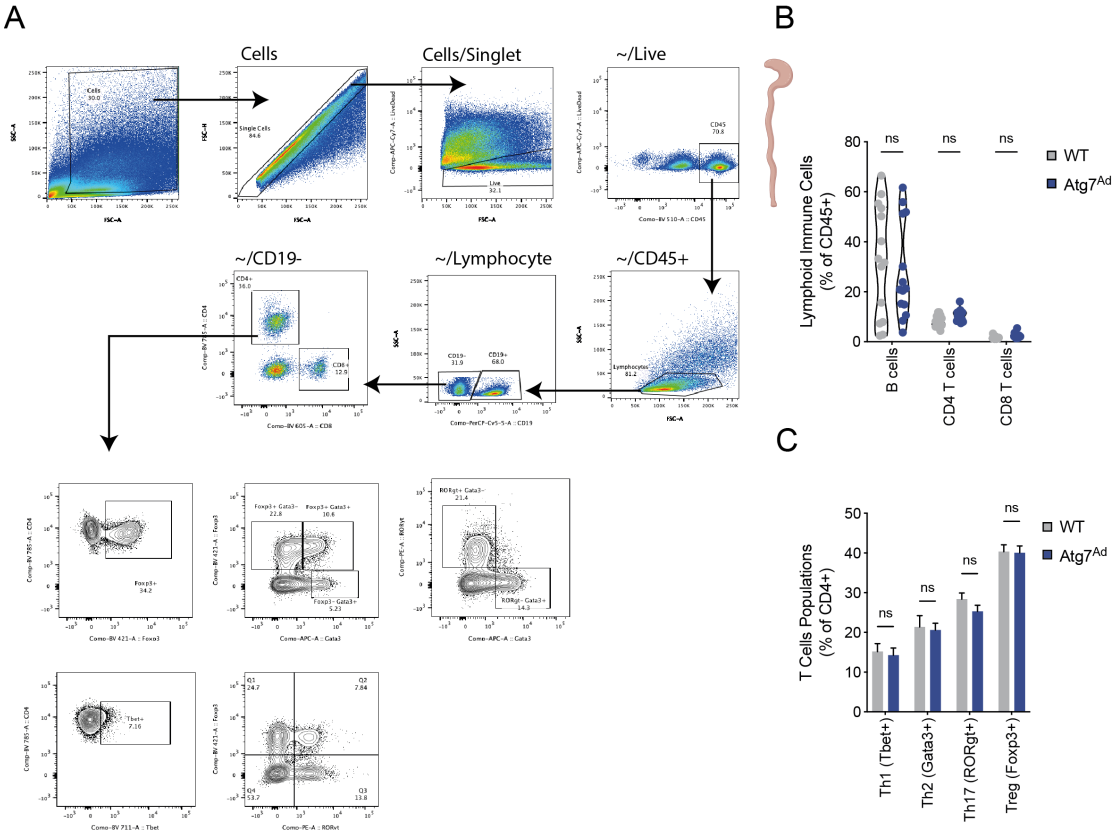

Figure 37: Intestinal lymphoid populations remain unaltered during homeostatic loss of adipocyte autophagy. (A) Lymphoid gating scheme for intestinal immune cells. (B) Frequency of lymphoid immune cell populations two weeks after autophagy deletion in adipocytes. (C) Frequency of $CD4^+$ T cell subsets in the colon. Statistical analysis by Two-Way ANOVA. Each data point represents one biological replicate, pooled from two independent experiments.

sought to challenge adipocyte autophagy-deficient mice with DSS. Two weeks after tamoxifen treatment, mice were treated with DSS for five days before samples were collected at peak inflammation at day seven (Fig.38A). Steady-state tamoxifen-treated wild-type and $Atg7^{Ad}$ mice were grouped together as 'control' (Ctrl) group in these experiments as they did not show significant differences under homeostasis. Across three independent cohorts, body weight loss trended to be stronger in $Atg7^{Ad}$ mice compared to DSS-treated wild-type controls (Fig.38B). In addition, colons from adipocyte autophagy-deficient mice trended to be shorter than in wild-type littermates, although not reaching statistical significance (Fig.38C).

Histopathological analysis of proximal, mid and distal colon tissue revealed increased intestinal tissue damage, which was confirmed by blinded scoring (Fig.38D). Of note, we found that the histopathological effect appeared to be more pronounced in females com-

pared to males, while colon shortening was observed equally in both sexes (Fig.38C,D (right graphs)). Intestinal inflammation tended to be increased at each individual colon site (Fig.38E). When stratified by genotype and tissue location, $Atg7^{Ad}$ show significantly higher histological inflammation. We further confirmed that autophagy loss increased the histologic subscore of inflammation, however the other criteria tended to be increased too (Fig.38F). Analysis across these subscores revealed a significant increase of inflammation based on genotype. To ensure that this phenotype was not just due to a particular scoring system, we verified the increase in colonic inflammation using a second scoring system of intestinal inflammation, typically used for the *Hh*-induced mouse models [350]. Both scoring systems showed the same results (data not shown), however the Dielemann scoring system allowed for greater detail into tissue alterations and is better adjusted for DSS-inflicted tissue injury [351].

In line with the increased histologic inflammation, we found that the expression of the alarmin *Il33* was significantly increased in the KO model compared to DSS treated wild type littermates (Fig.39A). Similarly, we found that *Tnfα* and the TNFα-inducible gene Pentraxin 3 (*Ptx3*) were increased upon tissue injury. Furthermore, we found that the expression of other pro-inflammatory cytokines (e.g. *Il1a*, *Il1b*, *S100a9*), which are known to be up-regulated during DSS-induced colitis, were also elevated (Fig.39B). A driver for DSS-induced colitis is *Ifnγ* expression (42). Both *Ifnγ* and IFNγ-regulated genes such as *Cxcl9* showed increased expression (Fig.39C). Overall, these phenotypes indicate that the loss of adipocyte autophagy aggravates DSS-induced inflammation in the intestine.

Total numbers of immune cells were not changed between genotypes upon DSS-induced intestinal inflammation (Fig.40A). When we assessed lymphoid cell populations, we found a trend to increased B cell frequency (Fig.40B). This increase was, however, not reflected in total B cell abundance in the colon (Fig.40C). Next, we quantified myeloid cell presence in the inflamed colon of wild-type and $Atg7^{Ad}$ mice. $Atg7^{Ad}$ mice showed a significant increase in monocyte frequency in the inflamed colon (Fig.40D). When separated into infiltrating (Ly6C$^+$ MHCII$^-$) and inflammatory monocytes (Ly6C$^+$ MHCII$^+$)

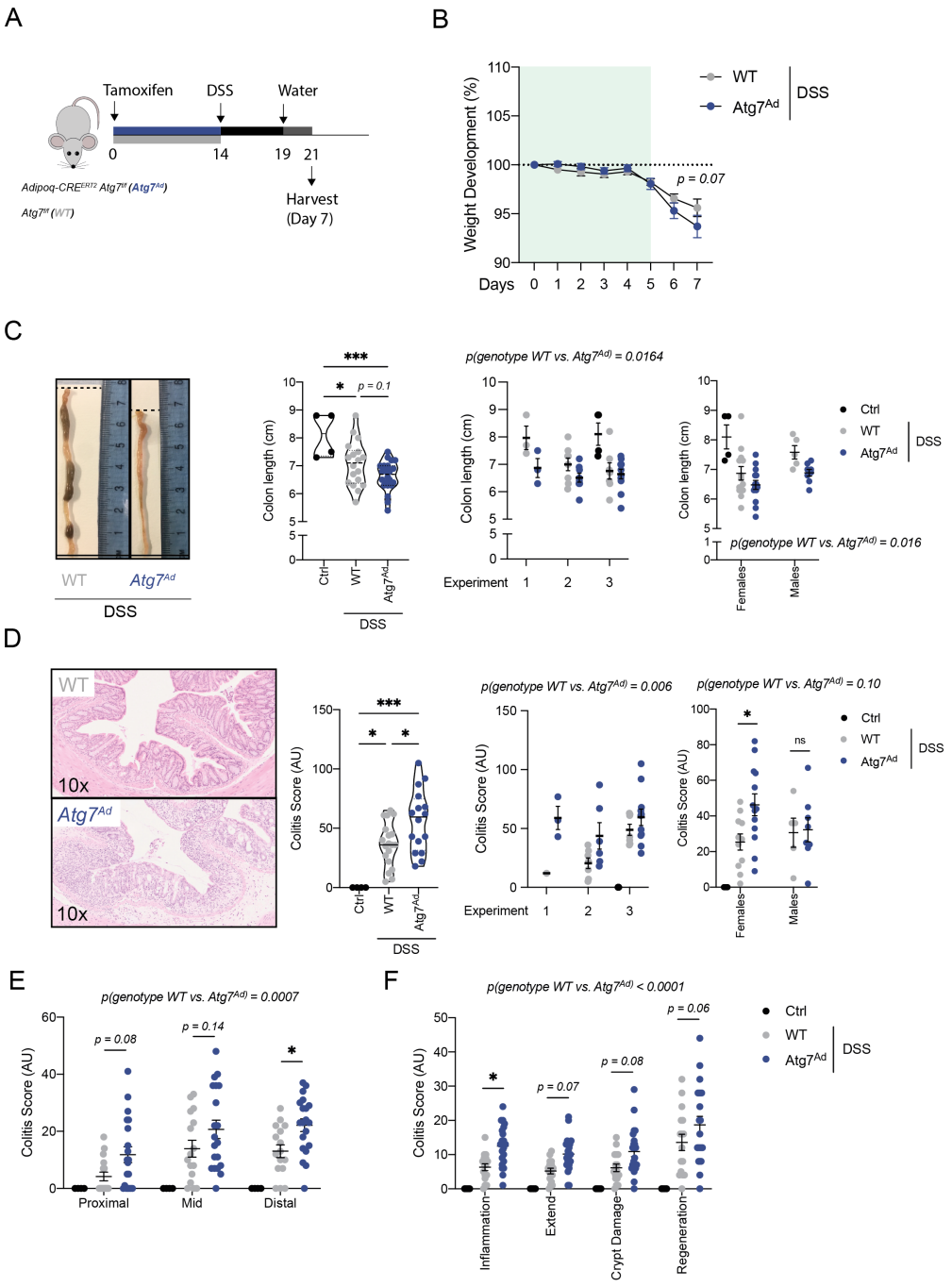

Figure 38: Loss of adipocyte autophagy leads to exacerbation of DSS-induced intestinal inflammation. (A) Experimental setup. (B) Weight development from start of DSS-treatment in WT and *Atg7*^{Ad} mice. (C) Representative image of colon length at days 7 after inflammation (left graph) and quantification of colon length of both sexes combined (middle left graph), separated by experiment (middle right graph) and separated by sex (right graph). (D) Representative image of colon histopathology (left graph) and quantification of colitis score of both sexes combined (middle left graph), separated by experiment (middle right graph) and separated by sex (right graph). (E) Histopathological scoring by colon location. (F) Histopathology scoring by tissue damage class according to Dieleman *et al.* [351]. Statistical analysis by Two-Way ANOVA (A,E-F) and One-Way ANOVA (C-D). Data pooled from three independent experiments; each data point is one biological replicate.

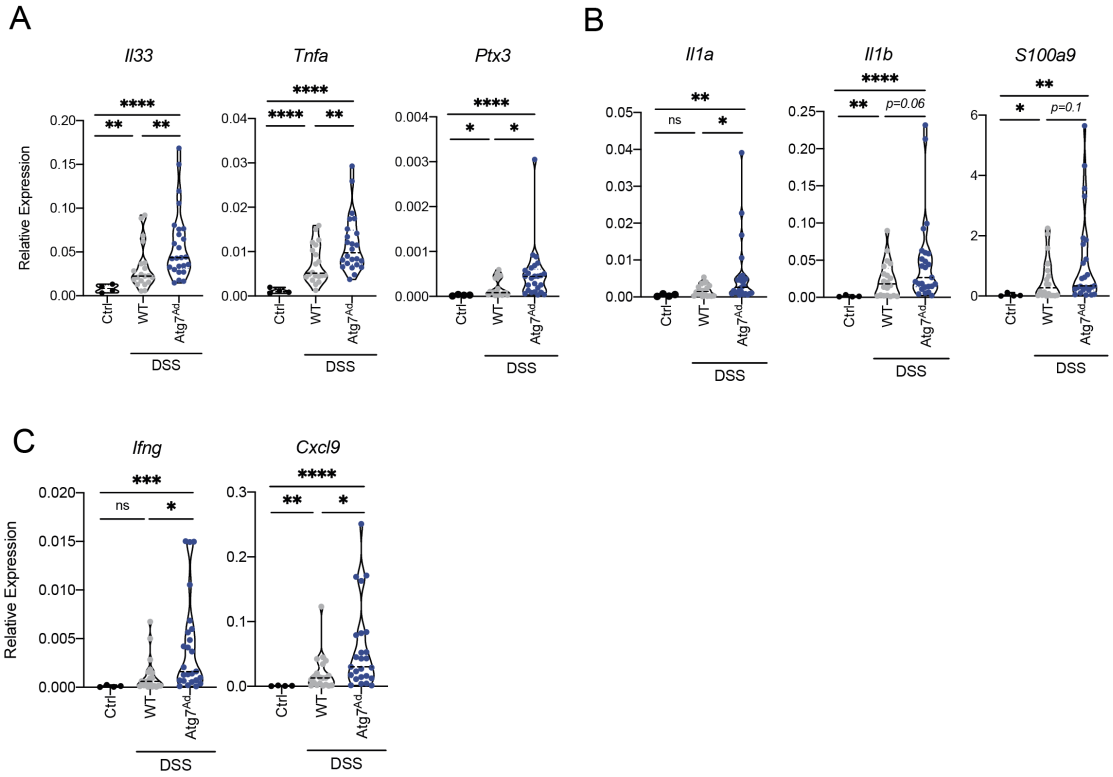

Figure 39: Loss of adipocyte autophagy increases the expression of several pro-inflammatory genes in the inflamed colon. Gene expression in whole colon tissues of (A) *Tnfα* and TNFα-inducible genes *Il33* and *Ptx3*, (B) classical innate pro-inflammatory gene and (C) *Ifnγ* and IFNγ-regulated gene *Cxcl9*. Statistical analysis by Two-Way ANOVA on log transformed values and confirmation of normal distribution. Data pooled from three independent experiments; each data point is one biological replicate.

this translated into a increased presence of MHCII+ inflammatory monocytes (Fig.40E). Two-Way ANOVA comparing the genotypes, independent of specific monocyte subsets, further demonstrates that the genotype increased monocyte presence in the colon of $Atg7^{Ad}$ compared to wild-type mice (Fig.40E). In summary, our data revealed a role of adipocyte autophagy in controlling acute intestinal inflammation.

Lastly, we were interested in whether loss of adipocyte autophagy would not only alter peak inflammation but also resolution. We therefore assessed intestinal health 14 days after the start of DSS treatment (Fig.41A). We were unable to detect substantial histopathological differences between the genotypes at the late inflammation/resolution time point (Fig.41B). In line with this, colon length was comparable between wild-type and $Atg7^{Ad}$ mice (Fig.41C). Interestingly, we observed an increased proportion and total cell number of FOXP3$^+$ Tregs in the colon of recovering wild-type mice com-

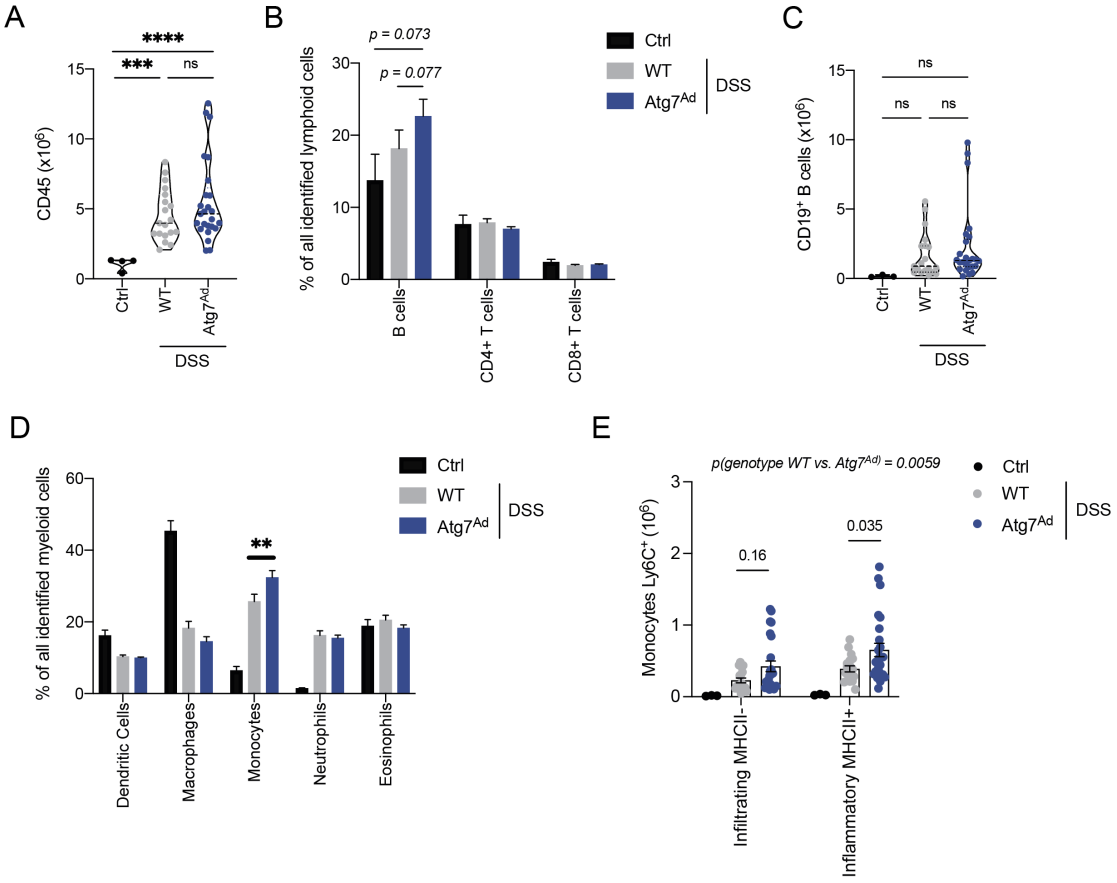

Figure 40: Immune cell infiltration was largely comparable between wild-type and *Atg7^{Ad}* mice. (A) Total number of CD45$^+$ immune cells in colon tissue at day 7 post-DSS start. (B) Fraction of lymphoid cells among all CD45$^+$ cells identified. (C) Total number of intestinal CD19$^+$ B cells. (D) Fraction of myeloid cells among all CD45$^+$ cells identified. (E) Total number of infiltrating monocytes (Ly6C$^+$ MHCII$^-$) and inflammatory monocytes (Ly6C$^+$ MHCII$^+$). Statistical analysis by One-Way ANOVA (A,C) and Two-Way ANOVA (B,D,E). Data pooled from three independent experiments; each datapoint is one biological replicate.

pared to adipocyte autophagy-deficient animals (Fig.41D). Intestinal FOXP3$^+$ Tregs can be further distinguished into three subsets depending on their co-expression of the transcription factors RORγt and GATA3 [352]. Using this classification, we aimed to further identify whether specific subsets of Tregs were affected by the loss of adipocyte autophagy during colitis remission. While all Treg subsets trended to be slightly reduced, only RORγt$^-$ Tregs frequencies were significantly decreased in recovering *Atg7^{Ad}* mice (Fig.41E). To see whether resolution was differentially regulated in the KO mouse model, we assessed gene expression of pro-resolving cytokines in whole colon tissue. Despite differences in Treg populations, neither *Il22* nor *Il10* nor *Tgfb1* showed consistent differential regulation between the models, indicating that the overall recovery is not

impaired in $Atg7^{Ad}$ mice upon DSS colitis (Fig.41F).

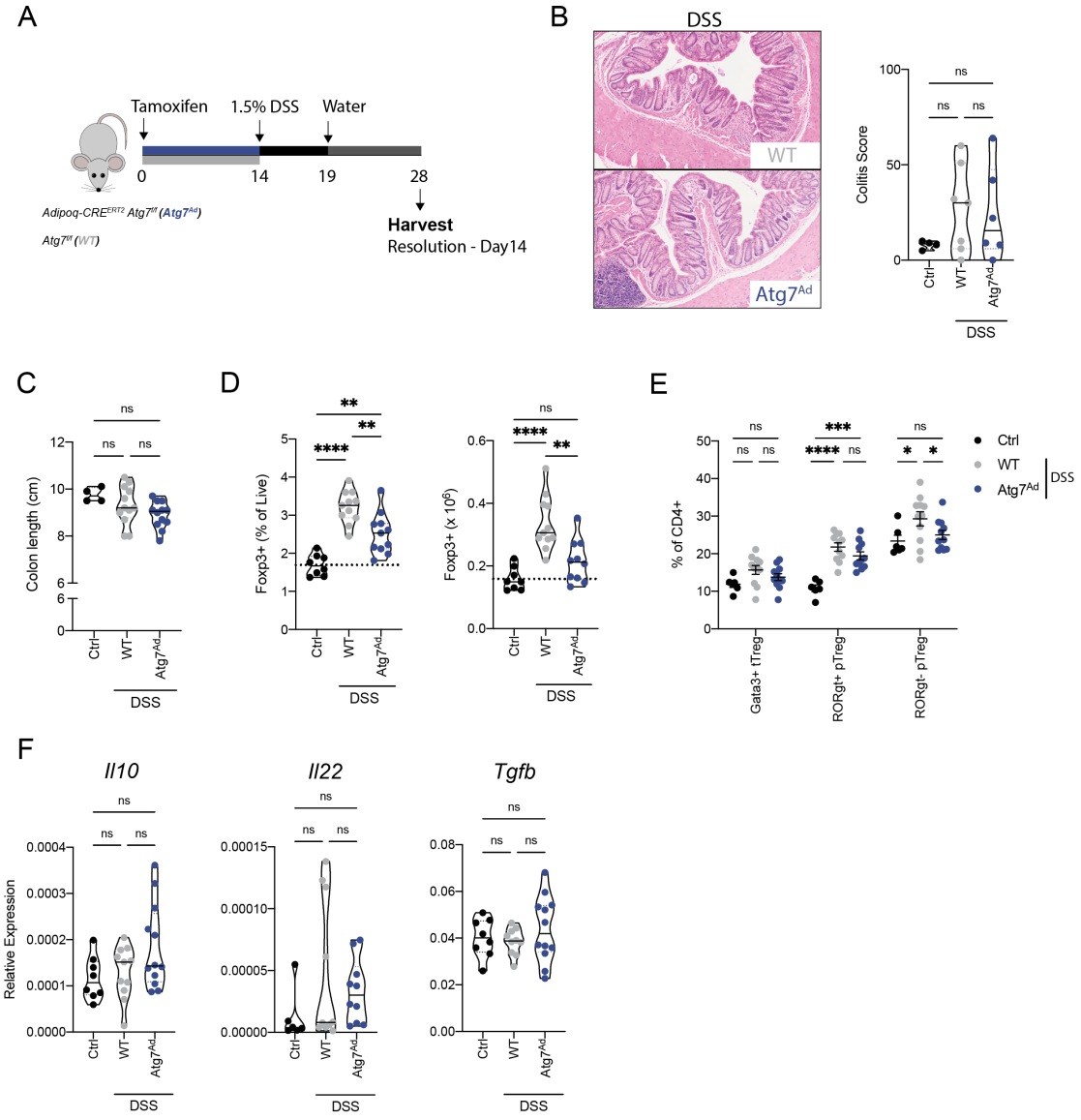

Figure 41: Blunted increase in intestinal Treg numbers during DSS recovery in $Atg7^{Ad}$ mice. (A) Schematic of experimental setup to investigate DSS recovery. (B) Representative histopathological images (left) and scoring (right) of proximal, mid and distal colon at resolution time point. (C) Colon length measured at resolution time point. (D) Frequency and total number of intestinal FOXP3$^+$ Tregs at day 14 after start of DSS treatment. (E) Frequency of FOXP3$^+$ Treg subsets in recovering colon. (F) Gene expression of pro-resolving/pro-repair cytokines in the colon at day 14 post-DSS start measured by qPCR. Statistical analysis by One-Way ANOVA (B-C), One-Way ANOVA on log transformed data (F) and Two-Way ANOVA (E). Data pooled from two independent experiments; each datapoint is one biological replicate.

In summary, we could demonstrate that the loss of adipocyte autophagy increases intestinal inflammation in response to DSS-induced injury by leading to increased tissue damage measured by both histology and pro-injury and pro-inflammatory cytokine ex-

pression in the colon. This exacerbation of the intestinal inflammation was accompanied by an increased infiltration of monocytes into the tissue. Although decreased FOXP3$^+$ Tregs were observed, loss of autophagy in adipocytes did not affect the overall recovery of the mice.

5.2.3 Helicobacter hepaticus-driven inflammation is not influenced by the loss of adipocyte autophagy

We next sought to understand whether adipocyte autophagy loss in chronic models of colitis would equally lead to an exacerbation of intestinal inflammation. The administration of *Hh* to susceptible hosts can drive disease phenotypes resembling human IBD. Experimentally, most protocols create a susceptible host environment by co-administration of IL-10R blocking antibody, which interrupts intestinal homeostatic control mechanism to *Hh* colonization. This model is driven by an IL-23-driven Th1/Th17 response as marked by the expression of IFNγ and IL-17, respectively. We therefore used the $Atg7^{Ad}$ mouse model to investigate whether adipocyte autophagy loss may also lead to increased intestinal inflammation in a more chronic model of murine colitis and the context of IL-10 pathway deficiency.

To assess this, mice were gavaged *Hh* for two consecutive days and administered two injections of anti-IL10R blocking antibodies one week apart (Fig.42A). Mice were either sacrificed after two weeks (peak inflammation) or six weeks (resolution). Histological sections stained by H&E revealed an influx of immune cell populations into the colonic lamina propria and epithelial erosion two weeks after *Hh* administration (Fig.42B). Upon resolution, epithelial damage was largely repaired, but some increased immune cell presence was still visible (Fig.42B). However, disease severity was comparable between the genotype groups at each of the time points (Fig.42C). Spleen weights, an indicator for adaptive immune cell activation, was increased after two weeks, however unaltered between the investigated genotypes. *Hh*-induced colitis is mainly driven by Th1 and Th17 cytokines [334]. Using colonic tissue RNA, we quantified the expression of several chemokines, and pro- and anti-inflammatory cytokines involved in the pathology. However, colon tissues from $Atg7^{Ad}$ mice showed comparable levels of *Hh*

colitis-induced gene expression as presented for key cytokines *Tnfα*, Th1/Th17 cytokine *Ifnγ* and Th17-inducing cytokine *Il23a* (Fig.42E).

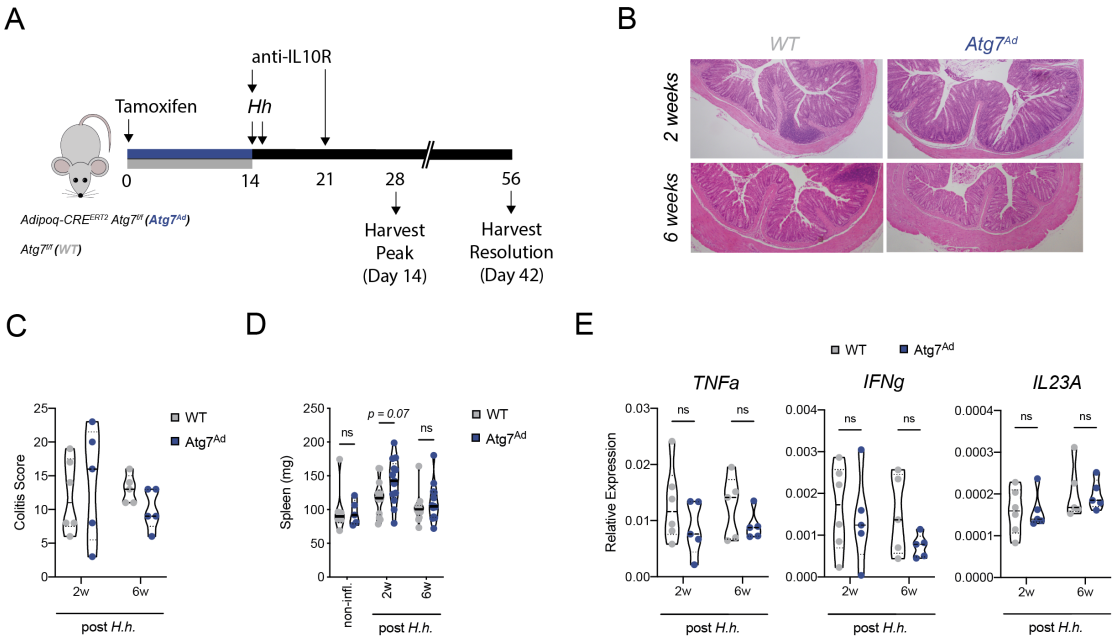

Figure 42: Loss of adipocyte autophagy does not alter the response to *Hh*-induced colitis. (A) Experimental setup of *Hh*-mediated colitis in wild-type and *Atg7*^{Ad} mice. (B) Representative pictures of distal colonic tissue sections stained with H&E. (C) Combined colitis scores from histological sections of proximal, mid and distal colon. (D) Spleen weight at different time points after *Hh*-induced colitis. (E) Gene expression of pro-inflammatory cytokines during *Hh*-induced colitis. Statistical analysis by Two-Way ANOVA (C-D) and Two-Way ANOVA on log transformed data (E) Data pooled from two independent experiments; each datapoint is one biological replicate.

In addition, both genotypes showed a comparable increase in immune cells two weeks (Fig.43A) and six weeks (Fig.43E) after *Hh* administration. At the two-week time point, an increased proportion of monocytes and neutrophils were present in the inflamed colon, however equal for both genotypes (Fig.43B). In line with the model used, we also found an increased presence of CD4$^+$ T cells although this increase was independent of the genotype used (Fig.43C), even after separating for CD4$^+$ T cell subsets (Fig. 43D). At the 6-week time point, the mice still showed an increased presence of immune cells in the colon (Fig.43E). While the proportion of myeloid cells had returned to baseline levels, CD4$^+$ T cell populations were still increased (Fig.43F,G). Total numbers of all CD4$^+$ T cell subpopulations was increased compared to non-inflamed control animals, however

no apparent difference was detected between the inflamed groups by their genotype (Fig.43H).

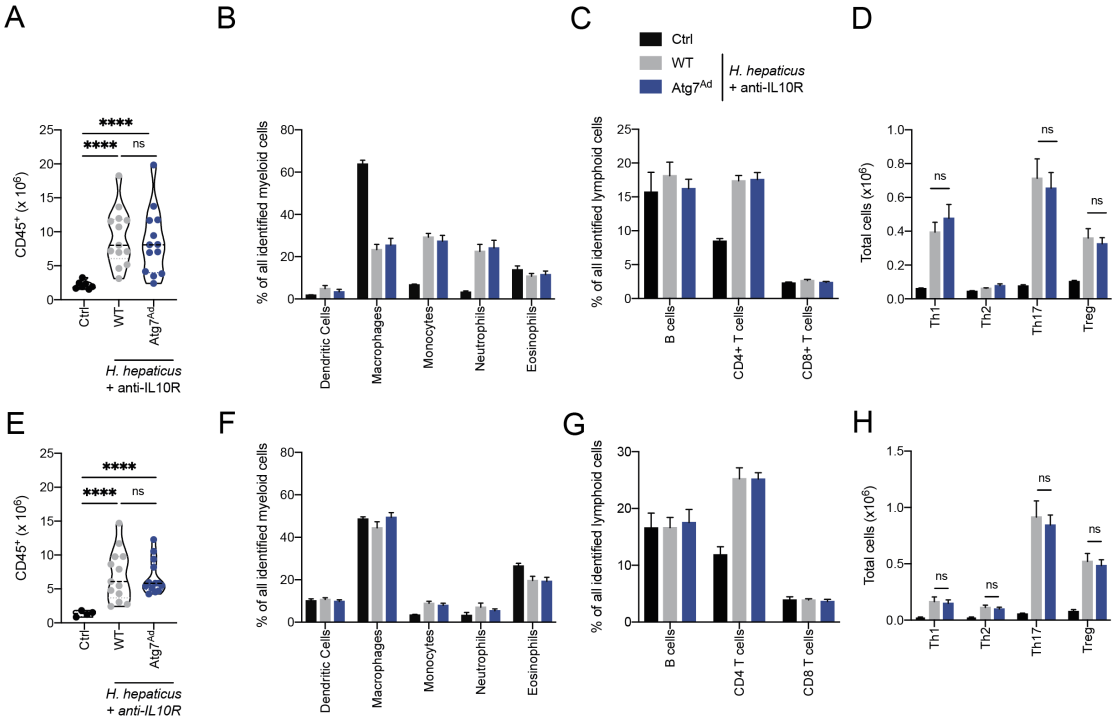

Figure 43: Intestinal immune cell populations were comparable between *Atg7^{Ad}* and control mice two and six weeks post-*Hh* treatment. Quantification of immune cell presence in colonic lamina propria after two weeks (A-D) and six weeks (E-H) after *Hh* administration. (A,E) Absolute number of colonic CD45$^+$ immune cells at given time point. (B,F) Frequency of myeloid cells at given time point. (C,G) Frequency of lymphoid cell populations at given time point. (D,H) Total number of CD4$^+$ T cell subsets in colon at given time point. Statistical analysis by One-Way ANOVA (A,E) and Two-Way ANOVA (B-D, F-H). Data pooled from two independent experiments; each datapoint is one biological replicate.

To summarize, the loss of autophagy in adipocytes did not affect *Hh*-induced colitis severity. Therefore, we dropped this model in the following chapter and focussed on the DSS-induced model of colitis to understand mechanisms of how adipocyte autophagy loss regulates intestinal inflammation.

5.3 Discussion

5.3.1 Adipose tissues respond to murine models of colitis and induce autophagy

Weight loss is a common denominator of IBD pathologies for both UC and CD patients [353]. This may be caused by malnutrition, decreased food intake, malabsorption and increased energy demands due to the ongoing inflammation. Many acute models of intestinal inflammation (such as DSS) show similar reductions in total body weight and adipose tissue mass. We applied a model of DSS-induced intestinal inflammation to mirror this pathology. The role of adipose tissues, especially the mesentery, during intestinal inflammation remains enigmatic. It was recently proposed that during DSS-induced colitis adipose tissues increase lipolysis thereby providing FFA to the circulation and meeting increased energy demands [354]. In contrast to their study, we did not observe an increase, but rather decrease of circulating FFA levels. These apparent contradicting findings may be explained by experimental differences in timing and possibly animal starting weight. The reduction in circulating FFA levels observed in our study correlates well with decreased levels in total visceral adipose tissues (a measurement that was not undertaken in the published study), suggesting that adipocytes may have already undergone peak lipolysis at the time of measurement.

CD36 is arguably the best characterized receptor for long-chain fatty acids contributing to intracellular FFA uptake, lipid homeostasis and dysfunction [346]. Furthermore, the uptake of lipids is essential to type 2 macrophage activation [355]. Interestingly, the CD36-dependent uptake of oxidized LDL particles into macrophages is characteristic for foam cell formation during atherosclerosis [356]. Beside macrophages, lymphocyte function and phenotype can be controlled via their CD36 expression. In the case of Tregs, loss of CD36 on intra-tumoral Tregs can reduce immune suppression and consequently limit cancer growth [357]. In tissues (e.g. gut, adipose tissues), CD36 expression is often increased on Tregs suggesting a critical role of CD36-mediated maintenance of tissue homeostasis [92, 146]. In addition, the uptake of exogenous lipids during high fat

diet in mice is restricted to CD36-expressing lymphocytes [358]. Upon DSS-induced colitis, macrophages in mesenteric and collective visceral adipose tissues up-regulate CD36 expression, possibly in response to the increased lipolytic output of the adipose tissue. ATMs are well-known to buffer toxic effects of adipose tissue lipolysis through uptake of exogenous lipids [283]. In addition, we observed that DSS-induced colitis increases the expression of the pro-inflammatory transcription factor IRF5 in both tested adipose tissues depots, whereas tissue resident CD206 marker expression remained unchanged. IRF5 is associated with increased expression of genes involved in pro-inflammatory pathways as seen previously in obesity and colitis [359, 360]. Observing an increase in IRF5 expression in ATM suggest that these cells may react to the inflammatory environment in the gut, either through the increase in lipolysis or through circulating pro-inflammatory factors (e.g. bacterial antigens or cytokines). To verify this, IRF5-dependent cytokines such as IL-12 and IL-23 could be quantified in adipose tissues.

Published data using the DSS colitis model suggest a possible involvement of the mesenteric adipose tissue to control bacterial translocation [189]. This study also shows significant increases of $F4/80^+$ macrophages and $CD3^+$ T cells into the mesenteric adipose tissue, but not in subcutaneous compartments. This is in line with the increase in macrophage and Treg numbers observed in our study supporting that the mesentery becomes densely packed with immune cells during colitis.

In contrast, infiltrating monocytes and neutrophils in the colon did not reveal any differences in CD36 expression. During colitis, the site of inflammation quickly becomes hypoxic and nutrient deprived [361]. This environment generally promotes a metabolic shift towards glycolysis in pro-inflammatory monocytes, macrophages and neutrophils [362]. Especially, neutrophils require production of ROS for bacterial killing. Interestingly, drugs targeting metabolic pathways such as dimethyl fumarate can reduce neutrophil induced inflammatory damage in models of experimental colitis in mice via the activation of the antioxidant transcriptional master regulator NRF2 [363, 364]. Using a targeted approach to alter the metabolism of pro-inflammatory cells to limit tissue damage may be promising for future anti-inflammatory therapies [362].

Lastly, induction of DSS colitis led to an increase in autophagic flux in the mesenteric

adipose tissue. Early studies from Leal *et al.* show that LC3-II levels are reduced in adipose tissue explants from human CD patients compared to controls [365]. Since the study did not use any lysosomal inhibitors to prevent LC3 degradation, the observed reduction in LC3-II could also be the consequence of an increased autophagic flux rather than a decrease in autophagy as LC3-II is degraded in the lysosomes. However, the changes we observed in whole tissue autophagy levels could be due to changes in either stromal cells or adipocytes or both. To identify which cell type increased its autophagic flux during DSS-induced colitis, we employed two experimental approaches [16]: First, double-membrane structures (possibly autophagosomes) were present in the cytoplasm of adipocytes during DSS-colitis but not in immune cells. Second, the *Atg8* homologues *Map1lc3b* and *Gabarapl1* were upregulated during DSS-induced colitis in visceral adipocytes but not in its stromal vascular fraction. In some instances, the induction of autophagy can be accompanied by an increase in autophagy related gene expression such as *Atg8* homologues. During muscle atrophy, activation of the transcription factor FOXO3 through the PI3K-AKT signalling pathway can control the expression of *Map1lc3b*, *Gabarapl1*, *Bnip3*, *Bnip3l* and *Vps34* [73, 366]. FOXO3 can directly bind to the promoter regions of the autophagy genes *Map1lc3b* and *Gabarapl1* to enhance their expression and autophagy levels [366]. Similar to the muscle atrophy and cachexia, DSS induced mice undergo a severe loss in adipose tissue mass possibly due to increased metabolic demands and insufficient calorie intake. However, it remains to be explored whether FOXO3 is activated in adipocytes during DSS induced colitis and is contributing to the loss of adipose tissue.

In general, these explorative experiments underline that autophagy is upregulated in wild-type animals and prompted us to investigate its role during DSS-induced colitis.

5.3.2 Adipocyte autophagy controls the inflammation in DSS but not *H. hepaticus*-induced colitis, and not under homeostatic conditions

The effects of genetic autophagy loss in the context of intestinal health have been studied in several cell types such as intestinal epithelial cells [367], Paneth cells [220, 368], macrophages [369, 370] and T cells [92]. However, the role of adipocyte autophagy

during intestinal inflammation remained unexplored. Genetic deletion of autophagy is often associated to an increase in inflammation [75]. For instance, autophagy loss in macrophages can lead to impaired LAP, increased inflammatory cytokine secretion and production of ROS [75, 31, 371, 98]. Interestingly, in our study, we found that adipocyte-specific loss of autophagy increases intestinal tissue inflammation in response to DSS-induced colitis. In contrast, the deletion had no impact on intestinal health under homeostatic conditions or in the chronic *Hh* colitis model. This suggest that autophagy may play a specific role during DSS-induced pathology. From a pathological and mechanistic perspective, the *Hh*- and DSS-induced colitis are quite distinct from one another. Whilst DSS-induced colitis causes epithelial barrier breakdown, *Hh* induces generally epithelial hyperplasia [372]. Even more important, the breakage of intestinal homeostasis by blocking the IL-10R is crucial for *Hh*-induced colitis [373]. While this is an acceptable compromise for studying pro-inflammatory pathways [359, 350], this model makes it more difficult to study compensatory anti-inflammatory mechanisms.

Increased inflammation in DSS-induced colitis upon adipocyte-specific loss of autophagy was predominantly marked by an elevated pro-inflammatory cytokine signature in the inflamed colons with a significant increase of infiltrating monocytes. This suggests that autophagy may control immune functions rather than abundance of immune cells. The alarmin IL-33 is upregulated upon tissue damage by epithelial cells and fibroblasts. Interestingly, single cell characterization of stromal intestinal fibroblasts demonstrated that a specific stromal subset, called S4, appears during DSS-induced inflammation [374] – and this subset expresses *Il33* and *Ptx3*. Overall, the expression of this gene set suggests an increased disease severity and increased tissue damage which was confirmed by histopathology scoring. Of note, future investigations could clarify whether the exacerbation of intestinal inflammation in the $Atg7^{Ad}$ mouse model is caused by affecting immune cell or stromal cell populations.

The role of mesenteric adipose tissue in human IBD patients remains controversial, with possibly initially well-intended protective effects which are subsequently subverted and become pathological [375]. Adipose tissues, and in particular the mesentery, may therefore have a role in the recovery from acute DSS colitis. In this study, no differences in

colon histology were observed at recovery when adipocyte autophagy was lost. Whilst the induction of inflammation is T and B cell independent [325], its recovery has been suggested to be promoted by both lymphoid cell types [376]. More specifically, Wang et al. show that adoptive transfer of Tregs into lymphocyte-deficient $Rag^{-/-}$ mice cannot improve recovery from DSS-colitis but requires B cells to promote IgA-producing plasma cell expansion [376, 377]. Curiously, we did find significantly lower presence of FOXP3-expressing Tregs in the colon of recovering $Atg7^{Ad}$ mice without an effect on the overall recovery of the animal. All Treg subsets trended to be diminished in $Atg7^{Ad}$ mice, however only RORγt$^-$ FOXP3$^+$ Tregs were significantly reduced. Although not much is known about this Treg subset in response to colitis, it has been shown to expand due to the presence of dietary antigens [378]. In contrast, GATA3$^+$ Treg subsets are well documented to participate in the response to injury through expression of the IL-33 receptor ST2 [379, 380]. Tregs in tissues express higher levels of CD36 compared to Tregs found in the circulation, potentially indicating that lipid uptake is important for T cell function at tissue sites. The usage of fatty acid oxidation for Treg proliferation and function remains arguable. Recent reports using genetic deletion of the mitochondrial fatty acid translocase *Cpt1a* showed that CPT1A, and hence FAO, is indeed dispensable for Treg homeostasis or function [381]. Even the Treg-specific deletion of CD36 was dispensable in controlling colitis in an adoptive T cell transfer model [357]. However, these findings do not necessarily allow conclusions about the role of CD36 in the expansion of tissue-resident Tregs in the colon upon colitis, as seen in the DSS model.

Lastly, in our study we did not investigate the impact that adipocyte autophagy deletion may have on the chronic course of colitis when administering repeated DSS cycles. Bacterial translocation into the mesentery is increased in CD patients [382]. Therefore, chronic DSS-induced colitis is used to study the effects of sustained bacterial translocation on the mesenteric and intestinal immune response over several weeks [189]. It remains to be seen if using a chronic DSS model would be affected by the reduced expansion of colonic Tregs observed after one cycle of DSS colitis. Studies depleting Tregs using anti-CD25 antibody did however not reveal a striking role of Tregs in controlling chronic intestinal inflammation using DSS colitis [383]. Whilst induction of chronic

colitis by *Hh* infection did not reveal any differences, the use of chronic DSS induced colitis may be an option for future experimentation looking to identify possible effects of reduced Treg presence after DSS recovery. It is plausible that the effects of increased intestinal inflammation upon DSS treatment are connected to pathogen translocation from the gut, which is not commonly seen for *Hh*-induced colitis.

5.4 Conclusion

In summary, this chapter sought to examine the role of adipocyte autophagy during intestinal inflammation. The induction of experimental colitis using DSS revealed an increase of autophagic flux in adipose tissues, which once inhibited by genetic deletion of *Atg7* led to a marked increase of intestinal inflammation. In addition, we found that immune cells in adipose tissue and intestine alter CD36 surface expression in response to DSS-induced colitis, possibly indicating changes in cellular fatty acid metabolism. Therefore, we sought to explore in the next chapter the possible mechanistic processes connecting adipocyte autophagy to increased intestinal inflammation in the DSS-induced colitis model.

6 Adipose tissues are a source of IL-10 and may contribute to the anti-inflammatory response during DSS-induced colitis

6.1 Introduction

6.1.1 Mesenteric adipose tissue in IBD pathologies and murine models of colitis

Adipose tissues have gained significant research interest due to a rise in obesity worldwide. It is generally thought that excess adipose tissue promotes inflammation, however, whether this increases the risk of IBD is unclear. Epidemiological studies show that the prevalence of obesity in the IBD population is similar to the prevalence of obesity in the general population [180]. Curiously, the results of smaller and larger studies of different ethnic and age groups have revealed conflicting results, with both positive and negative associations between overweight, obesity and IBD [384, 385, 319, 386]. However, the increase in global obesity demands more large-scale, long-term studies to assess this relationship systematically. Since obesity dramatically alters adipose tissue homeostasis and increases the risk of other chronic pathologies (e.g. rheumatoid arthritis), it appears plausible that obese-induced adipose tissue inflammation may be a contributing factor in the aggravation of IBD.

An unanswered question is, however, whether adipose tissues in lean individuals is adaptive or maladaptive in the context of IBD. The phenomenon of mesenteric adipose tissue expansion (the 'creeping fat') in CD patients has attracted much research attention in the past two decades, however its role and function in CD pathology still remains elusive. Since CD is characterized by transmural inflammation which is at least in part due to intestinal barrier breakage, it was proposed that the expansion of mesenteric adipose tissue may seal off leaky intestinal sites and therefore prevent bacteria from entering into circulation [189, 387]. Similarly, in humans, the omentum, a fat pad spanning across the stomach and intestine, has been commonly described to seal off sites of infection or

injury to prevent dissemination of bacteria [388]. These parallels highlight potentially important immune-regulatory and wound-healing properties of adipose tissues during intestinal injury. More evidence supporting this theory was provided by identification of an enriched translocation of specific bacteria into creeping fat tissues of CD patients [189, 382, 389]. Intriguingly, the study by Ha *et al.* identified a specific bacterial species, *Clostridium innocuum*, in creeping fat tissues capable of promoting adipogenesis, thus connecting bacterial translocation to the hyperplasic expansion of creeping fat tissue around the inflamed intestine [389].

However, the impact of the mesentery on CD pathology may depend on the current disease state. Several studies identified that mWAT from CD patients and murine models of colitis can express several pro-inflammatory cytokines [189, 390]. Secretion of other adipokines such as leptin may additionally be able to promote intestinal inflammation through promoting intestinal barrier dysfunction or TNFα-mediated immune exacerbation [323, 391]. Genetic leptin loss in *ob/ob* mice protects from DSS-induced colitis, possibly though STAT3-dependent mechanism [392].

In addition to cytokine mediated pro-inflammatory effects, it has been postulated that creeping fat tissues can lead to intestinal strictures and bowel obstruction. Early observations found that the creeping fat tissue becomes increasingly fibrotic with IBD progression. Unpublished data from the Rieder lab suggest a potential role of adipose tissue derived FFA in the development of intestinal fibrosis and stricture development [393]. *Vice versa*, activated muscularis propria fibroblasts may promote mesenteric creeping fat via production of fibronectin supporting the migration of pre-adipocytes out of the mesentery [394].

In summary, while the role of the mesentery and adipose tissues in general remains ambiguous, it is becoming increasingly clear that it may change over the course of disease progression providing different signals and functions at different times [375]. More research is needed to define adipose tissue function in IBD.

6.1.2 Adipose tissue macrophages in health and disease

ATMs have a central role in controlling metabolic homeostasis and inflammation in adipose tissues. Anecdotally, ATMs were traditionally separated into pro-inflammatory (M1-type) and anti-inflammatory (M2-type) phenotypes which show distinct metabolic profiles. Thereby, pro-inflammatory macrophages rely on glycolysis, whereas anti-inflammatory macrophages preferentially use OXPHOS. With the rise of single cell technologies, high plasticity in macrophage phenotypes has been revealed, challenging the bimodal "M1-type and M2-type model". A seminal study from Jaitin *et al.* demonstrated for instance that ATM phenotype shift over the course of high-fat induced obesity, consequently resulting in the accumulation of $CD9^+$ $TREM2^+$ lipid-associated macrophages (LAM) [285]. These LAMs have distinct functions in controlling lipid and energy metabolism of adipocytes and in preventing adipocyte hypertrophy. Under homeostatic conditions, the vast majority of ATMs express the mannose receptor CD206, a pattern recognition receptor sensing bacterial glycan and a classical marker for 'M2-type' macrophages. Upon obesity or aging, ATMs loose CD206 and increase CD11c expression, indicating a shift from 'M2-type' to 'M1-type' polarization. Strikingly, analysis of *in vivo* macrophages from obese mice and humans revealed a diverse regulation of both pro- and anti-inflammatory genes which was distinct from classical M1-type or M2-type phenotypes [395]. The same study found that ATMs from obese mice transcriptionally increase both *Tnfα* and *Il10* production. Intriguingly, co-culture of bone marrow derived macrophages (BMDM) with adipose tissues promotes a metabolically activated macrophage (MMe) polarization [284]. These MMe are essential for the clearance of dead adipocytes during obesity and contribute to the overall tissue inflammation through pro-inflammatory cytokine production [396]. In addition, MMe support cancer cell engraftment in adipose tissues of obese animals by increasing cancer cell stemness in an IL-6 dependent manner [397]. While MMe predominantly emerge in obesity, it remains unclear whether metabolic stimuli can also alter immune cell function in normal weight individuals.

In CD patients, expression of M-CSF in mWAT is increased which facilitates polariza-

tion of anti-inflammatory macrophages *in vitro* [398]. In models of lung cancer, the production of IL-10 from tumour associated macrophages can be regulated through the expression of M-CSF via activation of PPARβ/δ [399]. Intriguingly, this may provide an explanation for the accumulation of anti-inflammatory CD163$^+$ IL-10$^+$ ATM in creeping fat tissues [347]. Adipokines such as ADIPOQ and leptin can influence macrophage polarization. For instance, addition of ADIPOQ to BMDMs reduces TNFα and promotes IL-10 secretion in response to LPS stimulation [400, 401]. In contrast, leptin promotes the expression of several pro- and anti-inflammatory cytokines, however, it also increases expression of classical M2-type surface markers including CD206 [347, 402]. Whether adipocytes contribute to the changes observed in the function of ATMs in creeping fat remains largely unexplored. In general, ATMs are a heterogenous and plastic cell population with overlapping expression of surface markers and cytokine production, which depends on their direct metabolic and immunological cues.

6.1.3 Context and aim of this chapter

Adipose tissues are highly metabolic and secretory organs, which are capable of affecting the immune system at local and systemic levels. In the last chapter, we found that the loss of adipocyte autophagy led to an exacerbation of intestinal inflammation, however how this is mediated remains unclear. To gain mechanistic insights into possible interactions or crosstalk that could explain the phenotype, we sought to (1) investigate changes in the presence and secretion of key cytokine factors in serum and from adipose tissues, (2) screen for metabolic and transcriptional alterations in mature adipocytes and (3) assess adipocyte-immune cell communication.

6.2 Results

6.2.1 Adipose tissue increases IL-10 expression upon DSS colitis in an adipocyte autophagy dependent manner

Over the past years, the role of adipocytes as an endocrine cell has been clearly established, actively contributing to the regulation of systemic fatty acid metabolism, insulin secretion, extracellular matrix, vascularization and inflammation. A number

of adipokines (e.g. leptin, ADIPOQ, IL-6, TNFα) have been studied in detail and their physiological roles are well defined. Interestingly, adipokine levels of leptin and ADIPOQ are altered in inflammatory conditions including arthritis and IBD [403, 404]. Adipokines have gained interest in the context of IBD due to the cryptic emergence of creeping fat tissue. ADIPOQ has been found to have controversial effects on murine models of colitis. For instance, Fayad *et al.* found that *Adipoq*-KO mice were protected from DSS- and TNBS-induced colitis which was reversed upon ADIPOQ administration [405]. This suggested a pro-inflammatory role of ADIPOQ. In contrast, Nishihara *et al.* showed that genetic loss of *Adipoq* leads to an exacerbation of DSS- induced colitis, but not in the TNBS model [406]. The authors found that this effect may be mediated by direct action of ADIPOQ on epithelial cells, which was further substantiated by a study demonstrating that ADIPOQ receptor 1 silencing exacerbates TNBS-induced colitis [407]. More recent reports add to a growing body of evidence suggesting anti-inflammatory effects of ADIPOQ. For instance, administration of ADIPOQ reduces colonic inflammation, downregulates TNFα and IL-1β production and colonic apoptosis [408]. DSS-induced colitis was exacerbated in *Adipoq*-KO mice through STAT3-dependent pathways [409, 410].

Based on the secretory role of adipose tissues in regulating metabolism and inflammation, we sought to understand whether differentially secreted cytokines from the adipose tissue may explain the increased inflammation observed in $Atg7^{Ad}$ mice. To address this, serum samples were analysed for differential adipokine and cytokine expression profiles using ELISA-based or bead-based cytokine assays. Serum ADIPOQ levels were decreased with induction of DSS-induced colitis but were comparable between wild-type and $Atg7^{Ad}$ mice (Fig.44A). In addition, presence of serum leptin trended towards being decreased upon DSS-induced colitis but did not show any differences between wild-type and $Atg7^{Ad}$ mice (Fig.44B). Overall, these data suggest that secretion of these two key adipokines is unlikely to be the cause of exacerbation of intestinal inflammation observed in the $Atg7^{Ad}$ model upon DSS-colitis. Of note, it also provides evidence that the *Adipoq*-driven Cre system does not alter systemic ADIPOQ levels.

Next, serum samples were screened to a pre-defined inflammatory cytokine array. Strikingly, IL-10 and IL-27 levels were strongly increased in serum in response to DSS-induced colitis, but this increase was blunted in $Atg7^{Ad}$ mice (Fig.44C). Although no significant changes were observed for circulating pro-inflammatory cytokines using this array, we found that several key cytokines, such as TNFα and IL-6, trended towards being upregulated compared to non-DSS treated control mice.

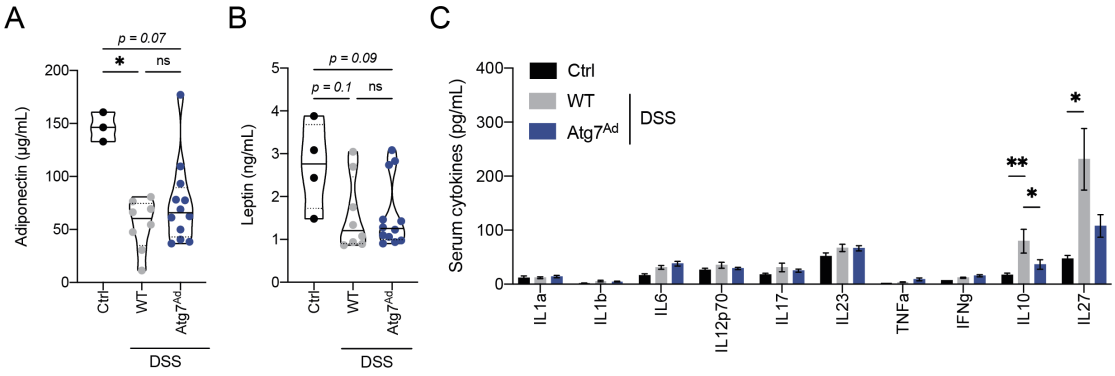

Figure 44: Presence of IL-10 is blunted in adipocyte autophagy-deficient mice upon DSS-induced colitis. Seven days after start of DSS administration the serum levels of (A) ADIPOQ, (B) leptin and (C) pro- and anti-inflammatory cytokines were assessed. Statistical analysis by One-Way ANOVA on log-transformed data. Data pooled from two independent experiments; each datapoint is one biological replicate.

As IL-10 is constitutively expressed in the intestine and is up-regulated during DSS-induced colitis in the colon, IL-10 expression levels in the colon were evaluated in wild-type and $Atg7^{Ad}$ mice upon DSS colitis. While DSS colitis expectedly increased *Il10* gene expression, no differences between mice based on their genotype was observed (Fig.45A), suggesting that the loss of adipocyte autophagy does not alter the local expression of IL-10 in the colon. In contrast, loss of adipocyte autophagy significantly increased the expression of *Il27* transcripts in the colon (Fig.45B). IL-27 is able to control IL-10 expression in the context of colitis and may promote therapeutic effects in an IL-10 dependent manner [411]. Interestingly, the same study showed that administration of recombinant IL-27 induces increased circulating levels of IL-10 and also expression of IL-10 in other tissues such as liver and mesenteric lymph nodes.

In human and murine IBD pathologies, several reports point towards a role of the

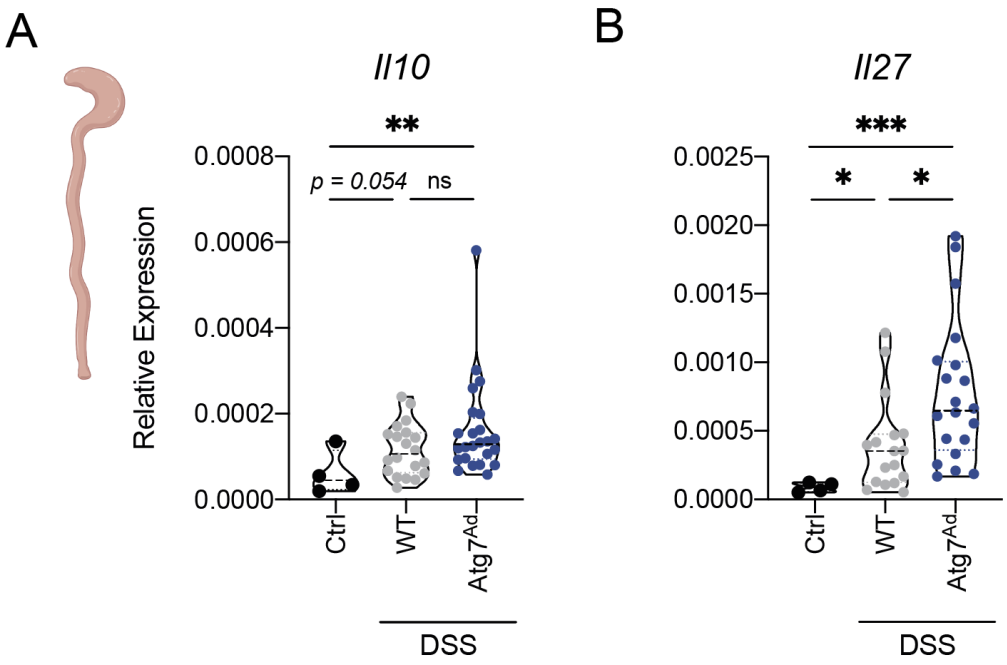

Figure 45: IL-27, but not IL-10 levels, are altered in the colon of adipocyte autophagy-deficient mice. (A) Gene expression of IL-10 in whole colon tissue at peak inflammation (7 days post-DSS) measured by qRT-PCR. (B) Gene expression of IL-27 in whole colon tissue at peak inflammation (7 days post-DSS) measured by qRT-PCR. Statistical analysis by One-Way ANOVA on log-transformed data. Data pooled from three independent experiments; each datapoint is one biological replicate.

mesentery in response to colitis by altering pro- and anti-inflammatory cytokine secretion [407, 382, 347, 390]. While many of these studies have focussed on dominant pro-inflammatory adipokines, we next sought to systematically screen for pro- and anti-inflammatory cytokines upon DSS- or *Hh*-induced colitis models. Both models were included in this analysis in order to comprehend common and model-specific cytokine signatures. To do this, mesenteric fat explants (without lymph nodes and colon) were cultured for 24 hours in medium containing 5% FBS. Strikingly, both models of colitis elicit a strong increase in cytokine secretion from mesenteric adipose tissues. Focussing on the wild-type animals, the data revealed four classes of cytokine profiles. The first set of cytokines, induced in both colitis models, contains the classical innate cytokines TNFα, IL-1β and monocyte attractant MCP-1 (Fig.46A). The next set consists of two interferon cytokines which were exclusively induced in *Hh*-induced colitis (Fig.46B). Especially IFNβ and IFNγ production was markedly increased in the mesentery at peak inflammation in the *Hh* model, in line with the central function of IFNγ in the disease

pathology. The third class of cytokines was elevated in the colitis models compared to non-inflamed controls, however, showed increased production during Hh colitis compared to DSS-induced mice (Fig.46C). These included both innate (e.g. IL-1α, GM-CSF) and adaptive cytokines (e.g. IL-17). The last group of cytokines were not differentially secreted from adipose tissues upon intestinal inflammation (IL-23 and IL-27, Fig.46D). These data demonstrate that mesenteric adipose tissue cells substantially alter their secreted cytokine profile in response to intestinal inflammation. Importantly, our data demonstrate that mesenteric adipose tissues are a considerable source of IL-10 during intestinal inflammation. It remains unclear whether adipose tissue-derived IL-10 can contribute to changes in circulating IL-10.

Next, we were wondering whether the loss of adipocyte autophagy may alter cytokine secretion from the adipose tissue. When including data from $Atg7^{Ad}$ mice, we were unable to detect any differences in the tested cytokines released from the mesentery based on the genotype, as exemplified for IL-10, IL-27 and TNFα (Fig.47B-D). Since all adipose tissues had been cultured in abundance of nutrients provided by fetal bovine serum (FBS), it is possible that the nutrient-rich culture conditions would cover any metabolic effects that arise from the autophagy-deficient adipose tissue. To test whether nutrient-deprivation would affect cytokine secretion, mWAT explants from DSS-inflamed were cultured in serum-deprived medium for 6 or 24 hours. Removing FBS from the culture conditions led to a decrease in IL-10 and TNFα secretion from $Atg7^{Ad}$ mesenteric fat explants (Fig.47E,F). To investigate, whether this effect was restricted to the adipose tissue proximal to the inflammation, gWAT were harvested from DSS-mice at peak inflammation and IL-10 and TNFα production were quantified by ELISA. In line with the results in the mesentery, gWAT increased IL-10 production in an autophagy-dependent manner, however, no differences were observed for TNFα (Fig.47G,H). This suggest that the secretion of adipose tissue-derived cytokines may not only be specific to the mesenteric adipose tissue but also occur in other distal adipose tissues. In summary, our data suggest that IL-10 is secreted from gWAT and mWAT in an autophagy dependent manner. Further, gWAT- and mWAT-derived IL-10 is possibly contributing to circulating IL-10 levels. This is of particular interest, since exogenous provision of recombinant

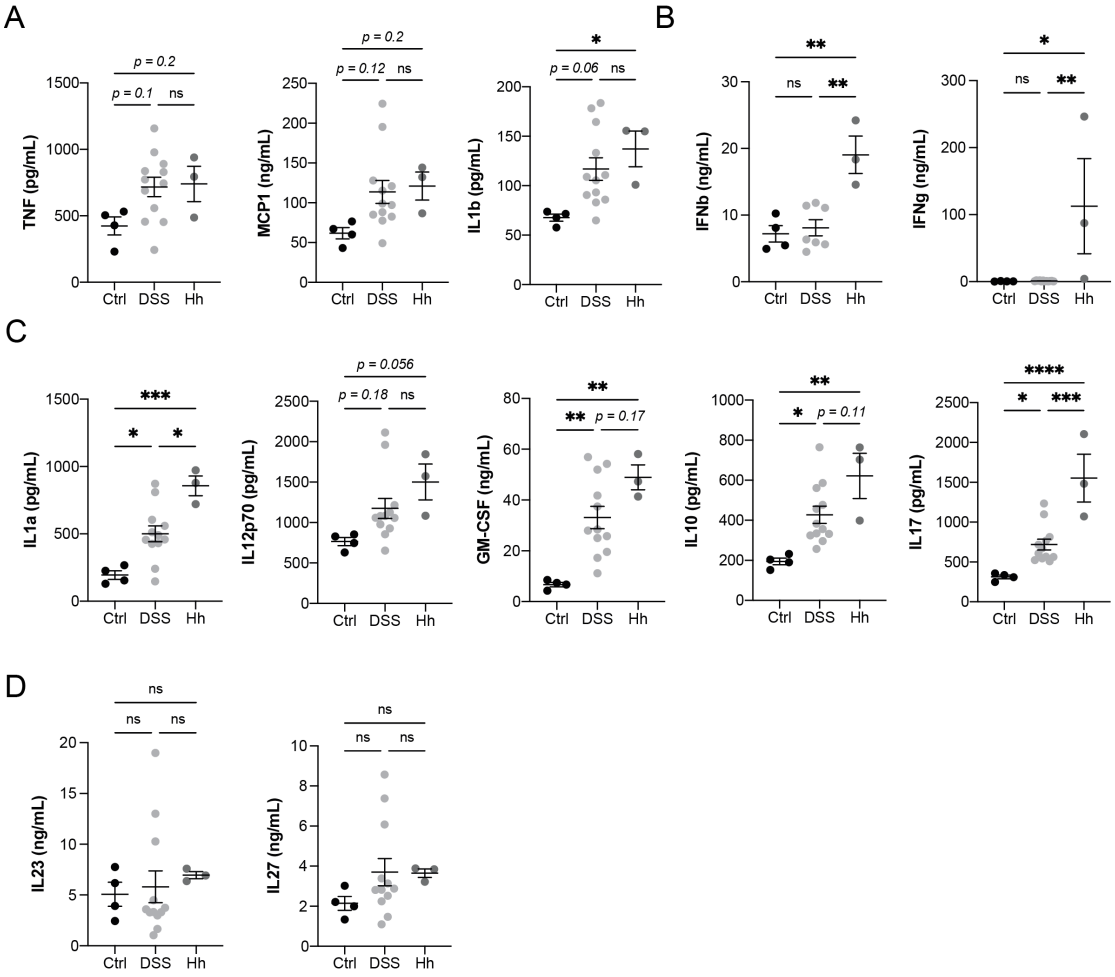

Figure 46: Mesenteric adipose tissues alter their cytokine profile upon DSS- and *Hh*-induced colitis in wild-type animals. Secreted cytokines from wild-type mWAT cultured in medium containing 5% FBS for 24h which are (A) increased to similar degree in both DSS- and *Hh*-induced colitis, (B) increased specifically in *Hh*-induced colitis, (C) increased in both colitis models, but more significantly in *Hh*-induced colitis and (D) not increased at all. Statistical analysis by One-Way ANOVA. Data pooled from one (*Hh*) or two independent (DSS) experiments; each datapoint is one biological replicate.

IL-10, via either bacterial or adenoviral overexpression systems, is capable of controlling DSS-induced intestinal inflammation [412, 413].

To test whether this observation is specific to the inflammatory environment created by intestinal inflammation or if it could be modelled *ex vivo*, adipose tissue explants from adipocyte autophagy-deleted or wild-type mice were cultured in the absence or presence of LPS or TNFα. The secretion of IL-10 and TNFα into the supernatant was measured. LPS treatment clearly upregulated TNFα and IL-10 production from both adipose tissues ($p < 0.0001$), whereas TNFα administration had no effect on IL-10 secretion

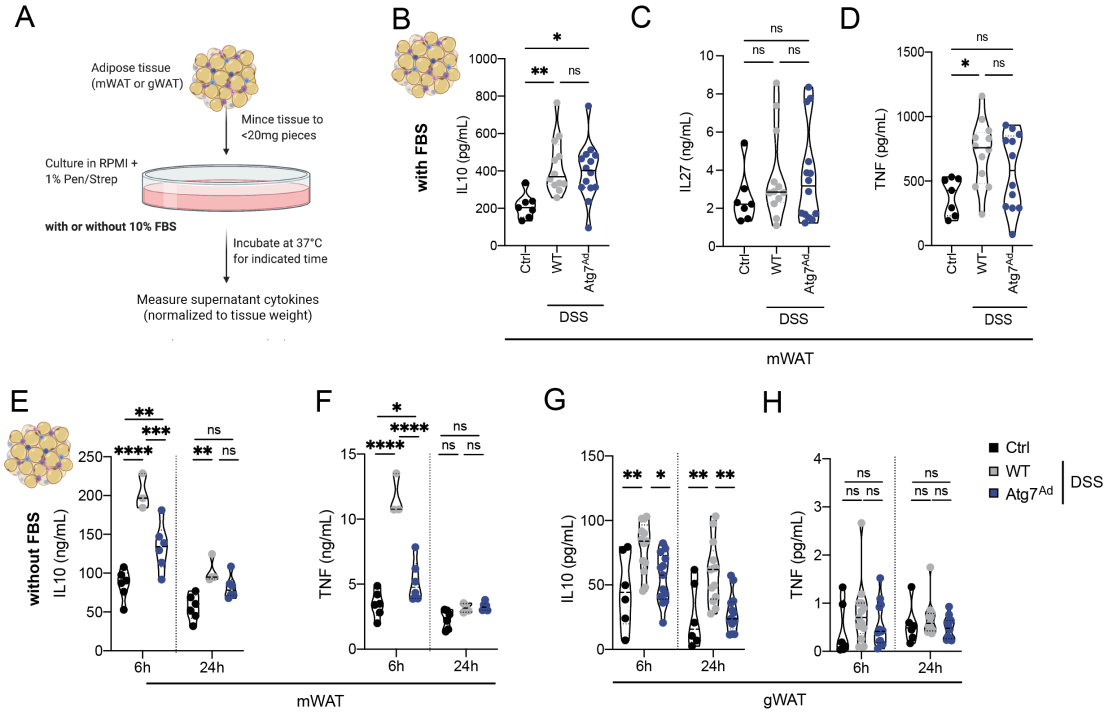

Figure 47: IL-10 is secreted from adipose tissues in an adipocyte autophagy-dependent manner. (A) Schematic overview of mWAT explant culture in the absence or presence 5% FBS. (B-D) Cytokine measurements in mWAT explant supernatant after 24h of culture in FBS containing medium. (E-F) Cytokine measurements in mWAT explant supernatant for the indicated time in the absence of FBS. (G-H) Cytokine measurements in gWAT explant supernatant for the indicated time in the absence of FBS. Statistical analysis by One-Way ANOVA. Data pooled from one to two independent experiments; each datapoint is one biological replicate.

(Fig.48A,B). Although we found a slight reduction in TNFα production in the mWAT, there were overall few changes in the secretory phenotype between autophagy-sufficient and -deficient adipose tissues. In particular, IL-10 secretion, despite being highly up-regulated upon LPS, did not show any differences between the genotypes. This suggests that DSS-induced colitis promotes a particular inflammatory environment that is not easily modelled by *ex vivo* stimulation. Over the seven days of DSS treatment, adipose tissues undergo significant changes, as previously discussed in Chapter 5.1, accompanied by loss of adipose tissue mass and an increase the number of ATMs and Tregs. These *in vivo* changes may be important to create a susceptible environment for differential cytokine secretion from autophagy-deficient adipose tissues.

In summary, our data revealed that IL-10 is specifically down-regulated in serum of $Atg7^{Ad}$ mice upon peak inflammation. In addition, IL-10 is secreted in an autophagy-

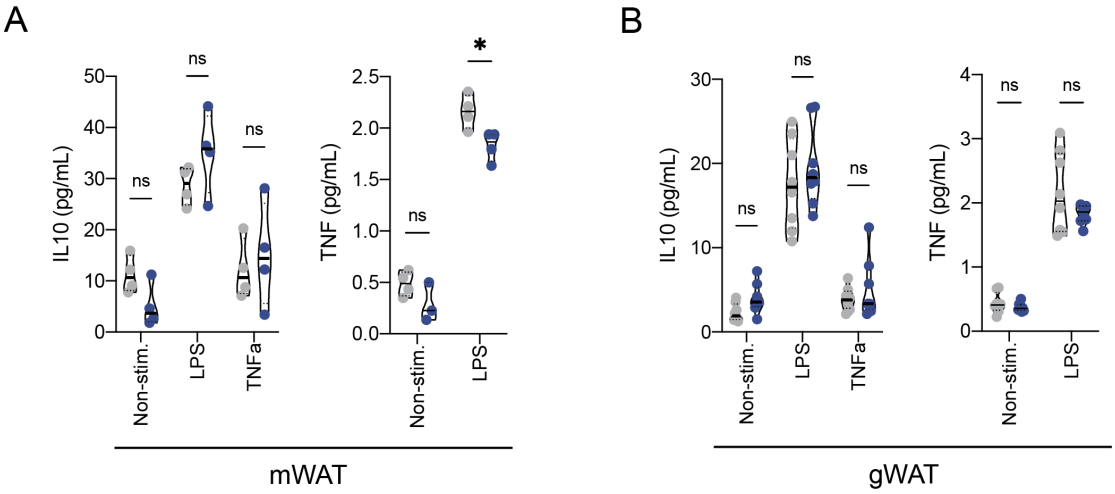

Figure 48: Adipocyte autophagy is dispensable for the production of IL-10 upon *ex vivo* stimulation of adipose tissues with LPS or TNFα. (A) Secretion of IL-10 and TNFα from mWAT into culture supernatant after 24h stimulation with either 100ng/mL LPS or 100ng/mL TNFα. (B) Secretion of IL-10 and TNFα from gWAT into culture supernatant after 24h stimulation with either 100ng/mL LPS or 100ng/mL TNFα. Statistical analysis by One-Way ANOVA. Data pooled from one independent experiments; each datapoint is one technical replicate from pooled adipose tissues from 2-4 mice.

dependent manner from proximal (mWAT) and distal (visWAT) adipose tissues to the site of inflammation. However, this effect is dependent on the absence of FBS, indicating that serum-derived nutrients or cytokines can influence the phenotype. The addition of LPS or TNFα to non-inflamed autophagy-sufficient or -deficient adipose tissue explants was not sufficient to alter cytokine secretion, indicating a complex inflammatory environment in adipose tissues during DSS-induced colitis. Interestingly, adipose tissues are source of IL-10 during inflammation and obesity and can be potentially secreted from adipocytes [414]. However, more recent analysis shows that adipose tissue-derived IL-10 originates predominantly from ATMs [415]. Similarly, ATMs increase IL-10 production during CD in creeping fat tissues [347].

6.2.2 Autophagy-deficient adipocytes differentially secrete free fatty acids

After identification of adipose tissue-derived IL-10 as a potential mediator controlling intestinal inflammation, we sought to characterize the macroscopic differences between wild-type and $Atg7^{Ad}$ adipose tissues during DSS-induced colitis. In line with the previously inflammation-induced observations in the wild-type animals, adipose

tissue mass is equally reduced in both male and female mice independent of their genotype (*p(inflammation) <0.0001*) (Fig.49A). Mesenteric lymph node weight was increased when compared to non-inflamed controls (*p(inflammation) <0.02*) but showed no change in the absence or presence of adipocyte autophagy during colitis (Fig.49B). Macroscopically, this suggests that adipose tissues react similarly to intestinal inflammation independent of their genotype. The development of creeping fat has been associated with a hyperplastic effect in the adipose tissues rather than an increase in adipocyte size [416, 417]. Histological analysis by H&E staining confirmed that non-inflamed $Atg7^{Ad}$ mice show increased adipocyte size and fewer number of adipocytes per square millimetre (Fig.49C-E). Interestingly, upon DSS-induced colitis, adipocyte size in autophagy-deficient mice decreases to wild-type level while wild-type mice show unchanged adipocyte size to non-inflamed animals (Fig.49D (left panel)). Conversely, the decrease in mWAT adipocyte size of DSS-treated $Atg7^{Ad}$ mice led to an increase in cell number (Fig.49E (left panel)). In line with hyperplasia observed in human creeping fat tissue, we found a significant increase in adipocyte number upon DSS-induced colitis across both genotypes (*p(inflammation) = 0.0003*). In DSS-treated female mice, no difference in cell size or number was observed based on their genotype (Fig.49D,E (right panels)). No water-treated females were included in this experiment. Overall, this suggests that autophagy-deficient adipose tissue reacts in a manner that is comparable to wild-type adipose tissues upon DSS-induced colitis. However, the increased loss of adipocyte size may indicate changes in lipid metabolism regulating the size of the lipid droplet in the adipocyte autophagy-deficient adipocytes.

To get a better understanding of how the loss of adipocyte autophagy may alter adipocyte cell biology under homeostasis and DSS colitis, we sought to purify visceral adipocytes by collecting the floating fraction after digestion from $Atg7^{Ad}$ and control mice (Fig.50A). In anticipation of possible sex-dependent effects on the transcriptome [418], three mice from each sex for each genotype and treatment group were included in the analysis. Strikingly, sex explained roughly 33% of the total variance (PC1), while DSS-induced inflammation explained 14% of the observed variance (PC2) in the dataset (Fig.50B). Although there was no obvious separation based on genotype, gene expression was anal-

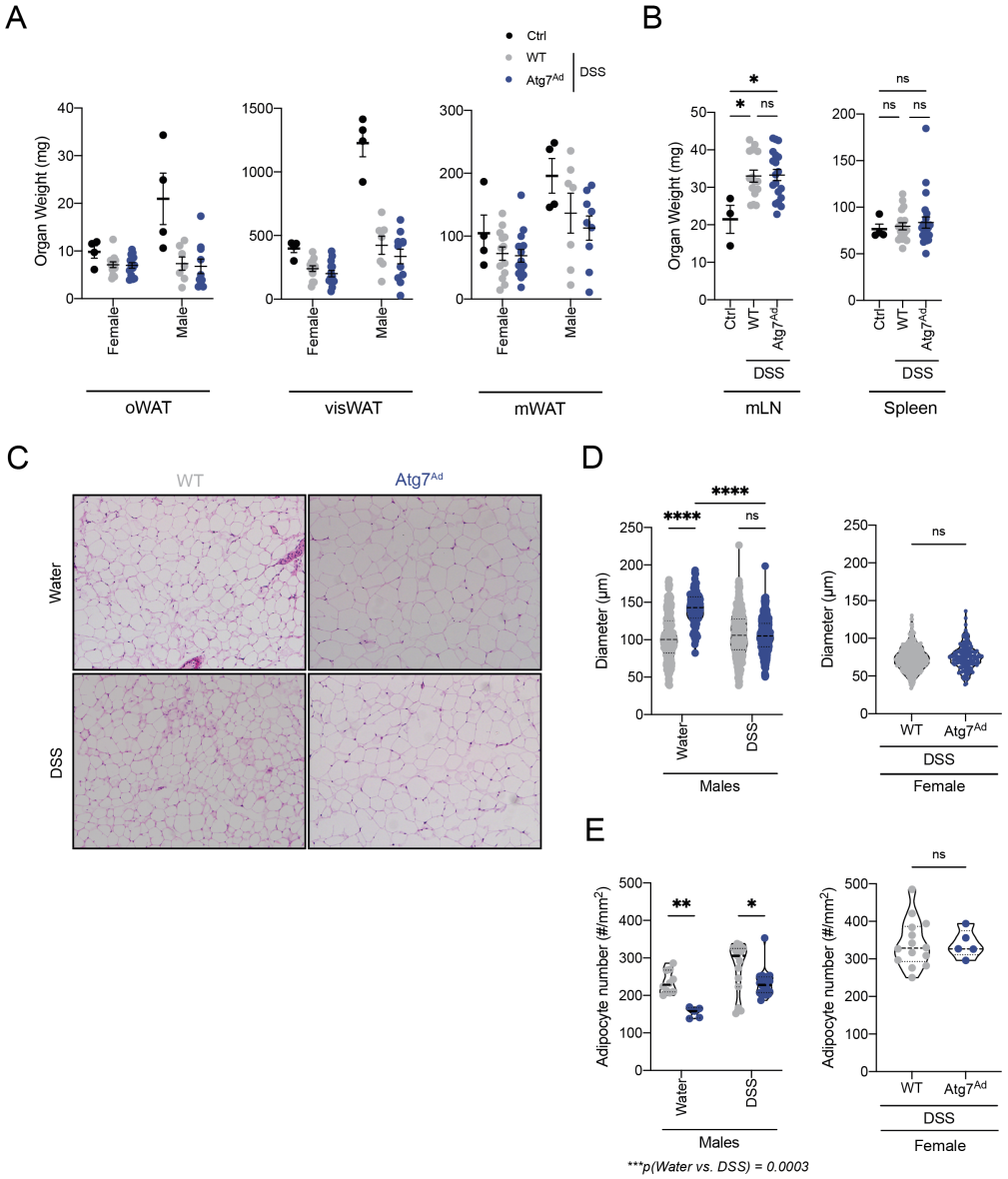

Figure 49: DSS-induced colitis leads to adipose tissue loss, but with signs of hyperplasia. (A) Weight of several visceral adipose tissue depots (oWAT, collective visWAT and mWAT) and measured at day 7 post-DSS treatment start. (B) Weight of mesenteric lymph nodes (mLN) and spleen at day 7 post-DSS treatment start. (C) Representative H&E staining of mWAT from males 7 days after start of DSS regime. (D) Adipocyte size presented as diameter in males (left panel) and females (right panel). (E) Total number of adipocytes in in males (left panel) and females (right panel). Statistical analysis by Two-Way ANOVA (A,D+E (left panel)), One-Way ANOVA (B) or Student's t-test (D+E(right panel)). Data pooled from three independent experiments (A,B) or one independent experiment (C-E); each datapoint is one biological replicate (A,B,E) and one adipocyte (D).

ysed in order to identify differential gene expression caused by the loss of adipocyte autophagy during either homeostasis or DSS-induced colitis. After separating mice based on treatment group, differential gene expression was performed using the DEseq2 R package [241]. Using this approach, visceral adipocytes from $Atg7^{Ad}$ mice showed a

strong and significant downregulation of *Atg7* transcripts, as expected (Fig.50C+D). Unsurprisingly, estrogen receptor 1 (*Esr1*) transcripts were upregulated in $Atg7^{Ad}$ mice, which is explained by *Adipoq*-driven overexpression of the *Cre* recombinase transgene coupled to the mutated human *ESR1* (∼76% sequence identity compared to murine *Esr1*). Due to the underlying breeding strategy, wild-type mice did not contain the recombinase allele (*Adipoq-*Cre^{ERT2} negative) whereas $Atg7^{Ad}$ mice were (*Adipoq-*Cre^{+}. In addition to *Atg7* and *Esr1*, autophagy loss led in both the water and the DSS treated group to a significant increase in the expression of *B630019A10Rik*, an uncharacterised gene located on chromosome 16 (Fig.50C+D). Across the treatment groups, a total of 17 genes were significantly upregulated in the *Atg7*-deficient adipocytes and 15 downregulated (Appendix A). Interestingly, the data did not reveal any differences in *Il10* gene expression in mature adipocytes upon DSS-induced colitis. This was further confirmed by qPCR (data not shown). Overall, this data suggests that autophagy loss in mature adipocytes does not fundamentally alter gene transcription.

Since the loss of autophagy did not reveal major transcriptional changes, one can presume that the acute loss of autophagy may change adipocyte physiology on a post-transcriptional level. Since the PCA revealed that the treatment explained a significant part of variance in the dataset, we next sought to understand effects of DSS-induced colitis on the transcriptome of visceral adipocytes. To do this, the dataset was stratified to include only wild-type animals. More than 1400 genes were differentially expressed upon DSS-induced colitis (Fig.51A). Among those, 738 were significantly upregulated during DSS-induced colitis, while 680 were down-regulated. Gene ontology analysis using the R package clusterProfiler [242] revealed an enriched gene set involving the production and regulation of TNFα (Fig.51B). Genes enriched in TNFα pathways were predominantly upregulated, possibly indicating activation of inflammatory pathways in visceral adipocytes upon DSS-induced colitis (Fig.51C). However, *Il10* expression in adipocytes was not upregulated during DSS-colitis. Although autophagy-regulated genes were not significantly enriched upon DSS-induced colitis, plotting z-scores of selected autophagy-related genes, showed a differential usage of this process upon intestinal inflammation (Fig.51D). In line with an increase of autophagy induction, mTOR signalling compo-

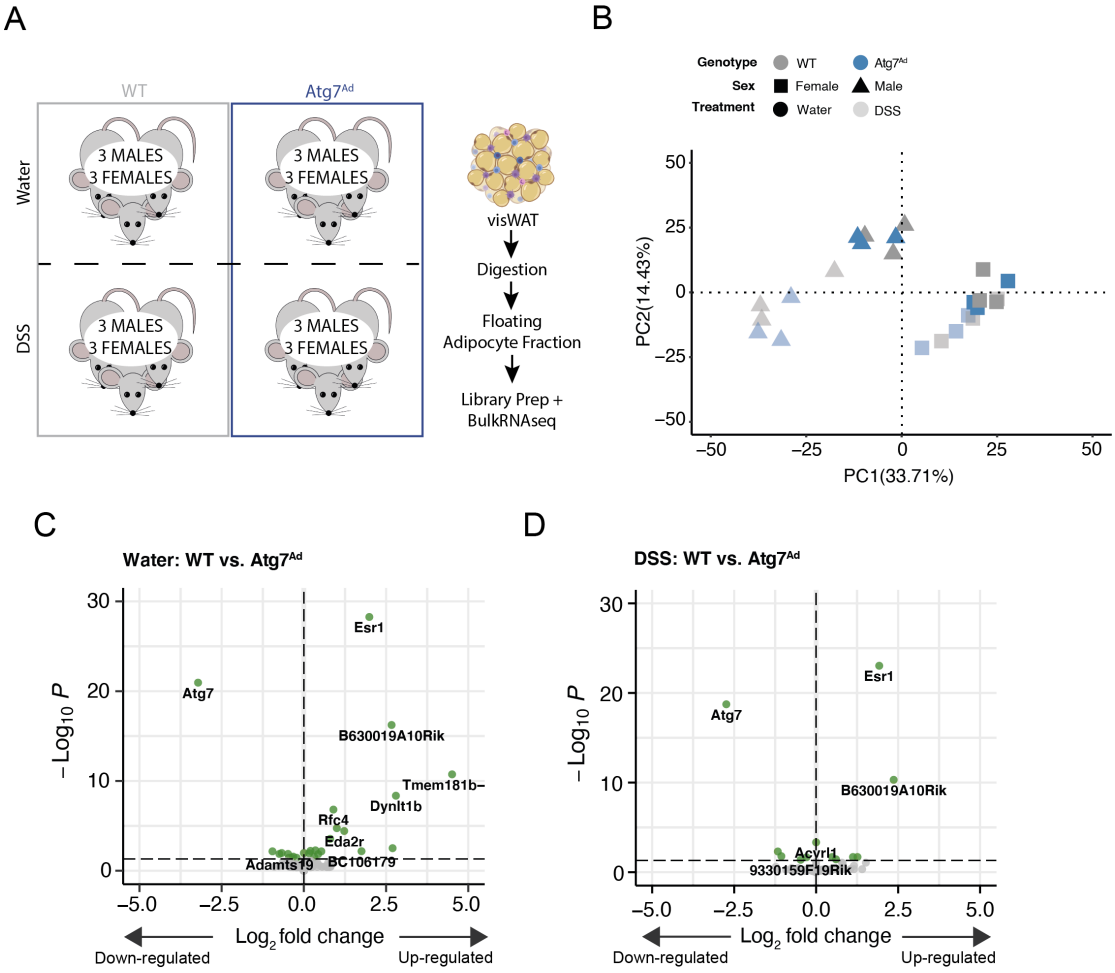

Figure 50: Genetic loss of *Atg7* in visceral adipocytes has no effect on overall transcriptome during homeostasis or DSS-induced colitis. (A) Schematic overview of transcriptomic experiment. Three female and three male mice were used per cohort and genotype. Visceral adipocytes were extracted and floating adipocyte fraction was collected after digestion. Total RNA from floating (adipocyte-enriched) fraction were harvested and sequenced. (B) PCA plot of individual datapoints. Each dot is one biological replicate. Genotype is presented by colour: Wild-type samples (grey) and $Atg7^{Ad}$ samples (blue). Sex is presented by shape: Square (female) and triangle (male). Treatment/cohort is presented by opacity: High opacity (water) and low opacity (DSS). (C) Volcano plot presenting differential expressed genes in female and male samples based on genotype under homeostasis. (D) Volcano plot presenting differential expressed genes in female and male samples based on genotype after DSS-induced colitis.

nents trended to be downregulated during DSS-induced colitis in adipocytes (Fig.51D).

TNFα is a classical pro-inflammatory cytokine induced in many chronic inflammatory conditions, including IBD. Therefore, it is unsurprising that absence or inhibition of TNFα can improve disease pathology in murine and human IBD [183]. However, TNFα has also been shown to elicit anti-inflammatory pathways, possibly to control immune exacerbation. Therapeutic inhibition of TNFα in an acute model of DSS-induced col-

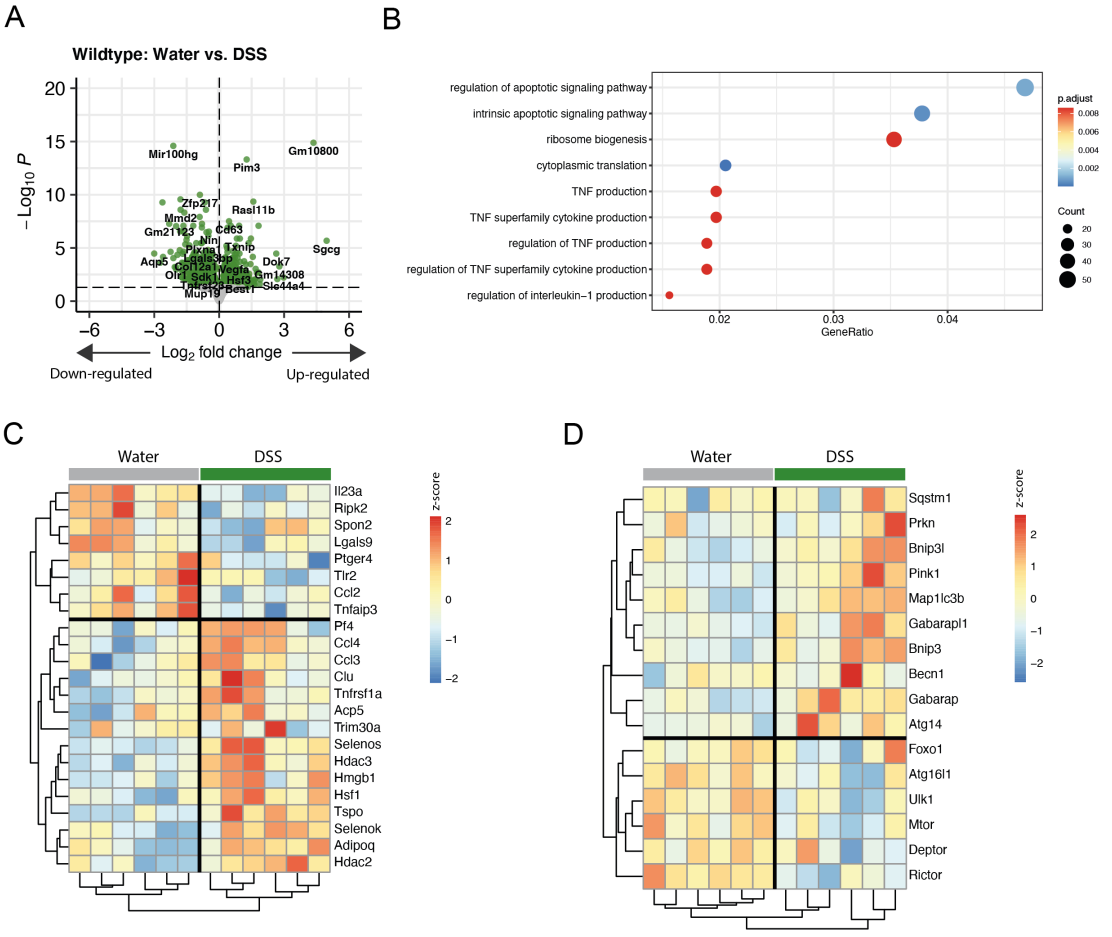

Figure 51: DSS-induced colonic inflammation results in transcriptional changes and distinct regulation of TNFα-related genes in visceral adipocytes. (A) Volcano plot presenting differential expressed genes in wild-type samples based on treatment (Water vs. DSS). (B) Gene ontology analysis of differentially regulated genes enriched in biological processes. (C) Heatmap of enriched genes based on gene ontology enrichment involved in the TNFα pathway. (D) Heatmap of selected genes involved in autophagy pathway.

itis leads to the exacerbation of inflammation [419]. Notably, *Tnf*α ablation leads to a reduction in colonic glucocorticoid synthesis, thereby exacerbating intestinal inflammation [420]. In addition, TNFα signalling has pleiotropic effects on adipose tissue biology, including inhibition of lipogenesis, adipogenesis and stimulation of adipocyte lipolysis [123]. Therefore, we sought to assess the effects of TNFα on lipolysis. First, we confirmed that serum TNFα levels were increased during peak inflammation in wild-type mice treated with 1.5% DSS (Fig.52A). Alike to isoproterenol-induced lipolysis, we hypothesized that loss of adipocyte autophagy would impair TNFα-induced release of FFA. To test this, gWAT explants were collected from mice two weeks after tamoxifen

treatment and were cultured for 24h in the absence or presence of TNFα. Interestingly, TNFα-stimulated adipose tissues showed reduced FFA in the supernatant (Fig.52B). To examine the putative effect *in vivo*, circulating FFA levels were measured in serum upon DSS-induced colitis. Notably, DSS-induced $Atg7^{Ad}$ mice showed a significant reduction in circulating FFA levels (Fig.52C). Overall, this suggests that autophagy impairs adipocyte lipolysis induced by both the β-adrenergic receptor and TNFα receptor signalling pathways. This is in line with findings from Ju *et al.* demonstrating that autophagy can control the degradation of the lipid droplet coating protein PLIN1 [238]. Interestingly, the same study provided evidence that TNFα can induce autophagy *in vitro*, thus linking lipolysis and autophagy. Whether TNFα controls adipocyte autophagy induction in DSS colitis remains unknown.

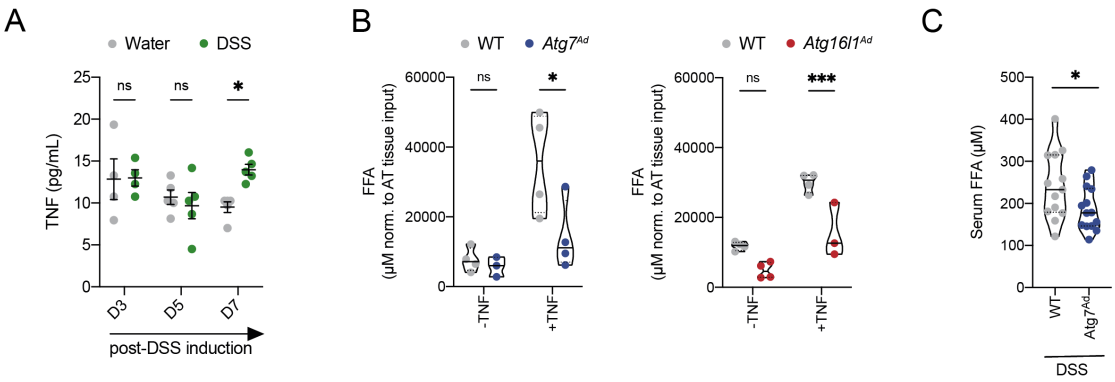

Figure 52: TNFα-induced release of FFA is decreased in autophagy-deficient explants and the serum of DSS-treated mice. (A) Circulating levels of TNFα 3, 5 and 7 days after start of treatment with 1.5% DSS in drinking water. (B) Release of FFA from gWAT explants into culture medium upon stimulation with TNFα (100ng/mL) for 24h and subsequent culture for 3h in fresh medium. (C) Serum FFA levels at day 7 post initial DSS administration. Statistical analysis by Two-Way ANOVA (A,B) or Student's t-test (C). Data representative for two independent experiments (A,B) and pooled from two independent experiments (C); each datapoint is one biological replicate.

FFA defines a diverse class of lipid species with distinct pleiotropic effects. To assess whether the reduction in circulating FFA levels is due to specific FFA levels being depleted in $Atg7^{Ad}$ mice, serum FFA species were measured by GC-MS. Intriguingly, the overall composition of serum FFA species were not altered between wild-type and adipocyte autophagy-deficient mice (Fig.53A,B). However, $Atg7^{Ad}$ mice showed decreases in all major FFA subspecies (Fig.53C,D): None of the individual FFA species were significantly reduced, but stratifying the data by Two-Way ANOVA revealed an

overall decrease in FFA concentration in the blood of adipocyte-autophagy deficient animals (Homeostasis: $p(genotype) = 0.042$; DSS: $p(genotype) = 0.056$). This confirms our previous results from the enzymatic FFA assay, revealing a reduction in serum FFA levels in $Atg7^{Ad}$ mice (Fig.52C).

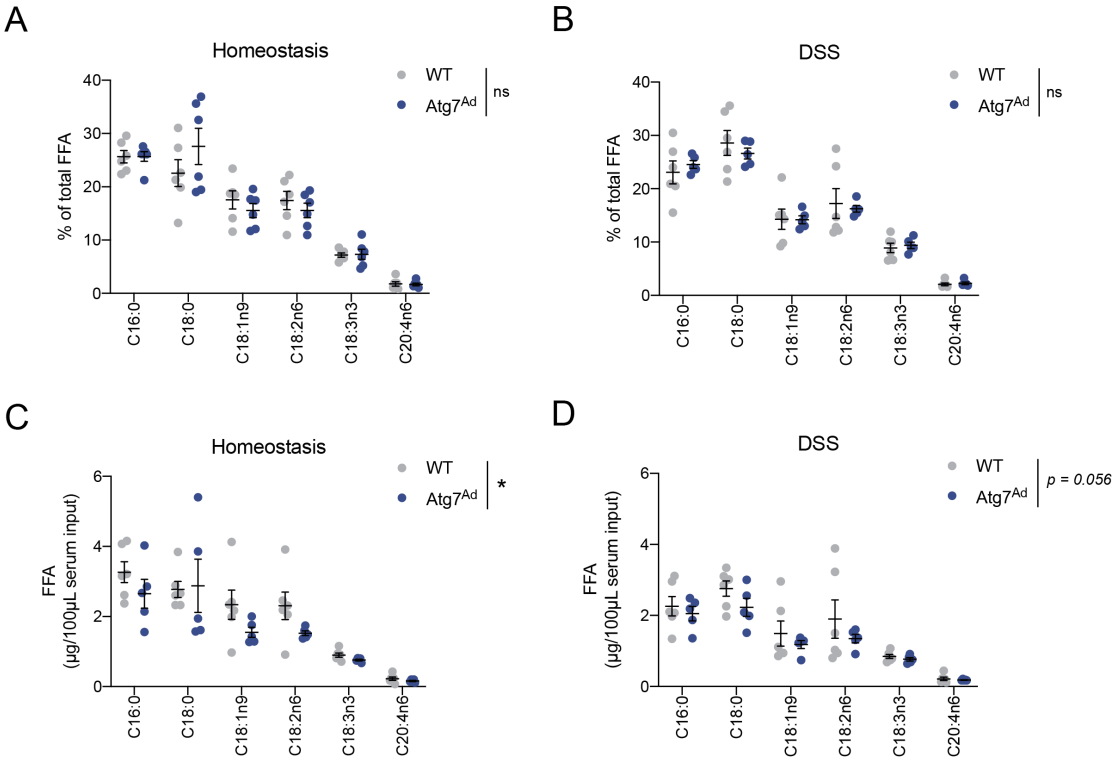

Figure 53: Serum FFA composition remains unaltered, while revealing an overall reduction in FFA concentration in adipocyte autophagy-deficient mice. (A,B) Composition of major FFA species in serum of wild-type or $Atg7^{Ad}$ mice after (A) 2 weeks post deletion or (B) after 2 weeks deletion and subsequent DSS-induced colitis for 7 days. (C,D) Concentration of major FFA species in serum of wild-type or $Atg7^{Ad}$ mice after (C) 2 weeks post deletion or (D) after 2 weeks deletion and subsequent DSS-induced colitis for 7 days. Major FFA species included were palmitic acid (C16:0), stearic acid (C18:0), oleic/elaidic acid (C18:1n9), linoleic/linoelaidic acid (C18:2n6), α-Linolenic acid (C18:3n3) and arachidonic acid (C20:4n6). Statistical analysis by Two-Way ANOVA. Data representative for one independent experiments; each datapoint is one biological replicate.

In addition to controlling circulating FFA levels, adipocytes take part in general lipid metabolism. Therefore, serum lipid composition was analysed using unbiased shotgun lipidomics from wild-type and $Atg7^{Ad}$ mice during peak DSS-induced intestinal inflammation. Returned data were processed as previously shown for homeostatic mice by stringent removal of all lipid species which were not complete in all analysed samples. Dimension reduction using PCA revealed no distinct segregation by genotype, however,

it indicates that PC1 may separate groups according to sex (Fig.54A). Since we had previously analysed the serum lipidome of wild-type and $Atg7^{Ad}$ mice under homeostatic conditions, the data was included in the final analysis. Interestingly, while PC1 still seems to predominantly discriminate between male and female mice, PC2 clearly separates the mouse lipidome by DSS treatment (Fig.54B). This being said, caution is required when analysing the data in context of DSS-specific effects on the lipidome since this may be confounded by different cohorts used for the two analysis. Thus, more detailed analysis is required to affirm the impact of intestinal inflammation on the serum lipidome. Differential lipid presence was measured using a linear regression based on sex and genotype. Interaction terms were initially included but showed a negligible effect on the overall dataset and were consequently removed as factor from the linear regression model. After correction for multiple testing, none of the measured lipid species were significantly changed in the serum lipidome of $Atg7^{Ad}$ mice compared to WT controls (Fig.54C). However, when separated by sex, we consistently found that $Atg7^{Ad}$ female mice trend towards reduced presence of some lipid classes. Exemplified, expression of dominant TAG species were significantly reduced in $Atg7^{Ad}$ females compared to WT females (Fig.54D). This was however not observed for male mice, which showed no statistical differences in lipid species. Since female $Atg7^{Ad}$ mice partially showed a stronger impact of DSS-induced colitis, this discrepancy in circulating lipid species may be caused by heightened inflammation observed in females compared to males. In line with this, overall TAG levels in males were elevated compared to females (data not shown).

In summary, analysis of the cell-intrinsic effects of autophagy deletion in mature adipocytes revealed that autophagy deletion reduces FFA secretion in response to TNFα-induced lipolysis. In line with this, total FFA levels in mouse serum were reduced upon autophagy deletion in DSS-inflamed animals as assessed by both FFA lipidomics and enzymatic assays. Interestingly, autophagy does not seem to influence specific FFA species that are produced and enter into circulation. However, it remains unclear whether local FFA availability in the adipose tissues may be altered by the loss of adipocyte autophagy and whether other cell types are responsive to these changes.

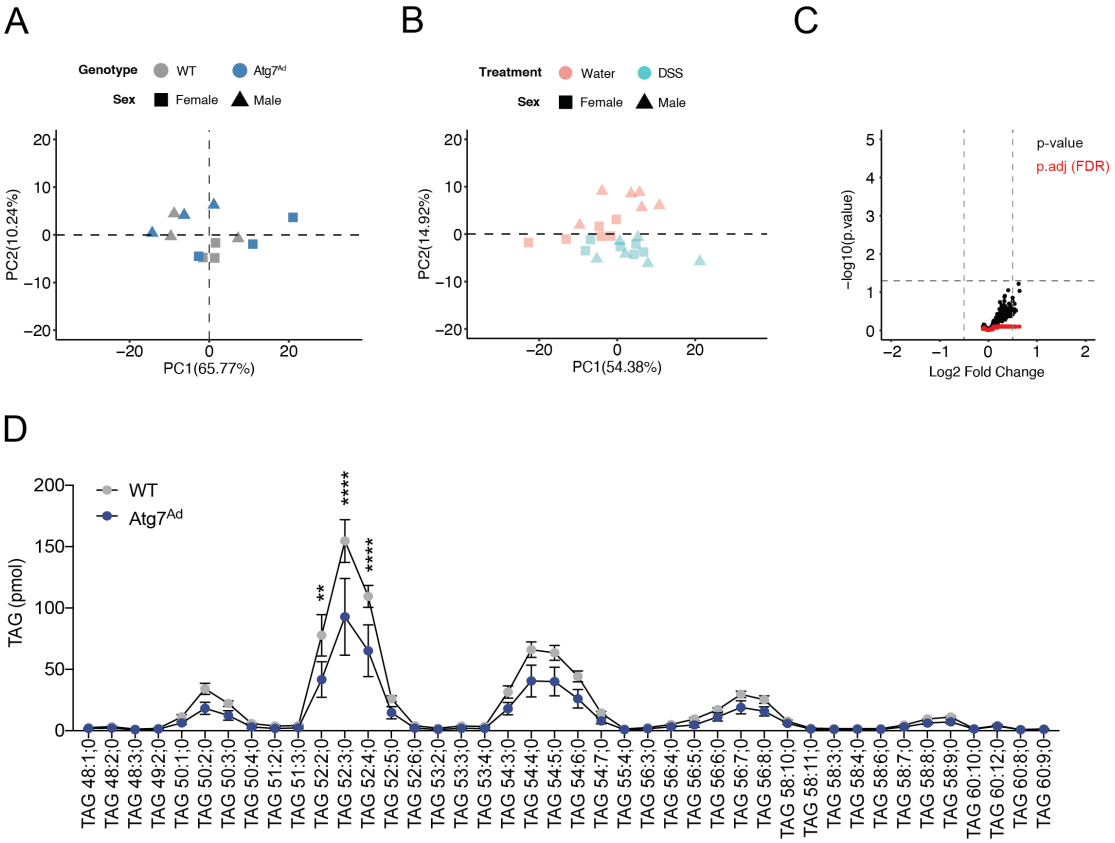

Figure 54: DSS-induced may alter serum lipidome, however this is largely independent of adipocyte autophagy. (A) PCA plot of serum lipidome from DSS-induced wild-type and $Atg7^{Ad}$ mice. (B) PCA plot of serum lipidome from homeostatic (red) and DSS-induced mice (blue) independent of genotype revealing a shift in serum lipidome upon DSS-induced colitis. (C) Differentially expressed lipid species in serum in the absence of adipocyte autophagy during DSS colitis after linear regression and multiple correction using Benjamini, Hochberg and Yekutieli correction (FDR). Data presented as non-corrected p-value (black dots) and adjusted p-value after FDR correction (red dots). (D) Serum TAG concentrations upon DSS-induced colitis in female wild-type and adipocyte autophagy-deficient mice.

6.2.3 IL-10 production in macrophages is dependent on FFA availability

Autophagy loss in mature adipocytes resulted in reduced FFA availability in serum and explant supernatants. In connection with the reduced secretion of anti-inflammatory IL-10 from adipocyte autophagy deficient adipose tissues, we hypothesized that the availability of FFA may alter local immune cell function in the adipose tissue. DSS-induced colitis increases the presence of ATMs (Chapter 5, Fig.33). However, it remains unclear whether the loss of adipocyte autophagy can change immune cell composition in adipose tissues during DSS-induced colitis. Expectedly, macrophages accumulated in mesenteric and visceral adipose tissues during intestinal inflammation, yet indepen-

dently of the loss of adipocyte autophagy (Fig.55A). This was predominantly due to an increased presence of CD206-expressing, tissue-resident macrophages (Fig.55B). In contrast, CD11c-expressing, pro-inflammatory macrophages were barely detectable (data not shown). An elevated presence of $Ly6C^+$ monocytes in visceral adipose tissues upon DSS-induced colitis (*p(inflammation)=0.08*) indicates that ATMs may originate from circulation (data not shown). ATMs derived from autophagy-deficient adipose tissues showed reduced levels of CD206 surface expression which was due to a small but significant shift in proportion of $CD206^+$:$CD206^-$ ATMs (Fig.55C). In contrast, the number of Tregs in visceral adipose tissue was comparable between wild-type and $Atg7^{Ad}$ mice upon DSS-induced colitis (Fig.55D). Overall, these data support the notion that macrophages are the primary cell type populating adipose tissues during DSS-induced colitis, independent of genotype. The slight reduction in CD206 expression, however, could indicate that the local adipose tissue environment may alter immune cell function rather than immune cell presence.

Next, we assessed possible changes in local FFA availability by measuring CD36 expression levels on immune cell populations from the colon or adipose tissues as a surrogate marker. While lymphoid cells and monocytes in the colon reduced CD36 expression during DSS-induced colitis (in line with their pro-inflammatory role), CD36 expression on intestinal macrophages and DCs remained unchanged (Fig.56A). However, surface expression of CD36 on colonic immune cell populations was comparable between the genotypes. For us, this finding indicated that colonic immune cell populations may not be the primary target cells susceptible to reduced systemic FFA availability. Therefore, we next sought to assess the expression of CD36 on immune cell populations in adipose tissues. Preliminary results from mWAT and visWAT recapitulate the increase in CD36 expression observed in mesenteric and visceral ATMs in response to DSS-induced colitis. Interestingly, this increase in CD36 expression was abrogated in ATMs from mWAT from $Atg7^{Ad}$ mice (Fig.56B). Although not reaching statistical significance, a similar trend was also observed on ATMs isolated from visWAT (Fig.56C). These findings are in line with the reduced lipolytic potential of autophagy-deficient adipocytes. However, it remains unclear whether the expression of CD36 on macrophages can be influenced

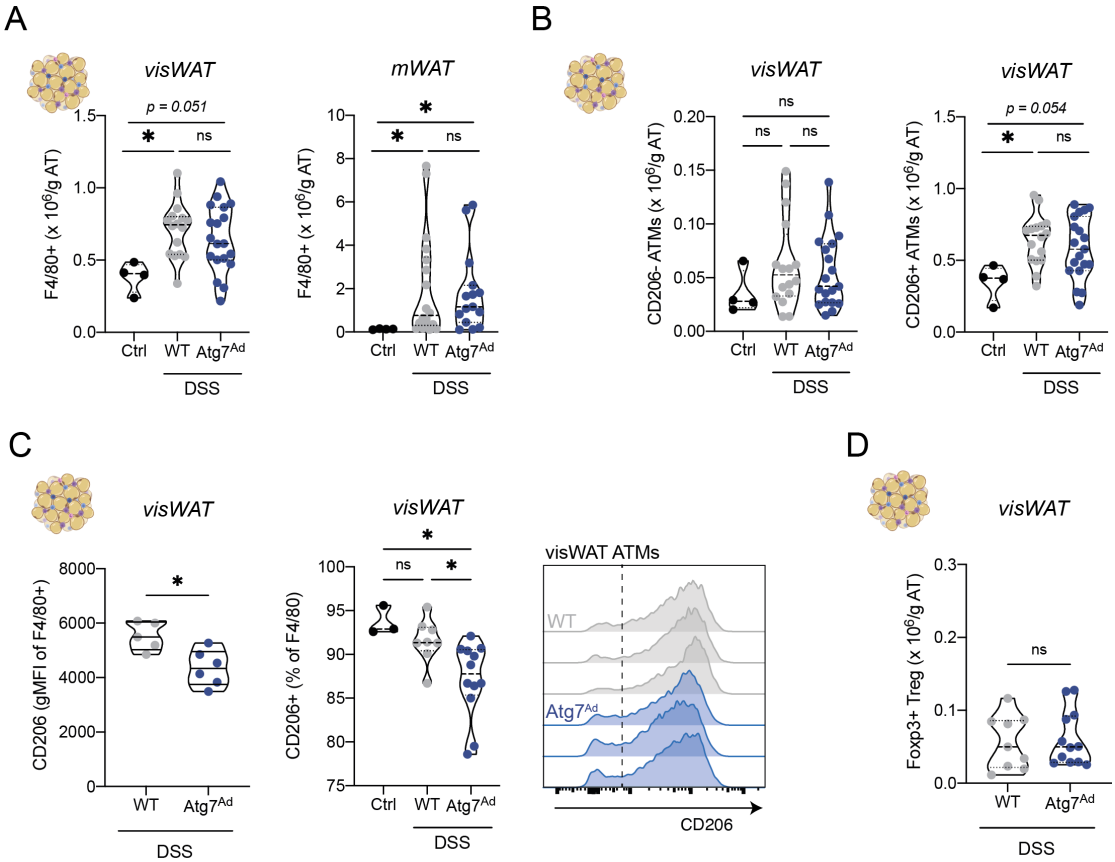

Figure 55: Loss of adipocyte autophagy results in a decrease of CD206 expression on ATMs. (A) Presence of ATMs in visceral and mesenteric adipose tissue during peak DSS-induced colitis. (B) Absolute number of CD206-expressing and -negative ATMs in visWAT upon DSS-induced inflammation at day 7. (C) Left: Representative results of surface CD206 expression on F4/80$^+$ ATMs. Center and right: frequency of CD206$^+$ ATMs. (D) Absolute number of Tregs in visceral adipose tissue during DSS-induced colitis. Statistical analysis by One-Way ANOVA (A-C) or Student's t-test (C,D). Data pooled from two-three independent experiments or representative for two independent experiments (C, left panel); each datapoint is one biological replicate.

by the local presence of FFA and thus can indicate differences in adipose tissue lipolysis *in vivo*.

Obesity and high fat diet feeding increase CD36 expression on several cell types, including macrophages [421, 422]. Molecularly, CD36 expression is controlled via the transcription factor PPARγ upon activation via binding of lipid ligands such as oxidized LDL [423, 424]. To confirm that CD36 expression on macrophages is sensitive to changes in its lipid environment, we next assessed the impact of increasing FFA concentrations on CD36 expression in BMDMs. After a seven-day differentiation with M-CSF, BMDM were polarized using either LPS and IFNγ (towards a pro-inflammatory pheno-

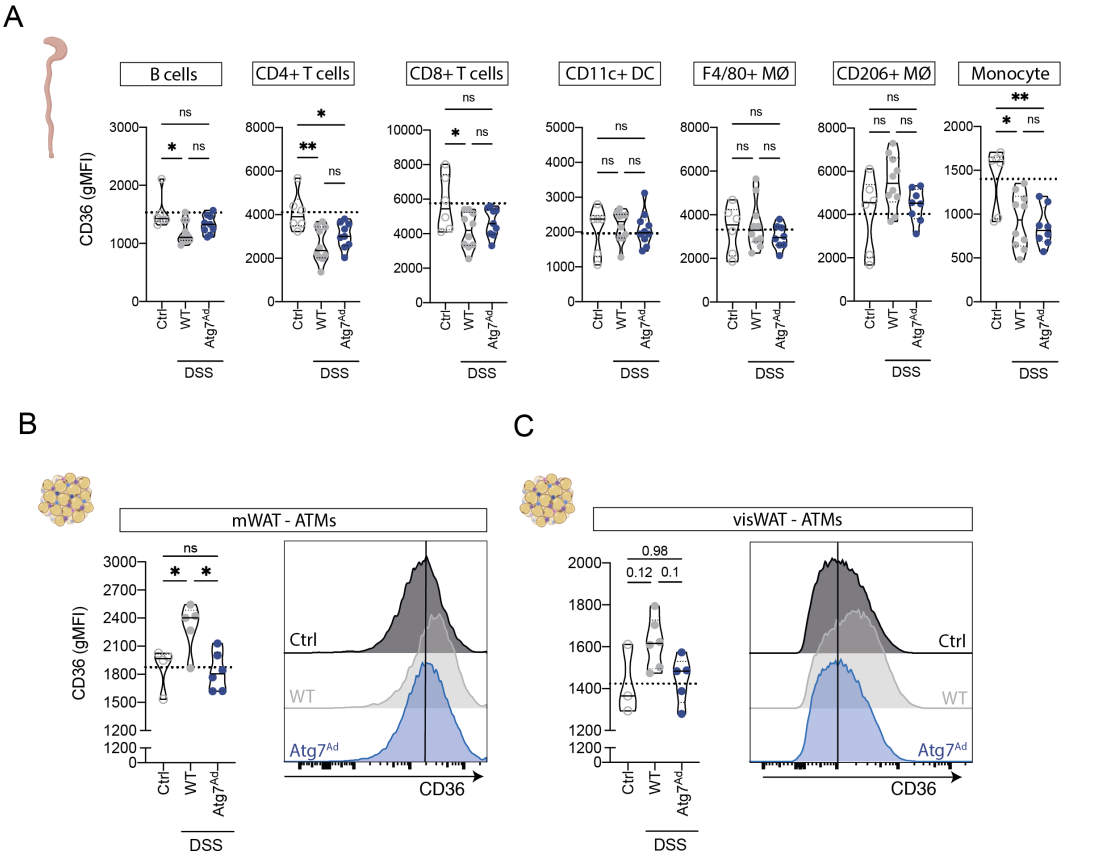

Figure 56: ATMs from *Atg7^{Ad}* mice expressed reduced surface expression of CD36, possibly indicating a reduced local FFA availability. Expression of CD36 on (A) intestinal immune cell populations, (B) mesenteric ATMs and (C) visceral ATMs. Data pooled from one-two independent experiments; each datapoint is one biological replicate.

type) or using IL-4 and IL-13 (towards an anti-inflammatory phenotype). Interestingly, polarizing BMDM in FBS-replete medium with increasing concentrations of a chemically defined lipid mix, led to a dose-dependent increase of CD36 expression on the surface of all BMDM subsets independent of their polarization (Fig.57). This suggests that macrophages are sensitive to increased local lipid availability and respond by promoting CD36 surface expression.

To investigate whether BMDM equally respond to deprivation of FFA from the culture medium, BMDM were either cultured in serum-rich (R_{10}) or serum-free medium (R_0). Since the latter condition would also reduce nutrients and protein factors from the medium, we opted to also use medium supplemented with the same quantity of charcoal treated FBS ($R_{Charcoal}$) that has been described to deplete FFA [425, 426]. First, we

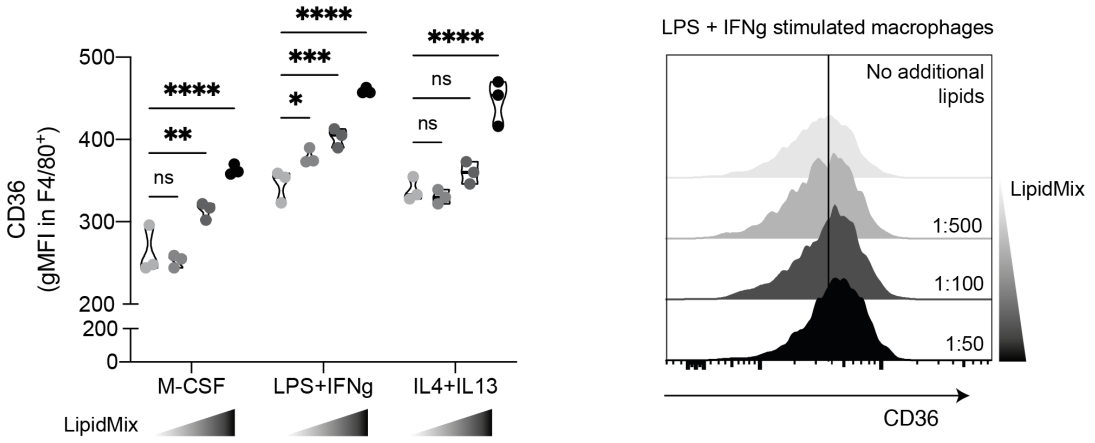

Figure 57: Lipid availability regulates expression of CD36 on the surface on BMDMs. M-CSF differentiated macrophages were stimulated using either LPS+IFNγ or IL4+IL13 in R_{10} medium for 16h with increasing amounts of a chemically defined lipid mix (2 µg/mL arachidonic and 10 µg/mL each linoleic, linolenic, myristic, oleic, palmitic and stearic, 0.22 mg/mL cholesterol). Expression of CD36 was analysed by flow cytometry after 16h of polarization. Data representative for one independent; each datapoint is one technical replicate.

verified that serum-deprivation and using charcoal-treated FBS results in a reduction of medium FFA levels in our system. Both R_0 and $R_{Charcoal}$ condition showed a reduction in FFA concentration in the medium with R_0 displaying the lowest levels (Fig.58A). Next, BMDMs were cultured during polarization in the corresponding medium conditions and CD36 expression was quantified. While stimulation with M-CSF did not alter CD36 expression across the medium conditions, BMDMs stimulated with either LPS and IFNγ or IL-4 and IL-13 seemed more reactive to a reduction in FFA availability (Fig.58B). This is in line with findings in RAW cells [427]. Interestingly, BMDMs stimulated with LPS and IFNγ showed a FFA-dependent increase in CD36 expression, whereas IL-4 and IL-13 treated BMDMs showed an inverse correlation of CD36 expression with decreasing FFA concentrations in the medium (Fig.58C).

Next, we investigated whether IL-10 secretion may be impacted by local FFA availability. Stimulation with LPS and IFNγ led to a significant increase in IL-10 and TNFα production in BMDMs. Intriguingly, the production of IL-10 in particular was blunted when cultured in a medium condition with low FFA content, while TNFα secretion was not affected by the FFA reduction (Fig.59A,B). Interestingly, we did not observe a strong IL-10 production from BMDM polarized in IL-4 and IL-13 containing medium,

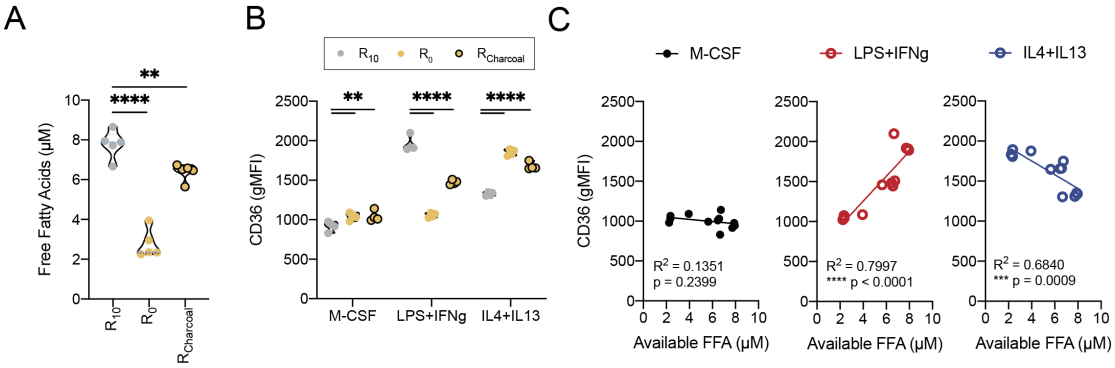

Figure 58: Limiting FFA availability differentially affects CD36 expression on BMDM dependent on their polarization. (A) FFA concentrations in freshly prepared medium supplemented with either 10% FBS (R_{10}) or without serum (R_0) or with 10% Charcoal-treated FBS ($R_{Charcoal}$). (B) Expression of CD36 on BMDMs 16h after start of polarization. (C) Correlation of medium FFA levels at start of polarization and expression of CD36 on polarized BMDMs. Data representative for three independent experiments; each datapoint is one technical replicate.

although the cells significantly increased expression of CD206 (Fig.59C). Focussing on LPS-stimulated macrophages, IL-10 secretion appeared to correlate with local concentrations of FFA in the media or surface expression of CD36 (Fig.59D). In addition, TNFα was not correlated to CD36 expression and FFA availability. Overall, these findings indicate that LPS-stimulated macrophages require sufficient FFA availability in their environment to elicit a strong IL-10 response.

To test whether LPS-stimulated macrophages require FFA for IL-10 production, we supplemented lipid-deprived medium with 200µM palmitic acid (PA) or linoleic acid (LA). Based on our preliminary data, we found that viability was specifically reduced in PA treated cells during LPS and IFNγ stimulation, which may be due to the low solubility of PA salts in medium. Viability was not affected by medium supplementation with water-soluble LA (Fig.60A). While the surface expression of CD36 was not affected by the addition of exogenous FFA in medium containing M-CSF, PA supplementation led unexpectedly to a decrease in CD36 expression (Fig.60B). In contrast, the addition of LA did not alter CD36 surface expression on BMDMs compared to LPS and IFNγ stimulated BMDMs in the absence of added FFAs (Fig.60B). Strikingly, however, the addition of LA recovered IL-10 expression in LPS-stimulated macrophages, without affecting TNFα levels (Fig.60C). Although the results are still preliminary, these data underline the requirement of specific FFA for the secretion IL-10 in response to pro-

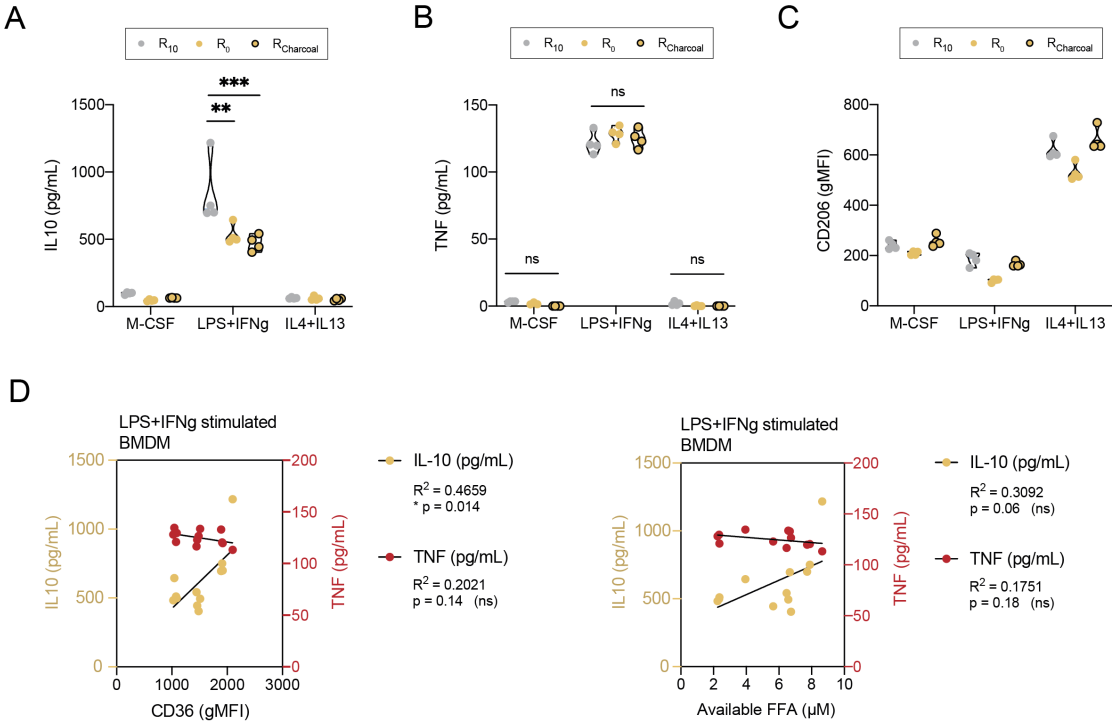

Figure 59: LPS-stimulated BMDM significantly decrease IL-10 secretion, but not TNFα, in medium with low concentrations of FFA. Secretion of (A) IL-10 or (B) TNFα into supernatant after 16h of polarization measured by ELISA. (C) Expression of CD206 on BMDM after 16h polarization. (D) Correlation of secreted cytokines with CD36 expression on LPS-stimulated macrophages or initial FFA concentration in polarization medium. Data representative of three independent experiments; each datapoint is one technical replicate. Data analyzed by Two-Way ANOVA.

inflammatory stimulation. Overall, these data support the notion that IL-10 secretion upon LPS stimulation requires the presence of FFA in its direct environment.

6.3 Discussion

6.3.1 An anti-inflammatory role of adipose tissues during inflammation

Adipose tissues are central players of systemic metabolism and inflammation through crosstalk with a multitude of organs including muscle, liver, gut and bone. In a study involving a lipodystrophic CD patients, regular injections of recombinant leptin were able to exacerbate intestinal inflammation in a TNFα-dependent manner. Animal studies using 'fatless' mice however have not been used to study its role in DSS-induced colitis. This may be due to the significant weight loss that most mice undergo during DSS-induced colitis. On the other hand, high-fat diet induced obesity exacerbates

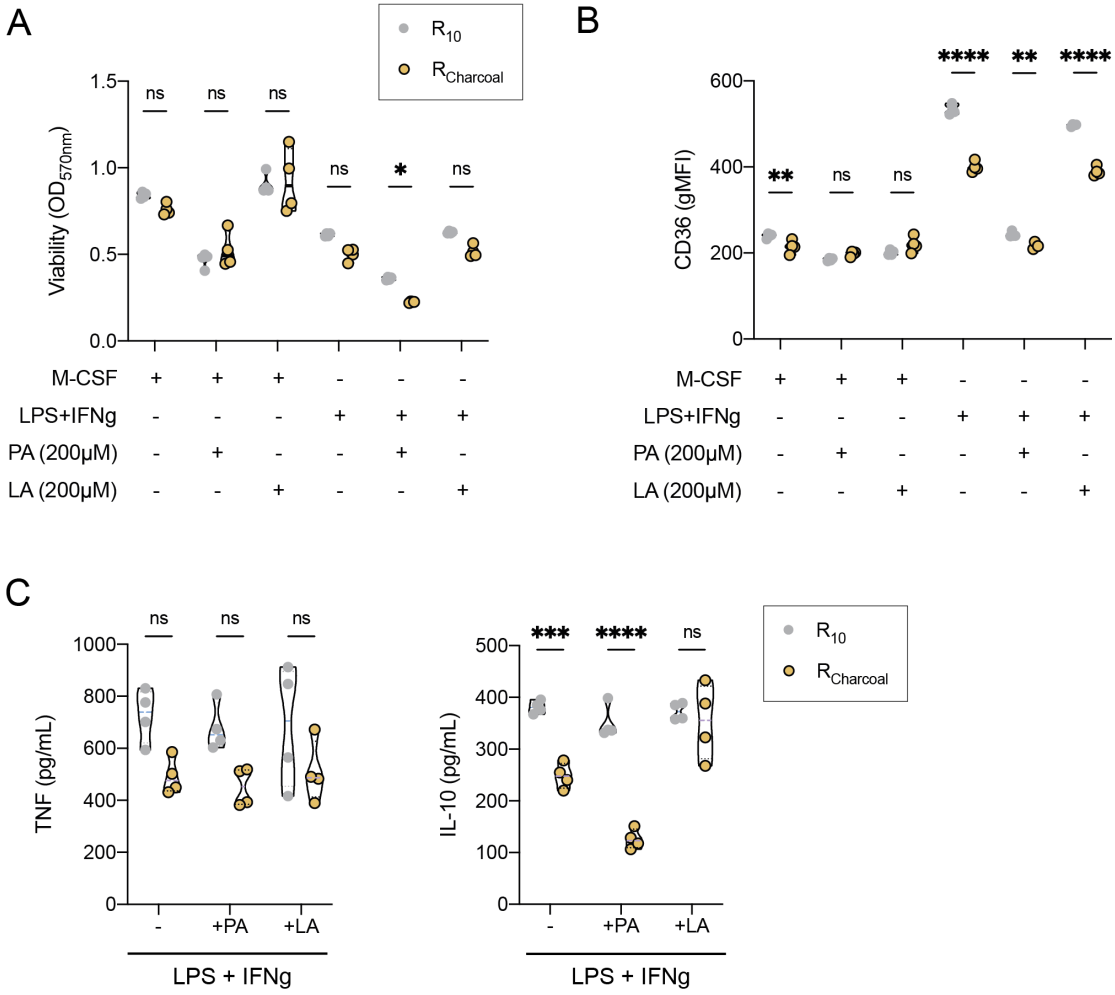

Figure 60: Linoleic acid supplementation rescues IL-10 secretion in LPS-stimulated BMDM. (A) Viability measured by MTT assay after 16h of polarization. (B) Surface expression of CD36 on BMDMs after 16h of polarization. (C) IL-10 and TNFα secretion into the supernatant after 16h of BMDM stimulation with LPS and IFNγ in the absence or presence of 200µM palmitic acid (PA) or linoleic acid (LA). Data representative for one independent experiments; each datapoint is one technical replicate. Data analyzed by Two-Way ANOVA.

DSS-induced colitis and can increase adipose tissue inflammation [428], suggesting a pro-inflammatory crosstalk between adipose tissues and the gut. Since obesity model promote adipose tissue dysfunction, the endogenous response of adipose tissues of metabolically health animals may therefore be different.

In this study, we found that adipose tissue explants increased the expression of several cytokines, some of which were found to be equally elevated in circulation upon DSS-induced colitis, intriguingly pointing towards a paracrine function of adipose tis-

sues in response to intestinal inflammation. This is in line with data from other groups demonstrating an upregulation of pro-inflammatory cytokine transcription in mesenteric adipose tissue [390]. This increase in cytokine expression may be due to enhanced bacterial translocation into the affected mesentery, which consequently stimulates innate immune signalling pathways. Blocking these signalling pathways using a *Myd88*-KO mouse model reduces adipose tissue cytokine production in response to DSS, while DSS-inflammation and bacterial translocation remains unaltered [189]. Intriguingly, in line with our own findings, the study found initial evidence that IL-10 is secreted from mWAT in response to DSS-induced colitis [189]. This corroborates our own findings which showed a robust upregulation of IL-10 upon DSS-induced colitis. An observation in line with previous reports from creeping fat tissues and murine models of colitis [347, 429]. Since the use of our model also revealed a simultaneous decrease of IL-10 from adipose tissues and in circulation in adipocyte autophagy-deficient animals, it may support the notion that adipose tissue derived IL-10 production contributes substantially to the total amount of IL-10 in circulation. In addition, the mWAT secretome data from different murine model of colitis (DSS-induced & *Hh*-induced) suggest that the response of adipose tissues to models of colitis are relatively well conserved. IL-10 is central to intestinal homeostasis controlling immune tolerance and wound healing [430]. We observed that IL-10 secretion from mWAT explants of *Hh*-inflamed mice was also (possibly more) increased compared to non-inflamed controls. Curiously, the IL-10 dependent mechanism could explain why there was no difference in the inflammation score of *Hh*-inflamed wild-type and $Atg7^{Ad}$ animals, since this model requires blockage of the tolerogenic IL-10 axis. Further experiments using *Hh* infections, in the absence of IL-10 blocking, could give additional evidence to whether adipocyte autophagy loss contributes to intestinal health via IL-10 production.

The fact that IL-10 production was only diminished when adipose tissue explants were cultured in serum-deprived medium suggests that the adipose tissue is incapable of providing specific signals or mediators (e.g. nutrients or cytokines) which may also be present in FBS. This could point towards specific metabolites such as lipid mediators

or growth factors or cytokines. Interestingly, even in serum starved conditions, wild-type adipocytes were fully functional in sparking an efficient cytokine response whereas only autophagy-deficient adipocytes could not provide these required signals. Another important note is that taking adipose tissue explants from mice prior to DSS-treatment did not reveal any differences in cytokine production, nor when they were stimulated with LPS or TNFα. This may indicate that the adipose tissue provides a specific environment, either through the influx or reshaping of local immune cells during DSS-induced colitis. Indeed, the complex environment induced by the intestinal inflammation may affect several adipose tissue cell types, many of which are known IL-10 producers; however, macrophages have been reported to be among the main producer of IL-10 in adipose tissues [415]. In addition, IL-10 may not be the only anti-inflammatory mediator involved in the observed phenotype, but one that is strongly associated to the development of IBD. Overall, this part mechanistically connects the adipose tissue to a reduction in systemic IL-10 levels and thus could explain the exacerbation of DSS-induced colitis in adipocyte autophagy deficient mice.

6.3.2 Acute loss of adipocyte autophagy contributes to FFA generation without fundamentally altering adipocyte identity

Adipose tissues from homeostatic mice present with a hypertrophic phenotype, which is largely lost upon DSS-induced colitis, which normalizes adipocyte size to wild-type levels. This may indicate that there is a significant utilization or liberation of lipids during DSS-induced colitis in autophagy-deficient adipocytes. Typically, increased adipocyte size correlates with lipolysis [431, 432]. However, *ex vivo* lipolysis studies suggested that autophagy-deficient adipocytes were impaired in isoproterenol- and TNFα-stimulated, and possibly in basic, lipolysis. Therefore, we conclude that in addition to impaired lipolysis, autophagy-deficient adipocytes may be defective in lipid uptake and storage, leading to increased adipocyte size during homeostasis and a reduction when lipid storage is limited during DSS-induced colitis. Lipid droplets arise from the endoplasmic reticulum and grow unless they are degraded through cytosolic lipases or lipophagy. It has previously been suggested that starvation-induced autophagy may take part in the

maintenance of lipid droplet size, thus connecting autophagy to regulating adipocyte size [433]. In general, the relationship between lipid droplets and autophagy seems to be tightly connected, reaching from lipid droplet degradation, to its formation, to providing lipids for autophagosomal membranes [434]. The control of lipid droplet size by autophagy may therefore be dependent on the nutritional and cellular situation.

To investigate whether autophagy loss in adipocytes would alter the response to intestinal inflammation and possibly to antigen exposure, the transcriptome of visceral adipocytes during homeostasis and DSS colitis was analysed. Deletion of *Atg7* was successful in the tested visceral adipocytes leading to a reduction of 80-90% in gene expression, which was in line with qPCR data from purified adipocytes. Strikingly, however, the loss of *Atg7* led to only very limited differential gene expression suggesting that autophagy loss does not alter the overall transcriptome of the adipocyte. It further provides evidence that inflammatory pathways are not altered by the loss of *Atg7* in visceral adipocytes during intestinal inflammation. In addition, the transcriptomic dataset did not reveal any striking changes in adipocyte phenotypes (no browning) or differential utilization of metabolic pathways on a transcriptional level. This is in contrast to other studies which performed whole adipose tissue transcriptomics from inducible adipocyte autophagy-deficient mice [269, 270]. Discrepancies will certainly arise from the different cellular source. While this study focussed specifically on transcriptional changes in the mature adipocytes, Cai *et al.* and Son *et al.* will have transcriptomic variation arising from the distinct cellular composition of their adipose tissues. Using visceral adipocytes from both sexes revealed a strong impact of sex on the overall adipocyte transcriptome, independent of treatment or genotype. Sex differences are quite common with more than 37% of all genes showing a sex-specific expression pattern [418], however, biomedical research often does not include these transcriptional changes in their analysis. Although there were no visible differences based on genotype, it is possible that expanding samples size for each sex, genotype and condition would reduce overall variation and thus enhance the potential of discovering differentially expressed genes. However, since we were unable to detect any major differentially expressed genes in our experimental

setup, we can presume that there are no obvious underlying transcriptional changes which would explain the increased inflammatory phenotype in $Atg7^{Ad}$ mice. Comparing the transcriptomic dataset of wild-type animals between homeostatic and DSS-treated animals revealed a significant shift in the adipocyte transcriptome. Interestingly, TNFα-regulated pathways seem predominantly differentially regulated possibly suggesting that TNFα-mediated signalling pathways induce changes in visceral adipose tissues during DSS-induced colitis. Yet, this data will require further validation in mice which have not previously received tamoxifen.

The transcriptomic data pointed towards a post-transcriptional role of autophagy in controlling adipocyte physiology. To this end, adipocytes were tested for their capacity to undergo TNFα-induced lipolysis. TNFα is a main driver of colitis and capable of inducing lipolysis [419, 123]. To functionally show that TNFα indeed increases adipose tissue lipolysis, one would require an adipocyte-specific deletion of *Tnfrs1a* which would prevent adipose tissue loss. Whole body deletion of *Tnfrs1a* or *Tnfrs1b* leads to an exacerbation of chronic DSS-induced colitis, therefore hinting towards an anti-inflammatory role of TNFR1 or TNFR2 signalling, respectively [435]. The same study showed that in particular *Tnfrs1a*-KO leads to an increased systemic inflammatory response, which seemed to involve increased presence of GM-CSF in circulation [435]. TNFα-induced lipolysis was significantly reduced in adipose tissues from adipocyte autophagy-deficient animals, which was reflected *in vivo* by lower serum FFA levels. This is of particular importance since this expands previous studies and our own which found that lipolysis is reduced after β-adrenergic receptor stimulation [269, 270, 272]. The reduced FFA release translated into lower serum FFA levels which showed a diminishment of several FFA species, rather than one in particular, indicating that autophagy does not influence the type of FFA that is released. This effect on lipid metabolism seemed to be specific, since no other changes in the serum lipidome have been observed. In summary, this data motivated further investigations examining the potential impact of FFA availability on the production of IL10 by adipose tissue immune cells.

6.3.3 Controlling IL-10 production in macrophages by FFA restriction

Macrophages, in concert with Ly6C-expressing monocytes, populate mWAT and collective visWAT upon DSS-induced colitis. This was in line with slightly (but not significantly) elevated levels of MCP1, a major chemoattractant for monocytes and macrophages, secreted from the adipose tissue [436]. Therefore, ATMs, in particular, became a central focus of this study, since this cell type predominately populates the adipose tissue upon DSS-colitis. In addition, ATMs were described to be sensitive to lipolysis induction through upregulation of CD36 during fasting phases following high fat diet feeding, thus allowing us to look for differences in CD36 expression as measure of *in vivo* lipolysis [283]. Intriguingly, ATMs from $Atg7^{Ad}$ mice failed to up-regulate CD36 expression, potentially indicating that the adipose tissues are less lipolytic. In addition, the expression of CD206 was slightly decreased, which could point towards a subtle shift in macrophage phenotype or to a decreased presence of oleic acid, a FFA which has been described to control CD206 expression on tumour associated macrophages [437]. Strikingly, reducing FFA levels in culture medium leads to a significant reduction in IL-10 levels and CD36 expression on BMDMs, when polarized using LPS and IFNγ. Somewhat surprising, we found consistently that M-CSF differentiated BMDMs produced the highest levels of IL-10 when stimulated with LPS, compared to IL-4 and IL-13 stimulated BMDMs. This is contrary to reports describing that IL-4 and IL-13 promotes an anti-inflammatory 'M2-type' macrophage polarization *in vitro*, characterized by a strong upregulation of IL-10. Despite the lack of IL-10 production, we verified that IL-4 and IL-13 enhanced the expression of other 'M2-type' factors such as CD206, suggesting that the polarization was working. Based on previous reports, initial differentiation of BMDM in either M-CSF or GM-CSF may present a stronger driver of anti-inflammatory or pro-inflammatory macrophage properties, respectively [438, 439]. Using these different differentiation cytokines has a strong impact on IL-10 production from BMDMs in response to LPS stimulation [440]. In addition, M-CSF and GM-CSF differentiated BMDMs show differential production of lipid mediators upon LPS stimulation, highlighting the importance of considering BMDM culture conditions to accurately represent the *in vivo* situation [441]. However, we believe LPS-induced macrophage presents an appro-

priate way to mimic *in vivo* situations. Both human IBD pathology and murine models of chemically-induced colitis are characterized by an increase in bacterial translocation [189, 382]. This was recently corroborated by a microbial study of bacteria translocating into the mesenteric under health and inflammatory conditions, which identified a set of lipophilic microbes enriched in the mesentery of CD patients [389]. Although most of ATMs were expressing the tissue-resident marker CD206 upon DSS colitis, we did find an increased secretion of GM-CSF from adipose tissues. This may provide an argument to test for IL-10 production in GM-CSF differentiated BMDMs upon reduction of local FFA availability.

Adipose tissues release a significant amount of FFA into their local and systemic environment. In adipose tissues, four fatty acids are particularly abundant. These include the saturated fatty acid palmitic acid and stearic acid and the unsaturated fatty acids oleic and linoleic acid [442, 443]. The presence of different FFA has distinct impacts on a variety of immune cell populations. For instance, the saturated fatty acid palmitate can bind to and activate the innate sensors Toll-like receptor (TLR) 2 and 4 [444, 445]. This induces the activation of pro-inflammatory cytokine production through activation of NFκB signalling pathways. However, other FFA have been shown to contribute to anti-inflammatory processes including polyunsaturated fatty acids such as omega-3 fatty acids. These dietary fatty acids include, among others, α-linolenic acid (ALA), eicosapentaenoic acid (EPA), and docosahexaenoic acid (DHA). Products from these fatty acids are classified as pro-resolving mediators, a group of metabolites that includes prostaglandins, leukotrienes, protectins, resolvins and others. In macrophages, the addition of DHA and EPA has been shown to significantly reduce pro-inflammatory gene expression in response to LPS stimulation in human, murine and cell line macrophages. Treatment with DHA can significantly increase IL-10 expression in a PPARγ-dependent manner [446]. In line with this, downregulation of FADS2, a key enzyme in synthesis of long-chain polyunsaturated fatty acids, in creeping fat tissue has been associated with reduced production of lipid mediators which are important for IL-10 production in ATMs [447]. Furthermore, omega-3 fatty acids can reduce NLRP3 inflammasome during high-

fat diet induced inflammation [448]. Beside omega-3 fatty acids, other unsaturated fatty acids such as oleic acid have known anti-inflammatory effects on immune cell function. Dietary supplementation of oleic acid promotes CD206 expression on mesenteric and tumour associated macrophages and are promoting an overall anti-inflammatory profile [437, 449]. It remains unclear however whether oleic acid can alter IL-10 production in ATMs. Macrophages can increase IL-10 production through mitochondrial respiration of FFA supplied through efferocytosis [450]. This was mediated via a SIRT1-PBX1 axis to promote wound healing in response to myocardial infarction. Using human cells, Pompura *et al.* recently demonstrated that Tregs respond to oleic acid by enhancing FAO and upregulating of IL-10 production [443]. Other cell types such as adipose tissue NKT cells have also been shown to respond to treatment with palmitic acid by promoting IL-10 production [451]. This effect was main driven activation of the unfolded protein response pathway mediated by IRE1α-XBP1s signalling pathway.

Future experiments will be required to further investigate the role of different FFA in the production of IL-10 in adipose tissue immune and ATMs specifically. At this current time, our data do not ultimately identify ATMs as the source of IL-10 during DSS-induced colitis. However due to their influx into the adipose tissue, they present an interesting candidate. Histological studies from creeping fat tissues also identified an increased production of IL-10 in mesenteric adipose tissues of CD patients, which was accompanied by an increased presence of $CD68^+$ macrophages [347]. Intriguingly, a seminal study from Ha *et al.* performed scRNAseq on immune cell populations in creeping fat tissue, which identified a central role of ATMs in wound healing and repair [389](10). Strikingly, ATMs in creeping fat tissue significantly upregulate IL-10 production compared to healthy controls. Overall, this evidence points to macrophages as a potential source of IL-10 which could influence systemic IL-10 levels. Therefore, we are currently investigating the effect of different FFA on BMDMs. In addition, administration of FFA to $Atg7^{Ad}$ mice could rescue the immune exacerbation phenotype in response to DSS-induced colitis and thus would allow more conclusive mechanistical insights *in vivo*.

6.4 Conclusion

In this chapter, we found evidence for the adipocyte autophagy-dependent production of IL-10 from adipose tissues. This may be controlled via a metabolic link between adipocytes and ATMs. TNFα-induced lipolysis, blunted in autophagy-deficient adipocytes, may lower local FFA availability. This local limitation in FFA availability then reduces the ATM's capacity to produce IL-10, which would otherwise enter into circulation and control intestinal inflammation. While some of these aspects require further investigation, the prospect of adipose tissue derived IL-10, contributing to intestinal homeostasis, may present an interesting new candidate for future therapeutic approaches.

7 General Discussion and Conclusion

7.1 Adipose tissues as a central hub for immunity

In this thesis, we describe an essential role of autophagy in the release of FFA from mature adipocytes during intestinal inflammation and its necessity for the anti-inflammatory inflammatory response. These findings underline the importance of adipocytes in regulating systemic immune homeostasis during inflammation.

While all animal species, including invertebrates and vertebrates, have evolved to store excess energy in the form of fat in cells, they differ in the cell types which are primarily responsible for fat storage and release. Worms (*Caenorhabditis elegans*) store lipids predominantly in intestinal cells, fruit flies (*Drosophila melanogaster*) have a dedicated organ called fat body, while humans use both visceral and subcutaneous adipose depots [452]. In addition to their vital role in regulating systemic energy balance, fat-storing cells have been also implicated in the regulation of host immunity early on in evolution. In fruit flies, the fat body, an organ with both liver and adipose tissue functions, has a central role in the immune response to invading pathogens, through production of antimicrobial peptides and ROS. In Drosophila, immunity-related ROS production requires the induction of lipophagy and lipolysis in enterocytes during inflammation [453]. Furthermore, innate immune pathways and metabolism often share common regulatory features and can regulate one another. This is for instance demonstrated by the NFκB-dependent regulation of the FOXO transcription factor, which fine-tunes fasting-induced lipolysis [454].

More recently, it was discovered that fat cells take part in wound healing responses. In *Drosophila*, fat body cells can migrate through peristaltic movement towards sites of tissue damage and seal the wounds to prevent infections [455]. Strikingly, this central function of adipocytes in wound healing is conserved in mammals, although through a different mechanism. Upon skin injury, dermal adipocytes induce lipolysis, which is important for macrophage recruitment and wound closure [456, 457]. This ability of adipocytes to take part in wound repair and prevention of bacterial spread appears to be evolutionary conserved. The omentum has been described as the "abdominal po-

liceman" more than a century ago, for its capacity to seal off abdominal hernias and perforated appendixes [458]. Analogous to the omentum, the mesentery may exert similar functions by restricting systemic bacterial dissemination from a hyperpermeable gut barrier. However, functional studies of visceral adipose tissues during acute and chronic inflammation in lean humans are challenging due to the invasive nature of sampling. Thus, the usage of functional animal models allow for a better understanding of the role of different mammalian adipose tissues in these pathologies.

Results from this thesis, generated by a comprehensive study of adipose tissue function in the mouse, advance our knowledge in the field by revealing that the adipose tissue is a significant source of anti-inflammatory cytokines, such as IL-10, during acute intestinal inflammation in lean animals. It remains to be seen whether similar effects would be observed in adipose tissues of obese animals or whether the underlying metabolic condition would subvert normal adipose tissue physiology. Previous findings show that mice fed with high fat diet prior to colitis induction have exacerbated disease severity and increased inflammatory cytokine production from mesenteric adipose tissues [407].

Thus far, our data indicates a role of autophagy in the provision of FFA, however its impact on exosome secretion remains to be explored. Adipocyte-derived exosomes contribute to intestinal homeostasis by controlling intestinal macrophage polarization [459]. This is in line with findings showing that adipocyte-derived exosomes containing specific microRNAs, such as miR-34a or miR-155, modulate adipose tissue inflammation by altering macrophage infiltration and function [460, 461]. During obesity, adipocytes also transfer neutral lipids via exosomes to macrophages and induce promote ATM-like gene expression [174]. The general contribution of adipocyte-derived exosomes to the total pool of circulating exosomes is still disputed. Reports suggest that a high percentage of circulating microRNA-containing exosomes may be derived from adipocytes, although labelling of adipocytes with tdTomato showed that not all $CD63^{+}$ exosomes are adipocyte-derived [174, 462]. Exosome secretion may represent an alternative and important route of adipocyte-immune cell communication.

An increasing body of evidence, included the one established in this thesis, demonstrates

that adipose tissues can be regarded as 'polyglot' (term coined by Prof. Philipp Scherrer), influencing processes even at distal tissue sites (e.g. gut, liver, brain). Overall, these findings point towards adipocytes as major evolutionary-conserved signal integrator of systemic inflammation and metabolism, which can be therefore regarded as a central hub for immunity in animals.

7.2 Adipose tissues – the Jekyll and Hyde of IBD?

The prevalence of IBD has increased over the past three decades and, thus IBD remains a major health challenge [463]. Further research is warranted to improve treatment options and to comprehend the complex immune environment during intestinal inflammation. In recent years, the advent of single cell technologies has allowed for a substantial improvement of our understanding of human IBD in various cell types [464]. These studies highlighted the diversity of the involved cell types, such as intestinal fibroblasts, epithelial cells and immune cells, and helped to understand the pathological differences between treatment responders and non-responders [465, 466, 374, 467]. All together, these studies provide new avenues for precision medicine approaches. However, more research is required to understand heterogeneous responses to treatments, wound healing processes and environmental triggers [468].

In the future, understanding of IBD comorbidities is of paramount importance for the establishment of new treatment strategies [469]. The global increase in obesity, and its subsequent pathological subversion of the adipose tissue, are likely to impact IBD. Curiously, the degree of adiposity seems to influence the risk of developing CD. In a study on young Danish men, underweight (BMI <18.5) men had an up-to 2-fold higher risk of CD compared to normal weight individuals [470]. Equally, overweight individuals were more likely develop CD, whereas this was not observed for UC [470]. Although the data did not address the influence of possible co-morbidities associated with weight change, it suggests that imbalancing the homeostatic adipose tissue response increases the risk for developing CD.

The function of the mesentery in IBD, in particular in CD, remains ambiguous. It can adopt both pro- and anti-inflammatory properties, which likely depend on disease

state, severity and co-morbidities. To get a better understanding of its role in IBD, a detailed study of the metabolic and immune dynamics in the mesentery in humans is needed. However, data collected from several groups support the argument that the initial involvement of the mesentery during IBD is protective rather than pathogenic [347, 389]. The hyperplastic expansion of the mesentery is typically associated with transmural inflammation, and may therefore close up sites of intestinal barrier leakage to prevent bacterial dissemination. Indeed, a specific subset of *Clostridium* bacteria, capable of surviving in a lipid-rich environment, is enriched in creeping fat tissue compared to distal sites in the same patient [389]. Strikingly, single cell transcriptomics of $CD45^+$ immune cells in creeping adipose tissue revealed that macrophages upregulate anti-inflammatory and pro-repair pathways, including the production of IL-10 [389]. This increase is in line with previous observations that there is a large number of IL-10-producing macrophages in creeping fat tissues [347]. Exposure to *Clostridium* further promotes the anti-inflammatory, pro-fibrotic macrophage functions through TGFβ and extracellular matrix protein production [389]. Overall, this ground-breaking study by Ha *et al.* pointed strongly towards a pro-wound healing function of the creeping fat tissue in CD pathology [389]. Similarly, our own study found that IL-10 secretion is highly upregulated during intestinal inflammation, in proximal mesenteric and distal gonadal adipose tissues. Our results, however, further reveal that the secretion of IL-10 from the adipose tissue depends on functional autophagy in the adipocytes.

The induction of pro-fibrotic gene signatures in macrophages and adipogenic progenitor cells may, however, become detrimental in chronic disease. Extensive intestinal and adipose tissue fibrosis has been linked to the development of intestinal strictures, which often require surgical intervention [393]. It remains unclear whether factors secreted from adipocytes can promote pro-fibrotic processes in the adipose tissue and intestine. Adipokine expression has been linked to anti-inflammatory, pro-fibrotic macrophage polarization [347]. Continuous excessive intestinal and mesenteric fibrosis may consequently lead to tissue hypoxia and immune exacerbation [471]. However, the precise sequence of tissue fibrosis and immune exacerbation remains arguable, with some evidence pointing towards immune exacerbation preceding tissue fibrosis. Although more

research will be required to address the possible pathological subversion of the mesentery over the course of CD, the chronic involvement of the mesentery may turn it from a well-intended (Dr. Jekyll) to an ultimately detrimental contributor (Mr. Hyde) to CD pathology.

In this thesis, adipocyte autophagy was critical for promoting the anti-inflammatory function of proximal and distal visceral adipose tissues. The DSS colitis model predominantly causes intestinal tissue injury. Therefore, it remains unclear whether bacterial translocation is required for the anti-inflammatory effects observed in our model. From the data presented, it appears likely that ATMs are a major contributor to IL-10 production during colitis, and that autophagy-dependent FFA release can modulate this response. Overall, this underpins the protective role of adipose tissues during colitis in lean mice and warrants translational studies in humans. A better understanding of the endogenous wound healing processes in IBD is critical to improving patient therapy and prolonging relapse-free periods.

7.3 Cell-extrinsic effects of autophagy

Autophagy is an essential cellular process for all cell types. Much of our understanding of autophagy is based on the cell-intrinsic functions of autophagy, such as differentiation, cell survival and metabolism. Only in recent years has the research field started appreciating that autophagy processes in one cell may impact the function of the cells surrounding it. These processes can be classified as "cell-extrinsic" or "non-autonomous" autophagy. From findings over the past decades, loss of autophagy in particular cell types influences other cell types through cytokine production, nutrient release or extracellular vesicle cross-communication.

The impact of autophagy on **cytokine secretion** has been well studied [472]. In this context, the secretion of IL-1β is arguably one of the most intensely and controversially studied cytokines. Induction of autophagy enhances the inflammasome-dependent secretion of IL-1β in LPS-stimulated macrophages [473]. In line with this, IL-1β and ferritin

are targeted towards secretory autophagosomes upon lysosomal damage [474]. In contrast, however, loss of *Atg16l1* in macrophages can also enhance the secretion of IL-1β and IL-18 and exacerbate colitis [369]. This effect is thought to be mediated by increased mitochondrial damage in response to autophagy loss, and consequently, damaged mitochondria increase the production of mitochondrial ROS, resulting in inflammasome activation [475]. Alternatively, autophagy regulates inflammasome activation via p62-mediated degradation of NLRP3 components [476]. Discrepancy in the findings may arise from differences in inflammasome activation and differences in autophagy pathways. Beside IL-1β, autophagy can also influence the expression and secretion of other cytokines including IL-6, IL-8, IL-18 [472]. Since the cytokine environment governs many immune cell functions, the autophagy-dependent alteration of cytokine secretion will impact on other immune and stromal cell types.

More recently, the classical role of autophagy in **nutrient provision** has been explored from a cell-extrinsic perspective. Findings from cancer research unravelled how host autophagy (i.e. in other cells than cancer cells) can promote cancer growth through regulating amino acid availability [161, 159, 162]. Pancreatic cancer cells can transform the tumour microenvironment to induce autophagy in local pancreatic stellate cells in order to increase amino acid availability [161]. Even more distant tissues such as the liver take part in the control of cancer growth by controlling circulating arginine levels in an autophagy-dependent manner [159]. While this intriguing metabolic cross-communication has been established in the context of cancer, future studies will be required to investigate this amino acid crosstalk under homeostatic and inflammatory conditions. In particular since the uptake of amino acids is central to the function of several immune cell subsets such as T cells and macrophages [477].

Although autophagy has been known to control some components of the lipolytic machinery, it remained unclear whether autophagy can control the **release of FFA** into the microenvironment and thus alter immune cell function. The research presented here demonstrates that autophagy in mature adipocyte regulates FFA secretion, and that

FFA availability modulates the anti-inflammatory response in macrophages. However, further *in vivo* links remain to be fully characterized. For instance, we have not fully demonstrated whether ATMs are ultimately responsible for the decrease in circulating IL-10 during DSS-induced colitis in $Atg7^{Ad}$ mice. Future scRNAseq experiments will allow for an unbiased characterization of the immune cell landscape in adipose tissues during colitis. Nevertheless, our data provides the first evidence of cell-extrinsic autophagy in the provision of FFA to immune cells under inflammatory conditions.

Finally, adipocyte autophagy may regulate intercellular communication through the **release of extracellular vesicles**. While LC3-containing extracellular vesicles have been described [35, 36], the precise involvement of different ATG proteins remains ill-defined. Recently, an elegant study highlighted the importance of ATG7 and ATG12, but not ATG14, in the secretion of LC3-exosomes from the cancer cell line HEK293T [35]. However, other reports found that LC3-exosome secretion can occur independent of ATG7 but required ATG16L1 and ATG5 [34]. This may be due to cell type-specific differences. It will therefore be part of future studies to better characterise the components of the autophagic machinery involved in LC3-exosome secretion specifically in adipocytes. However, it is plausible that LC3 helps to target specific cellular cargos into exosomes. This is substantiated by reports that classical autophagy receptors have been found in extracellular vesicles [478]. The impact of extracellular vesicles in the presented study has not been formally assessed, therefore it cannot be excluded that autophagy may be able to regulate the release of visceral adipose tissue-derived exosomes. Of note, the transcriptomic data set of visceral adipocytes included in this thesis, did indeed reveal an upregulation of exosome related genes (CD63, CD81, CD82) during DSS colitis in both genotype. This indicates that further assessment of exosome production from mice with adipocyte-specific loss of *Atg7* or *Atg16l1* is warranted. In conclusion, these early reported findings present a novel pathway through which parts of the autophagy machinery contribute to intercellular communication, and thus may have cell-extrinsic effects.

7.4 Adipocyte autophagy involvement for other pathologies

Since the research in this study was focussed predominantly on adipocyte autophagy during colitis, it remains unclear whether this adipocyte autophagy-dependent crosstalk is more generally transferable to other inflammatory conditions. Tmem are enriched in adipose tissues and peripheral adipose tissue loss leads to the migration of these cells to the adipose tissue-rich bone marrow during times of calorie restriction [150, 479]. Differentiation of $CD4^+$ and $CD8^+$ Tmem is reliant on endogenous FFA processing and it is a checkpoint for the generation of memory cell [480, 481, 482, 483]. The depletion of *Traf6* or *Cpt1a*, encoding for two proteins crucial for FAO, impairs the formation of $CD8^+$ Tmem, but does not impede $CD8^+$ cytotoxic effector functions upon infection [484, 485]. More importantly, PPARγ-dependent upregulation of fatty acid uptake in both human and mouse $CD4^+$ Tmems is essential for their optimal activation and proliferation *in vitro* [483]. This was similarly observed for $CD8^+$ Tmem in the skin and adipose tissues [150, 165]. Due to the close ties of Tmem and fatty acid uptake metabolism, we can speculate that changes in FFA liberation from adipocytes may impact adipose tissue-resident Tmem populations [156]. In line with the enhanced uptake of fatty acids in tissue-resident and effector memory populations [486], we found that these cell populations were significantly decreased in $Atg7^{Ad}$ mice upon DSS-induced intestinal inflammation in visceral adipose tissues (data not shown). This observation sparked a new project to assess the effect of adipocyte autophagy in Tmem formation, survival and re-activation.

On a cell-intrinsic level, it is well documented that autophagic flux decreases in most cell populations with age [487]. This decrease contributes to the 'inflamm-aging' process, a common low-grade inflammation observed in aged individuals on a cellular, tissue and systemic level. The overall metabolic function of adipose tissue declines with age. This is particularly evident by the decreased lipolytic potential of aged adipocytes [488]. Consequently, aberrant alterations in the circulating lipidome are commonly found in older animals. Conversely, supplementation of single lipid and fatty acid species have been shown to extend life and health span [489]. In addition, the aging process leads to an ac-

cumulation of ATMs, shifting the immune cell balance away from an anti-inflammatory to a pro-inflammatory environment and thus promote chronic low-grade tissue inflammation and insulin resistance [490]. As demonstrated here, autophagy contributes to the secretion of FFA into the environment and can alter the response to inflammation. However, it remains unclear whether a reduction in adipocyte autophagy can contribute to altered adipocyte metabolism and promote the inflamm-aging processes in adipose tissues. By studying the impact of autophagy-deficient adipocytes on macrophage polarization, it may be possible to identify specific FFA, or other factors, which are essential for the anti-inflammatory polarization and function of ATMs *in vivo*.

7.5 Thesis Summary and Outlook

Inflammation is an energy-demanding process and research into the metabolism of immune cells has highlighted the impact of differential nutrient availability on immune cell activation and disease severity. Adipocytes are vital for controlling systemic nutrient and energy balance. Thereby, adipocytes integrate a multitude of metabolic and immunological signals to coordinate the release of lipids and FFA into circulation and to their local environment. This process is predominantly driven through lipolytic processes in the cytoplasm. Although autophagy has previously been shown to be essential to adipocyte differentiation [116, 117], its contribution to the release of FFA and consequent regulation of inflammatory processes in metabolically healthy animals remained poorly understood.

In this thesis, evidence is presented which reveals that autophagy is induced in visceral adipocytes and that adipocyte autophagy is essential for mounting an anti-inflammatory immune response during acute intestinal inflammation. Adipocyte-specific loss of *Atg7* resulted in an exacerbation of intestinal inflammation. Simultaneously, lipolysis was impaired in *Atg7*-deficient adipocytes across all FFA species. This was reflected *in vivo* by the decreased expression of CD36 on ATMs, correlating with reduced FFA availability. Restriction of FFA availability reduced IL-10 production in macrophages but was rescued by exogenous FFA supplementation. In line with this, $Atg7^{Ad}$ visceral adipose tissue explants released less IL-10 and $Atg7^{Ad}$ mice had lower levels of circulating IL-10 upon DSS colitis. Together, this shows that adipocyte autophagy contributes to the release of FFA from adipocytes, which under inflammatory conditions can govern the systemic anti-inflammatory response and prevent immune exacerbation (Fig.61). This metabolic cross-communication extends our understanding of how autophagy can cell-extrinsically shape immune responses. While it is tempting to speculate about a general use of this mechanism in inflammatory conditions, it is still too early for these conclusions. For instance, it is still unknown whether bacterial translocation is required for this mechanism. In addition, further investigations into the cell-intrinsic mechanisms by which autophagy optimizes FFA release, either through degrading lipolytic proteins or regulating lipolysis-related signalling pathways or through lipophagy, remain to be

carried out. Taken together, this study has revealed a novel mechanism by which the adipose tissue maintains a balanced immune response, uncovering potential new targets for therapeutic intervention, by promoting adipocyte autophagy or through FFA supplementation.

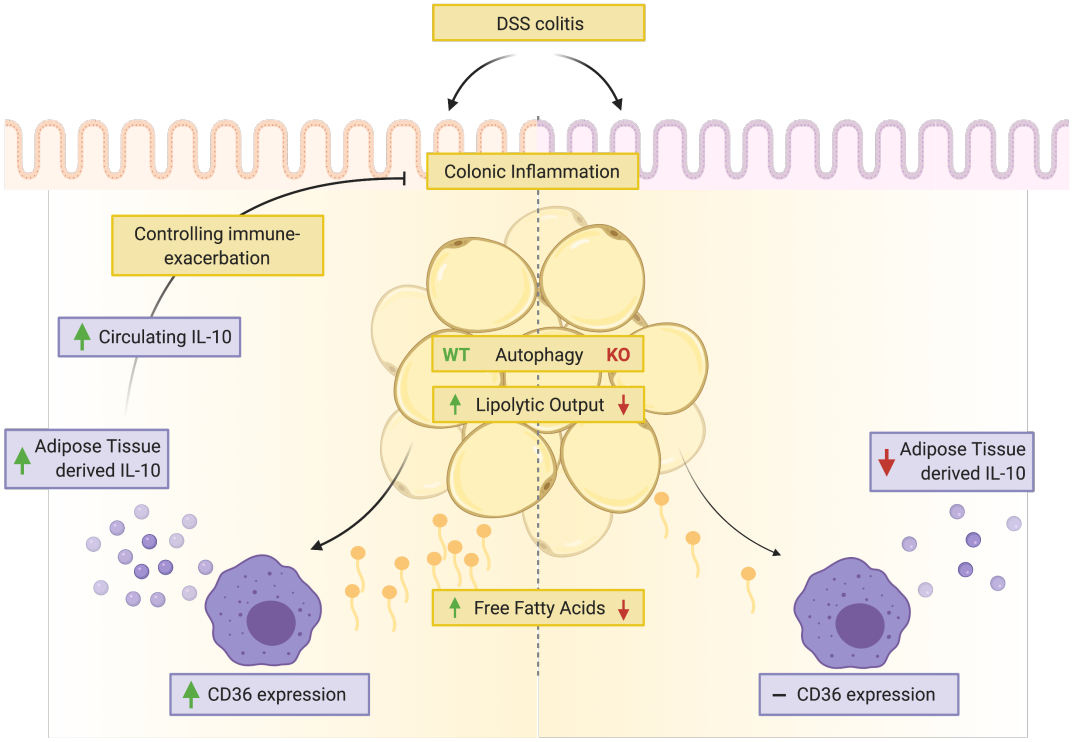

Figure 61: Graphical thesis summary. Adipocyte autophagy is required for the prevention of immune exacerbation to intestinal inflammation by promoting adipose tissue anti-inflammatory immune response. Left: Colonic inflammation due to DSS-induced colitis results in the upregulation of autophagy in adipocytes and increased FFA production. Upregulation of CD36 on macrophages is associated with an increased production and secretion of IL-10 from adipose tissues leading to high systemic levels of IL-10. Right: The absence of autophagy in adipocytes reduces FFA secretion and thus impedes on FFA-dependent IL-10 production in macrophages. This ultimately breaks an important anti-inflammatory pathway to prevent exacerbation of intestinal inflammation.

List of Figures

1 Types of autophagy. 21

2 Core autophagy pathway. 23

3 AMPK and mTOR regulatory pathways. 27

4 Relationship between autophagy and lipolysis. 34

5 Local FFA exchange in the adipose tissue. 39

6 Graphical presentation of the central hypothesis of the thesis. 47

7 Overview of cell line construction. 71

8 Lentiviral shRNA construct is tightly regulated and leads to strong and persistent induction of the construct after 5 days of doxycycline treatment. 72

9 Assessment of KD efficiency in ST2 cell constructs. 74

10 Increase of autophagic flux mostly proceeds expression of ADIPOQ during adipogenesis in ST2 cells. 76

11 *Adipoq* shows adipose tissue-specific gene expression and seems to be predominantly present in mature adipocyte. 78

12 Genotyping of *Adipoq*-driven Cre recombinase mice. 79

13 *Adipoq-Cre*^{ERT2} is adipose-tissue specific but shows minor leakage prior to tamoxifen administration. 81

14 *Adipoq-Cre*^{ERT2} has some off-target expression in adipose endothelial cells. 82

15 *Adipoq-Cre*^{ERT2} shows expression in predominantly mature adipocytes and is not expressed in the intestine. 83

16 Efficient deletion of *Atg7* on transcriptional and protein level. 85

17 *Atg7*^{Ad} mouse model efficiently inhibits LC3 lipidation and reduces autophagy. 86

18 Body weight and adipose tissue mass decreases 8 weeks after autophagy deletion. 96

19 Bone marrow adipose tissue development is impaired in adipocyte autophagy-deficient mice. 98

20 Adipocyte autophagy loss increases adipocyte size after 8 weeks. 99

21 Autophagy partially controls isoproterenol-induced lipolysis. 101
22 Serum free fatty acid and glycerol levels are not altered by autophagy loss in adipocytes. 102
23 Serum lipidome remained unchanged two weeks after autophagy deletion from adipocytes during homeostasis. 102
24 Adipocyte autophagy deletion does not alter myeloid presence in visceral adipose tissue depots. 104
25 Lymphoid cell populations were unaffected by the loss of autophagy. . . 105
26 Hematopoiesis is unchanged even 8 weeks after loss of adipocyte autophagy. 107
27 Hematopoietic recovery after irradiation shows trend to increased platelet recovery. 108
28 Loss of adipocyte autophagy shifts myeloid-lymphoid balance after irradiation. 109
29 Loss of adipocyte autophagy promotes hematopoietic progenitor expansion after irradiation. 110
30 DSS treatment regime results in significant intestinal inflammation. . . . 120
31 DSS treatment results in limited reduced body and adipose tissue weight 121
32 Expression of fatty acid translocase CD36 is increased on intestinal $CD206^{+}$ macrophages but decreased on antigen-experienced T cells. 123
33 Increased presence of ATMs and adipose tissue Tregs in mesenteric adipose tissue upon DSS-induced intestinal inflammation. 124
34 ATMs significantly upregulate CD36 and IRF5 expression during DSS-induced intestinal inflammation in both mWAT and visWAT. 126
35 Autophagy is increased during DSS-induced colitis in mesenteric, and potentially visceral adipose tissues. 127
36 Intestinal health is maintained in adipocyte-autophagy KO mice two weeks post-deletion. 129
37 Intestinal lymphoid populations remain unaltered during homeostatic loss of adipocyte autophagy. 130

38 Loss of adipocyte autophagy leads to exacerbation of DSS-induced intestinal inflammation. 132
39 Loss of adipocyte autophagy increases the expression of several pro-inflammatory genes in the inflamed colon. 133
40 Immune cell infiltration was largely comparable between wild-type and $Atg7^{Ad}$ mice. 134
41 Blunted increase in intestinal Treg numbers during DSS recovery in $Atg7^{Ad}$ mice. 135
42 Loss of adipocyte autophagy does not alter the response to *Hh*-induced colitis. 137
43 Intestinal immune cell populations were comparable between $Atg7^{Ad}$ and control mice two and six weeks post-*Hh* treatment. 138
44 Presence of IL-10 is blunted in adipocyte autophagy-deficient mice upon DSS-induced colitis. 150
45 IL-27, but not IL-10 levels, are altered in the colon of adipocyte autophagy-deficient mice. 151
46 Mesenteric adipose tissues alter their cytokine profile upon DSS- and *Hh*-induced colitis in wild-type animals. 153
47 IL-10 is secreted from adipose tissues in an adipocyte autophagy-dependent manner. 154
48 Adipocyte autophagy is dispensable for the production of IL-10 upon *ex vivo* stimulation of adipose tissues with LPS or TNFα. 155
49 DSS-induced colitis leads to adipose tissue loss, but with signs of hyperplasia. 157
50 Genetic loss of *Atg7* in visceral adipocytes has no effect on overall transcriptome during homeostasis or DSS-induced colitis. 159
51 DSS-induced colonic inflammation results in transcriptional changes and distinct regulation of TNFα-related genes in visceral adipocytes. 160
52 TNFα-induced release of FFA is decreased in autophagy-deficient explants and the serum of DSS-treated mice. 161

53 Serum FFA composition remains unaltered, while revealing an overall reduction in FFA concentration in adipocyte autophagy-deficient mice. . 162
54 DSS-induced may alter serum lipidome, however this is largely independent of adipocyte autophagy. 164
55 Loss of adipocyte autophagy results in a decrease of CD206 expression on ATMs. 166
56 ATMs from $Atg7^{Ad}$ mice expressed reduced surface expression of CD36, possibly indicating a reduced local FFA availability. 167
57 Lipid availability regulates expression of CD36 on the surface on BMDMs. 168
58 Limiting FFA availability differentially affects CD36 expression on BMDM dependent on their polarization. 169
59 LPS-stimulated BMDM significantly decrease IL-10 secretion, but not TNFα, in medium with low concentrations of FFA. 170
60 Linoleic acid supplementation rescues IL-10 secretion in LPS-stimulated BMDM. 171
61 Graphical thesis summary. 190

References

[1] C. De Duve et al. “Tissue fractionation studies. 6. Intracellular distribution patterns of enzymes in rat-liver tissue”. *Biochem J* 60.4 (1955), pp. 604–17. DOI: 10.1042/bj0600604.

[2] M. Tsukada and Y. Ohsumi. “Isolation and characterization of autophagy-defective mutants of Saccharomyces cerevisiae”. *FEBS Lett* 333.1-2 (1993), pp. 169–74. DOI: 10.1016/0014-5793(93)80398-e.

[3] N. Mizushima and B. Levine. “Autophagy in mammalian development and differentiation”. *Nat Cell Biol* 12.9 (2010), pp. 823–30. DOI: 10.1038/ncb0910-823.

[4] A. M. Choi, S. W. Ryter, and B. Levine. “Autophagy in human health and disease”. *N Engl J Med* 368.7 (2013), pp. 651–62. DOI: 10.1056/NEJMra1205406.

[5] L. Galluzzi et al. “Molecular definitions of autophagy and related processes”. *EMBO J* 36.13 (2017), pp. 1811–1836. DOI: 10.15252/embj.201796697.

[6] J. C. Farre and S. Subramani. “Peroxisome turnover by micropexophagy: an autophagy-related process”. *Trends Cell Biol* 14.9 (2004), pp. 515–23. DOI: 10.1016/j.tcb.2004.07.014.

[7] E. Kvam and D. S. Goldfarb. “Nvj1p is the outer-nuclear-membrane receptor for oxysterol-binding protein homolog Osh1p in Saccharomyces cerevisiae”. *J Cell Sci* 117.Pt 21 (2004), pp. 4959–68. DOI: 10.1242/jcs.01372.

[8] I. Kissova et al. “Selective and non-selective autophagic degradation of mitochondria in yeast”. *Autophagy* 3.4 (2007), pp. 329–36. DOI: 10.4161/auto.4034.

[9] J. D. Vevea et al. “Role for Lipid Droplet Biogenesis and Microlipophagy in Adaptation to Lipid Imbalance in Yeast”. *Dev Cell* 35.5 (2015), pp. 584–599. DOI: 10.1016/j.devcel.2015.11.010.

[10] R. J. Schulze et al. “Direct lysosome-based autophagy of lipid droplets in hepatocytes”. *Proc Natl Acad Sci U S A* 117.51 (2020), pp. 32443–32452. DOI: 10.1073/pnas.2011442117.

[11] R. Krick et al. “Piecemeal microautophagy of the nucleus requires the core macroautophagy genes”. *Mol Biol Cell* 19.10 (2008), pp. 4492–505. DOI: 10.1091/mbc.E08-04-0363.

[12] S. Schuck. “Microautophagy - distinct molecular mechanisms handle cargoes of many sizes”. *J Cell Sci* 133.17 (2020). DOI: 10.1242/jcs.246322.

[13] R. Singh et al. “Autophagy regulates lipid metabolism”. *Nature* 458.7242 (2009), pp. 1131–5. DOI: 10.1038/nature07976.

[14] S. Bernales, S. Schuck, and P. Walter. “ER-phagy: selective autophagy of the endoplasmic reticulum”. *Autophagy* 3.3 (2007), pp. 285–7. DOI: 10.4161/auto.3930.

[15] C. Mauvezin and T. P. Neufeld. “Bafilomycin A1 disrupts autophagic flux by inhibiting both V-ATPase-dependent acidification and Ca-P60A/SERCA-dependent autophagosome-lysosome fusion”. *Autophagy* 11.8 (2015), pp. 1437–8. DOI: 10.1080/15548627.2015.1066957.

[16] D. J. Klionsky et al. “Guidelines for the use and interpretation of assays for monitoring autophagy (3rd edition)”. *Autophagy* 12.1 (2016), pp. 1–222. DOI: 10.1080/15548627.2015.1100356.

[17] L. M. Lindqvist, A. K. Simon, and E. H. Baehrecke. “Current questions and possible controversies in autophagy”. *Cell Death Discov* 1 (2015). DOI: 10.1038/cddiscovery.2015.36.

[18] C. A. Lamb, T. Yoshimori, and S. A. Tooze. “The autophagosome: origins unknown, biogenesis complex”. *Nat Rev Mol Cell Biol* 14.12 (2013), pp. 759–74. DOI: 10.1038/nrm3696.

[19] S. A. Tooze and T. Yoshimori. “The origin of the autophagosomal membrane”. *Nat Cell Biol* 12.9 (2010), pp. 831–5. DOI: 10.1038/ncb0910-831.

[20] T. Nishimura and S. A. Tooze. “Emerging roles of ATG proteins and membrane lipids in autophagosome formation”. *Cell Discov* 6 (2020), p. 32. DOI: 10.1038/s41421-020-0161-3.

[21] T. N. Nguyen et al. "Atg8 family LC3/GABARAP proteins are crucial for autophagosome-lysosome fusion but not autophagosome formation during PINK1/Parkin mitophagy and starvation". *J Cell Biol* 215.6 (2016), pp. 857–874. DOI: 10.1083/jcb.201607039.

[22] S. Kaushik and A. M. Cuervo. "Chaperone-mediated autophagy: a unique way to enter the lysosome world". *Trends Cell Biol* 22.8 (2012), pp. 407–17. DOI: 10.1016/j.tcb.2012.05.006.

[23] J. F. Dice. "Peptide sequences that target cytosolic proteins for lysosomal proteolysis". *Trends Biochem Sci* 15.8 (1990), pp. 305–9. DOI: 10.1016/0968-0004(90)90019-8.

[24] U. Bandyopadhyay et al. "The chaperone-mediated autophagy receptor organizes in dynamic protein complexes at the lysosomal membrane". *Mol Cell Biol* 28.18 (2008), pp. 5747–63. DOI: 10.1128/MCB.02070-07.

[25] K. Morozova et al. "Structural and Biological Interaction of hsc-70 Protein with Phosphatidylserine in Endosomal Microautophagy". *J Biol Chem* 291.35 (2016), pp. 18096–106. DOI: 10.1074/jbc.M116.736744.

[26] A. M. Cuervo et al. "Impaired degradation of mutant alpha-synuclein by chaperone-mediated autophagy". *Science* 305.5688 (2004), pp. 1292–5. DOI: 10.1126/science.1101738.

[27] D. Zhou et al. "Lamp-2a facilitates MHC class II presentation of cytoplasmic antigens". *Immunity* 22.5 (2005), pp. 571–81. DOI: 10.1016/j.immuni.2005.03.009.

[28] R. Valdor et al. "Chaperone-mediated autophagy regulates T cell responses through targeted degradation of negative regulators of T cell activation". *Nat Immunol* 15.11 (2014), pp. 1046–54. DOI: 10.1038/ni.3003.

[29] J. L. Schneider, Y. Suh, and A. M. Cuervo. "Deficient chaperone-mediated autophagy in liver leads to metabolic dysregulation". *Cell Metab* 20.3 (2014), pp. 417–32. DOI: 10.1016/j.cmet.2014.06.009.

[30] J. Martinez et al. "Molecular characterization of LC3-associated phagocytosis reveals distinct roles for Rubicon, NOX2 and autophagy proteins". *Nat Cell Biol* 17.7 (2015), pp. 893–906. DOI: 10.1038/ncb3192.

[31] J. Martinez et al. "Noncanonical autophagy inhibits the autoinflammatory, lupus-like response to dying cells". *Nature* 533.7601 (2016), pp. 115–9. DOI: 10.1038/nature17950.

[32] C. D. Gonzalez, R. Resnik, and M. I. Vaccaro. "Secretory Autophagy and Its Relevance in Metabolic and Degenerative Disease". *Front Endocrinol (Lausanne)* 11 (2020), p. 266. DOI: 10.3389/fendo.2020.00266.

[33] M. Ponpuak et al. "Secretory autophagy". *Curr Opin Cell Biol* 35 (2015), pp. 106–16. DOI: 10.1016/j.ceb.2015.04.016.

[34] H. Guo et al. "Atg5 Disassociates the V1V0-ATPase to Promote Exosome Production and Tumor Metastasis Independent of Canonical Macroautophagy". *Dev Cell* 43.6 (2017), 716–730 e7. DOI: 10.1016/j.devcel.2017.11.018.

[35] A. M. Leidal et al. "The LC3-conjugation machinery specifies the loading of RNA-binding proteins into extracellular vesicles". *Nat Cell Biol* 22.2 (2020), pp. 187–199. DOI: 10.1038/s41556-019-0450-y.

[36] J. A. Nicolas-Avila et al. "A Network of Macrophages Supports Mitochondrial Homeostasis in the Heart". *Cell* 183.1 (2020), 94–109 e23. DOI: 10.1016/j.cell.2020.08.031.

[37] M. Zachari and I. G. Ganley. "The mammalian ULK1 complex and autophagy initiation". *Essays Biochem* 61.6 (2017), pp. 585–596. DOI: 10.1042/EBC20170021.

[38] P. M. Wong et al. "Regulation of autophagy by coordinated action of mTORC1 and protein phosphatase 2A". *Nat Commun* 6 (2015), p. 8048. DOI: 10.1038/ncomms9048.

[39] E. Karanasios et al. "Autophagy initiation by ULK complex assembly on ER tubulovesicular regions marked by ATG9 vesicles". *Nat Commun* 7 (2016), p. 12420. DOI: 10.1038/ncomms12420.

[40] R. C. Russell et al. “ULK1 induces autophagy by phosphorylating Beclin-1 and activating VPS34 lipid kinase”. *Nat Cell Biol* 15.7 (2013), pp. 741–50. DOI: 10.1038/ncb2757.

[41] E. Itakura et al. “Beclin 1 forms two distinct phosphatidylinositol 3-kinase complexes with mammalian Atg14 and UVRAG”. *Mol Biol Cell* 19.12 (2008), pp. 5360–72. DOI: 10.1091/mbc.E08-01-0080.

[42] G. M. Fimia et al. “Ambra1 regulates autophagy and development of the nervous system”. *Nature* 447.7148 (2007), pp. 1121–5. DOI: 10.1038/nature05925.

[43] H. C. Dooley et al. “WIPI2 links LC3 conjugation with PI3P, autophagosome formation, and pathogen clearance by recruiting Atg12-5-16L1”. *Mol Cell* 55.2 (2014), pp. 238–52. DOI: 10.1016/j.molcel.2014.05.021.

[44] T. Hanada et al. “The Atg12-Atg5 conjugate has a novel E3-like activity for protein lipidation in autophagy”. *J Biol Chem* 282.52 (2007), pp. 37298–302. DOI: 10.1074/jbc.C700195200.

[45] Y. Kabeya et al. “LC3, GABARAP and GATE16 localize to autophagosomal membrane depending on form-II formation”. *J Cell Sci* 117.Pt 13 (2004), pp. 2805–12. DOI: 10.1242/jcs.01131.

[46] S. Jager et al. “Role for Rab7 in maturation of late autophagic vacuoles”. *J Cell Sci* 117.Pt 20 (2004), pp. 4837–48. DOI: 10.1242/jcs.01370.

[47] Y. Nishida et al. “Discovery of Atg5/Atg7-independent alternative macroautophagy”. *Nature* 461.7264 (2009), pp. 654–8. DOI: 10.1038/nature08455.

[48] A. B. Birgisdottir, T. Lamark, and T. Johansen. “The LIR motif - crucial for selective autophagy”. *J Cell Sci* 126.Pt 15 (2013), pp. 3237–47. DOI: 10.1242/jcs.126128.

[49] S. Pankiv et al. “p62/SQSTM1 binds directly to Atg8/LC3 to facilitate degradation of ubiquitinated protein aggregates by autophagy”. *J Biol Chem* 282.33 (2007), pp. 24131–45. DOI: 10.1074/jbc.M702824200.

[50] G. Bjorkoy et al. “p62/SQSTM1 forms protein aggregates degraded by autophagy and has a protective effect on huntingtin-induced cell death”. *J Cell Biol* 171.4 (2005), pp. 603–14. DOI: 10.1083/jcb.200507002.

[51] P. Wild et al. “Phosphorylation of the autophagy receptor optineurin restricts Salmonella growth”. *Science* 333.6039 (2011), pp. 228–33. DOI: 10.1126/science.1205405.

[52] J. Korac et al. “Ubiquitin-independent function of optineurin in autophagic clearance of protein aggregates”. *J Cell Sci* 126.Pt 2 (2013), pp. 580–92. DOI: 10.1242/jcs.114926.

[53] Y. C. Wong and E. L. Holzbaur. “Optineurin is an autophagy receptor for damaged mitochondria in parkin-mediated mitophagy that is disrupted by an ALS-linked mutation”. *Proc Natl Acad Sci U S A* 111.42 (2014), E4439–48. DOI: 10.1073/pnas.1405752111.

[54] T. Johansen and T. Lamark. “Selective Autophagy: ATG8 Family Proteins, LIR Motifs and Cargo Receptors”. *J Mol Biol* 432.1 (2020), pp. 80–103. DOI: 10.1016/j.jmb.2019.07.016.

[55] V. V. Rogov et al. “Phosphorylation of the mitochondrial autophagy receptor Nix enhances its interaction with LC3 proteins”. *Sci Rep* 7.1 (2017), p. 1131. DOI: 10.1038/s41598-017-01258-6.

[56] Y. Zhu et al. “Modulation of serines 17 and 24 in the LC3-interacting region of Bnip3 determines pro-survival mitophagy versus apoptosis”. *J Biol Chem* 288.2 (2013), pp. 1099–113. DOI: 10.1074/jbc.M112.399345.

[57] Y. Kuang et al. “Structural basis for the phosphorylation of FUNDC1 LIR as a molecular switch of mitophagy”. *Autophagy* 12.12 (2016), pp. 2363–2373. DOI: 10.1080/15548627.2016.1238552.

[58] J. L. Sanwald et al. “The GABARAP Co-Secretome Identified by APEX2-GABARAP Proximity Labelling of Extracellular Vesicles”. *Cells* 9.6 (2020). DOI: 10.3390/cells9061468.

[59] F. Le Guerroue et al. "Autophagosomal Content Profiling Reveals an LC3C-Dependent Piecemeal Mitophagy Pathway". *Mol Cell* 68.4 (2017), 786–796 e6. DOI: 10.1016/j.molcel.2017.10.029.

[60] S. Zellner, M. Schifferer, and C. Behrends. "Systematically defining selective autophagy receptor-specific cargo using autophagosome content profiling". *Mol Cell* (2021). DOI: 10.1016/j.molcel.2021.01.009.

[61] A. E. Webb and A. Brunet. "FOXO transcription factors: key regulators of cellular quality control". *Trends Biochem Sci* 39.4 (2014), pp. 159–69. DOI: 10.1016/j.tibs.2014.02.003.

[62] C. Settembre et al. "TFEB links autophagy to lysosomal biogenesis". *Science* 332.6036 (2011), pp. 1429–33. DOI: 10.1126/science.1204592.

[63] H. Zhang et al. "Polyamines Control eIF5A Hypusination, TFEB Translation, and Autophagy to Reverse B Cell Senescence". *Mol Cell* 76.1 (2019), 110–125 e9. DOI: 10.1016/j.molcel.2019.08.005.

[64] D. M. Sabatini. "Twenty-five years of mTOR: Uncovering the link from nutrients to growth". *Proc Natl Acad Sci U S A* 114.45 (2017), pp. 11818–11825. DOI: 10.1073/pnas.1716173114.

[65] Y. Sancak et al. "Ragulator-Rag complex targets mTORC1 to the lysosomal surface and is necessary for its activation by amino acids". *Cell* 141.2 (2010), pp. 290–303. DOI: 10.1016/j.cell.2010.02.024.

[66] J. Kim et al. "AMPK and mTOR regulate autophagy through direct phosphorylation of Ulk1". *Nat Cell Biol* 13.2 (2011), pp. 132–41. DOI: 10.1038/ncb2152.

[67] N. Hosokawa et al. "Nutrient-dependent mTORC1 association with the ULK1-Atg13-FIP200 complex required for autophagy". *Mol Biol Cell* 20.7 (2009), pp. 1981–91. DOI: 10.1091/mbc.E08-12-1248.

[68] J. A. Martina et al. "MTORC1 functions as a transcriptional regulator of autophagy by preventing nuclear transport of TFEB". *Autophagy* 8.6 (2012), pp. 903–14. DOI: 10.4161/auto.19653.

[69] E. Jacinto et al. “Mammalian TOR complex 2 controls the actin cytoskeleton and is rapamycin insensitive”. *Nat Cell Biol* 6.11 (2004), pp. 1122–8. DOI: 10.1038/ncb1183.

[70] C. E. Gleason et al. “Phosphorylation at distinct subcellular locations underlies specificity in mTORC2-mediated activation of SGK1 and Akt”. *J Cell Sci* 132.7 (2019). DOI: 10.1242/jcs.224931.

[71] Z. Zhang et al. “Insulin-Dependent Regulation of mTORC2-Akt-FoxO Suppresses TLR4 Signaling in Human Leukocytes: Relevance to Type 2 Diabetes”. *Diabetes* 65.8 (2016), pp. 2224–34. DOI: 10.2337/db16-0027.

[72] S. M. Jung et al. “Non-canonical mTORC2 Signaling Regulates Brown Adipocyte Lipid Catabolism through SIRT6-FoxO1”. *Mol Cell* 75.4 (2019), 807–822 e8. DOI: 10.1016/j.molcel.2019.07.023.

[73] C. Mammucari et al. “FoxO3 controls autophagy in skeletal muscle in vivo”. *Cell Metab* 6.6 (2007), pp. 458–71. DOI: 10.1016/j.cmet.2007.11.001.

[74] M. Renna et al. “IGF-1 receptor antagonism inhibits autophagy”. *Hum Mol Genet* 22.22 (2013), pp. 4528–44. DOI: 10.1093/hmg/ddt300.

[75] T. Riffelmacher, F. C. Richter, and A. K. Simon. “Autophagy dictates metabolism and differentiation of inflammatory immune cells”. *Autophagy* 14.2 (2018), pp. 199–206. DOI: 10.1080/15548627.2017.1362525.

[76] J. Adams et al. “Intrasteric control of AMPK via the gamma1 subunit AMP allosteric regulatory site”. *Protein Sci* 13.1 (2004), pp. 155–65. DOI: 10.1110/ps.03340004.

[77] D. M. Gwinn et al. “AMPK phosphorylation of raptor mediates a metabolic checkpoint”. *Mol Cell* 30.2 (2008), pp. 214–26. DOI: 10.1016/j.molcel.2008.03.003.

[78] L. Wu et al. “AMP-Activated Protein Kinase (AMPK) Regulates Energy Metabolism through Modulating Thermogenesis in Adipose Tissue”. *Front Physiol* 9 (2018), p. 122. DOI: 10.3389/fphys.2018.00122.

[79] J. C. Rathmell. "Metabolism and autophagy in the immune system: immunometabolism comes of age". *Immunol Rev* 249.1 (2012), pp. 5–13. DOI: 10.1111/j.1600-065X.2012.01158.x.

[80] K. R. Menikdiwela et al. "Autophagy in metabolic syndrome: breaking the wheel by targeting the renin-angiotensin system". *Cell Death Dis* 11.2 (2020), p. 87. DOI: 10.1038/s41419-020-2275-9.

[81] P. L. Lee, S. M. Jung, and D. A. Guertin. "The Complex Roles of Mechanistic Target of Rapamycin in Adipocytes and Beyond". *Trends Endocrinol Metab* 28.5 (2017), pp. 319–339. DOI: 10.1016/j.tem.2017.01.004.

[82] A. J. Clarke and A. K. Simon. "Autophagy in the renewal, differentiation and homeostasis of immune cells". *Nat Rev Immunol* 19.3 (2019), pp. 170–183. DOI: 10.1038/s41577-018-0095-2.

[83] M. Mortensen et al. "Loss of autophagy in erythroid cells leads to defective removal of mitochondria and severe anemia in vivo". *Proc Natl Acad Sci U S A* 107.2 (2010), pp. 832–7. DOI: 10.1073/pnas.0913170107.

[84] H. Sandoval et al. "Essential role for Nix in autophagic maturation of erythroid cells". *Nature* 454.7201 (2008), pp. 232–5. DOI: 10.1038/nature07006.

[85] D. J. Puleston et al. "Autophagy is a critical regulator of memory CD8(+) T cell formation". *Elife* 3 (2014). DOI: 10.7554/eLife.03706.

[86] H. H. Pua et al. "Autophagy is essential for mitochondrial clearance in mature T lymphocytes". *J Immunol* 182.7 (2009), pp. 4046–55. DOI: 10.4049/jimmunol.0801143.

[87] L. Swadling et al. "Human Liver Memory CD8(+) T Cells Use Autophagy for Tissue Residence". *Cell Rep* 30.3 (2020), 687–698 e6. DOI: 10.1016/j.celrep.2019.12.050.

[88] T. Riffelmacher et al. "Autophagy-Dependent Generation of Free Fatty Acids Is Critical for Normal Neutrophil Differentiation". *Immunity* 47.3 (2017), 466–480 e5. DOI: 10.1016/j.immuni.2017.08.005.

[89] A. J. Clarke et al. "B1a B cells require autophagy for metabolic homeostasis and self-renewal". *J Exp Med* 215.2 (2018), pp. 399–413. DOI: 10.1084/jem.20170771.

[90] M. Ouimet et al. "Autophagy regulates cholesterol efflux from macrophage foam cells via lysosomal acid lipase". *Cell Metab* 13.6 (2011), pp. 655–67. DOI: 10.1016/j.cmet.2011.03.023.

[91] T. Riffelmacher. "Autophagy-dependent generation of free fatty acids is essential for normal neutrophil differentiation by guiding an energy-metabolic switch". Thesis. 2017.

[92] A. M. Kabat et al. "The autophagy gene Atg16l1 differentially regulates Treg and TH2 cells to control intestinal inflammation". *Elife* 5 (2016), e12444. DOI: 10.7554/eLife.12444.

[93] G. M. Carriche et al. "Regulating T-cell differentiation through the polyamine spermidine". *J Allergy Clin Immunol* 147.1 (2021), 335–348 e11. DOI: 10.1016/j.jaci.2020.04.037.

[94] S. N. Catlin et al. "The replication rate of human hematopoietic stem cells in vivo". *Blood* 117.17 (2011), pp. 4460–6. DOI: 10.1182/blood-2010-08-303537.

[95] M. Mortensen et al. "The autophagy protein Atg7 is essential for hematopoietic stem cell maintenance". *J Exp Med* 208.3 (2011), pp. 455–67. DOI: 10.1084/jem.20101145.

[96] G. Alsaleh et al. "Autophagy in T cells from aged donors is maintained by spermidine and correlates with function and vaccine responses". *Elife* 9 (2020). DOI: 10.7554/eLife.57950.

[97] C. Lopez-Otin et al. "The hallmarks of aging". *Cell* 153.6 (2013), pp. 1194–217. DOI: 10.1016/j.cell.2013.05.039.

[98] A. J. Stranks et al. "Autophagy Controls Acquisition of Aging Features in Macrophages". *J Innate Immun* 7.4 (2015), pp. 375–91. DOI: 10.1159/000370112.

[99] A. M. C. Faria, B. S. Reis, and D. Mucida. "Tissue adaptation: Implications for gut immunity and tolerance". *J Exp Med* 214.5 (2017), pp. 1211–1226. DOI: 10.1084/jem.20162014.

[100] G. Caputa, A. Castoldi, and E. J. Pearce. "Metabolic adaptations of tissue-resident immune cells". *Nat Immunol* 20.7 (2019), pp. 793–801. DOI: 10.1038/s41590-019-0407-0.

[101] C. R. Kahn, G. Wang, and K. Y. Lee. "Altered adipose tissue and adipocyte function in the pathogenesis of metabolic syndrome". *J Clin Invest* 129.10 (2019), pp. 3990–4000. DOI: 10.1172/JCI129187.

[102] E. D. Rosen and B. M. Spiegelman. "What we talk about when we talk about fat". *Cell* 156.1-2 (2014), pp. 20–44. DOI: 10.1016/j.cell.2013.12.012.

[103] A. Fedorenko, P. V. Lishko, and Y. Kirichok. "Mechanism of fatty-acid-dependent UCP1 uncoupling in brown fat mitochondria". *Cell* 151.2 (2012), pp. 400–13. DOI: 10.1016/j.cell.2012.09.010.

[104] P. Huttunen, J. Hirvonen, and V. Kinnula. "The occurrence of brown adipose tissue in outdoor workers". *Eur J Appl Physiol Occup Physiol* 46.4 (1981), pp. 339–45. DOI: 10.1007/BF00422121.

[105] J. T. English, S. K. Patel, and M. J. Flanagan. "Association of pheochromocytomas with brown fat tumors". *Radiology* 107.2 (1973), pp. 279–81. DOI: 10.1148/107.2.279.

[106] S. Altshuler-Keylin et al. "Beige Adipocyte Maintenance Is Regulated by Autophagy-Induced Mitochondrial Clearance". *Cell Metab* 24.3 (2016), pp. 402–419. DOI: 10.1016/j.cmet.2016.08.002.

[107] F. Sass et al. "TFEB-deficiency attenuates mitochondrial degradation upon brown adipose tissue whitening at thermoneutrality". *Mol Metab* (2021), p. 101173. DOI: 10.1016/j.molmet.2021.101173.

[108] L. Cheng et al. "Brown and beige adipose tissue: a novel therapeutic strategy for obesity and type 2 diabetes mellitus". *Adipocyte* 10.1 (2021), pp. 48–65. DOI: 10.1080/21623945.2020.1870060.

[109] S. H. Ro et al. "Autophagy in Adipocyte Browning: Emerging Drug Target for Intervention in Obesity". *Front Physiol* 10 (2019), p. 22. DOI: 10.3389/fphys.2019.00022.

[110] M. J. Lee, Y. Wu, and S. K. Fried. "Adipose tissue heterogeneity: implication of depot differences in adipose tissue for obesity complications". *Mol Aspects Med* 34.1 (2013), pp. 1–11. DOI: 10.1016/j.mam.2012.10.001.

[111] T. Tchkonia et al. "Mechanisms and metabolic implications of regional differences among fat depots". *Cell Metab* 17.5 (2013), pp. 644–656. DOI: 10.1016/j.cmet.2013.03.008.

[112] Y. Macotela et al. "Intrinsic differences in adipocyte precursor cells from different white fat depots". *Diabetes* 61.7 (2012), pp. 1691–9. DOI: 10.2337/db11-1753.

[113] R. M. Umek, A. D. Friedman, and S. L. McKnight. "CCAAT-enhancer binding protein: a component of a differentiation switch". *Science* 251.4991 (1991), pp. 288–92. DOI: 10.1126/science.1987644.

[114] P. Tontonoz, E. Hu, and B. M. Spiegelman. "Stimulation of adipogenesis in fibroblasts by PPAR gamma 2, a lipid-activated transcription factor". *Cell* 79.7 (1994), pp. 1147–56. DOI: 10.1016/0092-8674(94)90006-x.

[115] A. G. Cristancho and M. A. Lazar. "Forming functional fat: a growing understanding of adipocyte differentiation". *Nat Rev Mol Cell Biol* 12.11 (2011), pp. 722–34. DOI: 10.1038/nrm3198.

[116] R. Singh et al. "Autophagy regulates adipose mass and differentiation in mice". *J Clin Invest* 119.11 (2009), pp. 3329–39. DOI: 10.1172/JCI39228.

[117] Y. Zhang et al. "Adipose-specific deletion of autophagy-related gene 7 (atg7) in mice reveals a role in adipogenesis". *Proc Natl Acad Sci U S A* 106.47 (2009), pp. 19860–5. DOI: 10.1073/pnas.0906048106.

[118] C. Zhang et al. "Autophagy is involved in adipogenic differentiation by repressing proteasome-dependent PPARgamma2 degradation". *Am J Physiol Endocrinol Metab* 305.4 (2013), E530–9. DOI: 10.1152/ajpendo.00640.2012.

[119] G. S. Hotamisligil et al. "Increased adipose tissue expression of tumor necrosis factor-alpha in human obesity and insulin resistance". *J Clin Invest* 95.5 (1995), pp. 2409–15. DOI: 10.1172/JCI117936.

[120] J. L. Halaas et al. "Weight-reducing effects of the plasma protein encoded by the obese gene". *Science* 269.5223 (1995), pp. 543–6. DOI: 10.1126/science.7624777.

[121] A. E. Achari and S. K. Jain. "Adiponectin, a Therapeutic Target for Obesity, Diabetes, and Endothelial Dysfunction". *Int J Mol Sci* 18.6 (2017). DOI: 10.3390/ijms18061321.

[122] M. Ryden and P. Arner. "Tumour necrosis factor-alpha in human adipose tissue – from signalling mechanisms to clinical implications". *J Intern Med* 262.4 (2007), pp. 431–8. DOI: 10.1111/j.1365-2796.2007.01854.x.

[123] W. P. Cawthorn and J. K. Sethi. "TNF-alpha and adipocyte biology". *FEBS Lett* 582.1 (2008), pp. 117–31. DOI: 10.1016/j.febslet.2007.11.051.

[124] H. Du et al. "Lysosomal acid lipase-deficient mice: depletion of white and brown fat, severe hepatosplenomegaly, and shortened life span". *J Lipid Res* 42.4 (2001), pp. 489–500.

[125] C. Settembre et al. "TFEB controls cellular lipid metabolism through a starvation-induced autoregulatory loop". *Nat Cell Biol* 15.6 (2013), pp. 647–58. DOI: 10.1038/ncb2718.

[126] D. Lettieri Barbato et al. "FoxO1 controls lysosomal acid lipase in adipocytes: implication of lipophagy during nutrient restriction and metformin treatment". *Cell Death Dis* 4 (2013), e861. DOI: 10.1038/cddis.2013.404.

[127] K. Bersuker et al. "A Proximity Labeling Strategy Provides Insights into the Composition and Dynamics of Lipid Droplet Proteomes". *Dev Cell* 44.1 (2018), 97–112 e7. DOI: 10.1016/j.devcel.2017.11.020.

[128] A. Lass et al. "Adipose triglyceride lipase-mediated lipolysis of cellular fat stores is activated by CGI-58 and defective in Chanarin-Dorfman Syndrome". *Cell Metab* 3.5 (2006), pp. 309–19. DOI: 10.1016/j.cmet.2006.03.005.

[129] X. Yang et al. "The G(0)/G(1) switch gene 2 regulates adipose lipolysis through association with adipose triglyceride lipase". *Cell Metab* 11.3 (2010), pp. 194–205. DOI: 10.1016/j.cmet.2010.02.003.

[130] J. G. Granneman et al. "Perilipin controls lipolysis by regulating the interactions of AB-hydrolase containing 5 (Abhd5) and adipose triglyceride lipase (Atgl)". *J Biol Chem* 284.50 (2009), pp. 34538–44. DOI: 10.1074/jbc.M109.068478.

[131] H. Wang et al. "Activation of hormone-sensitive lipase requires two steps, protein phosphorylation and binding to the PAT-1 domain of lipid droplet coat proteins". *J Biol Chem* 284.46 (2009), pp. 32116–25. DOI: 10.1074/jbc.M109.006726.

[132] M. J. Watt and G. R. Steinberg. "Regulation and function of triacylglycerol lipases in cellular metabolism". *Biochem J* 414.3 (2008), pp. 313–25. DOI: 10.1042/BJ20080305.

[133] J. K. Sethi et al. "Characterisation of receptor-specific TNFalpha functions in adipocyte cell lines lacking type 1 and 2 TNF receptors". *FEBS Lett* 469.1 (2000), pp. 77–82. DOI: 10.1016/s0014-5793(00)01250-3.

[134] J. Lopez-Soriano et al. "Lipid metabolism in tumour-bearing mice: studies with knockout mice for tumour necrosis factor receptor 1 protein". *Mol Cell Endocrinol* 132.1-2 (1997), pp. 93–9. DOI: 10.1016/s0303-7207(97)00125-1.

[135] M. Ryden et al. "Mapping of early signaling events in tumor necrosis factor-alpha -mediated lipolysis in human fat cells". *J Biol Chem* 277.2 (2002), pp. 1085–91. DOI: 10.1074/jbc.M109498200.

[136] H. Ruan et al. "Profiling gene transcription in vivo reveals adipose tissue as an immediate target of tumor necrosis factor-alpha: implications for insulin resistance". *Diabetes* 51.11 (2002), pp. 3176–88. DOI: 10.2337/diabetes.51.11.3176.

[137] R. Zechner, F. Madeo, and D. Kratky. "Cytosolic lipolysis and lipophagy: two sides of the same coin". *Nat Rev Mol Cell Biol* 18.11 (2017), pp. 671–684. DOI: 10.1038/nrm.2017.76.

[138] N. Martinez-Lopez et al. "Autophagy proteins regulate ERK phosphorylation". *Nat Commun* 4 (2013), p. 2799. DOI: 10.1038/ncomms3799.

[139] N. Martinez-Lopez et al. "Autophagy in the CNS and Periphery Coordinate Lipophagy and Lipolysis in the Brown Adipose Tissue and Liver". *Cell Metab* 23.1 (2016), pp. 113–27. DOI: 10.1016/j.cmet.2015.10.008.

[140] Y. Peng et al. "ABHD5 interacts with BECN1 to regulate autophagy and tumorigenesis of colon cancer independent of PNPLA2". *Autophagy* 12.11 (2016), pp. 2167–2182. DOI: 10.1080/15548627.2016.1217380.

[141] S. P. Weisberg et al. "Obesity is associated with macrophage accumulation in adipose tissue". *J Clin Invest* 112.12 (2003), pp. 1796–808. DOI: 10.1172/JCI19246.

[142] J. I. Odegaard et al. "Macrophage-specific PPARgamma controls alternative activation and improves insulin resistance". *Nature* 447.7148 (2007), pp. 1116–20. DOI: 10.1038/nature05894.

[143] D. Y. Oh et al. "Increased macrophage migration into adipose tissue in obese mice". *Diabetes* 61.2 (2012), pp. 346–54. DOI: 10.2337/db11-0860.

[144] A. Vasanthakumar et al. "Sex-specific adipose tissue imprinting of regulatory T cells". *Nature* 579.7800 (2020), pp. 581–585. DOI: 10.1038/s41586-020-2040-3.

[145] A. Vasanthakumar et al. "The transcriptional regulators IRF4, BATF and IL-33 orchestrate development and maintenance of adipose tissue-resident regulatory T cells". *Nat Immunol* 16.3 (2015), pp. 276–85. DOI: 10.1038/ni.3085.

[146] D. Cipolletta et al. "PPAR-gamma is a major driver of the accumulation and phenotype of adipose tissue Treg cells". *Nature* 486.7404 (2012), pp. 549–53. DOI: 10.1038/nature11132.

[147] M. Feuerer et al. "Lean, but not obese, fat is enriched for a unique population of regulatory T cells that affect metabolic parameters". *Nat Med* 15.8 (2009), pp. 930–9. DOI: 10.1038/nm.2002.

[148] T. McLaughlin et al. "T-cell profile in adipose tissue is associated with insulin resistance and systemic inflammation in humans". *Arterioscler Thromb Vasc Biol* 34.12 (2014), pp. 2637–43. DOI: 10.1161/ATVBAHA.114.304636.

[149] S. Nishimura et al. “CD8+ effector T cells contribute to macrophage recruitment and adipose tissue inflammation in obesity”. *Nat Med* 15.8 (2009), pp. 914–20. DOI: 10.1038/nm.1964.

[150] S. J. Han et al. “White Adipose Tissue Is a Reservoir for Memory T Cells and Promotes Protective Memory Responses to Infection”. *Immunity* 47.6 (2017), 1154–1168 e6. DOI: 10.1016/j.immuni.2017.11.009.

[151] I. Misumi et al. “Obesity Expands a Distinct Population of T Cells in Adipose Tissue and Increases Vulnerability to Infection”. *Cell Rep* 27.2 (2019), 514–524 e5. DOI: 10.1016/j.celrep.2019.03.030.

[152] A. C. Kohlgruber et al. “gammadelta T cells producing interleukin-17A regulate adipose regulatory T cell homeostasis and thermogenesis”. *Nat Immunol* 19.5 (2018), pp. 464–474. DOI: 10.1038/s41590-018-0094-2.

[153] R. W. Grant and V. D. Dixit. “Adipose tissue as an immunological organ”. *Obesity (Silver Spring)* 23.3 (2015), pp. 512–8. DOI: 10.1002/oby.21003.

[154] Y. Qiu et al. “Eosinophils and type 2 cytokine signaling in macrophages orchestrate development of functional beige fat”. *Cell* 157.6 (2014), pp. 1292–1308. DOI: 10.1016/j.cell.2014.03.066.

[155] J. Vijay et al. “Single-cell analysis of human adipose tissue identifies depot and disease specific cell types”. *Nat Metab* 2.1 (2020), pp. 97–109. DOI: 10.1038/s42255-019-0152-6.

[156] F. C. Richter, S. Obba, and A. K. Simon. “Local exchange of metabolites shapes immunity”. *Immunology* 155.3 (2018), pp. 309–319. DOI: 10.1111/imm.12978.

[157] P. C. Rodriguez et al. “Arginase I production in the tumor microenvironment by mature myeloid cells inhibits T-cell receptor expression and antigen-specific T-cell responses”. *Cancer Res* 64.16 (2004), pp. 5839–49. DOI: 10.1158/0008-5472.CAN-04-0465.

[158] R. Geiger et al. “L-Arginine Modulates T Cell Metabolism and Enhances Survival and Anti-tumor Activity”. *Cell* 167.3 (2016), 829–842 e13. DOI: 10.1016/j.cell.2016.09.031.

[159] L. Poillet-Perez et al. “Autophagy maintains tumour growth through circulating arginine”. *Nature* 563.7732 (2018), pp. 569–573. DOI: 10.1038/s41586-018-0697-7.

[160] Laura Poillet-Perez et al. “Autophagy promotes growth of tumors with high mutational burden by inhibiting a T-cell immune response”. *Nature Cancer* 1.9 (2020), pp. 923–934. DOI: 10.1038/s43018-020-00110-7.

[161] C. M. Sousa et al. “Pancreatic stellate cells support tumour metabolism through autophagic alanine secretion”. *Nature* 536.7617 (2016), pp. 479–83. DOI: 10.1038/nature19084.

[162] N. S. Katheder et al. “Microenvironmental autophagy promotes tumour growth”. *Nature* 541.7637 (2017), pp. 417–420. DOI: 10.1038/nature20815.

[163] L. A. O’Neill, R. J. Kishton, and J. Rathmell. “A guide to immunometabolism for immunologists”. *Nat Rev Immunol* 16.9 (2016), pp. 553–65. DOI: 10.1038/nri.2016.70.

[164] C. Wilhelm et al. “Critical role of fatty acid metabolism in ILC2-mediated barrier protection during malnutrition and helminth infection”. *J Exp Med* 213.8 (2016), pp. 1409–18. DOI: 10.1084/jem.20151448.

[165] Y. Pan et al. “Survival of tissue-resident memory T cells requires exogenous lipid uptake and metabolism”. *Nature* 543.7644 (2017), pp. 252–256. DOI: 10.1038/nature21379.

[166] K. M. Nieman et al. “Adipocytes promote ovarian cancer metastasis and provide energy for rapid tumor growth”. *Nat Med* 17.11 (2011), pp. 1498–503. DOI: 10.1038/nm.2492.

[167] M. S. Shafat et al. “Leukemic blasts program bone marrow adipocytes to generate a protumoral microenvironment”. *Blood* 129.10 (2017), pp. 1320–1332. DOI: 10.1182/blood-2016-08-734798.

[168] A. Ladanyi et al. “Adipocyte-induced CD36 expression drives ovarian cancer progression and metastasis”. *Oncogene* 37.17 (2018), pp. 2285–2301. DOI: 10.1038/s41388-017-0093-z.

[169] H. Ye et al. “Leukemic Stem Cells Evade Chemotherapy by Metabolic Adaptation to an Adipose Tissue Niche”. *Cell Stem Cell* 19.1 (2016), pp. 23–37. DOI: 10.1016/j.stem.2016.06.001.

[170] C. H. Yao et al. “Exogenous Fatty Acids Are the Preferred Source of Membrane Lipids in Proliferating Fibroblasts”. *Cell Chem Biol* 23.4 (2016), pp. 483–93. DOI: 10.1016/j.chembiol.2016.03.007.

[171] K. Hayakawa et al. “Transfer of mitochondria from astrocytes to neurons after stroke”. *Nature* 535.7613 (2016), pp. 551–5. DOI: 10.1038/nature18928.

[172] M. N. Islam et al. “Mitochondrial transfer from bone-marrow-derived stromal cells to pulmonary alveoli protects against acute lung injury”. *Nat Med* 18.5 (2012), pp. 759–65. DOI: 10.1038/nm.2736.

[173] J. R. Brestoff et al. “Intercellular Mitochondria Transfer to Macrophages Regulates White Adipose Tissue Homeostasis and Is Impaired in Obesity”. *Cell Metab* 33.2 (2021), 270–282 e8. DOI: 10.1016/j.cmet.2020.11.008.

[174] 3rd Flaherty S. E. et al. “A lipase-independent pathway of lipid release and immune modulation by adipocytes”. *Science* 363.6430 (2019), pp. 989–993. DOI: 10.1126/science.aaw2586.

[175] G. Andrejeva and J. C. Rathmell. “Similarities and Distinctions of Cancer and Immune Metabolism in Inflammation and Tumors”. *Cell Metab* 26.1 (2017), pp. 49–70. DOI: 10.1016/j.cmet.2017.06.004.

[176] H. Wang and J. Ye. “Regulation of energy balance by inflammation: common theme in physiology and pathology”. *Rev Endocr Metab Disord* 16.1 (2015), pp. 47–54. DOI: 10.1007/s11154-014-9306-8.

[177] G. B. D. Causes of Death Collaborators. “Global, regional, and national age-sex-specific mortality for 282 causes of death in 195 countries and territories, 1980-2017: a systematic analysis for the Global Burden of Disease Study 2017”. *Lancet* 392.10159 (2018), pp. 1736–1788. DOI: 10.1016/S0140-6736(18)32203-7.

[178] D. Furman et al. “Chronic inflammation in the etiology of disease across the life span”. *Nat Med* 25.12 (2019), pp. 1822–1832. DOI: 10.1038/s41591-019-0675-0.

[179] T. J. Pasvol et al. "Incidence and prevalence of inflammatory bowel disease in UK primary care: a population-based cohort study". *BMJ Open* 10.7 (2020), e036584. DOI: 10.1136/bmjopen-2019-036584.

[180] S. Singh et al. "Obesity in IBD: epidemiology, pathogenesis, disease course and treatment outcomes". *Nat Rev Gastroenterol Hepatol* 14.2 (2017), pp. 110–121. DOI: 10.1038/nrgastro.2016.181.

[181] M. Fakhoury et al. "Inflammatory bowel disease: clinical aspects and treatments". *J Inflamm Res* 7 (2014), pp. 113–20. DOI: 10.2147/JIR.S65979.

[182] M. A. McGuckin et al. "Intestinal barrier dysfunction in inflammatory bowel diseases". *Inflamm Bowel Dis* 15.1 (2009), pp. 100–13. DOI: 10.1002/ibd.20539.

[183] M. Friedrich, M. Pohin, and F. Powrie. "Cytokine Networks in the Pathophysiology of Inflammatory Bowel Disease". *Immunity* 50.4 (2019), pp. 992–1006. DOI: 10.1016/j.immuni.2019.03.017.

[184] M. Murai et al. "Interleukin 10 acts on regulatory T cells to maintain expression of the transcription factor Foxp3 and suppressive function in mice with colitis". *Nat Immunol* 10.11 (2009), pp. 1178–84. DOI: 10.1038/ni.1791.

[185] E. Breese et al. "Interleukin-2- and interferon-gamma-secreting T cells in normal and diseased human intestinal mucosa". *Immunology* 78.1 (1993), pp. 127–31.

[186] I. J. Fuss et al. "Disparate CD4+ lamina propria (LP) lymphokine secretion profiles in inflammatory bowel disease. Crohn's disease LP cells manifest increased secretion of IFN-gamma, whereas ulcerative colitis LP cells manifest increased secretion of IL-5". *J Immunol* 157.3 (1996), pp. 1261–70.

[187] F. Heller et al. "Interleukin-13 is the key effector Th2 cytokine in ulcerative colitis that affects epithelial tight junctions, apoptosis, and cell restitution". *Gastroenterology* 129.2 (2005), pp. 550–64. DOI: 10.1016/j.gastro.2005.05.002.

[188] R. Atreya and B. Siegmund. "Location is important: differentiation between ileal and colonic Crohn's disease". *Nat Rev Gastroenterol Hepatol* 18 (2021), pp. 544–558. DOI: 10.1038/s41575-021-00424-6.

[189] A. Batra et al. "Mesenteric fat - control site for bacterial translocation in colitis?" *Mucosal Immunol* 5.5 (2012), pp. 580–91. DOI: 10.1038/mi.2012.33.

[190] J. Verdier et al. "Compartmentalized expression of Th1 and Th17 cytokines in pediatric inflammatory bowel diseases". *Inflamm Bowel Dis* 18.7 (2012), pp. 1260–6. DOI: 10.1002/ibd.21905.

[191] H. Schmitt et al. "Expansion of IL-23 receptor bearing TNFR2+ T cells is associated with molecular resistance to anti-TNF therapy in Crohn's disease". *Gut* 68.5 (2019), pp. 814–828. DOI: 10.1136/gutjnl-2017-315671.

[192] W. J. Sandborn et al. "Ustekinumab induction and maintenance therapy in refractory Crohn's disease". *N Engl J Med* 367.16 (2012), pp. 1519–28. DOI: 10.1056/NEJMoa1203572.

[193] P. J. Mannon et al. "Anti-interleukin-12 antibody for active Crohn's disease". *N Engl J Med* 351.20 (2004), pp. 2069–79. DOI: 10.1056/NEJMoa033402.

[194] C. Becker et al. "Constitutive p40 promoter activation and IL-23 production in the terminal ileum mediated by dendritic cells". *J Clin Invest* 112.5 (2003), pp. 693–706. DOI: 10.1172/JCI17464.

[195] N. Kamada et al. "Unique CD14 intestinal macrophages contribute to the pathogenesis of Crohn disease via IL-23/IFN-gamma axis". *J Clin Invest* 118.6 (2008), pp. 2269–80. DOI: 10.1172/JCI34610.

[196] T. Kobayashi et al. "IL23 differentially regulates the Th1/Th17 balance in ulcerative colitis and Crohn's disease". *Gut* 57.12 (2008), pp. 1682–9. DOI: 10.1136/gut.2007.135053.

[197] C. T. Weaver et al. "The Th17 pathway and inflammatory diseases of the intestines, lungs, and skin". *Annu Rev Pathol* 8 (2013), pp. 477–512. DOI: 10.1146/annurev-pathol-011110-130318.

[198] O. Wera, P. Lancellotti, and C. Oury. "The Dual Role of Neutrophils in Inflammatory Bowel Diseases". *J Clin Med* 5.12 (2016). DOI: 10.3390/jcm5120118.

[199] U. Jain et al. “Debaryomyces is enriched in Crohn’s disease intestinal tissue and impairs healing in mice”. *Science* 12.371 (2021), pp. 1154–1159. DOI: 10.1126/science.abd0919.

[200] W. Hueber et al. “Secukinumab, a human anti-IL-17A monoclonal antibody, for moderate to severe Crohn’s disease: unexpected results of a randomised, double-blind placebo-controlled trial”. *Gut* 61.12 (2012), pp. 1693–700. DOI: 10.1136/gutjnl-2011-301668.

[201] M. F. Neurath. “Targeting immune cell circuits and trafficking in inflammatory bowel disease”. *Nat Immunol* 20.8 (2019), pp. 970–979. DOI: 10.1038/s41590-019-0415-0.

[202] R. S. Wildin, S. Smyk-Pearson, and A. H. Filipovich. “Clinical and molecular features of the immunodysregulation, polyendocrinopathy, enteropathy, X linked (IPEX) syndrome”. *J Med Genet* 39.8 (2002), pp. 537–45. DOI: 10.1136/jmg.39.8.537.

[203] M. C. Fantini et al. “Smad7 controls resistance of colitogenic T cells to regulatory T cell-mediated suppression”. *Gastroenterology* 136.4 (2009), 1308–16, e1–3. DOI: 10.1053/j.gastro.2008.12.053.

[204] P. P. Ahern et al. “Interleukin-23 drives intestinal inflammation through direct activity on T cells”. *Immunity* 33.2 (2010), pp. 279–88. DOI: 10.1016/j.immuni.2010.08.010.

[205] D. S. Shouval et al. “Interleukin-10 receptor signaling in innate immune cells regulates mucosal immune tolerance and anti-inflammatory macrophage function”. *Immunity* 40.5 (2014), pp. 706–19. DOI: 10.1016/j.immuni.2014.03.011.

[206] K. J. Maloy and F. Powrie. “Intestinal homeostasis and its breakdown in inflammatory bowel disease”. *Nature* 474.7351 (2011), pp. 298–306. DOI: 10.1038/nature10208.

[207] H.H. Uhlig. “Monogenic diseases associated with intestinal inflammation: implications for the understanding of inflammatory bowel disease”. *Gut* 62.12 (2013), pp. 1795–805. DOI: 10.1136/gutjnl-2012-303956.

[208] K. Atarashi et al. “Induction of colonic regulatory T cells by indigenous Clostridium species”. *Science* 331.6015 (2011), pp. 337–41. DOI: 10.1126/science.1198469.

[209] J. F. Colombel et al. “Interleukin 10 (Tenovil) in the prevention of postoperative recurrence of Crohn’s disease”. *Gut* 49.1 (2001), pp. 42–6. DOI: 10.1136/gut.49.1.42.

[210] S. Schreiber et al. “Safety and efficacy of recombinant human interleukin 10 in chronic active Crohn’s disease. Crohn’s Disease IL-10 Cooperative Study Group”. *Gastroenterology* 119.6 (2000), pp. 1461–72. DOI: 10.1053/gast.2000.20196.

[211] J. Hampe et al. “A genome-wide association scan of nonsynonymous SNPs identifies a susceptibility variant for Crohn disease in ATG16L1”. *Nat Genet* 39.2 (2007), pp. 207–11. DOI: 10.1038/ng1954.

[212] M. Parkes et al. “Sequence variants in the autophagy gene IRGM and multiple other replicating loci contribute to Crohn’s disease susceptibility”. *Nat Genet* 39.7 (2007), pp. 830–2. DOI: 10.1038/ng2061.

[213] S. A. McCarroll et al. “Deletion polymorphism upstream of IRGM associated with altered IRGM expression and Crohn’s disease”. *Nat Genet* 40.9 (2008), pp. 1107–12. DOI: 10.1038/ng.215.

[214] K. Y. Hui et al. “Functional variants in the LRRK2 gene confer shared effects on risk for Crohn’s disease and Parkinson’s disease”. *Sci Transl Med* 10.423 (2018). DOI: 10.1126/scitranslmed.aai7795.

[215] L. Jostins et al. “Host-microbe interactions have shaped the genetic architecture of inflammatory bowel disease”. *Nature* 491.7422 (2012), pp. 119–24. DOI: 10.1038/nature11582.

[216] B. Khor, A. Gardet, and R. J. Xavier. “Genetics and pathogenesis of inflammatory bowel disease”. *Nature* 474.7351 (2011), pp. 307–17. DOI: 10.1038/nature10209.

[217] P. Kuballa et al. "Impaired autophagy of an intracellular pathogen induced by a Crohn's disease associated ATG16L1 variant". *PLoS One* 3.10 (2008), e3391. DOI: 10.1371/journal.pone.0003391.

[218] L. H. Travassos et al. "Nod1 and Nod2 direct autophagy by recruiting ATG16L1 to the plasma membrane at the site of bacterial entry". *Nat Immunol* 11.1 (2010), pp. 55–62. DOI: 10.1038/ni.1823.

[219] R. Cooney et al. "NOD2 stimulation induces autophagy in dendritic cells influencing bacterial handling and antigen presentation". *Nat Med* 16.1 (2010), pp. 90–7. DOI: 10.1038/nm.2069.

[220] K. Cadwell et al. "A key role for autophagy and the autophagy gene Atg16l1 in mouse and human intestinal Paneth cells". *Nature* 456.7219 (2008), pp. 259–63. DOI: 10.1038/nature07416.

[221] K. Cadwell et al. "A common role for Atg16L1, Atg5 and Atg7 in small intestinal Paneth cells and Crohn disease". *Autophagy* 5.2 (2009), pp. 250–2. DOI: 10.4161/auto.5.2.7560.

[222] B. Liu et al. "Irgm1-deficient mice exhibit Paneth cell abnormalities and increased susceptibility to acute intestinal inflammation". *Am J Physiol Gastrointest Liver Physiol* 305.8 (2013), G573–84. DOI: 10.1152/ajpgi.00071.2013.

[223] P. Brest et al. "A synonymous variant in IRGM alters a binding site for miR-196 and causes deregulation of IRGM-dependent xenophagy in Crohn's disease". *Nat Genet* 43.3 (2011), pp. 242–5. DOI: 10.1038/ng.762.

[224] S. Mehto et al. "The Crohn's Disease Risk Factor IRGM Limits NLRP3 Inflammasome Activation by Impeding Its Assembly and by Mediating Its Selective Autophagy". *Mol Cell* 73.3 (2019), 429–445 e7. DOI: 10.1016/j.molcel.2018.11.018.

[225] B. Z. Shao et al. "The Role of Autophagy in Inflammatory Bowel Disease". *Front Physiol* 12 (2021), p. 621132. DOI: 10.3389/fphys.2021.621132.

[226] A. Sassmann, S. Offermanns, and N. Wettschureck. "Tamoxifen-inducible Cre-mediated recombination in adipocytes". *Genesis* 48.10 (2010), pp. 618–25. DOI: 10.1002/dvg.20665.

[227] M. Komatsu et al. "Impairment of starvation-induced and constitutive autophagy in Atg7-deficient mice". *J Cell Biol* 169.3 (2005), pp. 425–34. DOI: 10.1083/jcb.200412022.

[228] S. Hwang et al. "Nondegradative role of Atg5-Atg12/ Atg16L1 autophagy protein complex in antiviral activity of interferon gamma". *Cell Host Microbe* 11.4 (2012), pp. 397–409. DOI: 10.1016/j.chom.2012.03.002.

[229] L. Madisen et al. "A robust and high-throughput Cre reporting and characterization system for the whole mouse brain". *Nat Neurosci* 13.1 (2010), pp. 133–40. DOI: 10.1038/nn.2467.

[230] C. Danne et al. "A Large Polysaccharide Produced by Helicobacter hepaticus Induces an Anti-inflammatory Gene Signature in Macrophages". *Cell Host Microbe* 22.6 (2017), 733–745 e5. DOI: 10.1016/j.chom.2017.11.002.

[231] O. Naveiras et al. "Bone-marrow adipocytes as negative regulators of the haematopoietic microenvironment". *Nature* 460.7252 (2009), pp. 259–63. DOI: 10.1038/nature08099.

[232] M. Ogawa et al. "B cell ontogeny in murine embryo studied by a culture system with the monolayer of a stromal cell clone, ST2: B cell progenitor develops first in the embryonal body rather than in the yolk sac". *EMBO J* 7.5 (1988), pp. 1337–43.

[233] H. Green and M. Meuth. "An established pre-adipose cell line and its differentiation in culture". *Cell* 3.2 (1974), pp. 127–33. DOI: 10.1016/0092-8674(74)90116-0.

[234] E. V. Morris et al. "Myeloma Cells Down-Regulate Adiponectin in Bone Marrow Adipocytes Via TNF-Alpha". *J Bone Miner Res* 35.5 (2020), pp. 942–955. DOI: 10.1002/jbmr.3951.

[235] C. Fellmann et al. “An optimized microRNA backbone for effective single-copy RNAi”. *Cell Rep* 5.6 (2013), pp. 1704–13. DOI: 10.1016/j.celrep.2013.11.020.

[236] P. Ebner et al. “The IAP family member BRUCE regulates autophagosome-lysosome fusion”. *Nat Commun* 9.1 (2018), p. 599. DOI: 10.1038/s41467-018-02823-x.

[237] M. Schweiger et al. “Measurement of lipolysis”. *Methods Enzymol* 538 (2014), pp. 171–93. DOI: 10.1016/B978-0-12-800280-3.00010-4.

[238] L. Ju et al. “Obesity-associated inflammation triggers an autophagy-lysosomal response in adipocytes and causes degradation of perilipin 1”. *Cell Death Dis* 10.2 (2019), p. 121. DOI: 10.1038/s41419-019-1393-8.

[239] Y. M. Lim et al. “Systemic autophagy insufficiency compromises adaptation to metabolic stress and facilitates progression from obesity to diabetes”. *Nat Commun* 5 (2014), p. 4934. DOI: 10.1038/ncomms5934.

[240] N. L. Bray et al. “Near-optimal probabilistic RNA-seq quantification”. *Nat Biotechnol* 34.5 (2016), pp. 525–7. DOI: 10.1038/nbt.3519.

[241] M. I. Love, W. Huber, and S. Anders. “Moderated estimation of fold change and dispersion for RNA-seq data with DESeq2”. *Genome Biol* 15.12 (2014), p. 550. DOI: 10.1186/s13059-014-0550-8.

[242] G. Yu et al. “clusterProfiler: an R package for comparing biological themes among gene clusters”. *OMICS* 16.5 (2012), pp. 284–7. DOI: 10.1089/omi.2011.0118.

[243] M. A. Surma et al. “An automated shotgun lipidomics platform for high throughput, comprehensive, and quantitative analysis of blood plasma intact lipids”. *Eur J Lipid Sci Technol* 117.10 (2015), pp. 1540–1549. DOI: 10.1002/ejlt.201500145.

[244] R. Herzog et al. “A novel informatics concept for high-throughput shotgun lipidomics based on the molecular fragmentation query language”. *Genome Biol* 12.1 (2011), R8. DOI: 10.1186/gb-2011-12-1-r8.

[245] J. Folch, M. Lees, and G. H. Sloane Stanley. "A simple method for the isolation and purification of total lipides from animal tissues". *J Biol Chem* 226.1 (1957), pp. 497–509.

[246] R. Berry and M. S. Rodeheffer. "Characterization of the adipocyte cellular lineage in vivo". *Nat Cell Biol* 15.3 (2013), pp. 302–8. DOI: 10.1038/ncb2696.

[247] X. Chen, Y. He, and F. Lu. "Autophagy in Stem Cell Biology: A Perspective on Stem Cell Self-Renewal and Differentiation". *Stem Cells Int* 2018 (2018), p. 9131397. DOI: 10.1155/2018/9131397.

[248] B. M. Spiegelman. "PPAR-gamma: adipogenic regulator and thiazolidinedione receptor". *Diabetes* 47.4 (1998), pp. 507–14. DOI: 10.2337/diabetes.47.4.507.

[249] E. Jeffery et al. "Characterization of Cre recombinase models for the study of adipose tissue". *Adipocyte* 3.3 (2014), pp. 206–11. DOI: 10.4161/adip.29674.

[250] J. Liu et al. "Cre Recombinase Strains Used for the Study of Adipose Tissues and Adipocyte Progenitors". *J Cell Physiol* 232.10 (2017), pp. 2698–2703. DOI: 10.1002/jcp.25675.

[251] Z. V. Wang et al. "Identification and characterization of a promoter cassette conferring adipocyte-specific gene expression". *Endocrinology* 151.6 (2010), pp. 2933–9. DOI: 10.1210/en.2010-0136.

[252] U. Gurriaran-Rodriguez et al. "Obestatin as a regulator of adipocyte metabolism and adipogenesis". *J Cell Mol Med* 15.9 (2011), pp. 1927–40. DOI: 10.1111/j.1582-4934.2010.01192.x.

[253] Z. Cao, R. M. Umek, and S. L. McKnight. "Regulated expression of three C/EBP isoforms during adipose conversion of 3T3-L1 cells". *Genes Dev* 5.9 (1991), pp. 1538–52. DOI: 10.1101/gad.5.9.1538.

[254] D. J. Klemm et al. "Insulin-induced adipocyte differentiation. Activation of CREB rescues adipogenesis from the arrest caused by inhibition of prenylation". *J Biol Chem* 276.30 (2001), pp. 28430–5. DOI: 10.1074/jbc.M103382200.

[255] H. Hauner. "Complete adipose differentiation of 3T3 L1 cells in a chemically defined medium: comparison to serum-containing culture conditions". *Endocrinology* 127.2 (1990), pp. 865–72. DOI: 10.1210/endo-127-2-865.

[256] J. N. Fain et al. "Dexamethasone and the inflammatory response in explants of human omental adipose tissue". *Mol Cell Endocrinol* 315.1-2 (2010), pp. 292–8. DOI: 10.1016/j.mce.2009.10.004.

[257] M. J. Harms et al. "Mature Human White Adipocytes Cultured under Membranes Maintain Identity, Function, and Can Transdifferentiate into Brown-like Adipocytes". *Cell Rep* 27.1 (2019), 213–225 e5. DOI: 10.1016/j.celrep.2019.03.026.

[258] Consortium Tabula Muris et al. "Single-cell transcriptomics of 20 mouse organs creates a Tabula Muris". *Nature* 562.7727 (2018), pp. 367–372. DOI: 10.1038/s41586-018-0590-4.

[259] W. P. Cawthorn et al. "Bone marrow adipose tissue is an endocrine organ that contributes to increased circulating adiponectin during caloric restriction". *Cell Metab* 20.2 (2014), pp. 368–375. DOI: 10.1016/j.cmet.2014.06.003.

[260] Y. Fan et al. "Parathyroid Hormone Directs Bone Marrow Mesenchymal Cell Fate". *Cell Metab* 25.3 (2017), pp. 661–672. DOI: 10.1016/j.cmet.2017.01.001.

[261] Y. Y. Chau et al. "Visceral and subcutaneous fat have different origins and evidence supports a mesothelial source". *Nat Cell Biol* 16.4 (2014), pp. 367–75. DOI: 10.1038/ncb2922.

[262] R. Yi et al. "Overexpression of exportin 5 enhances RNA interference mediated by short hairpin RNAs and microRNAs". *RNA* 11.2 (2005), pp. 220–6. DOI: 10.1261/rna.7233305.

[263] A. Josephrajan et al. "Unconventional Secretion of Adipocyte Fatty Acid Binding Protein 4 Is Mediated By Autophagic Proteins in a Sirtuin-1-Dependent Manner". *Diabetes* 68.9 (2019), pp. 1767–1777. DOI: 10.2337/db18-1367.

[264] B. E. Fitzwalter et al. "Autophagy Inhibition Mediates Apoptosis Sensitization in Cancer Therapy by Relieving FOXO3a Turnover". *Dev Cell* 44.5 (2018), 555–565 e3. DOI: 10.1016/j.devcel.2018.02.014.

[265] A. Vij et al. "Investigating regulatory signatures of human autophagy related gene 5 (ATG5) through functional in silico analysis". *Meta Gene* 9 (2016), pp. 237–48. DOI: 10.1016/j.mgene.2016.07.012.

[266] K. Zebisch et al. "Protocol for effective differentiation of 3T3-L1 cells to adipocytes". *Anal Biochem* 425.1 (2012), pp. 88–90. DOI: 10.1016/j.ab.2012.03.005.

[267] W. He et al. "Adipose-specific peroxisome proliferator-activated receptor gamma knockout causes insulin resistance in fat and liver but not in muscle". *Proc Natl Acad Sci U S A* 100.26 (2003), pp. 15712–7. DOI: 10.1073/pnas.2536828100.

[268] M. Iwaki et al. "Induction of adiponectin, a fat-derived antidiabetic and antiatherogenic factor, by nuclear receptors". *Diabetes* 52.7 (2003), pp. 1655–63. DOI: 10.2337/diabetes.52.7.1655.

[269] J. Cai et al. "Autophagy Ablation in Adipocytes Induces Insulin Resistance and Reveals Roles for Lipid Peroxide and Nrf2 Signaling in Adipose-Liver Crosstalk". *Cell Rep* 25.7 (2018), 1708–1717 e5. DOI: 10.1016/j.celrep.2018.10.040.

[270] Y. Son et al. "Adipocyte-specific Beclin1 deletion impairs lipolysis and mitochondrial integrity in adipose tissue". *Mol Metab* (2020), p. 101005. DOI: 10.1016/j.molmet.2020.101005.

[271] T. Yamamuro et al. "Age-dependent loss of adipose Rubicon promotes metabolic disorders via excess autophagy". *Nat Commun* 11.1 (2020), p. 4150. DOI: 10.1038/s41467-020-17985-w.

[272] Xing Zhang et al. "Sustained activation of autophagy suppresses adipocyte maturation via a lipolysis-dependent mechanism". *Autophagy* 16.9 (2020), pp. 1668–1682. DOI: 10.1080/15548627.2019.1703355.

[273] S. Hayashi and A. P. McMahon. "Efficient recombination in diverse tissues by a tamoxifen-inducible form of Cre: a tool for temporally regulated gene activa-

tion/inactivation in the mouse". *Dev Biol* 244.2 (2002), pp. 305–18. DOI: 10.1006/dbio.2002.0597.

[274] A. K. Indra et al. "Temporally-controlled site-specific mutagenesis in the basal layer of the epidermis: comparison of the recombinase activity of the tamoxifen-inducible Cre-ER(T) and Cre-ER(T2) recombinases". *Nucleic Acids Res* 27.22 (1999), pp. 4324–7. DOI: 10.1093/nar/27.22.4324.

[275] N. Hesselbarth et al. "Tamoxifen affects glucose and lipid metabolism parameters, causes browning of subcutaneous adipose tissue and transient body composition changes in C57BL/6NTac mice". *Biochem Biophys Res Commun* 464.3 (2015), pp. 724–9. DOI: 10.1016/j.bbrc.2015.07.015.

[276] L. Zhao et al. "Even a low dose of tamoxifen profoundly induces adipose tissue browning in female mice". *Int J Obes (Lond)* 44.1 (2020), pp. 226–234. DOI: 10.1038/s41366-019-0330-3.

[277] M. Schmidt-Supprian and K. Rajewsky. "Vagaries of conditional gene targeting". *Nat Immunol* 8.7 (2007), pp. 665–8. DOI: 10.1038/ni0707-665.

[278] G. Haemmerle et al. "Defective lipolysis and altered energy metabolism in mice lacking adipose triglyceride lipase". *Science* 312.5774 (2006), pp. 734–7. DOI: 10.1126/science.1123965.

[279] M. B. Schott et al. "Lipid droplet size directs lipolysis and lipophagy catabolism in hepatocytes". *J Cell Biol* 218.10 (2019), pp. 3320–3335. DOI: 10.1083/jcb.201803153.

[280] I. Kojta, M. Chacinska, and A. Blachnio-Zabielska. "Obesity, Bioactive Lipids, and Adipose Tissue Inflammation in Insulin Resistance". *Nutrients* 12.5 (2020). DOI: 10.3390/nu12051305.

[281] Felix Clemens Richter et al. "Impact of obesity on host defences: Implications for SARS-CoV-2 infection". *Oxford Open Immunology* (2021). DOI: 10.1093/oxfimm/iqab001.

[282] R. S. Sappati Biyyani, B. S. Putka, and K. D. Mullen. "Dyslipidemia and lipoprotein profiles in patients with inflammatory bowel disease". *J Clin Lipidol* 4.6 (2010), pp. 478–82. DOI: 10.1016/j.jacl.2010.08.021.

[283] A. Kosteli et al. "Weight loss and lipolysis promote a dynamic immune response in murine adipose tissue". *J Clin Invest* 120.10 (2010), pp. 3466–79. DOI: 10.1172/JCI42845.

[284] M. Kratz et al. "Metabolic dysfunction drives a mechanistically distinct proinflammatory phenotype in adipose tissue macrophages". *Cell Metab* 20.4 (2014), pp. 614–25. DOI: 10.1016/j.cmet.2014.08.010.

[285] D. A. Jaitin et al. "Lipid-Associated Macrophages Control Metabolic Homeostasis in a Trem2-Dependent Manner". *Cell* 178.3 (2019), 686–698 e14. DOI: 10.1016/j.cell.2019.05.054.

[286] S. Cinti et al. "Adipocyte death defines macrophage localization and function in adipose tissue of obese mice and humans". *J Lipid Res* 46.11 (2005), pp. 2347–55. DOI: 10.1194/jlr.M500294-JLR200.

[287] S. Talukdar et al. "Neutrophils mediate insulin resistance in mice fed a high-fat diet through secreted elastase". *Nat Med* 18.9 (2012), pp. 1407–12. DOI: 10.1038/nm.2885.

[288] L. Lynch et al. "Adipose tissue invariant NKT cells protect against diet-induced obesity and metabolic disorder through regulatory cytokine production". *Immunity* 37.3 (2012), pp. 574–87. DOI: 10.1016/j.immuni.2012.06.016.

[289] L. Lynch et al. "Regulatory iNKT cells lack expression of the transcription factor PLZF and control the homeostasis of T(reg) cells and macrophages in adipose tissue". *Nat Immunol* 16.1 (2015), pp. 85–95. DOI: 10.1038/ni.3047.

[290] F. A. Ververs et al. "Immunometabolic Activation of Invariant Natural Killer T Cells". *Front Immunol* 9 (2018), p. 1192. DOI: 10.3389/fimmu.2018.01192.

[291] K. J. Suchacki et al. "Bone marrow adipose tissue is a unique adipose subtype with distinct roles in glucose homeostasis". *Nat Commun* 11.1 (2020), p. 3097. DOI: 10.1038/s41467-020-16878-2.

[292] E. L. Scheller et al. "Bone marrow adipocytes resist lipolysis and remodeling in response to beta-adrenergic stimulation". *Bone* 118 (2019), pp. 32–41. DOI: 10.1016/j.bone.2018.01.016.

[293] C. Attane et al. "Human Bone Marrow Is Comprised of Adipocytes with Specific Lipid Metabolism". *Cell Rep* 30.4 (2020), 949–958 e6. DOI: 10.1016/j.celrep.2019.12.089.

[294] T. H. Ambrosi et al. "Adipocyte Accumulation in the Bone Marrow during Obesity and Aging Impairs Stem Cell-Based Hematopoietic and Bone Regeneration". *Cell Stem Cell* 20.6 (2017), 771–784 e6. DOI: 10.1016/j.stem.2017.02.009.

[295] L. Zhong et al. "Single cell transcriptomics identifies a unique adipose lineage cell population that regulates bone marrow environment". *Elife* 9 (2020). DOI: 10.7554/eLife.54695.

[296] B. O. Zhou et al. "Bone marrow adipocytes promote the regeneration of stem cells and haematopoiesis by secreting SCF". *Nat Cell Biol* 19.8 (2017), pp. 891–903. DOI: 10.1038/ncb3570.

[297] E. L. Scheller et al. "Region-specific variation in the properties of skeletal adipocytes reveals regulated and constitutive marrow adipose tissues". *Nat Commun* 6 (2015), p. 7808. DOI: 10.1038/ncomms8808.

[298] Z. Zhang et al. "Bone marrow adipose tissue-derived stem cell factor mediates metabolic regulation of hematopoiesis". *Haematologica* 104.9 (2019), pp. 1731–1743. DOI: 10.3324/haematol.2018.205856.

[299] C. Valet et al. "Adipocyte Fatty Acid Transfer Supports Megakaryocyte Maturation". *Cell Rep* 32.1 (2020), p. 107875. DOI: 10.1016/j.celrep.2020.107875.

[300] O. Kajkenova et al. "Increased adipogenesis and myelopoiesis in the bone marrow of SAMP6, a murine model of defective osteoblastogenesis and low turnover osteopenia". *J Bone Miner Res* 12.11 (1997), pp. 1772–9. DOI: 10.1359/jbmr.1997.12.11.1772.

[301] A. L. Boyd et al. "Acute myeloid leukaemia disrupts endogenous myelo-erythropoiesis by compromising the adipocyte bone marrow niche". *Nat Cell Biol* 19.11 (2017), pp. 1336–1347. DOI: 10.1038/ncb3625.

[302] G. Schoiswohl et al. "Impact of Reduced ATGL-Mediated Adipocyte Lipolysis on Obesity-Associated Insulin Resistance and Inflammation in Male Mice". *Endocrinology* 156.10 (2015), pp. 3610–24. DOI: 10.1210/en.2015-1322.

[303] W. P. Cawthorn et al. "Expansion of Bone Marrow Adipose Tissue During Caloric Restriction Is Associated With Increased Circulating Glucocorticoids and Not With Hypoleptinemia". *Endocrinology* 157.2 (2016), pp. 508–21. DOI: 10.1210/en.2015-1477.

[304] P. Tandon, R. Wafer, and J. E. N. Minchin. "Adipose morphology and metabolic disease". *J Exp Biol* 221.Pt Suppl 1 (2018). DOI: 10.1242/jeb.164970.

[305] S. Wueest et al. "Basal lipolysis, not the degree of insulin resistance, differentiates large from small isolated adipocytes in high-fat fed mice". *Diabetologia* 52.3 (2009), pp. 541–6. DOI: 10.1007/s00125-008-1223-5.

[306] C. Lelliott and A. J. Vidal-Puig. "Lipotoxicity, an imbalance between lipogenesis de novo and fatty acid oxidation". *Int J Obes Relat Metab Disord* 28 Suppl 4 (2004), S22–8. DOI: 10.1038/sj.ijo.0802854.

[307] K. W. Cho, D. L. Morris, and C. N. Lumeng. "Flow cytometry analyses of adipose tissue macrophages". *Methods Enzymol* 537 (2014), pp. 297–314. DOI: 10.1016/B978-0-12-411619-1.00016-1.

[308] C. Benezech et al. "Inflammation-induced formation of fat-associated lymphoid clusters". *Nat Immunol* 16.8 (2015), pp. 819–828. DOI: 10.1038/ni.3215.

[309] M. C. Horowitz et al. "Bone marrow adipocytes". *Adipocyte* 6.3 (2017), pp. 193–204. DOI: 10.1080/21623945.2017.1367881.

[310] W. W. Pang et al. "Human bone marrow hematopoietic stem cells are increased in frequency and myeloid-biased with age". *Proc Natl Acad Sci U S A* 108.50 (2011), pp. 20012–7. DOI: 10.1073/pnas.1116110108.

[311] J. Osuga et al. "Targeted disruption of hormone-sensitive lipase results in male sterility and adipocyte hypertrophy, but not in obesity". *Proc Natl Acad Sci U S A* 97.2 (2000), pp. 787–92. DOI: 10.1073/pnas.97.2.787.

[312] S. Kaushik and A. M. Cuervo. "Degradation of lipid droplet-associated proteins by chaperone-mediated autophagy facilitates lipolysis". *Nat Cell Biol* 17.6 (2015), pp. 759–70. DOI: 10.1038/ncb3166.

[313] T. Yokota et al. "Adiponectin, a fat cell product, influences the earliest lymphocyte precursors in bone marrow cultures by activation of the cyclooxygenase-prostaglandin pathway in stromal cells". *J Immunol* 171.10 (2003), pp. 5091–9. DOI: 10.4049/jimmunol.171.10.5091.

[314] F. A. Bilwani and K. L. Knight. "Adipocyte-derived soluble factor(s) inhibits early stages of B lymphopoiesis". *J Immunol* 189.9 (2012), pp. 4379–86. DOI: 10.4049/jimmunol.1201176.

[315] J. Z. Liu et al. "Association analyses identify 38 susceptibility loci for inflammatory bowel disease and highlight shared genetic risk across populations". *Nat Genet* 47.9 (2015), pp. 979–986. DOI: 10.1038/ng.3359.

[316] J. D. Rioux et al. "Genome-wide association study identifies new susceptibility loci for Crohn disease and implicates autophagy in disease pathogenesis". *Nat Genet* 39.5 (2007), pp. 596–604. DOI: 10.1038/ng2032.

[317] A. Larabi, N. Barnich, and H. T. T. Nguyen. "New insights into the interplay between autophagy, gut microbiota and inflammatory responses in IBD". *Autophagy* 16.1 (2020), pp. 38–51. DOI: 10.1080/15548627.2019.1635384.

[318] A. Blain et al. "Crohn's disease clinical course and severity in obese patients". *Clin Nutr* 21.1 (2002), pp. 51–7. DOI: 10.1054/clnu.2001.0503.

[319] T. Greuter et al. "Impact of obesity on disease activity and disease outcome in inflammatory bowel disease: Results from the Swiss inflammatory bowel disease cohort". *United European Gastroenterol J* 8.10 (2020), pp. 1196–1207. DOI: 10.1177/2050640620954556.

[320] B. B. Crohn, L. Ginzburg, and G. D. Oppenheimer. "Landmark article Oct 15, 1932. Regional ileitis. A pathological and clinical entity. By Burril B. Crohn, Leon Ginzburg, and Gordon D. Oppenheimer". *JAMA* 251.1 (1984), pp. 73–9. DOI: 10.1001/jama.251.1.73.

[321] P. Althoff et al. "Creeping Fat Assessed by Small Bowel MRI Is Linked to Bowel Damage and Abdominal Surgery in Crohn's Disease". *Dig Dis Sci* 64.1 (2019), pp. 204–212. DOI: 10.1007/s10620-018-5303-1.

[322] A. L. Sheehan et al. "Fat-wrapping in Crohn's disease: pathological basis and relevance to surgical practice". *Br J Surg* 79.9 (1992), pp. 955–8. DOI: 10.1002/bjs.1800790934.

[323] J. F. Ziegler et al. "Leptin induces TNFalpha-dependent inflammation in acquired generalized lipodystrophy and combined Crohn's disease". *Nat Commun* 10.1 (2019), p. 5629. DOI: 10.1038/s41467-019-13559-7.

[324] P. Kiesler, I. J. Fuss, and W. Strober. "Experimental Models of Inflammatory Bowel Diseases". *Cell Mol Gastroenterol Hepatol* 1.2 (2015), pp. 154–170. DOI: 10.1016/j.jcmgh.2015.01.006.

[325] L. A. Dieleman et al. "Dextran sulfate sodium-induced colitis occurs in severe combined immunodeficient mice". *Gastroenterology* 107.6 (1994), pp. 1643–52. DOI: 10.1016/0016-5085(94)90803-6.

[326] C. F. Krieglstein et al. "Collagen-binding integrin alpha1beta1 regulates intestinal inflammation in experimental colitis". *J Clin Invest* 110.12 (2002), pp. 1773–82. DOI: 10.1172/JCI15256.

[327] B. Chami et al. "The role of CXCR3 in DSS-induced colitis". *PLoS One* 9.7 (2014), e101622. DOI: 10.1371/journal.pone.0101622.

[328] J. C. Masterson et al. "Eosinophil-mediated signalling attenuates inflammatory responses in experimental colitis". *Gut* 64.8 (2015), pp. 1236–47. DOI: 10.1136/gutjnl-2014-306998.

[329] R. Kuhn et al. "Interleukin-10-deficient mice develop chronic enterocolitis". *Cell* 75.2 (1993), pp. 263–74. DOI: 10.1016/0092-8674(93)80068-p.

[330] D. J. Berg et al. "Enterocolitis and colon cancer in interleukin-10-deficient mice are associated with aberrant cytokine production and CD4(+) TH1-like responses". *J Clin Invest* 98.4 (1996), pp. 1010–20. DOI: 10.1172/JCI118861.

[331] Y. P. Rubtsov et al. "Regulatory T cell-derived interleukin-10 limits inflammation at environmental interfaces". *Immunity* 28.4 (2008), pp. 546–58. DOI: 10.1016/j.immuni.2008.02.017.

[332] A. Roers et al. "T cell-specific inactivation of the interleukin 10 gene in mice results in enhanced T cell responses but normal innate responses to lipopolysaccharide or skin irritation". *J Exp Med* 200.10 (2004), pp. 1289–97. DOI: 10.1084/jem.20041789.

[333] M. C. Kullberg et al. "Helicobacter hepaticus triggers colitis in specific-pathogen-free interleukin-10 (IL-10)-deficient mice through an IL-12- and gamma interferon-dependent mechanism". *Infect Immun* 66.11 (1998), pp. 5157–66. DOI: 10.1128/IAI.66.11.5157-5166.1998.

[334] M. C. Kullberg et al. "IL-23 plays a key role in Helicobacter hepaticus-induced T cell-dependent colitis". *J Exp Med* 203.11 (2006), pp. 2485–94. DOI: 10.1084/jem.20061082.

[335] B. Bernshtein et al. "IL-23-producing IL-10Ralpha-deficient gut macrophages elicit an IL-22-driven proinflammatory epithelial cell response". *Sci Immunol* 4.36 (2019). DOI: 10.1126/sciimmunol.aau6571.

[336] P. J. Morrison et al. "Th17-cell plasticity in Helicobacter hepaticus-induced intestinal inflammation". *Mucosal Immunol* 6.6 (2013), pp. 1143–56. DOI: 10.1038/mi.2013.11.

[337] F. Powrie et al. "Phenotypically distinct subsets of CD4+ T cells induce or protect from chronic intestinal inflammation in C. B-17 scid mice". *Int Immunol* 5.11 (1993), pp. 1461–71. DOI: 10.1093/intimm/5.11.1461.

[338] L. Eckmann. "Animal models of inflammatory bowel disease: lessons from enteric infections". *Ann N Y Acad Sci* 1072 (2006), pp. 28–38. DOI: 10.1196/annals.1326.008.

[339] D. Kontoyiannis et al. "Impaired on/off regulation of TNF biosynthesis in mice lacking TNF AU-rich elements: implications for joint and gut-associated immunopathologies". *Immunity* 10.3 (1999), pp. 387–98. DOI: 10.1016/s1074-7613(00)80038-2.

[340] M. Tschurtschenthaler et al. "Defective ATG16L1-mediated removal of IRE1alpha drives Crohn's disease-like ileitis". *J Exp Med* 214.2 (2017), pp. 401–422. DOI: 10.1084/jem.20160791.

[341] T. T. Pizarro et al. "SAMP1/YitFc mouse strain: a spontaneous model of Crohn's disease-like ileitis". *Inflamm Bowel Dis* 17.12 (2011), pp. 2566–84. DOI: 10.1002/ibd.21638.

[342] S. Read and F. Powrie. "Induction of Inflammatory Bowel Disease in Immunodeficient Mice by Depletion of Regulatory T Cells". *Current Protocols in Immunology* 30 (1999), pp. 15.13.1–15.13.10. DOI: 10.1002/0471142735.im1513s30.

[343] I. Olivier et al. "Is Crohn's creeping fat an adipose tissue?" *Inflamm Bowel Dis* 17.3 (2011), pp. 747–57. DOI: 10.1002/ibd.21413.

[344] P. Czarnewski et al. "Conserved transcriptomic profile between mouse and human colitis allows unsupervised patient stratification". *Nat Commun* 10.1 (2019), p. 2892. DOI: 10.1038/s41467-019-10769-x.

[345] I. Okayasu et al. "A novel method in the induction of reliable experimental acute and chronic ulcerative colitis in mice". *Gastroenterology* 98.3 (1990), pp. 694–702. DOI: 10.1016/0016-5085(90)90290-h.

[346] M. Y. Pepino et al. "Structure-function of CD36 and importance of fatty acid signal transduction in fat metabolism". *Annu Rev Nutr* 34 (2014), pp. 281–303. DOI: 10.1146/annurev-nutr-071812-161220.

[347] L. I. Kredel et al. "Adipokines from local fat cells shape the macrophage compartment of the creeping fat in Crohn's disease". *Gut* 62.6 (2013), pp. 852–62. DOI: 10.1136/gutjnl-2011-301424.

[348] B. Levine, N. Mizushima, and H. W. Virgin. "Autophagy in immunity and inflammation". *Nature* 469.7330 (2011), pp. 323–35. DOI: 10.1038/nature09782.

[349] G. R. Jones et al. "Dynamics of Colon Monocyte and Macrophage Activation During Colitis". *Front Immunol* 9 (2018), p. 2764. DOI: 10.3389/fimmu.2018.02764.

[350] G. Ryzhakov et al. "Alpha kinase 1 controls intestinal inflammation by suppressing the IL-12/Th1 axis". *Nat Commun* 9.1 (2018), p. 3797. DOI: 10.1038/s41467-018-06085-5.

[351] L. A. Dieleman et al. "Chronic experimental colitis induced by dextran sulphate sodium (DSS) is characterized by Th1 and Th2 cytokines". *Clin Exp Immunol* 114.3 (1998), pp. 385–91. DOI: 10.1046/j.1365-2249.1998.00728.x.

[352] N. Whibley, A. Tucci, and F. Powrie. "Regulatory T cell adaptation in the intestine and skin". *Nat Immunol* 20.4 (2019), pp. 386–396. DOI: 10.1038/s41590-019-0351-z.

[353] R. Shamir. "Nutritional aspects in inflammatory bowel disease". *J Pediatr Gastroenterol Nutr* 48 Suppl 2 (2009), S86–8. DOI: 10.1097/MPG.0b013e3181a15ca0.

[354] L. Liu et al. "Fibroblast Growth Factor 21 Deficiency Attenuates Experimental Colitis-Induced Adipose Tissue Lipolysis". *Gastroenterol Res Pract* 2017 (2017), p. 3089378. DOI: 10.1155/2017/3089378.

[355] S. C. Huang et al. "Cell-intrinsic lysosomal lipolysis is essential for alternative activation of macrophages". *Nat Immunol* 15.9 (2014), pp. 846–55. DOI: 10.1038/ni.2956.

[356] Y. M. Park. "CD36, a scavenger receptor implicated in atherosclerosis". *Exp Mol Med* 46 (2014), e99. DOI: 10.1038/emm.2014.38.

[357] H. Wang et al. "CD36-mediated metabolic adaptation supports regulatory T cell survival and function in tumors". *Nat Immunol* 21.3 (2020), pp. 298–308. DOI: 10.1038/s41590-019-0589-5.

[358] J. Couturier et al. "Lymphocytes upregulate CD36 in adipose tissue and liver". *Adipocyte* 8.1 (2019), pp. 154–163. DOI: 10.1080/21623945.2019.1609202.

[359] A. L. Corbin et al. "IRF5 guides monocytes toward an inflammatory CD11c(+) macrophage phenotype and promotes intestinal inflammation". *Sci Immunol* 5.47 (2020). DOI: 10.1126/sciimmunol.aax6085.

[360] E. Dalmas et al. "Irf5 deficiency in macrophages promotes beneficial adipose tissue expansion and insulin sensitivity during obesity". *Nat Med* 21.6 (2015), pp. 610–8. DOI: 10.1038/nm.3829.

[361] C. T. Taylor and S. P. Colgan. "Hypoxia and gastrointestinal disease". *J Mol Med (Berl)* 85.12 (2007), pp. 1295–300. DOI: 10.1007/s00109-007-0277-z.

[362] E. M. Palsson-McDermott and L. A. J. O'Neill. "Targeting immunometabolism as an anti-inflammatory strategy". *Cell Res* 30.4 (2020), pp. 300–314. DOI: 10.1038/s41422-020-0291-z.

[363] G. Casili et al. "Dimethyl Fumarate Reduces Inflammatory Responses in Experimental Colitis". *J Crohns Colitis* 10.4 (2016), pp. 472–83. DOI: 10.1093/ecco-jcc/jjv231.

[364] X. Liu et al. "Dimethyl fumarate ameliorates dextran sulfate sodium-induced murine experimental colitis by activating Nrf2 and suppressing NLRP3 inflammasome activation". *Biochem Pharmacol* 112 (2016), pp. 37–49. DOI: 10.1016/j.bcp.2016.05.002.

[365] R. F. Leal et al. "Autophagy is decreased in mesenteric fat tissue but not in intestinal mucosae of patients with Crohn's disease". *Cell Tissue Res* 350.3 (2012), pp. 549–52. DOI: 10.1007/s00441-012-1491-8.

[366] J. Zhao et al. "FoxO3 coordinately activates protein degradation by the autophagic/lysosomal and proteasomal pathways in atrophying muscle cells". *Cell Metab* 6.6 (2007), pp. 472–83. DOI: 10.1016/j.cmet.2007.11.004.

[367] J. Pott, A. M. Kabat, and K. J. Maloy. "Intestinal Epithelial Cell Autophagy Is Required to Protect against TNF-Induced Apoptosis during Chronic Colitis in Mice". *Cell Host Microbe* 23.2 (2018), 191–202 e4. DOI: 10.1016/j.chom.2017.12.017.

[368] N. Wittkopf et al. "Lack of intestinal epithelial atg7 affects paneth cell granule formation but does not compromise immune homeostasis in the gut". *Clin Dev Immunol* 2012 (2012), p. 278059. DOI: 10.1155/2012/278059.

[369] T. Saitoh et al. "Loss of the autophagy protein Atg16L1 enhances endotoxin-induced IL-1beta production". *Nature* 456.7219 (2008), pp. 264–8. DOI: 10.1038/nature07383.

[370] K. G. Lassen et al. "Atg16L1 T300A variant decreases selective autophagy resulting in altered cytokine signaling and decreased antibacterial defense". *Proc Natl Acad Sci U S A* 111.21 (2014), pp. 7741–6. DOI: 10.1073/pnas.1407001111.

[371] Q. Lu et al. "Homeostatic Control of Innate Lung Inflammation by Vici Syndrome Gene Epg5 and Additional Autophagy Genes Promotes Influenza Pathogenesis". *Cell Host Microbe* 19.1 (2016), pp. 102–13. DOI: 10.1016/j.chom.2015.12.011.

[372] J. G. Fox et al. "Helicobacter hepaticus infection in mice: models for understanding lower bowel inflammation and cancer". *Mucosal Immunol* 4.1 (2011), pp. 22–30. DOI: 10.1038/mi.2010.61.

[373] M. C. Kullberg et al. "Helicobacter hepaticus-induced colitis in interleukin-10-deficient mice: cytokine requirements for the induction and maintenance of intestinal inflammation". *Infect Immun* 69.7 (2001), pp. 4232–41. DOI: 10.1128/IAI.69.7.4232-4241.2001.

[374] J. Kinchen et al. "Structural Remodeling of the Human Colonic Mesenchyme in Inflammatory Bowel Disease". *Cell* 175.2 (2018), 372–386 e17. DOI: 10.1016/j.cell.2018.08.067.

[375] J. C. Coffey et al. "The mesentery in Crohn's disease: friend or foe?" *Curr Opin Gastroenterol* 32.4 (2016), pp. 267–73. DOI: 10.1097/MOG.0000000000000280.

[376] L. Wang et al. "T regulatory cells and B cells cooperate to form a regulatory loop that maintains gut homeostasis and suppresses dextran sulfate sodium-induced colitis". *Mucosal Immunol* 8.6 (2015), pp. 1297–312. DOI: 10.1038/mi.2015.20.

[377] Y. Cong et al. "A dominant, coordinated T regulatory cell-IgA response to the intestinal microbiota". *Proc Natl Acad Sci U S A* 106.46 (2009), pp. 19256–61. DOI: 10.1073/pnas.0812681106.

[378] K. S. Kim et al. "Dietary antigens limit mucosal immunity by inducing regulatory T cells in the small intestine". *Science* 351.6275 (2016), pp. 858–63. DOI: 10.1126/science.aac5560.

[379] C. Schiering et al. "The alarmin IL-33 promotes regulatory T-cell function in the intestine". *Nature* 513.7519 (2014), pp. 564–568. DOI: 10.1038/nature13577.

[380] E. A. Wohlfert et al. "GATA3 controls Foxp3(+) regulatory T cell fate during inflammation in mice". *J Clin Invest* 121.11 (2011), pp. 4503–15. DOI: 10.1172/JCI57456.

[381] B. Raud et al. "Etomoxir Actions on Regulatory and Memory T Cells Are Independent of Cpt1a-Mediated Fatty Acid Oxidation". *Cell Metab* 28.3 (2018), 504–515 e7. DOI: 10.1016/j.cmet.2018.06.002.

[382] L. Peyrin-Biroulet et al. "Mesenteric fat as a source of C reactive protein and as a target for bacterial translocation in Crohn's disease". *Gut* 61.1 (2012), pp. 78–85. DOI: 10.1136/gutjnl-2011-300370.

[383] B. Creyns et al. "Fibrogenesis in Chronic DSS Colitis is Not Influenced by Neutralisation of Regulatory T Cells, of Major T Helper Cytokines or Absence of IL-13". *Sci Rep* 9.1 (2019), p. 10064. DOI: 10.1038/s41598-019-46472-6.

[384] Q. Hu et al. "The Impact of Obesity on the Clinical Course of Inflammatory Bowel Disease: A Meta-Analysis". *Med Sci Monit* 23 (2017), pp. 2599–2606. DOI: 10.12659/msm.901969.

[385] A. Flores et al. "Obesity in Inflammatory Bowel Disease: A Marker of Less Severe Disease". *Dig Dis Sci* 60.8 (2015), pp. 2436–45. DOI: 10.1007/s10620-015-3629-5.

[386] N. Pavelock et al. "Effects of obesity on the course of inflammatory bowel disease". *Proc (Bayl Univ Med Cent)* 32.1 (2019), pp. 14–17. DOI: 10.1080/08998280.2018.1542887.

[387] T. Kruis, A. Batra, and B. Siegmund. "Bacterial translocation - impact on the adipocyte compartment". *Front Immunol* 4 (2014), p. 510. DOI: 10.3389/fimmu.2013.00510.

[388] V. Di Nicola. "Omentum a powerful biological source in regenerative surgery". *Regen Ther* 11 (2019), pp. 182–191. DOI: 10.1016/j.reth.2019.07.008.

[389] Connie W. Y. Ha et al. "Translocation of Viable Gut Microbiota to Mesenteric Adipose Drives Formation of Creeping Fat in Humans". *Cell* 183.3 (2020), 666–683.e17. DOI: 10.1016/j.cell.2020.09.009.

[390] W. C. Mustain et al. "Inflammatory cytokine gene expression in mesenteric adipose tissue during acute experimental colitis". *PLoS One* 8.12 (2013), e83693. DOI: 10.1371/journal.pone.0083693.

[391] J. E. Hu et al. "Leptin Downregulates Angulin-1 in Active Crohn's Disease via STAT3". *Int J Mol Sci* 21.21 (2020). DOI: 10.3390/ijms21217824.

[392] B. Siegmund, H. A. Lehr, and G. Fantuzzi. "Leptin: a pivotal mediator of intestinal inflammation in mice". *Gastroenterology* 122.7 (2002), pp. 2011–25. DOI: 10.1053/gast.2002.33631.

[393] R. Mao et al. "The Mesenteric Fat and Intestinal Muscle Interface: Creeping Fat Influencing Stricture Formation in Crohn's Disease". *Inflamm Bowel Dis* 25.3 (2019), pp. 421–426. DOI: 10.1093/ibd/izy331.

[394] R. Mao et al. "Activated intestinal muscle cells promote preadipocyte migration: a novel mechanism for creeping fat formation in Crohn's disease". *Gut* (2021). DOI: 10.1136/gutjnl-2020-323719.

[395] L. Boutens et al. "Unique metabolic activation of adipose tissue macrophages in obesity promotes inflammatory responses". *Diabetologia* 61.4 (2018), pp. 942–953. DOI: 10.1007/s00125-017-4526-6.

[396] B. R. Coats et al. "Metabolically Activated Adipose Tissue Macrophages Perform Detrimental and Beneficial Functions during Diet-Induced Obesity". *Cell Rep* 20.13 (2017), pp. 3149–3161. DOI: 10.1016/j.celrep.2017.08.096.

[397] P. Tiwari et al. "Metabolically activated adipose tissue macrophages link obesity to triple-negative breast cancer". *J Exp Med* 216.6 (2019), pp. 1345–1358. DOI: 10.1084/jem.20181616.

[398] G. Paul et al. "Profiling adipocytokine secretion from creeping fat in Crohn's disease". *Inflamm Bowel Dis* 12.6 (2006), pp. 471–7. DOI: 10.1097/00054725-200606000-00005.

[399] J. Park et al. "M-CSF from Cancer Cells Induces Fatty Acid Synthase and PPAR-beta/delta Activation in Tumor Myeloid Cells, Leading to Tumor Progression". *Cell Rep* 10.9 (2015), pp. 1614–1625. DOI: 10.1016/j.celrep.2015.02.024.

[400] A. M. Wolf et al. "Adiponectin induces the anti-inflammatory cytokines IL-10 and IL-1RA in human leukocytes". *Biochem Biophys Res Commun* 323.2 (2004), pp. 630–5. DOI: 10.1016/j.bbrc.2004.08.145.

[401] C. M. van Stijn et al. "Macrophage polarization phenotype regulates adiponectin receptor expression and adiponectin anti-inflammatory response". *FASEB J* 29.2 (2015), pp. 636–49. DOI: 10.1096/fj.14-253831.

[402] S. C. Acedo et al. "Participation of leptin in the determination of the macrophage phenotype: an additional role in adipocyte and macrophage crosstalk". *In Vitro Cell Dev Biol Anim* 49.6 (2013), pp. 473–8. DOI: 10.1007/s11626-013-9629-x.

[403] E. Toussirot, G. Streit, and D. Wendling. "The contribution of adipose tissue and adipokines to inflammation in joint diseases". *Curr Med Chem* 14.10 (2007), pp. 1095–100. DOI: 10.2174/092986707780362826.

[404] C. Weidinger et al. "Adipokines and Their Role in Intestinal Inflammation". *Front Immunol* 9 (2018), p. 1974. DOI: 10.3389/fimmu.2018.01974.

[405] R. Fayad et al. "Adiponectin deficiency protects mice from chemically induced colonic inflammation". *Gastroenterology* 132.2 (2007), pp. 601–14. DOI: 10.1053/j.gastro.2006.11.026.

[406] T. Nishihara et al. "Effect of adiponectin on murine colitis induced by dextran sulfate sodium". *Gastroenterology* 131.3 (2006), pp. 853–61. DOI: 10.1053/j.gastro.2006.06.015.

[407] A. Sideri et al. “Effects of obesity on severity of colitis and cytokine expression in mouse mesenteric fat. Potential role of adiponectin receptor 1”. *Am J Physiol Gastrointest Liver Physiol* 308.7 (2015), G591–604. DOI: 10.1152/ajpgi.00269.2014.

[408] Q. Zhao et al. “Adiponectin administration alleviates DSS-induced colonic inflammation in Caco-2 cells and mice”. *Inflamm Res* 67.8 (2018), pp. 663–670. DOI: 10.1007/s00011-018-1155-6.

[409] S. Obeid et al. “Adiponectin confers protection from acute colitis and restricts a B cell immune response”. *J Biol Chem* 292.16 (2017), pp. 6569–6582. DOI: 10.1074/jbc.M115.712646.

[410] A. Saxena et al. “Effect of exercise on chemically-induced colitis in adiponectin deficient mice”. *J Inflamm (Lond)* 9.1 (2012), p. 30. DOI: 10.1186/1476-9255-9-30.

[411] M. L. Hanson et al. “Oral delivery of IL-27 recombinant bacteria attenuates immune colitis in mice”. *Gastroenterology* 146.1 (2014), 210–221 e13. DOI: 10.1053/j.gastro.2013.09.060.

[412] M. Sasaki et al. “Reversal of experimental colitis disease activity in mice following administration of an adenoviral IL-10 vector”. *J Inflamm (Lond)* 2.1 (2005), p. 13. DOI: 10.1186/1476-9255-2-13.

[413] L. Steidler et al. “Treatment of murine colitis by Lactococcus lactis secreting interleukin-10”. *Science* 289.5483 (2000), pp. 1352–5. DOI: 10.1126/science.289.5483.1352.

[414] C. E. Juge-Aubry et al. “Adipose tissue is a regulated source of interleukin-10”. *Cytokine* 29.6 (2005), pp. 270–4. DOI: 10.1016/j.cyto.2004.10.017.

[415] J. R. Acosta et al. “Human-Specific Function of IL-10 in Adipose Tissue Linked to Insulin Resistance”. *J Clin Endocrinol Metab* 104.10 (2019), pp. 4552–4562. DOI: 10.1210/jc.2019-00341.

[416] L. I. Kredel and B. Siegmund. "Adipose-tissue and intestinal inflammation - visceral obesity and creeping fat". *Front Immunol* 5 (2014), p. 462. DOI: 10.3389/fimmu.2014.00462.

[417] L. Peyrin-Biroulet et al. "Mesenteric fat in Crohn's disease: a pathogenetic hallmark or an innocent bystander?" *Gut* 56.4 (2007), pp. 577–83. DOI: 10.1136/gut.2005.082925.

[418] M. Oliva et al. "The impact of sex on gene expression across human tissues". *Science* 369.6509 (2020). DOI: 10.1126/science.aba3066.

[419] G. Kojouharoff et al. "Neutralization of tumour necrosis factor (TNF) but not of IL-1 reduces inflammation in chronic dextran sulphate sodium-induced colitis in mice". *Clin Exp Immunol* 107.2 (1997), pp. 353–8. DOI: 10.1111/j.1365-2249.1997.291-ce1184.x.

[420] M. Noti et al. "TNF suppresses acute intestinal inflammation by inducing local glucocorticoid synthesis". *J Exp Med* 207.5 (2010), pp. 1057–66. DOI: 10.1084/jem.20090849.

[421] X. Luo et al. "Obesity induces preadipocyte CD36 expression promoting inflammation via the disruption of lysosomal calcium homeostasis and lysosome function". *EBioMedicine* 56 (2020), p. 102797. DOI: 10.1016/j.ebiom.2020.102797.

[422] C. P. Liang et al. "Increased CD36 protein as a response to defective insulin signaling in macrophages". *J Clin Invest* 113.5 (2004), pp. 764–73. DOI: 10.1172/JCI19528.

[423] L. Nagy et al. "Oxidized LDL regulates macrophage gene expression through ligand activation of PPARgamma". *Cell* 93.2 (1998), pp. 229–40. DOI: 10.1016/s0092-8674(00)81574-3.

[424] P. Tontonoz et al. "PPARgamma promotes monocyte/macrophage differentiation and uptake of oxidized LDL". *Cell* 93.2 (1998), pp. 241–52. DOI: 10.1016/s0092-8674(00)81575-5.

[425] R. F. Chen. "Removal of fatty acids from serum albumin by charcoal treatment". *J Biol Chem* 242.2 (1967), pp. 173–81.

[426] A. E. Ringel et al. "Obesity Shapes Metabolism in the Tumor Microenvironment to Suppress Anti-Tumor Immunity". *Cell* 183.7 (2020), 1848–1866 e26. DOI: 10.1016/j.cell.2020.11.009.

[427] K. R. Feingold et al. "Mechanisms of triglyceride accumulation in activated macrophages". *J Leukoc Biol* 92.4 (2012), pp. 829–39. DOI: 10.1189/jlb.1111537.

[428] L. G. Teixeira et al. "The combination of high-fat diet-induced obesity and chronic ulcerative colitis reciprocally exacerbates adipose tissue and colon inflammation". *Lipids Health Dis* 10 (2011), p. 204. DOI: 10.1186/1476-511X-10-204.

[429] A. Schaffler et al. "Secretion of RANTES (CCL5) and interleukin-10 from mesenteric adipose tissue and from creeping fat in Crohn's disease: regulation by steroid treatment". *J Gastroenterol Hepatol* 21.9 (2006), pp. 1412–8. DOI: 10.1111/j.1440-1746.2006.04300.x.

[430] M. Quiros et al. "Macrophage-derived IL-10 mediates mucosal repair by epithelial WISP-1 signaling". *J Clin Invest* 127.9 (2017), pp. 3510–3520. DOI: 10.1172/JCI90229.

[431] B. Jacobsson and U. Smith. "Effect of cell size on lipolysis and antilipolytic action of insulin in human fat cells". *J Lipid Res* 13.5 (1972), pp. 651–6.

[432] J. Laurencikiene et al. "Regulation of lipolysis in small and large fat cells of the same subject". *J Clin Endocrinol Metab* 96.12 (2011), E2045–9. DOI: 10.1210/jc.2011-1702.

[433] A. S. Rambold, S. Cohen, and J. Lippincott-Schwartz. "Fatty acid trafficking in starved cells: regulation by lipid droplet lipolysis, autophagy, and mitochondrial fusion dynamics". *Dev Cell* 32.6 (2015), pp. 678–92. DOI: 10.1016/j.devcel.2015.01.029.

[434] T. Shpilka et al. "Lipid droplets and their component triglycerides and steryl esters regulate autophagosome biogenesis". *EMBO J* 34.16 (2015), pp. 2117–31. DOI: 10.15252/embj.201490315.

[435] Y. Wang et al. "Protective role of tumor necrosis factor (TNF) receptors in chronic intestinal inflammation: TNFR1 ablation boosts systemic inflammatory response". *Lab Invest* 93.9 (2013), pp. 1024–35. DOI: 10.1038/labinvest.2013.89.

[436] H. Kanda et al. "MCP-1 contributes to macrophage infiltration into adipose tissue, insulin resistance, and hepatic steatosis in obesity". *J Clin Invest* 116.6 (2006), pp. 1494–505. DOI: 10.1172/JCI26498.

[437] H. Wu et al. "Lipid droplet-dependent fatty acid metabolism controls the immune suppressive phenotype of tumor-associated macrophages". *EMBO Mol Med* 11.11 (2019), e10698. DOI: 10.15252/emmm.201910698.

[438] F. O. Martinez et al. "Transcriptional profiling of the human monocyte-to-macrophage differentiation and polarization: new molecules and patterns of gene expression". *J Immunol* 177.10 (2006), pp. 7303–11. DOI: 10.4049/jimmunol.177.10.7303.

[439] M. Orecchioni et al. "Macrophage Polarization: Different Gene Signatures in M1(LPS+) vs. Classically and M2(LPS-) vs. Alternatively Activated Macrophages". *Front Immunol* 10 (2019), p. 1084. DOI: 10.3389/fimmu.2019.01084.

[440] D. C. Lacey et al. "Defining GM-CSF- and macrophage-CSF-dependent macrophage responses by in vitro models". *J Immunol* 188.11 (2012), pp. 5752–65. DOI: 10.4049/jimmunol.1103426.

[441] A. Lukic et al. "GM-CSF- and M-CSF-primed macrophages present similar resolving but distinct inflammatory lipid mediator signatures". *FASEB J* 31.10 (2017), pp. 4370–4381. DOI: 10.1096/fj.201700319R.

[442] L. Hodson, C. M. Skeaff, and B. A. Fielding. "Fatty acid composition of adipose tissue and blood in humans and its use as a biomarker of dietary intake". *Prog Lipid Res* 47.5 (2008), pp. 348–80. DOI: 10.1016/j.plipres.2008.03.003.

[443] S. L. Pompura et al. "Oleic acid restores suppressive defects in tissue-resident FOXP3 Tregs from patients with multiple sclerosis". *J Clin Invest* 131.2 (2021). DOI: 10.1172/JCI138519.

[444] M. T. Nguyen et al. "A subpopulation of macrophages infiltrates hypertrophic adipose tissue and is activated by free fatty acids via Toll-like receptors 2 and 4 and JNK-dependent pathways". *J Biol Chem* 282.48 (2007), pp. 35279–92. DOI: 10.1074/jbc.M706762200.

[445] T. Suganami et al. "Role of the Toll-like receptor 4/NF-kappaB pathway in saturated fatty acid-induced inflammatory changes in the interaction between adipocytes and macrophages". *Arterioscler Thromb Vasc Biol* 27.1 (2007), pp. 84–91. DOI: 10.1161/01.ATV.0000251608.09329.9a.

[446] H. Y. Chang et al. "Docosahexaenoic acid induces M2 macrophage polarization through peroxisome proliferator-activated receptor gamma activation". *Life Sci* 120 (2015), pp. 39–47. DOI: 10.1016/j.lfs.2014.10.014.

[447] R. Liu et al. "Disturbance of Fatty Acid Desaturation Mediated by FADS2 in Mesenteric Adipocytes Contributes to Chronic Inflammation of Crohn's Disease". *J Crohns Colitis* 14.11 (2020), pp. 1581–1599. DOI: 10.1093/ecco-jcc/jjaa086.

[448] Y. Yan et al. "Omega-3 fatty acids prevent inflammation and metabolic disorder through inhibition of NLRP3 inflammasome activation". *Immunity* 38.6 (2013), pp. 1154–63. DOI: 10.1016/j.immuni.2013.05.015.

[449] C. Camell and C. W. Smith. "Dietary oleic acid increases m2 macrophages in the mesenteric adipose tissue". *PLoS One* 8.9 (2013), e75147. DOI: 10.1371/journal.pone.0075147.

[450] S. Zhang et al. "Efferocytosis Fuels Requirements of Fatty Acid Oxidation and the Electron Transport Chain to Polarize Macrophages for Tissue Repair". *Cell Metab* 29.2 (2019), 443–456 e5. DOI: 10.1016/j.cmet.2018.12.004.

[451] N. M. LaMarche et al. "Distinct iNKT Cell Populations Use IFNgamma or ER Stress-Induced IL-10 to Control Adipose Tissue Homeostasis". *Cell Metab* (2020). DOI: 10.1016/j.cmet.2020.05.017.

[452] S. Gesta, Y. H. Tseng, and C. R. Kahn. "Developmental origin of fat: tracking obesity to its source". *Cell* 131.2 (2007), pp. 242–56. DOI: 10.1016/j.cell.2007.10.004.

[453] K. A. Lee et al. “Inflammation-Modulated Metabolic Reprogramming Is Required for DUOX-Dependent Gut Immunity in Drosophila”. *Cell Host Microbe* 23.3 (2018), 338–352 e5. DOI: 10.1016/j.chom.2018.01.011.

[454] M. Molaei, C. Vandehoef, and J. Karpac. “NF-kappaB Shapes Metabolic Adaptation by Attenuating Foxo-Mediated Lipolysis in Drosophila”. *Dev Cell* 49.5 (2019), 802–810 e6. DOI: 10.1016/j.devcel.2019.04.009.

[455] A. Franz, W. Wood, and P. Martin. “Fat Body Cells Are Motile and Actively Migrate to Wounds to Drive Repair and Prevent Infection”. *Dev Cell* 44.4 (2018), 460–470 e3. DOI: 10.1016/j.devcel.2018.01.026.

[456] B. A. Shook et al. “Dermal Adipocyte Lipolysis and Myofibroblast Conversion Are Required for Efficient Skin Repair”. *Cell Stem Cell* 26.6 (2020), 880–895 e6. DOI: 10.1016/j.stem.2020.03.013.

[457] B. A. Schmidt and V. Horsley. “Intradermal adipocytes mediate fibroblast recruitment during skin wound healing”. *Development* 140.7 (2013), pp. 1517–27. DOI: 10.1242/dev.087593.

[458] R. Morison. “Remarks ON SOME FUNCTIONS OF THE OMENTUM”. *Br Med J* 1.2350 (1906), pp. 76–8. DOI: 10.1136/bmj.1.2350.76.

[459] M. Wei et al. “Visceral Adipose Tissue Derived Exosomes Exacerbate Colitis Severity via Pro-inflammatory MiRNAs in High Fat Diet Fed Mice”. *ACS Nano* 14.4 (2020), pp. 5099–5110. DOI: 10.1021/acsnano.0c01860.

[460] Y. Pan et al. “Adipocyte-secreted exosomal microRNA-34a inhibits M2 macrophage polarization to promote obesity-induced adipose inflammation”. *J Clin Invest* 129.2 (2019), pp. 834–849. DOI: 10.1172/JCI123069.

[461] Y. Zhang et al. “Adipocyte-derived microvesicles from obese mice induce M1 macrophage phenotype through secreted miR-155”. *J Mol Cell Biol* 8.6 (2016), pp. 505–517. DOI: 10.1093/jmcb/mjw040.

[462] T. Thomou et al. “Adipose-derived circulating miRNAs regulate gene expression in other tissues”. *Nature* 542.7642 (2017), pp. 450–455. DOI: 10.1038/nature21365.

[463] G. B. D. Inflammatory Bowel Disease Collaborators. "The global, regional, and national burden of inflammatory bowel disease in 195 countries and territories, 1990-2017: a systematic analysis for the Global Burden of Disease Study 2017". *Lancet Gastroenterol Hepatol* 5.1 (2020), pp. 17–30. DOI: 10.1016/S2468-1253(19)30333-4.

[464] D. Corridoni et al. "Inflammatory Bowel Disease Through the Lens of Single-cell RNA-seq Technologies". *Inflamm Bowel Dis* 26.11 (2020), pp. 1658–1668. DOI: 10.1093/ibd/izaa089.

[465] D. Corridoni et al. "Single-cell atlas of colonic CD8(+) T cells in ulcerative colitis". *Nat Med* 26.9 (2020), pp. 1480–1490. DOI: 10.1038/s41591-020-1003-4.

[466] K. Parikh et al. "Colonic epithelial cell diversity in health and inflammatory bowel disease". *Nature* 567.7746 (2019), pp. 49–55. DOI: 10.1038/s41586-019-0992-y.

[467] J. C. Martin et al. "Single-Cell Analysis of Crohn's Disease Lesions Identifies a Pathogenic Cellular Module Associated with Resistance to Anti-TNF Therapy". *Cell* 178.6 (2019), 1493–1508 e20. DOI: 10.1016/j.cell.2019.08.008.

[468] Crohns Foundation and Colitis. "Challenges in IBD Research". *Inflamm Bowel Dis* 25.Suppl 2 (2019), S1–S4. DOI: 10.1093/ibd/izz074.

[469] M. Argollo et al. "Comorbidities in inflammatory bowel disease: a call for action". *Lancet Gastroenterol Hepatol* 4.8 (2019), pp. 643–654. DOI: 10.1016/S2468-1253(19)30173-6.

[470] M. A. Mendall et al. "Body mass index in young men and risk of inflammatory bowel disease through adult life: A population-based Danish cohort study". *Sci Rep* 9.1 (2019), p. 6360. DOI: 10.1038/s41598-019-42642-8.

[471] M. C. Manresa, C. Godson, and C. T. Taylor. "Hypoxia-sensitive pathways in inflammation-driven fibrosis". *Am J Physiol Regul Integr Comp Physiol* 307.12 (2014), R1369–80. DOI: 10.1152/ajpregu.00349.2014.

[472] I. Cotzomi-Ortega et al. “Autophagy and Its Role in Protein Secretion: Implications for Cancer Therapy”. *Mediators Inflamm* 2018 (2018), p. 4231591. DOI: 10.1155/2018/4231591.

[473] N. Dupont et al. “Autophagy-based unconventional secretory pathway for extracellular delivery of IL-1beta”. *EMBO J* 30.23 (2011), pp. 4701–11. DOI: 10.1038/emboj.2011.398.

[474] T. Kimura et al. “Dedicated SNAREs and specialized TRIM cargo receptors mediate secretory autophagy”. *EMBO J* 36.1 (2017), pp. 42–60. DOI: 10.15252/embj.201695081.

[475] K. Nakahira et al. “Autophagy proteins regulate innate immune responses by inhibiting the release of mitochondrial DNA mediated by the NALP3 inflammasome”. *Nat Immunol* 12.3 (2011), pp. 222–30. DOI: 10.1038/ni.1980.

[476] C. S. Shi et al. “Activation of autophagy by inflammatory signals limits IL-1beta production by targeting ubiquitinated inflammasomes for destruction”. *Nat Immunol* 13.3 (2012), pp. 255–63. DOI: 10.1038/ni.2215.

[477] B. Kelly and E. L. Pearce. “Amino Assets: How Amino Acids Support Immunity”. *Cell Metab* 32.2 (2020), pp. 154–175. DOI: 10.1016/j.cmet.2020.06.010.

[478] N. P. Hessvik et al. “PIKfyve inhibition increases exosome release and induces secretory autophagy”. *Cell Mol Life Sci* 73.24 (2016), pp. 4717–4737. DOI: 10.1007/s00018-016-2309-8.

[479] N. Collins et al. “The Bone Marrow Protects and Optimizes Immunological Memory during Dietary Restriction”. *Cell* 178.5 (2019), 1088–1101 e15. DOI: 10.1016/j.cell.2019.07.049.

[480] X. Xu et al. “Autophagy is essential for effector CD8(+) T cell survival and memory formation”. *Nat Immunol* 15.12 (2014), pp. 1152–61. DOI: 10.1038/ni.3025.

[481] D. O’Sullivan et al. “Memory CD8(+) T cells use cell-intrinsic lipolysis to support the metabolic programming necessary for development”. *Immunity* 41.1 (2014), pp. 75–88. DOI: 10.1016/j.immuni.2014.06.005.

[482] Y. Endo et al. “ACC1 determines memory potential of individual CD4(+) T cells by regulating de novo fatty acid biosynthesis”. *Nat Metab* 1.2 (2019), pp. 261–275. DOI: 10.1038/s42255-018-0025-4.

[483] M. Angela et al. “Fatty acid metabolic reprogramming via mTOR-mediated inductions of PPARgamma directs early activation of T cells”. *Nat Commun* 7 (2016), p. 13683. DOI: 10.1038/ncomms13683.

[484] E. L. Pearce et al. “Enhancing CD8 T-cell memory by modulating fatty acid metabolism”. *Nature* 460.7251 (2009), pp. 103–7. DOI: 10.1038/nature08097.

[485] G. J. van der Windt et al. “Mitochondrial respiratory capacity is a critical regulator of CD8+ T cell memory development”. *Immunity* 36.1 (2012), pp. 68–78. DOI: 10.1016/j.immuni.2011.12.007.

[486] D. O’Sullivan. “The metabolic spectrum of memory T cells”. *Immunol Cell Biol* 97.7 (2019), pp. 636–646. DOI: 10.1111/imcb.12274.

[487] A. M. Leidal, B. Levine, and J. Debnath. “Autophagy and the cell biology of age-related disease”. *Nat Cell Biol* 20.12 (2018), pp. 1338–1348. DOI: 10.1038/s41556-018-0235-8.

[488] F. Lonnqvist et al. “Catecholamine-induced lipolysis in adipose tissue of the elderly”. *J Clin Invest* 85.5 (1990), pp. 1614–21. DOI: 10.1172/JCI114612.

[489] A. A. Johnson and A. Stolzing. “The role of lipid metabolism in aging, lifespan regulation, and age-related disease”. *Aging Cell* 18.6 (2019), e13048. DOI: 10.1111/acel.13048.

[490] C. N. Lumeng et al. “Aging is associated with an increase in T cells and inflammatory macrophages in visceral adipose tissue”. *J Immunol* 187.12 (2011), pp. 6208–16. DOI: 10.4049/jimmunol.1102188.

A Appendix 1: Differentially expressed genes - WT vs. $Atg7^{Ad}$

Gene Symbol	Full Gene Name	Log_2-Fold Change	Adjusted p-value
Tmem181b-ps	Tmem181b-ps	4.51	1.84E-11
Dynlt1b	Dynein Light Chain Tctex-Type 1	2.80	4.41E-09
Gm14308	Predicted Gene 14308	2.70	0.003072571
B630019A10Rik	B630019A10Rik	2.67	5.82E-17
Esr1	Estrogen Receptor 1	1.99	5.43E-29
BC106179	cDNA sequence BC106179	1.75	0.006712794
Eda2r	Ectodysplasin A2 Receptor	1.23	3.75E-05
Ephx1	Epoxide Hydrolase 1	1.00	1.82E-05
Rfc4	Replication Factor C Subunit 4	0.90	1.55E-07
Gm3435	Predicted Gene 3435	0.80	0.000281161
Ccn5	Cellular Communication Network Factor 5	0.53	0.006926866
Apoe	Apolipoprotein E	0.43	0.014085464
Ccng1	Cyclin G1	0.35	0.005376878
Exoc4	Exocyst Complex Component 4	0.31	0.029922866
Rpl30	Ribosomal Protein L30	0.20	0.006137911
Rps25	Ribosomal Protein S25	0.16	0.011377989

Table 1: Significantly upregulated genes in visceral adipocytes from water-treated $Atg7^{Ad}$ compared to WT mice

Gene Symbol	Full Gene Name	Log_2-Fold Change	Adjusted p-value
Trib2	Tribbles Pseudokinase 2	-0.000024	0.010641562
Grn	Granulin Precursor	-0.22	0.036176645
Rsrp1	Arginine And Serine Rich Protein 1	-0.32	0.02707597
Col3a1	Collagen Type III Alpha 1 Chain	-0.37	0.036176645
Axl	AXL Receptor Tyrosine Kinase	-0.46	0.036176645
Pde2a	Phosphodiesterase 2A	-0.48	0.013422994
Tfr2	Transferrin Receptor 2	-0.68	0.010641562
Adamts19	ADAM Metallopeptidase With Thrombospondin Type 1 Motif 19	-0.75	0.013422994
F830016B08Rik	Interferon-gamma-inducible GTPase Ifgga4 protein	-0.96	0.006926866
Atg7	Autophagy Related 7	-3.22	1.12E-21

Table 2: Significantly downregulated genes in visceral adipocytes from water-treated $Atg7^{Ad}$ compared to WT mice

Gene Symbol	Full Gene Name	Log_2-Fold Change	Adjusted p-value
B630019A10Rik	B630019A10Rik	2.36	4.95E-11
Esr1	Estrogen Receptor 1	1.92	9.18E-24
Eda2r	Ectodysplasin A2 Receptor	1.26	0.020606108
Ephx1	Epoxide Hydrolase 1	1.12	0.020576813
Vit	Vitrin	0.60	0.036813531
Rfc4	Replication Factor C Subunit 4	0.49	0.020576813

Table 3: Significantly upregulated genes in visceral adipocytes from DSS-treated $Atg7^{Ad}$ compared to WT mice

Gene Symbol	Full Gene Name	Log_2-Fold Change	Adjusted p-value
Acvrl1	Activin A Receptor Like Type 1	-4.39E-05	0.000471573
Calr	Calreticulin	-0.29	0.021953765
9330159F19Rik	9330159F19Rik	-0.47	0.041899377
Jam3	Junctional Adhesion Molecule 3	-1.06	0.016819224
Fgfbp3	Fibroblast Growth Factor Binding Protein 3	-1.17	0.004962239
Atg7	Autophagy Related 7	-2.74	1.83E-19

Table 4: Significantly downregulated genes in visceral adipocytes from DSS-treated $Atg7^{Ad}$ compared to WT mice